DETERMINING THE CONTRIBUTION OF EXERCISE IN PREVENTING ABERRANT MYELOPOIESIS WITH OBESITY AND ITS IMPLICATIONS FOR COLORECTAL CANCER ONSET

James Joseph George Vanhie, M.Sc.

Thesis submitted to the University of Ottawa
in partial fulfillment of the requirements for the
Doctor of Philosophy degree in Human Kinetics

School of Human Kinetics
Faculty of Health Sciences
University of Ottawa

Thesis Abstract

Obesity continues in its severity on a global scale, where by 2030 it is anticipated that a third of adults will be overweight and another half will be classified as having obesity[1]. Several components contribute to the elevating trend; a lack of physical activity and Western diet consumption are at the forefront[2]. Western diets are rich in saturated fats that promote adipocyte hypertrophy and chronic low-grade systemic inflammation that is driven by aberrant myelopoiesis in the bone marrow[2–6]. The bone marrow is a complex environment that hosts hematopoiesis—the process of blood cell formation. Hematopoietic stem cells (HSCs) are the most primitive pluripotent cells that can divide asymmetrically to form more committed progenitor cells of the lymphoid and myeloid lineages. Our lab has previously demonstrated that high-fat diet-induced obesity promotes inflammatory myeloid cell formation, termed *myelopoiesis*, that is attenuated by exercise training under conditions of radiation-induced stress hematopoiesis[7]. Previous reports suggest that cells in the HSC niche could be communicating via extracellular vesicles to affect myelopoiesis[8,9]. Therefore, obesity may alter EV signaling, and by extension, myelopoiesis. Targeting obesity-induced aberrant myelopoiesis through exercise training could have important implications for peripheral disease.

Colorectal cancer (CRC) is being diagnosed at ever increasing rates in young people that is due, in part, to Western diet consumption alongside a sedentary lifestyle[10–12]. Since obesity also promotes chronic low-grade inflammation and aberrant myelopoiesis, obesity may promote CRC onset through these mechanisms. A previous report demonstrated a partial reliance on macrophage accumulation in CRC development, where transient macrophage depletion attenuated carcinogenesis[13]. Importantly, our group[14] and others[15] have shown that weight loss

alone does not attenuate CRC formation. Instead, we reported previously that colorectal carcinogenesis is mitigated only with the introduction of exercise alongside weight loss[14]. However, whether inflammatory cell accumulation is marrow-derived and precedes colorectal carcinogenesis and localized inflammation remains unknown. Further, alterations to EV communication and HSC differentiation patterns during steady state hematopoiesis remain unknown. Therefore, the overall objective of the thesis was to deepen our understanding of how obesity and exercise exert differential effects on steady state hematopoiesis, and in turn, whether the differential effects of obesity and exercise on hematopoiesis underlie colon cancer aetiology.

Our main findings were that obesity promotes HSC and progenitor cell expansion alongside aberrant myelopoiesis during steady state hematopoiesis. EVs had altered cargo, where miRNA-331-5p and miR-193 were lower in EVs derived from exercised mice with obesity compared to sedentary counterparts. Further, EVs from exercised mice with obesity attenuated HSC and progenitor cell expansion that was observed in sedentary counterparts. Finally, obesity led to enhanced myeloid cell accumulation in the colon without any effect of exercise, yet exercise attenuated colorectal carcinogenesis, which may be due to β-Catenin and STAT3 molecular pathway maintenance. Overall, the current thesis found that high-fat diet-induced obesity alters HSC niche EV communication, promotes aberrant myelopoiesis and colon myeloid cell accumulation, and colon cancer formation. However, exercise training attenuates aberrant myelopoiesis and colon cancer formation, which may be due to cell proliferation pathway management.

Acknowledgements

I want to thank my supervisor, Dr. Michael De Lisio, for providing the opportunity to complete my final degree in his lab. Mike, thank you very much for all of your support and patience throughout the program. Beginning this program on the eve of the COVID-19 pandemic provided a unique opportunity to understand how to navigate through unexpected twists in a (to me) brand-new field. Your unwavering professionalism, advice, and commitment to science have provided an exemplary standard for me to aspire to in my own career.

I would also like to thank my thesis advisory committee, Dr. Krista Power and Dr. Kristi Adamo, for their invaluable suggestions, feedback, and support throughout the program.

This thesis could not have been completed without extensive collaboration from all of the current and previous De Lisio Lab members. Special mentions must be made to previous members Eadan Farber and Matthew Ngu, whose support and friendship continues today. To current members, especially Dr. Nicolás Collao, Dr. Kayleigh Beaudry, and (soon to be Dr.) Lisa Ek Orloff, thank you for providing the best possible lab environment. Thank you to all of my friends outside of the lab who have always taken interest in my research and supported me at every step.

Thank you to my family for their unconditional support throughout the years. Mom and dad, a special appreciation goes to both of you for your endless support in this ultimate endeavor. It's been a long road, but it has been worth the sacrifice.

Finally, a special thank you to my partner, Natalie, for having accompanied me in the final stretch of this academic marathon. Thank you for the countless times you listened, supported,

and motivated me. You've made a greater impact than you know on helping me achieve this milestone. Love you, Nat.

Table of Contents

List of Figures

List of Tables

List of Supplemental Figures

List of Supplemental Tables

List of Appendix Figures

List of Appendix Tables

List of Abbreviations

Abca1 – ATP-binding cassette transporter ABCA1

Abcg1 – ATP-binding cassette sub-family G member 1

ACF – Aberrant crypt foci

AIBP – A-I binding protein

Akt – Protein Kinase B

AML – Acute myeloid leukemia

AOM – Azoxymethane

APOC2 – Apolipoprotein C-II

APC – adenomatous polyposis coli protein

Apoe – Apolipoprotein E

ATF4 – Activating transcription factor 4

BFU-E – Blast forming unit-erythroid

BMI – Body mass index

BRAF – v-Raf murine sarcoma viral oncogene homolog B

BSA – Bovine serum albumin

c-Kit – Receptor tyrosine kinase

CAR – C-X-C motif chemokine ligand 12-abundant reticular

CCL2 – C-C chemokine ligand type 2

Ccnd1 – Cyclin D1 gene

CCR2 – C-C chemokine receptor type 2

CD4 – Cluster of differentiation 4

CD9 – Cluster of differentiation 9

CD36 – Cluster of differentiation 36

CD40 – Cluster of differentiation 40

CD48 – Cluster of differentiation 48

CD49d – Cluster of differentiation 49d

CD86 - Cluster of differentiation 86

CD150 – Cluster of differentiation 150

CD229 – Cluster of differentiation 229

CD244 – Cluster of differentiation 244

CFU – Colony forming unit

CFU-E – Colony forming unit-erythroid

CFU-GEMM – Colony forming unit granulocyte, erythroid, macrophage, megakaryocyte

CFU-GM – Colony forming unit-granulocyte, macrophage

CLP – Common lymphoid progenitor cell

CMP – Common myeloid progenitor cell

CON - Control

CPT1 – Carnitine palmitoyl transferase 1

CSF1 – Colony stimulating factor

CXCL4 – C-X-C motif chemokine ligand 4

CXCL12 – C-X-C motif chemokine ligand 12

DMEM – Dulbecco's modified Eagle's medium

DNA – deoxyribonucleic acid

DSS – Dextran sodium sulfate

Na_2-EDTA (or K_2-EDTA) – Disodium (or dipotassium) ethylenediaminetetraacetic acid

EdU – 5-Ethynyl-2'-deoxyuridine

ERK – extracellular signal-regulated kinase

EV – Extracellular vesicle

EX - Exercise

FABP4 – Fatty acid-binding protein 4

FACS – Fluorescence-activated cell sorting

FAK – Focal adhesion kinase

FAP – Familial (hereditary) adenomatous polyposis

FBS – Fetal bovine serum

G-CSF – Granulocyte colony stimulating factor

GMPs – Granulocyte-monocyte progenitor cells

GO:BP – Gene ontology: Biological processes

IFNγ – Interferon γ

IL-1β – Interleukin-1β

IL-2 – Interleukin-2

IL-3 – Interleukin 3

IL-6 – Interleukin-6

IL-10 – Interleukin-10

IL-12 – Interleukin-12

IL-17 – Interleukin-17

IL-23 – Interleukin-23

ISEV – International Society for Extracellular Vesicles

HDL – High-density lipoprotein

HFD – High-fat diet

HNPCC – hereditary non-polyposis colorectal cancer (Lynch syndrome)

HSC – Hematopoietic stem cell

HSPC – Hematopoietic stem and progenitor cell

JAK – Janus kinase

JNK – c-Jun N-terminal kinase

KEGG – Kyoto encyclopedia of genes and genomes

KRAS – kirsten rat sarcoma

LDL – Low-density lipoprotein

LEPR – Leptin receptor

LGR4 – Leucine-rich repeat-containing G-protein coupled receptor 4

LT-HSC – Long-term hematopoietic stem cell

LXR – Liver X receptor

MACS – Magnetic-activated cell sorting

MAPK – mitogen-activated protein kinase

M1 – Classically activated macrophage

M2 – Alternatively activated macrophage

MCP-1 – Monocyte chemoattractant protein-1

M-CSF – Macrophage colony stimulating factor

MEPs – Megakaryocyte-erythroid progenitor cells

MIP-2 – Macrophage inflammatory protein 2

mmu-miR – Mus musculus (mouse) micro ribonucleic acid

miRNA – Micro ribonucleic acid

MISEV2014 – Minimal Information for Studies of Extracellular Vesicles 2014

MLH1 – MutL Homolog 1

MPP – Multipotent progenitor

MSC – Mesenchymal stromal/stem cell

MSH2 – MutS homolog 2

MSH6 – MutS homolog 6

mTOR – mechanistic target of rapamycin

MyD88 – Myeloid differentiation primary response 88

NaOH – Sodium hydroxide

NF-κB – Nuclear factor kappa B

NK Cell – Natural killer cell

Notch1 – Neurogenic locus notch homolog protein 1

PBS – Phosphate-buffered saline

PCR – Polymerase chain reaction

PD-L1 – Programmed death-ligand 1

PDGFR-α – Platelet-derived growth factor receptor α

PI3K – Phosphatidylinositol-3-kinase

PMS1 – Postmeiotic segregation increased 1 homolog 1

PMS2 - Postmeiotic segregation increased 1 homolog 2

PPARγ – Peroxisome proliferator-activated receptor γ

PUFA – Polyunsaturated fatty acid

RANKL – Receptor activator of nuclear factor kappa-B ligand

Rap1 – Ras-associated protein 1

RCN2 – Reticulocalbin-2

RIPA Buffer – Radioimmunoprecipitation assay buffer

RT-qPCR – Reverse transcription quantitative polymerase chain reaction

scATAC-seq – Single cell analysis for assay for transposase-accessible chromatin using sequencing

SDS-PAGE – Sodium dodecyl sulfate-polyacrylamide gel eletrophoresis

SED - Sedentary

SLAM – signaling lymphocytic activation molecule

SnapATAC – Single nucleus analysis pipeline for assay for transposase-accessible chromatin

SPARC – Secreted protein acidic and rich in cysteine

SREBP2 – Sterol regulatory element-binding protein 2

STAT1 – Signal transducer and activator of transcription 1

STAT3 – Signal transducer and activator of transcription 3

STAT6 – Signal transducer and activator of transcription 6

ST-HSC – Short-term hematopoietic stem cell

Sca-1 – Stem cell antigen 1

SCF – Stem cell factor

TBST – Tris buffered saline – Tween 20

TGF-β1 – Transforming growth factor β1

TLR4 – Toll-like receptor 4

TNF-α – Tumor necrosis factor-α

TREM2 – Triggering receptor expressed on myeloid cells 2

TSG101 – Tumor susceptibility gene 101

TP53 – Tumor protein 53

VDR – Vitamin D receptor

VEGFR2 – Vascular endothelial growth factor 2

Copyright Authorization

Chapter IV: This manuscript was published in the journal *Frontiers in Physiology.*

Title: **The role of exercise and high fat diet-induced bone marrow extracellular vesicles in stress hematopoiesis**

Authors: James J. Vanhie, Wooseok Kim, Lisa Ek Orloff, Matthew Ngu, Nicolas Collao, and Michael De Lisio

DOI: https://doi.org/10.3389/fphys.2022.1054463

Chapter V: This manuscript was submitted to the journal *Medicine and Science in Sports and Exercise*

Title: **High fat diets promote hematopoietic stem cell expansion and myeloid skewing during steady state hematopoiesis**

Assigned Paper A#: MSSE-D-24-00242

Chapter VI: This manuscript was submitted to the journal *Medicine and Science in Sports and Exercise*

Title: **Obesity promotes marrow-derived myeloid cell accumulation while exercise reduces proliferative signaling in colon cancer**

Assigned Paper #: MSSE-D-24-00410

Schematic figures were created with Biorender.com under an institutional annual subscription: De Lisio Lab, University of Ottawa.

Funding Sources

James Vanhie was supported by the University of Ottawa Admission Scholarship, Ontario Graduate Scholarship, and the University of Ottawa/Children's Hospital of Eastern Ontario Research Institute's Doctoral Fellowship for Advancement of Biological Perspectives for Exercise Interventions Across the Lifespan.

Chapter I: Literature Review – Exercise, Obesity, Hematopoiesis, and the Bone Marrow Microenvironment

How does lifestyle affect hematopoiesis and the bone marrow microenvironment?

James J. Vanhie[1] and Michael De Lisio[1]

[1]University of Ottawa, Ottawa, Ontario, Canada

Keywords: exercise, physical activity, obesity, hematopoiesis, myelopoiesis, extracellular vesicles

Toxicologic Pathology

2022 Oct; 50(7): 858-866

DOI: https://doi.org/10.1177/01926233221123523

Contribution: James J. Vanhie drafted and edited the manuscript and figures.

***Correspondence to:**
Michael De Lisio, PhD
Roger Guindon Hall, University of Ottawa
Phone: +1 613-562-5800 ext. 6987
Email: mdelisio@uottawa.ca

Abstract

Lifestyle factors are modifiable behavioural factors that have a significant impact on health and longevity. Diet-induced obesity and physical activity/exercise are two prevalent lifestyle factors that have strong relationships to overall health. The mechanisms linking obesity to negative health outcomes, and the mechanisms linking increased participation in physical activity/exercise to positive health outcomes are beginning to be elucidated. Chronic inflammation, due in part to overproduction of myeloid cells from hematopoietic stem cells (HSCs) in the bone marrow, is an established mechanism responsible for the negative health effects of obesity. Recent work has shown that exercise training can reverse the aberrant myelopoiesis present in obesity in part by restoring the bone marrow microenvironment. Specifically, exercise training reduces marrow adipose tissue, increases HSC retention factor expression, and reduces pro-inflammatory cytokine levels in the bone marrow. Other, novel mechanistic factors responsible for these exercise-induced effects, including intercellular communication via extracellular vesicles (EVs), is beginning to be explored. This review will summarize the recent literature describing the effects of exercise on hematopoiesis in individuals with obesity and introduce the potential contribution of EVs to this process.

Introduction

Acute stresses are typically consequent to foreign body intrusion (e.g., puncture wounds), internal injury (e.g., muscle strain), or by infection (e.g., bacterial or viral). However, diet-induced obesity induces a chronic, low-grade, systemic inflammatory condition. This chronic inflammatory state has wide-reaching consequences with long-term health effects including an increased risk of developing high blood pressure, heart disease, type 2 diabetes, and many cancers. Immune cells are composed of white blood cells that originate from the bone marrow. Inflammatory cells of the innate immune system include monocytes, macrophages, and granulocytes. These cells are a part of the myeloid cell lineage which is one of two lineages that develop from rare, primitive hematopoietic stem cells (HSCs). HSCs are located in the bone marrow and are responsible for the formation of all blood cells, a process termed hematopoiesis. HSCs proliferate and differentiate when subject to stressed conditions to replenish the blood system. Under chronic inflammatory conditions HSCs proliferate and differentiate more quickly than they would during steady-state conditions. This leads to pre-emptive HSC pool exhaustion and myeloid-skewed hematopoiesis (i.e., myelopoiesis), resulting in the overproduction of inflammatory cells[1–3].

While obesity induces a chronic inflammatory condition that promotes myeloid cell development, exercise promotes opposing effects. Previous work from our lab showed that exercise reduces myelopoiesis within a high-fat diet-induced (HFD) obesity mouse model, where peripheral monocyte populations decreased[4–7]. These effects were seen independent of weight loss, suggesting the effects were specific to exercise. Obesity and exercise also have opposing impacts on the bone marrow environment. Obesity promotes marrow adipose tissue formation

that physically replaces the space available for red marrow, where hematopoiesis occurs[5]. Adipocytes also secrete pro-inflammatory cytokines including tumour necrosis factor-α (TNF-α), interleukin-6 (IL-6), and free fatty acids, thereby promoting HSC differentiation into myeloid cells[8]. Exercise can reverse these effects by offsetting leptin signaling in the marrow and promoting HSC quiescence factor signaling through leptin receptor-positive mesenchymal stromal cells[9].

The opposing effects obesity and exercise impart on the bone marrow environment are consequent to altered intra- and intercellular signaling. Most of the literature to date has focused on the role of soluble proteins (i.e., cytokines, growth factors, and neurotransmitters) as the language for intercellular communication in the bone marrow[5]. While important insights have been derived from these studies, the role of other mediators of intercellular communication, such as extracellular vesicles (EVs), have received relatively less attention. EVs are small, membrane-bound nanoparticles (<1000 nm) that often contain cell-specific cargo, including proteins and microRNAs (miRNAs). When irradiated mouse donor EVs are injected into healthy mice subsequent sample analysis shows hematopoietic injury similar to those seen in the irradiated mice[10]. Similarly, EV injection from healthy donor mice into irradiated mice promotes hematopoietic recovery[11]. Further, an emerging body of literature has described the EV response to acute exercise and exercise training with these studies implicating exercise-induced EVs as potential mediators of the systemic effects of exercise[12]. These data demonstrate a role for EVs in impacting HSC activity; however, the role of exercise-induced EVs in regulating hematopoiesis has not been previously explored. The purpose of this review is to provide an updated overview of the current literature describing the role of obesity and exercise on hematopoiesis and the

bone marrow microenvironment and introduce exercise-induced EVs as novel potential mediators of these effects.

Obesity and Systemic Inflammation

Obesogenic conditions promote systemic inflammation that persists in a chronic, low-grade fashion. During chronic caloric excess, adipocytes respond by undergoing hypertrophy and hyperplasia[13]. Lowered vascular density surrounding the enlarged adipocytes can eventually lead to hypoxia and increased inflammatory cytokine release (i.e., IL-6 and TNF-α)[14,15]. In response to the inflammatory environment, circulating monocytes enter the tissue and differentiate into macrophages via C-C chemokine ligand type 2 (CCL2) chemokine interactions with its receptor, CCR2, on the monocyte cell surface[16,17]. Of these macrophages, pro-inflammatory macrophages (M1) propagate the inflammatory condition through IL-6 and TNF-α cytokine release[18,19]. Together, adipocyte and M1 macrophage cytokine release promote a positive feedback loop[20,21]. Interestingly, adipose tissue in lean individuals contains a greater proportion of anti-inflammatory macrophages (M2) that act as a mediator for resolving inflammation[22]. Nevertheless, the chronic low-grade inflammatory state seen in obesity has far-reaching effects on multiple organ systems, where TNF-α and IL-6 impact nuclear factor kappa B (NF-κB) and Janus kinase-signal transducer and activator of transcription proteins (JAK-STAT) signaling[23,24]. Chronic inflammation characterized by both an upregulation of pro-inflammatory cytokines and overproduction of myeloid lineage cells, including macrophages, termed myelopoiesis has detrimental effects on several tissues that contribute to the long-term health effects of obesity.

Bone Marrow – The Home for Hematopoiesis

All erythrocytes, leukocytes, and thrombocytes originate from a select set of cells termed hematopoietic stem cells (HSCs). The majority of these cells reside in the bone marrow and represent the most primitive cells in the hematopoietic hierarchy[25–28]. HSCs were originally discovered by Ernest McCullogh and James Till in 1961 by their unique capability to self-renew and produce pluripotent progenitors[29,30]. They make up a rare cell population, accounting for approximately 1 in every 10,000 bone marrow cells[30,31].

As a foundational cell for the entire blood system, maintenance of HSC genetic and functional integrity is critical for proper immune system health. Consequently, HSCs largely remain quiescent, with less than 5% activated at a given time[32]. Cell population maintenance occurs through the asymmetric division of HSCs, with the division rate occurring once per year up to a rate of once every three months[32]. This asymmetric division gives rise to HSC subpopulations, including long-term HSCs (LT-HSCs) that give rise to short-term HSCs (ST-HSCs), which further differentiate into multi-potent progenitor cells (MPPs)[33]. Of the HSC subpopulations, LT-HSCs have the greatest self-renewal capacity, and the MPPs the lowest. Conversely, LT-HSCs contain the lowest proliferative capacity and MPPs the highest. HSCs can be identified through specific cell surface markers. In mice, HSCs can be identified through the presence or absence of the lineage, Sca-1, and c-kit (LSK) surface markers. LT-HSCs, ST-HSCs, and MPPs can be individually identified by the signaling lymphocytic activation molecule (SLAM) markers cluster of differentiation 48 (CD48), CD150, CD229, and CD244[28]. The interplay between these cell populations underlies the importance of hematopoietic maintenance throughout the

lifespan, leading to complex bone marrow organisation, where distinct locations for each cell type can be found[34,35].

MPPs are set in a juxtaposition for differentiation into either the myeloid or lymphoid lineages. Myeloid cells form most blood cell populations, including erythrocytes, megakaryocytes, dendritic cells, and cells that form the innate immune system (granulocytes, monocytes, and macrophages). Lymphoid cells are responsible for adaptive immunity, whose cells include T lymphocytes, B lymphocytes, and natural killer (NK) cells.

Bone Marrow – Regulation of Hematopoiesis by the Hematopoietic Stem Cell Niche

Hematopoiesis is impacted by the local tissue microenvironment in the bone marrow, termed the HSC niche, where all components required for HSC function and regulation are located[36]. The HSC niche is a highly complex organisation of many cell populations that work together to give rise to all mature blood cells. These other cell groups include, but are not limited to, mesenchymal stem cells (MSCs), osteoblasts, adipocytes, endothelial cells, and mature hematopoietic cells. With respect to hematopoiesis, two distinct HSC niches have been described: the arteriolar and sinusoidal regions. Quiescent HSCs are found in close proximity to arterioles while less-quiescent HSCs are found close to sinusoids[37,38].

Common secreted factors affecting the HSC pool involve complex interplay between C-X-C motif chemokine ligand 4 (CXCL4), CXCL12, transforming growth factor beta 1 (TGF-β1), and stem cell factor (SCF)[38–41]. MSCs, like HSCs, are relatively rare cells capable of self-renewal and differentiation into chondrocytes, adipocytes, and osteoblasts[42–44]. They are located in the vicinity of arterioles and sinusoids[38,45–47] and can be identified as nestin^{+}, CXCL12-abundant reticular (CAR), platelet-derived growth factor receptor-α (PDGFR-α), and leptin receptor (LEPR^{+})

cells[48,49]. The importance of these cells in HSC maintenance was shown through the ablation of CXCL12^{+} bone marrow cells in mice, which led to HSC pool and osteogenic cell reductions[50,51]. Osteoblasts were once thought to play a direct role in hematopoietic control, but recent developments suggest their role may be indirect[52,53]. Unlike osteoblasts, adipocytes appear to directly affect HSC regulation. Adipocytes are derived mainly from LEPR^{+} cells and can alter the HSC niche by producing marrow adipose tissue[54]. Throughout life, progressive marrow adipose tissue accumulation has a demonstrated effect on lowering hematopoietic activity and bone regeneration[55–57]. Marrow adipose tissue accumulation negatively affects hematopoiesis through physical replacement of red marrow, thereby decreasing the space available for hematopoiesis[55]. Adipocytes also promote premature HSC exhaustion through pro-inflammatory cytokine secretion, including TNF-α, IL-6, and free fatty acids[8,58,59].

Mature leukocytes also influence HSC activity. Macrophages can regulate MSC CXCL12 expression via liver X receptor (LXR) when clearing aged neutrophils within the bone marrow, thereby promoting HSC retention[60]. Neutrophils affect osteogenic cells via prostaglandin E2 to reduce HSC release from the marrow into the circulation[61]. Lymphocytes are widely distributed within the HSC niche and appear to play several roles in HSC maintenance[62]. Natural killer cells may play an inhibitory role in HSC differentiation via NK cell-derived colony-inhibiting activity soluble factor[63]. CD4^{+} regulatory T cell deletion similarly depresses HSC myeloid differentiation in addition to reduced HSC colony growth[64]. However, regulatory T cells may also provide a protective effect on HSC survival through IL-10[65–67]. Finally, endothelial cells surrounding sinusoids play a pivotal role in HSC maintenance, as Butler and colleagues (2010) found an expansion of the HSC pool following the disruption of vascular endothelial growth factor 2

(VEGFR2) and vascular endothelial (VE)-cadherin-dependent angiogenic signaling both *in vivo* and *in vitro* via notch signaling[68]. Coculture experiments have further demonstrated a promotional effect of arteriolar and sinusoidal endothelial cells on HSC maintenance, with arteriolar endothelial cells being the major producer of SCF[69]. Altogether, the HSC niche undergoes complex cell intercommunication to control HSC production and differentiation. Exercise and obesity impact this cell communication to induce downstream changes in myeloid and lymphoid cell production, and by extension, alterations to systemic inflammatory responses.

Bone Marrow – Obesity and Exercise's Effects on Bone Marrow Structure and Hematopoietic Stem Cell Function

Chronic inflammation, as seen in obesity, has a demonstrated role in affecting hematopoiesis, the HSC niche, and circulating blood cell populations, while exercise opposes these effects (Figure 1.1)[5]. Chronic inflammatory conditions are linked to marrow adipose tissue accumulation and elevated circulating leukocyte content in humans[2]. Under obesogenic conditions, these leukocytes are predominantly myeloid in origin[3]. The observed alterations to blood cell populations are consequent to upregulated HSC proliferation that can lead to HSC pool exhaustion and myeloid cell overproduction[6,70]. In mice, myeloid skewing has been documented to occur at as early as 6 weeks following a HFD regimen[71]. Within the bone marrow, obesity promotes the inflammatory state[72]. Even following subsequent weight loss the chronic inflammatory state placed on the HSC niche leads to the accumulation of myeloid progenitors and LT- and ST-HSC depletion[4,73,74]. However, exercise mitigates these alterations in HSC activity.

Circulating HSC concentrations have a noted increase following acute and endurance exercise training in mice[75–77]. These elevations have also been observed in healthy, well-trained humans

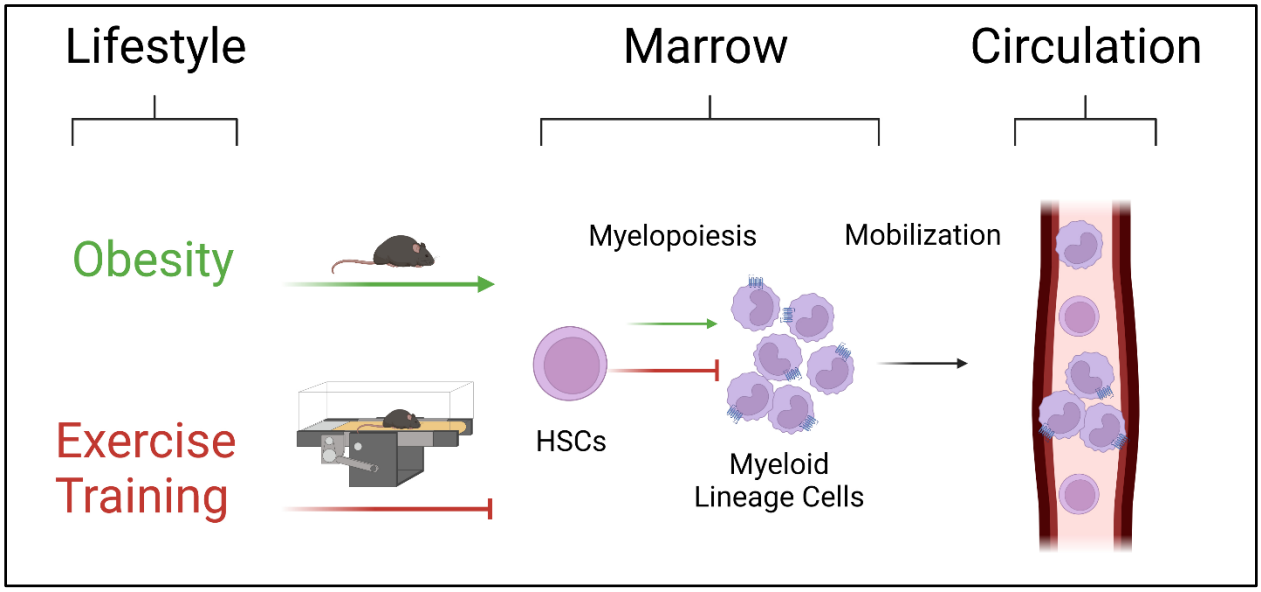

Figure 1.1. Exercise training reverses aberrant myelopoiesis in obesity. In obesity, hematopoietic stem cell (HSC) differentiation skews toward myelopoiesis, resulting in an overproduction of pro-inflammatory myeloid lineage cells in circulation and HSC exhaustion. Exercise reverses these effects by promoting HSC maintenance and inhibiting aberrant myelopoiesis. Green lines indicate the effects of obesity and red lines indicate the effects of exercise. Figure created with BioRender.com.

following an acute exercise bout[78]. In mice, treadmill exercise increases bone marrow HSC proportion in healthy mice[79], while exposing mice to voluntary wheel running did no change in bone marrow HSC frequency in healthy mice[9]. Discrepant findings in healthy mice may be due to the exercise model used. Although voluntary wheel running is generally considered less stressful, increases in stress hormones have been observed[80]. Further, given that mice provided with a running wheel will run 8-15 km/day[9] while treadmill exercise allows for a translatable dose of exercise to be administered, the treadmill exercise intervention is more relevant to human populations. In disease models, atherosclerotic mice exposed to a running wheel have reduced HSC frequency[9]. Similarly, in adults with obesity, exercise training reduces the content of

inflammatory primed-HSCs in circulation[81]. Further, exercise training in previously obese mice who had undergone weight loss and were at increased risk of carcinogenesis restored the HSC frequency to levels in never obese mice[4]. Thus, the effects of exercise appear to be dependent on exercise dose and model in healthy conditions and to reduce aberrant HSC expansion in disease.

Functionally, Baker and colleagues (2011) reported increased HSC colony forming unit capacity with exercise training[82]. *In vivo*, exercise training does not reduce HSC activity in a transplantation assay[79] but improves hematopoietic recovery in stress hematopoiesis[7] and in response to infection[9,83]. Importantly, this increased hematopoietic activity in exercise trained mice in the context of stress hematopoiesis does not appear to result in increased risk of hematological malignancies; however, the risk of hematological malignancies is increased in experimental models of obesity[84]. With respect to HSC fate decisions, exercise training induces a notable decrease in HSC myeloid-skewing under obesogenic conditions[4] and an increase in lymphopoiesis[83]. Collectively, these results suggest that regardless of the effects of exercise training on HSC content, exercise training improves the functional capacity of HSCs to respond to hematopoietic stress and may restore HSC lineage commitment to reverse the inflammatory phenotype in obesity.

New technologies have allowed for dissection of molecular alterations induced by exercise that may explain the effects of exercise training on hematopoiesis at the single cell level. Using single cell RNA-sequencing, Liu and colleagues characterized molecular changes in bone marrow following 5-weeks of voluntary wheel running[85]. The authors found that HSCs had the fewest number of differentially expressed genes in response to wheel running while mature

monocytes had the greatest number and that this effect was diminished in aged animals[85]. Interestingly, a separate study, also using 4-weeks of wheel running as their exercise model, observed an increase in common lymphoid progenitors in aged animals with no effect on HSCs or other hematopoietic progenitor cell subsets[86]. Perhaps unsurprisingly, pathways involved in oxidative phosphorylation were among the most upregulated by exercise, while cytokine signaling pathways were among the most downregulated[85]. These findings aligned with cellular analyses which indicated that exercise directs immune cell composition towards an anti-inflammatory profile[85]. Combined, these findings led the authors to conclude that wheel running led to anti-inflammatory adaptations in hematopoietic cells[85].

Within the HSC niche, chronic elevations of IL-6 and TNF-α in obesity promote MSC differentiation away from the osteogenic lineage and toward the adipogenic lineage, thereby enhancing marrow adipose tissue formation[87–89]. In a TNF-α knockout mouse model there was an increase in bone density and a reduction in marrow adipose tissue despite being on a long-term HFD regimen[88,89]. There was also a decrease in bone density and a tendency towards adipogenic differentiation of MSCs with elevated monocyte chemoattractant protein-1 (MCP-1) content, an inflammatory chemokine that is elevated in obesity[90,91]. Combined, these results suggest a strong relationship between the content of pro-inflammatory markers and detrimental effects on homeostasis in individuals with obesity. Exercise, however, increases bone mineral density and decreases marrow adipose tissue formation, even in conditions where peroxisome proliferator-activated receptor gamma (PPARγ) agonists are provided to promote marrow adipose tissue formation[6]. Exercise decreases TNF-α and IL-1β signaling in the bone marrow, which may be responsible for mitigated marrow adipose tissue formation and increased bone

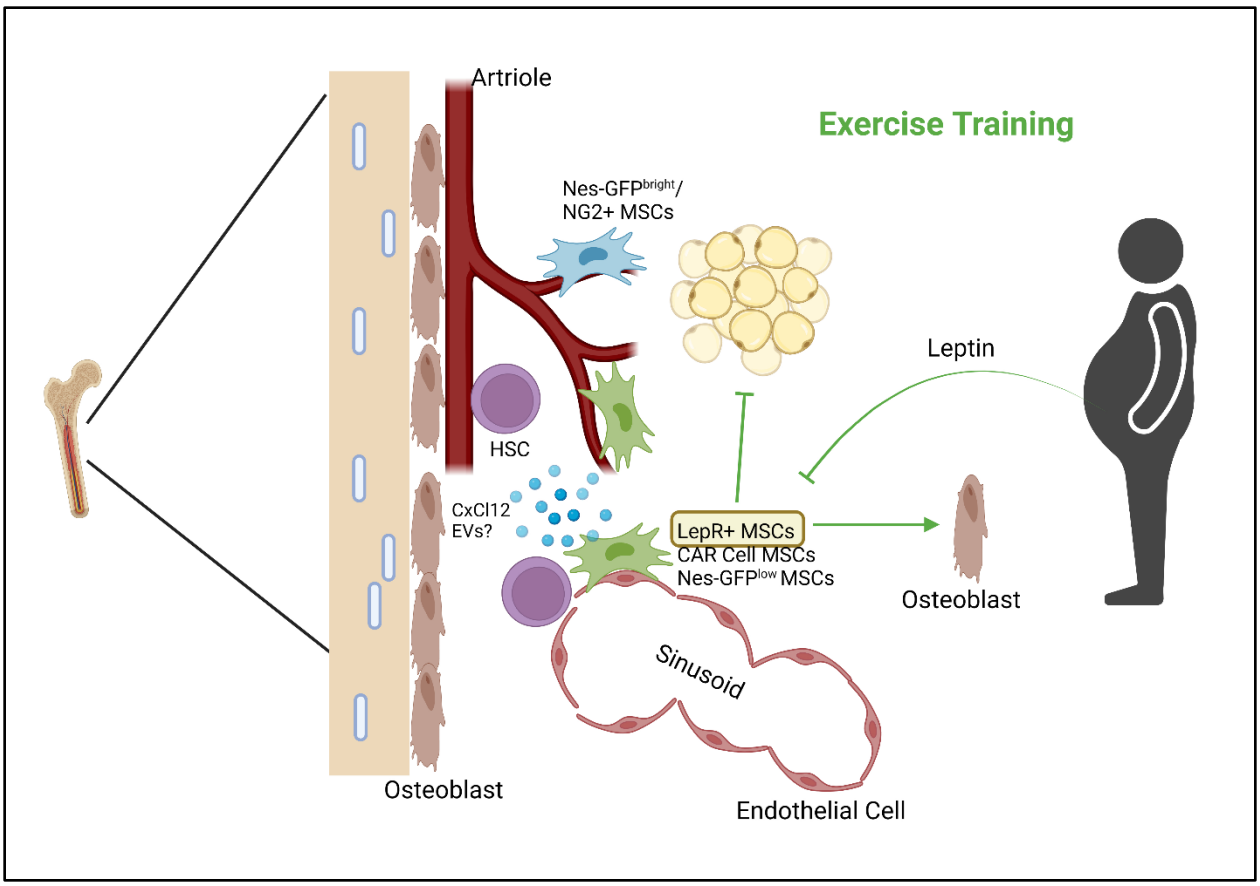

Figure 1.2. Exercise training remodels the HSC niche. Exercise training reduces marrow adipose tissue and stimulates osteogenic differentiation of MSCs. Furthermore, exercise training promotes the expression and release of HSC retention factors (i.e., CxCl12), specifically from LepR+ MSCs, and reduces leptin production from peripheral adipose tissue. A relatively unexplored mechanism of the effects of exercise involves the release of EVs from other sources that contribute to the restoration of hematopoiesis in obesity. Green lines indicate the effects of exercise training. Figure created with BioRender.com. CxCl12, C-X-C motif chemokine ligand; EV, extracellular vesicle; LepR+, leptin receptor-positive; MSC, mesenchymal stem cell.

density compared to sedentary obesogenic conditions[23]. In addition, exercise preconditioning of the HSC niche prior to bone marrow transplantation accelerates hematopoietic recovery in mice[92] and perhaps also in humans[93]. These effects are due, in part, to preservation of the HSC niche (Figure 1.2)[92,94].

Several groups have investigated the effects of exercise training on the HSC niche. It has been well-established that exercise training reduces marrow adipose tissue content[4,6,7]. These effects can be traced back to exercise-induced alterations in cell fate decisions of bone marrow-MSCs that favour osteogenic over adipogenic differentiation[6,82]. Bone marrow-MSCs proliferate in response to acute exercise[75] and recent work has demonstrated that chronic wheel running increased the content of osteoprogenitors in the bone marrow of aged mice while unloading reduced their content[86]. Further, chronic wheel running increases the expression of *Cxcl12* in $LepR^{+}$ bone marrow MSCs via reducing leptin release from adipocytes[9]. Recently, Peng and colleagues used a 5-week treadmill exercise intervention to determine that exercise training increased osteoblast and common lymphoid progenitor cell content[83]. Mechanistically, mechanical stimulation induced by running resulted in reticulocalbin-2 (RCN2) release from bone marrow macrophages that stimulated fatty acid release from marrow adipocytes that fueled osteogenic and lymphopoietic fate decisions by mesenchymal stromal cells and HSCs respectively[83]. Collectively, these reports suggest cells within the marrow alter their communication in response to obesity- and exercise-induced stressors. A full understanding of mediators of this cell communication within the bone with obesity and exercise, however, is lacking.

Extracellular Vesicles – An Overview

First discovered in 1946, EVs were initially thought of as pro-coagulant particles due to their release from platelets[95]. EVs are now appreciated to be membrane-bound particles released by cells for intercellular communication and waste[96,97]. The term “EV” is an umbrella term for membrane-bound particles that are most commonly referred to as exosomes and microvesicles,

among other less-commonly used names[97–100]. Exosomes are small EVs that form within multivesicular endosomes while microvesicles are larger than exosomes and are a product of direct budding of the cell membrane. To address inconsistent nomenclature in the literature, a group of EV experts formed the International Society for Extracellular Vesicles (ISEV) along with an all-encompassing document in 2014 titled *Minimal Information for Studies of Extracellular Vesicles 2014* (MISEV2014), which outlined rationale for EV isolation recommendations and established standards that should be met for a sound study design[101]. These recommendations were updated and refined in 2018[99].

Challenges remain in identifying EVs from other particles due to unknown surface marker characteristics[102,103]. Defining EV presence in a solution has therefore been commonly attributed to particle size and ubiquitous protein expression. The first step in identifying EV presence is to isolate them from a tissue sample. When choosing an EV isolation method, important considerations must be made regarding recovery capabilities, sample purity, volume, and protocol duration[104]. Four isolation methods are typically used: ultracentrifugation, immunoaffinity capture, ultrafiltration, and precipitation, each with their own drawbacks and advantages[104,105]. Once isolated, EVs can be identified by high-resolution flow cytometry, nanoparticle tracking analysis, transmission electron microscopy, and western blot. Cargo can be analysed by transcriptomics and proteomics techniques[106].

Extracellular Vesicles – Vehicles for Cell-Cell Communication in the Bone Marrow

EV release from cells is a highly conserved cell-cell communication method that is present in all cells of the body[107]. Wen and colleagues (2016) examined the role of bone marrow-derived EVs on irradiated hematopoietic cell injury recovery *in vitro*[11]. Specifically, exosomes,

microvesicles, and their combination were introduced to murine HSCs following irradiation. The microvesicle-exosome collection showed a 6-fold increase in cell proliferation compared to the vehicle control, suggesting a positive role for EVs in radiation injury hematopoietic recovery[11]. When observed individually, exosomes doubled cell proliferation compared to control while microvesicles quadrupled cell proliferation compared to control[11]. These results suggest microvesicles substantially facilitate hematopoietic cell recovery from injury while exosomes have a relatively minor effect on recovery. Despite these findings, discriminating possible differences between exosome and microvesicle-driven influences in cell activity across the literature remains a challenge due to nomenclature inconsistencies. However, growing evidence suggests EVs can invoke HSC activity alterations which may be useful for understanding disease development and creating therapeutic options[107–109].

Studies are continually finding that EVs carry cell-specific contents originating from the source cell, which may be used to understand the influence of specific cell populations on their surroundings[110,111]. These findings extend to pathological or healthy cells[112,113]. For example, Haraszti and colleagues (2016) examined the surface content and cargo of exosomes and microvesicles of U87 glioblastoma cells, Huh7 hepatocellular carcinoma cells, and healthy human bone marrow-derived MSCs[110]. They found similar proteomes in U87- and Huh7-derived EVs, while healthy MSC cell-derived EV proteomes were significantly different, suggesting cells curate their cargo based on internal cues[110]. The ability for EVs to bind and release cargo into a target cell is dependent upon surface adhesion protein expression on both the EVs and the target cells. Understanding the interplay between pathological cell EV release, target cell adhesion and

uptake, and target cell activity alterations will provide great insight in mitigating or halting negative effects.

Within the context of exercise, EV cargo and release from skeletal muscle has been primarily studied with little information available for other tissues. In general, exercise alters circulating blood EV content. For example, Whitham and colleagues (2018) showed a single 1 hour cycling exercise bout altered circulating EV protein content and increased total circulating EV count[114], thereby corroborating the findings of others[115]. In muscle-derived EVs there have been notable alterations to EV cargo in response to exercise. For example, miR-486 is downregulated in muscle-derived EVs following an acute bout of exercise[116]. miR-486 has been linked to promoting erythroid cell differentiation, indicating a potential role for exercise-induced EV signaling in impacting distant hematopoietic cells[117]. Furthermore, downregulated miRNA linked to inhibited mesenchymal stromal cell osteogenic differentiation has been observed in circulating blood of rats following exercise[118,119] suggesting that exercise-induced EVs may alter the HSC niche. Collectively, these data suggest exercise alters EV cargo in a manner that can impact cell activity of distant tissues. However, the impacts of exercise on bone marrow-derived EV release and cargo, and their role in hematopoiesis have not been directly investigated.

Conclusions and Future Directions

Obesity and exercise have opposing effects on hematopoiesis and the bone marrow microenvironment that contributes to their divergent effects on health. Obesity skews hematopoiesis to favour myelopoiesis, increases marrow adipose tissue, creates a pro-inflammatory HSC niche, and impairs HSC regenerative potential, while these effects are generally reversed by exercise. However, the effects of exercise training on the HSC niche do not

appear to be durable, suggesting that consistent participation in exercise training interventions is necessary. The role of other signaling factors as regulators of hematopoiesis, including but not limited to EVs and their cargo, are beginning to be appreciated; however, their role in regulating hematopoiesis in the context of obesity and exercise remains understudied. Further, the exercise prescription that can be translated to humans which induces the beneficial effects of exercise on bone marrow remodeling in obesity remains unknown. Making progress towards these two key gaps in literature will improve both our understanding as well as application of exercise training in the context of obesity-associated pathologies.

Author Contribution

Authors contributed to conception of the topic of this review (MD); and writing and editing the manuscript (MD, JV). All authors gave final approval and agree to be accountable for all aspects of work in ensuring that questions relating to the accuracy or integrity of any part of the work are appropriately investigated and resolved.

Declaration of Conflicting Interests

The author(s) declared no potential conflicts of interest with respect to the research, authorship, and/or publication of this article.

Funding

The author(s) disclosed receipt of the following financial support for the research, authorship, and/or publication of this article: Funds were provided by the National Sciences and Engineering Council (NSERC) and the American Institute for Cancer Research (AICR) to Michael De Lisio. James J. Vanhie received support from the uOttawa/CHEO-RI Doctoral Fellowship and an Ontario Graduate Scholarship.

References

1. Niemiro GM, Raine LB, Khan NA, et al. Circulating progenitor cells are positively associated with cognitive function among overweight/obese children. *Brain Behav Immun*. 2016;57:47-52. doi:10.1016/j.bbi.2016.03.018

2. Trottier MD, Naaz A, Li Y, Fraker PJ. Enhancement of hematopoiesis and lymphopoiesis in diet-induced obese mice. *Proc Natl Acad Sci*. 2012;109(20):7622-7629. doi:10.1073/pnas.1205129109

3. Singer K, DelProposto J, Lee Morris D, et al. Diet-induced obesity promotes myelopoiesis in hematopoietic stem cells. *Mol Metab*. 2014;3(6):664-675. doi:10.1016/j.molmet.2014.06.005

4. Emmons R, Xu G, Hernández-Saavedra D, et al. Effects of obesity and exercise on colon cancer induction and hematopoiesis in mice. *Am J Physiol-Endocrinol Metab*. 2018;316(2):E210-E220. doi:10.1152/ajpendo.00237.2018

5. Emmons R, Niemiro GM, De Lisio M. Hematopoiesis with obesity and exercise: Role of the bone marrow niche. *Exerc Immunol Rev*. 2017;23:82-95.

6. Styner M, Thompson WR, Galior K, et al. Bone marrow fat accumulation accelerated by high fat diet is suppressed by exercise. *Bone*. 2014;64:39-46. doi:10.1016/j.bone.2014.03.044

7. Emmons R, Ngu M, Xu G, Hernández-Saavedra D, Chen H, De Lisio M. Effects of obesity and exercise on bone marrow progenitor cells after radiation. *Med Sci Sports Exerc*. 2019;51(6):1126-1136. doi:10.1249/MSS.0000000000001894

8. Halade GV, Rahman MM, Williams PJ, Fernandes G. High fat diet-induced animal model of age-associated obesity and osteoporosis. *J Nutr Biochem*. 2010;21(12):1162-1169. doi:10.1016/j.jnutbio.2009.10.002

9. Frodermann V, Rohde D, Courties G, et al. Exercise reduces inflammatory cell production and cardiovascular inflammation via instruction of hematopoietic progenitor cells. *Nat Med*. 2019;25:1761-1771. doi:10.1038/s41591-019-0633-x

10. Szatmári T, Kis D, Bogdándi EN, et al. Extracellular Vesicles Mediate Radiation-Induced Systemic Bystander Signals in the Bone Marrow and Spleen. *Front Immunol*. 2017;8. doi:10.3389/fimmu.2017.00347

11. Wen S, Dooner M, Cheng Y, et al. Mesenchymal stromal cell-derived extracellular vesicles rescue radiation damage to murine marrow hematopoietic cells. *Leukemia*. 2016;30(11):2221-2231. doi:10.1038/leu.2016.107

12. Nederveen JP, Warnier G, Di Carlo A, Nilsson MI, Tarnopolsky MA. Extracellular Vesicles and Exosomes: Insights From Exercise Science. *Front Physiol*. 2020;11:604274. doi:10.3389/fphys.2020.604274

13. Halberg N, Wernstedt-Asterholm I, Scherer PE. The Adipocyte as an Endocrine Cell. *Endocrinol Metab Clin North Am*. 2008;37(3):753-768. doi:10.1016/j.ecl.2008.07.002

14. Cinti S, Mitchell G, Barbatelli G, et al. Adipocyte death defines macrophage localization and function in adipose tissue of obese mice and humans. *J Lipid Res*. 2005;46(11):2347-2355. doi:10.1194/jlr.M500294-JLR200

15. Trayhurn P, Wood IS. Adipokines: inflammation and the pleiotropic role of white adipose tissue. *Br J Nutr*. 2004;92(3):347-355. doi:10.1079/BJN20041213

16. Italiani P, Boraschi D. From Monocytes to M1/M2 Macrophages: Phenotypical vs. Functional Differentiation. *Front Immunol*. 2014;5. doi:10.3389/fimmu.2014.00514

17. Fujimura N, Xu B, Dalman J, Deng H, Aoyama K, Dalman RL. CCR2 inhibition sequesters multiple subsets of leukocytes in the bone marrow. *Sci Rep*. 2015;5(1):11664. doi:10.1038/srep11664

18. Murano I, Barbatelli G, Parisani V, et al. Dead adipocytes, detected as crown-like structures, are prevalent in visceral fat depots of genetically obese mice. *J Lipid Res*. 2008;49(7):1562-1568. doi:10.1194/jlr.M800019-JLR200

19. Revelo XS, Luck H, Winer S, Winer DA. Morphological and Inflammatory Changes in Visceral Adipose Tissue During Obesity. *Endocr Pathol*. 2014;25(1):93-101. doi:10.1007/s12022-013-9288-1

20. Weisberg SP, McCann D, Desai M, Rosenbaum M, Leibel RL, Ferrante AW. Obesity is associated with macrophage accumulation in adipose tissue. *J Clin Invest*. 2003;112(12):1796-1808. doi:10.1172/JCI200319246

21. Hotamisligil GS, Shargill NS, Spiegelman BM. Adipose Expression of Tumor Necrosis Factor-α: Direct Role in Obesity-Linked Insulin Resistance. *Science*. 1993;259(5091):87-91. doi:10.1126/science.7678183

22. Lauterbach MAR, Wunderlich FT. Macrophage function in obesity-induced inflammation and insulin resistance. *Pflüg Arch - Eur J Physiol*. 2017;469(3-4):385-396. doi:10.1007/s00424-017-1955-5

23. Kern L, Mittenbühler M, Vesting A, Ostermann A, Wunderlich C, Wunderlich F. Obesity-Induced TNFα and IL-6 Signaling: The Missing Link between Obesity and Inflammation—Driven Liver and Colorectal Cancers. *Cancers*. 2018;11(1):24. doi:10.3390/cancers11010024

24. Jais A, Brüning JC. Hypothalamic inflammation in obesity and metabolic disease. *J Clin Invest*. 2017;127(1):24-32. doi:10.1172/JCI88878

25. Gazit R, Weissman IL, Rossi DJ. Hematopoietic Stem Cells and the Aging Hematopoietic System. *Semin Hematol*. 2008;45(4):218-224. doi:10.1053/j.seminhematol.2008.07.010

26. Seita J, Weissman IL. Hematopoietic stem cell: self-renewal versus differentiation: Hematopoietic stem cell. *Wiley Interdiscip Rev Syst Biol Med*. 2010;2(6):640-653. doi:10.1002/wsbm.86

27. Pang WW, Price EA, Sahoo D, et al. Human bone marrow hematopoietic stem cells are increased in frequency and myeloid-biased with age. *Proc Natl Acad Sci*. 2011;108(50):20012-20017. doi:10.1073/pnas.1116110108

28. Oguro H, Ding L, Morrison SJ. SLAM Family Markers Resolve Functionally Distinct Subpopulations of Hematopoietic Stem Cells and Multipotent Progenitors. *Cell Stem Cell*. 2013;13(1):102-116. doi:10.1016/j.stem.2013.05.014

29. Siminovitch L, McCulloch EA, Till JE. The distribution of colony-forming cells among spleen colonies. *J Cell Comp Physiol*. 1963;62(3):327-336. doi:10.1002/jcp.1030620313

30. Till JE, McCulloch EA. A Direct Measurement of the Radiation Sensitivity of Normal Mouse Bone Marrow Cells [1]. *Radiat Res*. 2011;175(2):145-149. doi:10.1667/RRXX28.1

31. Spangrude G, Heimfeld S, Weissman I. Purification and characterization of mouse hematopoietic stem cells. *Science*. 1988;241(4861):58-62. doi:10.1126/science.2898810

32. Catlin SN, Busque L, Gale RE, Guttorp P, Abkowitz JL. The replication rate of human hematopoietic stem cells in vivo. *Blood*. 2011;117(17):4460-4466. doi:10.1182/blood-2010-08-303537

33. Yamamoto R, Morita Y, Ooehara J, et al. Clonal Analysis Unveils Self-Renewing Lineage-Restricted Progenitors Generated Directly from Hematopoietic Stem Cells. *Cell*. 2013;154(5):1112-1126. doi:10.1016/j.cell.2013.08.007

34. Kiel MJ, Yilmaz ÖH, Iwashita T, Yilmaz OH, Terhorst C, Morrison SJ. SLAM Family Receptors Distinguish Hematopoietic Stem and Progenitor Cells and Reveal Endothelial Niches for Stem Cells. *Cell*. 2005;121(7):1109-1121. doi:10.1016/j.cell.2005.05.026

35. Boulais PE, Frenette PS. Making sense of hematopoietic stem cell niches. *Blood*. 2015;125(17):2621-2629. doi:10.1182/blood-2014-09-570192

36. Morrison SJ, Spradling AC. Stem Cells and Niches: Mechanisms That Promote Stem Cell Maintenance throughout Life. *Cell*. 2008;132(4):598-611. doi:10.1016/j.cell.2008.01.038

37. Itkin T, Gur-Cohen S, Spencer JA, et al. Distinct bone marrow blood vessels differentially regulate haematopoiesis. *Nature*. 2016;532(7599):323-328. doi:10.1038/nature17624

38. Kunisaki Y, Bruns I, Scheiermann C, et al. Arteriolar niches maintain haematopoietic stem cell quiescence. *Nature*. 2013;502(7473):637-643. doi:10.1038/nature12612

39. Bruns I, Lucas D, Pinho S, et al. Megakaryocytes regulate hematopoietic stem cell quiescence through CXCL4 secretion. *Nat Med*. 2014;20(11):1315-1320. doi:10.1038/nm.3707

40. Yamazaki S, Ema H, Karlsson G, et al. Nonmyelinating Schwann Cells Maintain Hematopoietic Stem Cell Hibernation in the Bone Marrow Niche. *Cell*. 2011;147(5):1146-1158. doi:10.1016/j.cell.2011.09.053

41. Hérault A, Binnewies M, Leong S, et al. Myeloid progenitor cluster formation drives emergency and leukaemic myelopoiesis. *Nature*. 2017;544(7648):53-58. doi:10.1038/nature21693

42. Sacchetti B, Funari A, Michienzi S, et al. Self-Renewing Osteoprogenitors in Bone Marrow Sinusoids Can Organize a Hematopoietic Microenvironment. *Cell*. 2007;131(2):324-336. doi:10.1016/j.cell.2007.08.025

43. Chan CKF, Chen CC, Luppen CA, et al. Endochondral ossification is required for haematopoietic stem-cell niche formation. *Nature*. 2009;457(7228):490-494. doi:10.1038/nature07547

44. Frenette PS, Pinho S, Lucas D, Scheiermann C. Mesenchymal Stem Cell: Keystone of the Hematopoietic Stem Cell Niche and a Stepping-Stone for Regenerative Medicine. *Annu Rev Immunol*. 2013;31(1):285-316. doi:10.1146/annurev-immunol-032712-095919

45. Katayama Y, Battista M, Kao WM, et al. Signals from the Sympathetic Nervous System Regulate Hematopoietic Stem Cell Egress from Bone Marrow. *Cell*. 2006;124(2):407-421. doi:10.1016/j.cell.2005.10.041

46. Lucas D, Battista M, Shi PA, Isola L, Frenette PS. Mobilized Hematopoietic Stem Cell Yield Depends on Species-Specific Circadian Timing. *Cell Stem Cell*. 2008;3(4):364-366. doi:10.1016/j.stem.2008.09.004

47. Méndez-Ferrer S, Lucas D, Battista M, Frenette PS. Haematopoietic stem cell release is regulated by circadian oscillations. *Nature*. 2008;452(7186):442-447. doi:10.1038/nature06685

48. Birbrair A, Frenette PS. Niche heterogeneity in the bone marrow. *Ann N Y Acad Sci*. 2016;1370(1):82-96. doi:10.1111/nyas.13016

49. Pinho S, Frenette PS. Haematopoietic stem cell activity and interactions with the niche. *Nat Rev Mol Cell Biol*. 2019;20(5):303-320. doi:10.1038/s41580-019-0103-9

50. Marie P. Strontium as therapy for osteoporosis. *Curr Opin Pharmacol*. 2005;5(6):633-636. doi:10.1016/j.coph.2005.05.005

51. Roberts EW, Deonarine A, Jones JO, et al. Depletion of stromal cells expressing fibroblast activation protein-α from skeletal muscle and bone marrow results in cachexia and anemia. *J Exp Med*. 2013;210(6):1137-1151. doi:10.1084/jem.20122344

52. Calvi LM, Adams GB, Weibrecht KW, et al. Osteoblastic cells regulate the haematopoietic stem cell niche. *Nature*. 2003;425(6960):841-846. doi:10.1038/nature02040

53. Zhang J, Niu C, Ye L, et al. Identification of the haematopoietic stem cell niche and control of the niche size. *Nature*. 2003;425(6960):836-841. doi:10.1038/nature02041

54. Scheller EL, Troiano N, VanHoutan JN, et al. Use of Osmium Tetroxide Staining with Microcomputerized Tomography to Visualize and Quantify Bone Marrow Adipose Tissue In Vivo. In: *Methods in Enzymology*. Vol 537. Elsevier; 2014:123-139. doi:10.1016/B978-0-12-411619-1.00007-0

55. Ambrosi TH, Scialdone A, Graja A, et al. Adipocyte accumulation in the bone marrow during obesity and eging impairs stem cell-based hematopoietic and bone regeneration. *Cell Stem Cell*. 2017;20(6):771-784.e6. doi:10.1016/j.stem.2017.02.009

56. Kricun ME. Red-yellow marrow conversion: Its effect on the location of some solitary bone lesions. *Skeletal Radiol*. 1985;14(1):10-19. doi:10.1007/BF00361188

57. Naveiras O, Nardi V, Wenzel PL, Hauschka PV, Fahey F, Daley GQ. Bone-marrow adipocytes as negative regulators of the haematopoietic microenvironment. *Nature*. 2009;460(7252):259-263. doi:10.1038/nature08099

58. Aaron N, Costa S, Rosen C, Qiang L. The implications of bone marrow adipose tissue on inflammaging. *Front Endocrinol*. 2022;13:1-10. doi:10.3389/fendo.2022.853765

59. Hermetet F, Buffière A, Aznague A, et al. High-fat diet disturbs lipid raft/TGF-β signaling-mediated maintenance of hematopoietic stem cells in mouse bone marrow. *Nat Commun*. 2019;10(1):523. doi:10.1038/s41467-018-08228-0

60. Chow A, Huggins M, Ahmed J, et al. CD169+ macrophages provide a niche promoting erythropoiesis under homeostasis and stress. *Nat Med*. 2013;19(4):429-436. doi:10.1038/nm.3057

61. Kawano Y, Fukui C, Shinohara M, et al. G-CSF-induced sympathetic tone provokes fever and primes antimobilizing functions of neutrophils via PGE2. *Blood*. 2017;129(5):587-597. doi:10.1182/blood-2016-07-725754

62. Mercier FE, Ragu C, Scadden DT. The bone marrow at the crossroads of blood and immunity. *Nat Rev Immunol*. 2012;12(1):49-60. doi:10.1038/nri3132

63. Degliantoni G, Murphy M, Kobayashi M, Francis MK, Perussia B, Trinchieri G. Natural killer (NK) cell-derived hematopoietic colony-inhibiting activity and NK cytotoxic factor. Relationship with tumor necrosis factor and synergism with immune interferon. *J Exp Med*. 1985;162(5):1512-1530. doi:10.1084/jem.162.5.1512

64. Urbieta M, Barao I, Jones M, et al. Hematopoietic progenitor cell regulation by CD4+CD25+ T cells. *Blood*. 2010;115(23):4934-4943. doi:10.1182/blood-2009-04-218826

65. Gandy KL, Domen J, Aguila H, Weissman IL. CD8+TCR+ and CD8+TCR- cells in whole bone marrow facilitate the engraftment of hematopoietic stem cells across allogeneic barriers. *Immunity*. 1999;11(5):579-590. doi:10.1016/s1074-7613(00)80133-8

66. Fujisaki J, Wu J, Carlson AL, et al. In vivo imaging of Treg cells providing immune privilege to the haematopoietic stem-cell niche. *Nature*. 2011;474(7350):216-219. doi:10.1038/nature10160

67. Hirata Y, Furuhashi K, Ishii H, et al. CD150high Bone Marrow Tregs Maintain Hematopoietic Stem Cell Quiescence and Immune Privilege via Adenosine. *Cell Stem Cell*. 2018;22(3):445-453.e5. doi:10.1016/j.stem.2018.01.017

68. Butler JM, Nolan DJ, Vertes EL, et al. Endothelial Cells Are Essential for the Self-Renewal and Repopulation of Notch-Dependent Hematopoietic Stem Cells. *Cell Stem Cell*. 2010;6(3):251-264. doi:10.1016/j.stem.2010.02.001

69. Xu C, Gao X, Wei Q, et al. Stem cell factor is selectively secreted by arterial endothelial cells in bone marrow. *Nat Commun*. 2018;9(1):2449. doi:10.1038/s41467-018-04726-3

70. Van Den Berg SM, PSeijkens TT, HKusters PJ, et al. Diet-induced obesity in mice diminishes hematopoietic stem and progenitor cells in the bone marrow. *FASEB J*. 2016;30(5):1779-1788. doi:10.1096/fj.201500175

71. Liu A, Chen M, Kumar R, et al. Bone marrow lympho-myeloid malfunction in obesity requires precursor cell-autonomous TLR4. *Nat Commun*. 2018;9:708. doi:10.1038/s41467-018-03145-8

72. Adler BJ, Kaushansky K, Rubin CT. Obesity-driven disruption of haematopoiesis and the bone marrow niche. *Nat Rev Endocrinol*. 2014;10:737-748. doi:10.1038/nrendo.2014.169

73. Robsahm TE, Aagnes B, Hjartåker A, Langseth H, Bray FI, Larsen IK. Body mass index, physical activity, and colorectal cancer by anatomical subsites: a systematic review and meta-analysis of cohort studies. *Eur J Cancer Prev*. 2013;22(6):492-505. doi:10.1097/CEJ.0b013e328360f434

74. Je Y, Jeon JY, Giovannucci EL, Meyerhardt JA. Association between physical activity and mortality in colorectal cancer: A meta-analysis of prospective cohort studies: Physical activity and colorectal cancer mortality. *Int J Cancer*. 2013;133(8):1905-1913. doi:10.1002/ijc.28208

75. Emmons R, Niemiro GM, Owolabi O, De Lisio M. Acute exercise mobilizes hematopoietic stem and progenitor cells and alters the mesenchymal stromal cell secretome. *J Appl Physiol*. 2016;120(6):624-632. doi:10.1152/japplphysiol.00925.2015

76. Mooren FC, Krüger K. Apoptotic lymphocytes induce progenitor cell mobilization after exercise. *J Appl Physiol*. 2015;119(2):135-139. doi:10.1152/japplphysiol.00287.2015

77. Marycz K, Mierzejewska K, Śmieszek A, et al. Endurance Exercise Mobilizes Developmentally Early Stem Cells into Peripheral Blood and Increases Their Number in Bone Marrow: Implications for Tissue Regeneration. *Stem Cells Int*. 2016;2016:1-10. doi:10.1155/2016/5756901

78. Kröpfl JM, Beltrami FG, Gruber HJ, Stelzer I, Spengler CM. Exercise-Induced Circulating Hematopoietic Stem and Progenitor Cells in Well-Trained Subjects. *Front Physiol*. 2020;11(308):1-10. doi:10.3389/fphys.2020.00308

79. De Lisio M, Parise G. Characterization of the Effects of Exercise Training on Hematopoietic Stem Cell Quantity and Function. *J Appl Physiol Bethesda Md 1985*. Published online September 27, 2012. doi:10.1152/japplphysiol.00717.2012

80. Fuss J, Ben Abdallah NMB, Vogt MA, et al. Voluntary exercise induces anxiety-like behavior in adult C57BL/6J mice correlating with hippocampal neurogenesis. *Hippocampus*. 2010;20(3):364-376. doi:10.1002/hipo.20634

81. Niemiro GM, Allen JM, Mailing LJ, et al. Effects of endurance exercise training on inflammatory circulating progenitor cell content in lean and obese adults. *J Physiol*. 2018;596(14):2811-2822. doi:10.1113/JP276023

82. Baker JM, De Lisio M, Parise G. Endurance exercise training promotes medullary hematopoiesis. *FASEB J*. 2011;25(12):4348-4357. doi:10.1096/fj.11-189043

83. Peng H, Hu B, Xie LQ, et al. A mechanosensitive lipolytic factor in the bone marrow promotes osteogenesis and lymphopoiesis. *Cell Metab*. Published online June 7, 2022:S1550-4131(22)00191-7. doi:10.1016/j.cmet.2022.05.009

84. Farber E, Kwiecien JM, Bojic D, et al. Exercise Improves Cancer-free Survival and Health Span in a Model of Radiation-induced Cancer. *Med Sci Sports Exerc*. 2021;53(11):2254-2263. doi:10.1249/MSS.0000000000002711

85. Liu L, Buckley MT, Reyes JM, et al. Exercise reprograms the inflammatory landscape of multiple stem cell compartments during mammalian aging. Published online January 12, 2022:2022.01.12.475145. doi:10.1101/2022.01.12.475145

86. Shen B, Tasdogan A, Ubellacker JM, et al. A mechanosensitive peri-arteriolar niche for osteogenesis and lymphopoiesis. *Nature*. 2021;591(7850):438-444. doi:10.1038/s41586-021-03298-5

87. Kaneki H, Guo R, Chen D, et al. Tumor Necrosis Factor Promotes Runx2 Degradation through Up-regulation of Smurf1 and Smurf2 in Osteoblasts. *J Biol Chem*. 2006;281(7):4326-4333. doi:10.1074/jbc.M509430200

88. Liu W, Konermann A, Guo T, Jäger A, Zhang L, Jin Y. Canonical Wnt signaling differently modulates osteogenic differentiation of mesenchymal stem cells derived from bone marrow and from periodontal ligament under inflammatory conditions. *Biochim Biophys Acta BBA - Gen Subj*. 2014;1840(3):1125-1134. doi:10.1016/j.bbagen.2013.11.003

89. Lu X, Gilbert L, He X, Rubin J, Nanes MS. Transcriptional Regulation of the Osterix (Osx, Sp7) Promoter by Tumor Necrosis Factor Identifies Disparate Effects of Mitogen-activated Protein Kinase and NFκB Pathways. *J Biol Chem*. 2006;281(10):6297-6306. doi:10.1074/jbc.M507804200

90. Sul OJ, Ke K, Kim WK, et al. Absence of MCP-1 leads to elevated bone mass via impaired actin ring formation. *J Cell Physiol*. 2012;227(4):1619-1627. doi:10.1002/jcp.22879

91. Sullivan CB, Porter RM, Evans CH, et al. TNFα and IL-1β influence the differentiation and migration of murine MSCs independently of the NF-κB pathway. *Stem Cell Res Ther*. 2014;5(4):104. doi:10.1186/scrt492

92. De Lisio M, Baker JM, Parise G. Exercise promotes bone marrow cell survival and recipient reconstitution post-bone marrow transplantation, which is associated with increased survival. *Exp Hematol*. Published online October 11, 2012. doi:10.1016/j.exphem.2012.10.003

93. Aziz JA, Smith C, Slobodian M, et al. Impact of Exercise Training on Hematological Outcomes Following Hematopoietic Cell Transplantation: A Scoping Review. *Clin Investig Med Med Clin Exp*. 2021;44(2):E19-26. doi:10.25011/cim.v44i2.36369

94. De Lisio M, Phan N, Boreham DR, Parise G. Exercise-induced protection of bone marrow cells following exposure to radiation. *Appl Physiol Nutr Metab Physiol Appliquée Nutr Métabolisme*. 2011;36(1):80-87. doi:10.1139/H10-087

95. Chargaff E, West R. The biological significance of the thromboplastic protein of blood. *J Biol Chem*. 1946;166(1):189-197. doi:10.1016/S0021-9258(17)34997-9

96. Zaborowski MP, Balaj L, Breakefield XO, Lai CP. Extracellular Vesicles: Composition, Biological Relevance, and Methods of Study. *BioScience*. 2015;65(8):783-797. doi:10.1093/biosci/biv084

97. Yáñez-Mó M, Siljander PRM, Andreu Z, et al. Biological properties of extracellular vesicles and their physiological functions. *J Extracell Vesicles*. 2015;4(1):27066. doi:10.3402/jev.v4.27066

98. Ratajczak MZ, Ratajczak J. Extracellular microvesicles/exosomes: discovery, disbelief, acceptance, and the future? *Leukemia*. 2020;34(12):3126-3135. doi:10.1038/s41375-020-01041-z

99. Théry C, Witwer KW, Aikawa E, et al. Minimal information for studies of extracellular vesicles 2018 (MISEV2018): a position statement of the International Society for Extracellular Vesicles and update of the MISEV2014 guidelines. *J Extracell Vesicles*. 2018;7(1):1535750. doi:10.1080/20013078.2018.1535750

100. Witwer KW, Théry C. Extracellular vesicles or exosomes? On primacy, precision, and popularity influencing a choice of nomenclature. *J Extracell Vesicles*. 2019;8(1):1648167. doi:10.1080/20013078.2019.1648167

101. Lötvall J, Hill AF, Hochberg F, et al. Minimal experimental requirements for definition of extracellular vesicles and their functions: a position statement from the International Society for Extracellular Vesicles. *J Extracell Vesicles*. 2014;3(1):26913. doi:10.3402/jev.v3.26913

102. Stein JM, Luzio JP. Ectocytosis caused by sublytic autologous complement attack on human neutrophils. The sorting of endogenous plasma-membrane proteins and lipids into shed vesicles. *Biochem J*. 1991;274(2):381-386. doi:10.1042/bj2740381

103. Cocucci E, Meldolesi J. Ectosomes and exosomes: shedding the confusion between extracellular vesicles. *Trends Cell Biol*. 2015;25(6):364-372. doi:10.1016/j.tcb.2015.01.004

104. Doyle L, Wang M. Overview of Extracellular Vesicles, Their Origin, Composition, Purpose, and Methods for Exosome Isolation and Analysis. *Cells*. 2019;8(7):727. doi:10.3390/cells8070727

105. Peterson MF, Otoc N, Sethi JK, Gupta A, Antes TJ. Integrated systems for exosome investigation. *Methods*. 2015;87:31-45. doi:10.1016/j.ymeth.2015.04.015

106. Kormelink TG, Arkesteijn GJA, Nauwelaers FA, van den Engh G, Nolte-'t Hoen ENM, Wauben MHM. Prerequisites for the analysis and sorting of extracellular vesicle subpopulations by high-resolution flow cytometry: Sorting Extracellular Vesicle Subpopulations. *Cytometry A*. 2016;89(2):135-147. doi:10.1002/cyto.a.22644

107. Wiklander OPB, Brennan MÁ, Lötvall J, Breakefield XO, EL Andaloussi S. Advances in therapeutic applications of extracellular vesicles. *Sci Transl Med*. 2019;11(492):eaav8521. doi:10.1126/scitranslmed.aav8521

108. Machhi J, Shahjin F, Das S, et al. A Role for Extracellular Vesicles in SARS-CoV-2 Therapeutics and Prevention. *J Neuroimmune Pharmacol*. Published online February 5, 2021. doi:10.1007/s11481-020-09981-0

109. György B, Hung ME, Breakefield XO, Leonard JN. Therapeutic Applications of Extracellular Vesicles: Clinical Promise and Open Questions. *Annu Rev Pharmacol Toxicol*. 2015;55(1):439-464. doi:10.1146/annurev-pharmtox-010814-124630

110. Haraszti RA, Didiot MC, Sapp E, et al. High-resolution proteomic and lipidomic analysis of exosomes and microvesicles from different cell sources. *J Extracell Vesicles*. 2016;5(1):32570. doi:10.3402/jev.v5.32570

111. Kowal J, Arras G, Colombo M, et al. Proteomic comparison defines novel markers to characterize heterogeneous populations of extracellular vesicle subtypes. *Proc Natl Acad Sci*. 2016;113(8):E968-E977. doi:10.1073/pnas.1521230113

112. Kitamura Y, Kojima M, Kurosawa T, et al. Proteomic Profiling of Exosomal Proteins for Blood-based Biomarkers in Parkinson's Disease. *Neuroscience*. 2018;392:121-128. doi:10.1016/j.neuroscience.2018.09.017

113. Ohshima K, Hatakeyama K, Kanto K, et al. Comparative proteomic analysis identifies exosomal Eps8 protein as a potential metastatic biomarker for pancreatic cancer. *Oncol Rep*. Published online November 15, 2018. doi:10.3892/or.2018.6869

114. Whitham M, Parker BL, Friedrichsen M, et al. Extracellular Vesicles Provide a Means for Tissue Crosstalk during Exercise. *Cell Metab*. 2018;27(1):237-251.e4. doi:10.1016/j.cmet.2017.12.001

115. Frühbeis C, Helmig S, Tug S, Simon P, Krämer-Albers EM. Physical exercise induces rapid release of small extracellular vesicles into the circulation. *J Extracell Vesicles*. 2015;4(1):28239. doi:10.3402/jev.v4.28239

116. Aoi W, Ichikawa H, Mune K, et al. Muscle-enriched microRNA miR-486 decreases in circulation in response to exercise in young men. *Front Physiol*. 2013;4. doi:10.3389/fphys.2013.00080

117. Shi XF, Wang H, Kong FX, et al. Exosomal miR-486 regulates hypoxia-induced erythroid differentiation of erythroleukemia cells through targeting Sirt1. *Exp Cell Res*. 2017;351(1):74-81. doi:10.1016/j.yexcr.2016.12.023

118. Oliveira GP, Porto WF, Palu CC, et al. Effects of Acute Aerobic Exercise on Rats Serum Extracellular Vesicles Diameter, Concentration and Small RNAs Content. *Front Physiol*. 2018;9:532. doi:10.3389/fphys.2018.00532

119. Sol Kim D, Young Lee S, Hee Lee J, Chan Bae Y, Sup Jung J. MicroRNA-103a-3p controls proliferation and osteogenic differentiation of human adipose tissue-derived stromal cells. *Exp Mol Med*. 2015;47(7):e172-e172. doi:10.1038/emm.2015.39

Chapter II: Literature Review Continued – The Role of High-Fat Diets on Hematopoiesis and the Bone Marrow Microenvironment

Recent advances in understanding the role of high fat diets and their components on hematopoiesis and the hematopoietic stem cell niche

James J. Vanhie[1], Matthew Ngu[1], and Michael De Lisio[1,2]

[1]School of Human Kinetics, University of Ottawa, 451 Smyth Road, Ottawa, Ontario, K1H 8L1, Canada

[2]Department of Cellular and Molecular Medicine, University of Ottawa, 451 Smyth Road, Ottawa, Ontario, K1H 8L1, Canada

Current Opinion in Food Science

2020 Aug; 34: 30-37

DOI: https://doi.org/10.1016/j.cofs.2020.11.004

Contribution: James J. Vanhie drafted and edited the manuscript.

Correspondence to:
Michael De Lisio, PhD
Roger Guindon Hall, University of Ottawa
Phone: +1 613-562-5800 ext. 6987
Email: mdelisio@uottawa.ca

Abstract

Hematopoietic stem/progenitor cells (HSPCs) are self-renewing, multipotent progenitors that sustain hematopoiesis and occupy the bone marrow. The increasing incidence of obesity has led to an expanding body of literature examining the effects of high fat diet-induced obesity on HSPCs. These studies indicate that diet-induced obesity results in HSPC depletion and overproduction of myeloid cells during stress and steady state hematopoiesis. These effects are mediated by cell autonomous mechanisms and alterations in the HSPC niche. Emerging work is revealing that dietary components in high fat diets or altered by obesity, such as, saturated fatty acids, cholesterol, and vitamin D, have effects on HSPC function that are distinct from obesity.

Introduction

The prevalence of obesity has increased globally, and most recent Canadian data indicate that 6 in 10 adults aged 18 to 79 are classified as overweight or obese (Government of Canada; URL: https://www150.statcan.gc.ca/n1/pub/82-625-x/2019001/article/00005-eng.htm). Obesity is defined as a body mass index of ≥30 kg/m^2 with the accumulation of excess adipose tissue that results in elevated risks to health through the development of comorbidities, including hyperlipidemia, insulin resistance, and a state of chronic systemic inflammation [1,2]. Obesity is considered a risk factor for several metabolic and cardiovascular diseases as well as several types of cancer. The increased disease risk in persons with obesity is due, in part, to alterations in immune and inflammatory cell content and function. Indeed, persons with obesity have compromised immunity and increased risk of developing severe symptoms from infection, and are in a state of chronic inflammation characterized by an expansion of proinflammatory myeloid cells [3,4]. The involvement of hematopoietic cells in obesity-associated complications has inspired several recent investigations into the effects of obesity on hematopoietic stem/progenitor cells (HSPCs). HSPCs are responsible for the production of all mature blood and immune cells in a process termed hematopoiesis. Excess caloric consumption combined with physical inactivity are the primary behavioural factors contributing to obesity in humans, and these conditions are modeled in rodents by feeding a high-fat diet (HFD) that typically consists of 45-60% fat as a measure of total kilocalories. Rodent models of diet-induced obesity have revealed significantly altered hematopoiesis that results in skewing of mature cell production along the myeloid lineage. These recent findings suggest chronic inflammation and reduced immune function characteristic of obesity could be due, in part, to alterations in hematopoiesis.

HSPCs are regulated by cell autonomous and niche factors that are altered with obesity. While several recent reports have used diet-induced and pharmacological methods of obesity induction in murine models to evaluate the effects of obesity and/or increased adiposity on hematopoiesis, relatively few studies have examined the role of individual dietary components that are enriched in high fat diets. Thus, creating a gap in the literature related to the extent to which the diet-induced obesity phenotype in HSPCs is due to adipose tissue expansion or specific components of the high fat diet. Here, we provide a concise overview of the recent literature examining the effects of diet-induced obesity on HSPCs and hematopoiesis as well as the role of dietary components in high fat diets or altered by obesity on hematopoiesis and the hematopoietic stem cell niche.

High Fat Diets

Most rodent studies examining the effects of obesity on hematopoiesis have induced obesity by high fat diet feeding. This model is a good approximation of human obesity which is due to excess caloric consumption and physical inactivity. Rodent and human obesity is characterized by an overproduction of mature myeloid lineage cells [5,6] contributing to the chronic inflammatory state characteristic of obesity [7]. Indeed, monocytes, which are derived from common myeloid progenitors contribute to the elevation of pro-inflammatory cytokines TNF-α, IL-6, and IL1β in obesity [8–10]. Adipose tissue depots expand in obesity and are known to contribute to proinflammatory conditions via the upregulation of several inflammatory cytokines [11]. Aberrant myelopoiesis contributes to this pro-inflammatory environment as monocytes home to adipose depots and contribute to the local inflammatory response. Indeed, inflammatory cytokine concentrations in peripheral tissues are decreased when monocyte homing is blocked

by genetic ablation of C-C chemokine receptor type 2 (CCR2) [12], indicating a role of altered hematopoiesis on the inflammatory state of extramedullary tissues. As obesity progresses and extramedullary tissues become more inflamed, they signal back to HSPCs to continue a cycle of chronic inflammatory cell overproduction.

Since mature hematopoietic cells are short-lived in circulation, recent investigations have begun to trace obesity-induced alterations in these populations back to HSPCs from which all mature hematopoietic cells are derived. Using the diet-induced obesity model in rodents, HSPC skewing towards the myeloid lineage has commonly been shown [5,9,13–15], and these findings have been confirmed in human studies in adults with obesity [6]. Nagareddy and colleagues (2014) also observed aberrant myelopoiesis in a genetic model of obesity (i.e. *Ob/Ob* mice) [5], suggesting that the effects of obesity on hematopoiesis are, at least in part, independent of diet. Following weight loss, macrophage populations decrease with an accompanied lowered expression of inflammatory markers; however, alterations to HSPCs persist [13]. Singer and colleagues (2014) determined that 12 weeks of obesity induction by high fat diet, followed by 8 week on normal diet restored several HSPC population to that observed in mice maintained on a normal diet for the full 20 weeks; however, myeloid progenitors remained significantly elevated [15]. Similarly, we observed a persistent elevation of myeloid progenitors in mice fed a high fat diet to induced obesity followed by normal diet feeding to induce weigh loss in a model of colorectal cancer, and extended these findings by showing that the addition of exercise to the normal diet-induced weight loss restored healthy hematopoiesis [16]. Together, these findings raise the alarming possibility that weight loss may not fully reverse obesity-induced alterations to HSPC differentiation.

The mechanisms responsible for aberrant myelopoiesis in obesity are only beginning to be identified. Aberrant myelopoiesis was maintained when bone marrow from high fat diet-fed mice was transplanted into normal diet-fed mice indicating that the effects of high fat diet on hematopoiesis are, at least in part, cell-autonomous [15]. TLR4-MyD88 signaling has been implicated in HSPC response to bacterial infection, and as such, has been examined in the context of diet-induced obesity. TLR4 is a member of the pattern recognition family that recognizes invading pathogens as well as endogenous molecules, including saturated fatty acids and gut microbiota-derived lipopolysaccharide [17]. On HSPCs, TLR4 acts as an important transducer of the extracellular signal from fatty acids to activation of intracellular inflammatory pathways [18,19]. These preclinical findings are supported by data from human HSPCs as *in vitro* stimulation of the TLR4 receptor increased myeloid differentiation [20]. Singer and colleagues implicated the TLR4-MyD88 pathway in aberrant myelopoiesis by showing that myeloid progenitor content was reduced when *MyD88*$^{-/-}$ donor cells were transplanted into high fat diet-fed mice compared to wild type donor cells [15]. Interestingly, when similar experiments were performed with *Tlr4*$^{-/-}$ donors, the content of the most primitive HSPC population (i.e., long-term HSCs) was reduced, but aberrant myelopoiesis was not detected, suggesting a potential uncoupling of TLR4-MyD88 axis in stress hematopoiesis [15]. Liu and colleagues (2018) similarly found no significant changes in steady state hematopoiesis under obesogenic conditions in *Tlr4*$^{-/-}$ mice [19]. However, under conditions of stress hematopoiesis induced by chemotherapy, *Tlr4*$^{-/-}$ mice fed a HFD had improved hematopoietic reconstitution compared to wild type mice under identical conditions [19]. Further, when *Tlr4*$^{-/-}$ bone marrow was competitively transplanted with wild type bone marrow into recipients fed a high fat diet, aberrant myelopoiesis was only

detected from wild type donor cells, suggesting a cell autonomous effect of TLR4 signaling in HSPCs [19]. Together, these findings implicate the TLR4-MyD88 pathway as a potential mechanistic link between obesity and HSPC regulation; however, given the pleiotropic nature of obesity, several other mechanisms are also likely involved that remain to be elucidated.

Whether diet-induced obesity influences HSPC content and proliferation is controversial and appears to depend on both the fat content of the diet and the length of exposure to the diet. van den Berg and colleagues reported that long-term high fat feeding (45% kcal fat) in rodents attenuated HSPC proliferation leading to an eventual reduction in several HSPC populations in the bone marrow and reduced repopulating capacity upon transplantation [9]. HSPC reduction may be accelerated when the diet consists of 60% kcal fat as Singer and colleagues (2014) demonstrated that the proportion of long-term HSCs were significantly reduced following only one week of high fat (60% kcal fat) feeding [15]. This reduction in primitive HSPC proportion was delayed until 4 weeks when mice were fed a high fat diet consisting of only 45% kcal fat [5]. Conversely, using Ob/Ob mice, Nagareddy and colleagues observed an increase in the proportion of HSPCs with no change in cell cycle status compared to wild type; however, when they used a model of diet-induced obesity (60% kcal for 20 weeks), no difference in HSPCs content or cell cycle status was observed [5]. Interestingly, Liu and colleagues (2018) found that the absolute number of HSPCs were significantly reduced, while the proportion of HSPCs was increased following long-term feeding with a high fat diet consisting of 40% kcal fat [19]. In contrast to van den Berg and colleagues, Liu et al observed an increase in HSPC proliferation in obese mice [19]. The reduction in absolute HSPC content is supported in models of stress hematopoiesis. Work from our lab has shown that long-term obesity reduces primitive, long-term HSPC content during

recovery from a non-myeloablative radiation dose suggesting that long-term obesity and/or high fat diet consumption impairs hematopoietic regeneration [10]. Similarly, Liu and colleagues (2018) showed impaired recovery from chemotherapy-induced hematopoietic stress in mice fed a high fat diet compared to control [19]. These findings suggest that considerations need to be made for how HSPC content is expressed, that obesity is a dynamic process with HSPC content changing depending on length of time from obesity induction, and that a strong obesity-induced phenotype might require the induction of hematopoietic stress [9,21,22].

In addition to its direct effects on HSPCs, diet-induced obesity induces a significant remodeling of the bone marrow environment. Elevated bone marrow adiposity induced by obesity reduces the physical space available for hematopoiesis and elevates the content of pro-inflammatory cytokines, thereby directly affecting HSC fate [23]. Diet-induced obesity acts on leptin receptor positive (LepR+) mesenchymal stromal cells (MSCs) to substantially increase marrow adipose tissue by inducing adipogenic differentiation at the expense of osteoblastogenesis through upregulated JAK2/STAT3 pathway activity [11,24–26]. Early work suggested that marrow adipose tissue was a negative regulator of hematopoiesis and was associated with reduced HSPC content due in part to decreasing the space available for hematopoietically active marrow [27]. These data were supported by a recent study that showed that co-injection of preadipocytes in a bone marrow transplant model significantly reduced HSPC content, while injection of primitive MSCs boosted HSPC engraftment [28]. Similarly, data from our lab indicates that marrow adipose tissue accumulates in mice fed a high fat diet, long-term, and these changes to the bone marrow were associated with reduced multipotent- and lymphoid-progenitor cell content during radiation recovery [10]. Using a murine bone marrow

transplantation model, Singer and colleagues observed that myelopoiesis was elevated in obese recipient mice who received marrow from lean mice compared to recipients fed a normal diet, suggesting that the niche plays a significant role in myelopoiesis [15]. Supporting this notion, Liu and colleagues found that hematopoietic regeneration following chemotherapy was reduced in mice fed a high fat diet, but was restored when bone marrow from high fat diet-fed mice was transplanted into control diet-fed mice [19]. Boyd and colleagues showed that myelopoiesis was linked to marrow adipose tissue content using a pharmacological method of marrow adipose tissue induction in a leukemia model [29]. These data suggest that in the context of stress hematopoiesis, obesity or marrow adipose tissue expansion may accelerate hematopoietic recovery and attenuate immunosuppression by promoting HSPC proliferation and myeloid differentiation; however, under chronic obesogenic conditions, this process may exhaust primitive HSPC populations and contribute to systemic inflammation.

In addition to cellular changes in the bone marrow, obesity also remodels the bone marrow paracrine environment by increasing pro-inflammatory factors known to induce HSPC proliferation while reducing paracrine factors involved in HSPC maintenance [7]. Specifically, obesity increases bone marrow leptin, IL-1β, IL-6, and TNF-α [8–10] content and reduces levels of CXCL12 [10,16]. Recently, leptin was specifically identified as a paracrine factor that indirectly alters hematopoiesis through $LepR^{+}$ MSCs [30]. Leptin is secreted from adipose tissue and its concentration increases with adipose tissue expansion [31]. Lean mice continuously injected subcutaneously with leptin for 6 weeks had increased leukocytosis, while genetically disrupting leptin signaling in MSCs reduced leukocytosis and increased their expression of HSPC maintenance factors [30]. Whether high fat diet directly induces alterations in the MSC

secretome remains to be determined. Beyond the bone marrow, obesity induces changes to the secretome of white adipose tissue depots and their associated macrophages that influence HSPCs. Indeed, Nagareddy and colleagues (2014) identified a cell non-autonomous role for the TLR4-MyD88 pathway in obesity-induced myelopoiesis by showing that TLR4 activation on adipose tissue macrophages leads to increased secretion of Il-1β which promotes monocytosis from myeloid progenitors in the bone marrow [5]. Collectively, a growing body of literature describes how diet-induced obesity alters HSPC content and hematopoiesis via direct and indirect factors. However, the role of specific dietary components in HFDs or altered by obesity on HSPC function is less well-known and will be the focus of the rest of this review.

Fatty Acids

Fatty acids are hydrophobic compounds composed of hydrocarbon branches of varying length and saturation. Major classes include saturated and polyunsaturated fatty acids (PUFAs). Eicosanoids are a group of signaling lipids that are primarily derived from arachidonic acid (an omega-6 PUFA) that are integral to controlling inflammation [32]. The Mediterranean diet which is high in PUFAs, is associated with reduced myeloid progenitor cell production compared to the Western diet which contains a larger composition of saturated fatty acids (33% vs. 21%), thereby providing anti-inflammatory effects that may contribute to its associated reduced cardiovascular disease risk [33–35]. In a clinical study involving 14,586 healthy individuals, Bonaccio an colleagues (2014) found a significant correlation between adherence to consuming a Mediterranean diet and a reduction in white blood cell populations [36]. In 106 individuals with diabetes or more than 2 cardiovascular disease risk factors, Mena and colleagues (2009) measured decreases in monocyte CD49d and CD40 expression (pro-inflammatory markers)

following an introduction of the Mediterranean diet, but not with a low-fat diet [37]. These findings indicate a significant role of dietary compounds found within the Mediterranean diet on mitigating chronic inflammation. *In vivo*, eicosapentaenoic acid and docosahexanoic acid (omega-3 PUFAs) supplementation downregulates T- and B- cell activation and NF-κB transcription (regulator of the transcription of pro-inflammatory cytokines, including IL-6, IL-12, and TNF-α) compared to a control and corn oil-based HFD, indicating a role for omega-3 fatty acids in reducing the inflammatory profile in mature hematopoietic cells [38]. Direct effects of PUFAs on HSPCs and hematopoiesis have been less well-studied. *In vitro* the addition of docosahexanoic acid and arachidonic acid increases HSPC differentiation to megakaryocytes [39], and α-linoleic acid (an omega-3 PUFA) and linoleic acid (an omega-6 PUFA) supplementation stimulates HSPC proliferation, improves spleen colony formation, and increases engraftment potential of transplanted bone marrow cells from non-supplemented donor mice [40]. These findings suggest PUFA supplementation may provide favourable conditions for HSPC regeneration during stress hematopoiesis, and that different PUFAs may have distinct effects on hematopoiesis. Mechanistically, it is known that HSPCs require functioning fatty acid metabolism. When fatty acid metabolism is disrupted via inhibition of the free fatty acid transporter carnitine palmitoyl transferase 1 (CPT1), or deletion of 12/15-lioxygenase, a key enzyme in unsaturated fatty acid metabolism, HSPC repopulation capacity is impaired [41,42]. Similar results are seen in acute myeloid leukemia (AML) cell lines, which are derived from HSPCs, and have high fatty acid-binding protein 4 (FABP4) expression and reduced proliferation when exposed to a FABP4 inhibitor [41,43]. As such, these initial studies indicate that PUFAs and/or alterations to fatty acid metabolism can directly influence HSPC function.

Cholesterol

Cholesterol is a lipid compound that is involved in cell membrane formation and cell signaling, and high cholesterol levels are associated with diet-induced obesity. Cholesterol is carried throughout circulation via lipoproteins, including low-density, cholesterol-rich lipoproteins (LDL) and high-density, cholesterol-poor lipoproteins (HDL). Plasma concentrations of LDL and HDL are affected by downstream metabolism of other nutrients, including saturated and trans fatty acids that primarily elevate LDL [44]. Hypercholesterolemia (particularly that characterized by high LDL) promotes HSPC proliferation, differentiation, and mobilization [45–47]. Interestingly, hypercholesterolemic non-obese mice lacking the LDL receptor also display enhanced HSC proliferation [48]. These results suggest that direct signaling through the LDL receptor may be responsible for its effects on differentiation and mobilization, but distinct mechanisms connect hypercholesterolemia to HSPC proliferation. Hypercholesterolemia elevates bone marrow triglyceride content downstream through a complex set of mechanisms originating with lipoprotein lipase (LPL) on the vascular endothelium [49]. LPL forms free fatty acids by hydrolyzing triglycerides bound to lipoproteins in circulation with the critical cofactor apolipoprotein C-II (APOC2) [50–53]. Without proper LPL or APOC2 function hyperlipidemia occurs, resulting in HSPC expansion, dysregulated hematopoiesis, and anemia [53]. This phenotype has been observed in APOC2- or LPL-deficient human patients, where triglyceride and cholesterol levels severely increase [52,54]. Cholesterol accumulation in HSPCs can also be caused by defective or downregulated cholesterol efflux genes (Apoe, Abca1, and Abcg1) [55,56]. Hematopoietic cell-specific Abca1/Abcg1 knockout display HSPC proliferation in marrow in addition to elevated granulocyte production and upregulated extramedullary hematopoiesis

[57]. These alterations are attributed to elevated G-CSF concentration in the blood through the pro-inflammatory IL-23/IL-17/G-CSF signaling axis, as G-CSF levels were normalised following IL-17-blocking antibody injection in wild type recipients [57,58]. Collectively, these data suggest that signaling through the LDL receptor is involved in HSPC differentiation and mobilization, while intracellular cholesterol content plays a critical role in HSPC expansion.

HSPC cellular cholesterol content is maintained by several mechanisms, including cholesterol efflux to HDL, LDL cholesterol uptake, and endogenous cholesterol synthesis [49]. The capacity of HDL to accept cholesterol is regulated in part by the presence of apolipoprotein A-I binding protein (AIBP) [49]. AIBP mediates cholesterol efflux by activating sterol regulatory element-binding protein 2 (SREBP2), the master transcription factor for Notch1 signaling, leading to HSC specification [49,59]. Interestingly, in mature hematopoietic cells, HDL administration can prevent or in some cases reverse HSPC proliferation and differentiation by promoting cholesterol efflux [57,60]. Cholesterol accumulation in HSPCs also elevates blood monocyte populations by enhancing HSPC proliferation and mobilization, which are necessary for the development of atherosclerotic plaques [61]. Monocytosis and upregulated monocytic recruitment to atherosclerotic legions can be reversed via HDL administration as described earlier [55,57], providing a novel link between hematopoiesis, diet, and cardiovascular disease. Therefore, attenuating the accumulation of cholesterol within HSPCs appears to have downstream effects in reducing the systemic inflammatory profile displayed in diet-induced obesity. Despite the advancement in understanding the role of HDL and LDL on HSPC proliferation and differentiation patterns, questions remain unanswered on the effects of dietary cholesterol uptake on hematopoiesis in healthy and diseased states and how HSPC niche cell populations are affected.

Vitamin D

The study of vitamin D on hematopoiesis and the hematopoietic stem cell niche remains of interest for individuals with obesity, as obesity is linked to vitamin D deficiency [62]. Vitamin D is a cholesterol-derived compound, is often enriched in high-fat foods, and is classically understood for its integral role in the proper function of calcium homeostasis and metabolism. Beyond these functions vitamin D plays a pleiotropic role due to the ubiquitous expression of the vitamin D receptor (VDR) in almost all body tissues, including HSPCs [63]. In HSPCs, vitamin D plays an important role in stimulating differentiation and proliferation [64,65]. Cortes *et al.* defined a direct role of vitamin D in modulating zebrafish HSPC production *in vitro* and *in vivo* during development which was independent from its role in maintaining calcium homeostasis [65]. This modulation of HSPC production may be translatable to a human model, as the zebrafish hematopoietic system closely resembles human hematopoiesis [66]. Vitamin D has long been known to induce myeloid progenitor differentiation into monocytes through downstream signaling from VDR in immature HSPC and myeloid progenitor cells in healthy bone marrow and AML [63,67]. Interestingly, mature monocyte populations remain unaltered in VDR knockout mice during steady state hematopoiesis [63]. Despite this, common myeloid and granulocyte-monocyte progenitor cell populations both decrease in VDR knockout mice compared to wild-type, suggesting VDR activation is partially responsible for monocytic differentiation and/or maintenance of monocyte precursors [63]. VDR activation is also important in regulating the HSPC niche. Activation of the VDR on osteoblasts induces receptor activator of nuclear factor kappa-B ligand (RANKL) upregulation, leading to enhanced proteolytic enzyme secretion from osteoclasts and concurrent degradation of HSC anchoring proteins resulting in HSPC mobilization

[68,69]. Despite understanding the role of VDR on HSPC mobilization, the mechanistic effects of vitamin D supplementation and deficiency on HSPC subpopulation proliferation/differentiation and the cellular makeup of the HSC niche remains largely unknown.

Conclusion

Bone marrow is the primary location for hematopoiesis, which involves a complex interplay of autonomous cell signaling and cell-cell communication between HSPCs and their niche. This interplay can be significantly altered by the introduction of HFDs, which can induce HSPC proliferation, myeloid differentiation, and migration at steady state, and impairing stress hematopoiesis. When the HSPC niche is altered by HFDs, pro-inflammatory pathways and marrow adipose tissue accumulation encourage myeloid skewing. It is beginning to be appreciated that these obesity-induced alterations in HSPCs and hematopoiesis are an important contributing factor to the chronic inflammation and reduced immune function observed in obesity. While the literature regarding the role of specific dietary components enriched in or modulated by high fat diets/obesity on HSPCs and hematopoiesis is in its infancy, interesting findings are beginning to emerge. Specifically, these early studies seem to indicate that fatty acids, cholesterol, and vitamin D directly influence HSPC proliferation and differentiation (Figure 2.1). A diet rich with omega-3 PUFAs play a significant role in decreasing inflammation and provides substrates for β-oxidation which is known to play a significant role in HSPC regulation. Hypercholesterolemia increases HSPC proliferation, differentiation, and mobilization due to cholesterol accumulation within HSPCs. However, supplementation of HDL can promote cholesterol efflux, thereby mitigating HSPC expansion and differentiation. Finally, vitamin D induces HSPC proliferation and differentiation, and induce HSPC mobilization indirectly via

regulating the osteoblast secretome. The role of dietary components on the HSPC niche has yet to be thoroughly investigated. Future work should further elucidate the role and mechanisms responsible for HSPC regulation by specific dietary components in order to develop dietary strategies to reduce obesity-associated disease through the modulation of hematopoiesis.

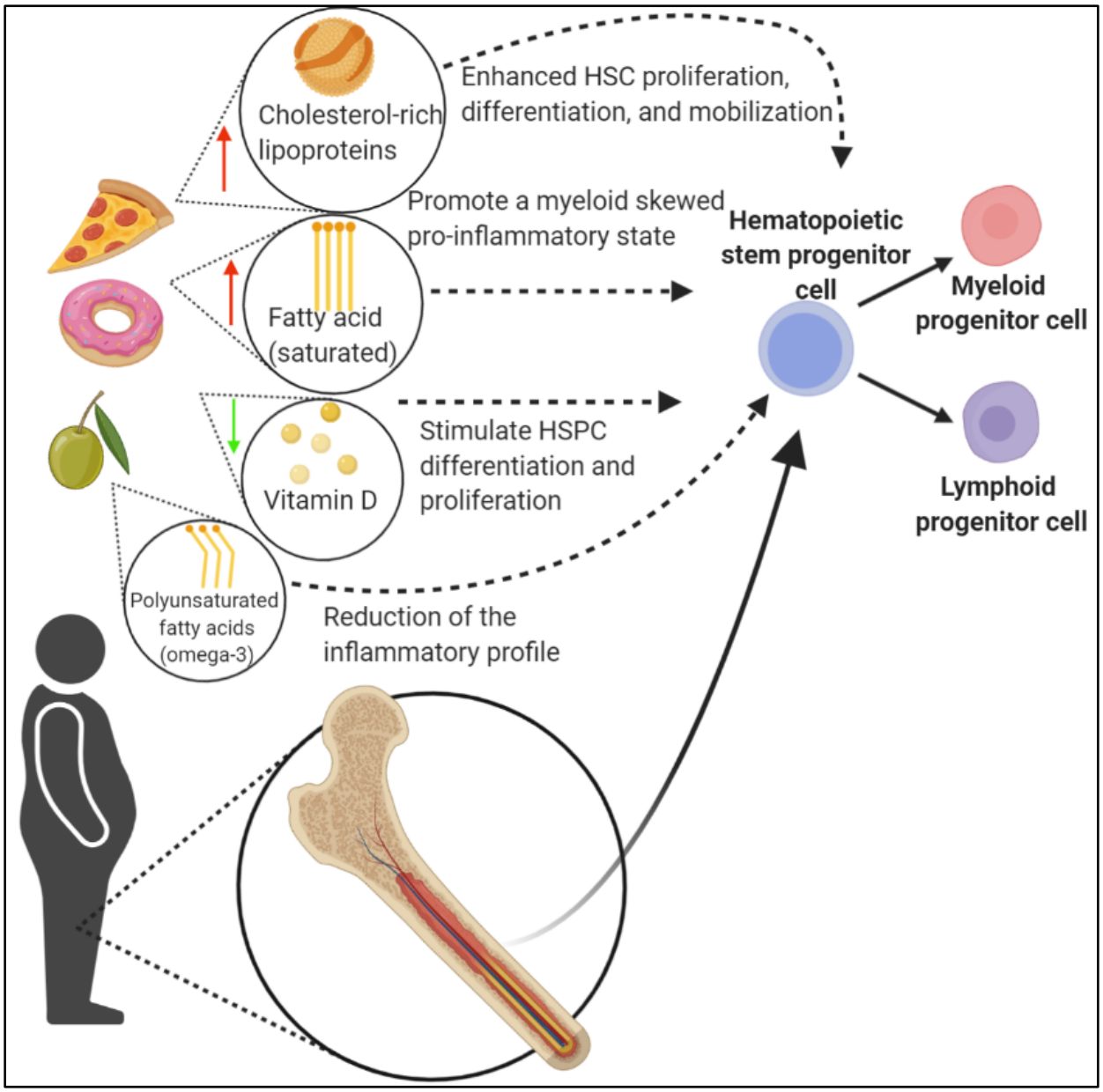

Figure 2.1. The effects of dietary components enriched in high fat diets on hematopoietic stem and progenitor cells of the bone marrow. Obesity induced by high fat diet reduces HSPC content and increases myelopoiesis. Initial evidence suggests that fatty acids, cholesterol-rich lipoproteins, and signaling through the vitamin D receptor all contribute in distinct but related ways to the obesity-associated phenotype in HSPCs, while diets rich in polyunsaturated fatty acids may reverse some of the effects of obesity on HSPCs.

Conflict of interest statement

Nothing declared.

Acknowledgements

This work was supported by the Natural Sciences and Engineering Council [grant number RGPIN-2017-04320] and the American Institute for Cancer Research.

References

1. Lutz TA, Woods SC: **Overview of Animal Models of Obesity**. *Current Protocols in Pharmacology* 2012, **58**:5.61.1-5.61.18.

2. Hruby A, Hu FB: **The Epidemiology of Obesity: A Big Picture**. *PharmacoEconomics* 2015, **33**:673–689.

3. Himbert C, Delphan M, Scherer D, Bowers LW, Hursting S, Ulrich CM: **Signals from the adipose microenvironment and the obesity-cancer link-A systematic review**. *Cancer Prev Res* 2017, **10**:494–506.

4. McLaughlin T, Ackerman SE, Shen L, Engleman E: **Role of innate and adaptive immunity in obesity-associated metabolic disease**. *Journal of Clinical Investigation* 2017, **127**:5–13.

5. Nagareddy PR, Kraakman M, Masters SL, Stirzaker RA, Gorman DJ, Grant RW, Dragoljevic D, Hong ES, Abdel-Latif A, Smyth SS, et al.: **Adipose tissue macrophages promote myelopoiesis and monocytosis in obesity**. *Cell Metabolism* 2014, **19**:821–835.

6. Niemiro GM, Allen JM, Mailing LJ, Khan NA, Holscher HD, Woods JA, De Lisio M: **Effects of endurance exercise training on inflammatory circulating progenitor cell content in lean and obese adults: Exercise and circulating progenitor cells in obesity**. *J Physiol* 2018, **596**:2811–2822.

7. Emmons R, Niemiro GM, De Lisio M: **Hematopoiesis with obesity and exercise: Role of the bone marrow niche**. *Exercise immunology review* 2017, **23**:82–95.

8. Trottier MD, Naaz A, Li Y, Fraker PJ: **Enhancement of hematopoiesis and lymphopoiesis in diet-induced obese mice**. *Proc Natl Acad Sci U S A* 2012, **109**:7622–7629.

9. Van Den Berg SM, PSeijkens TT, HKusters PJ, Beckers L, DenToom M, Smeets E, Levels J, De Winther MPJ, Lutgens E: **Diet-induced obesity in mice diminishes hematopoietic stem and progenitor cells in the bone marrow**. *FASEB Journal* 2016, **30**:1779–1788.

10. Emmons R, Ngu M, Xu G, Hernández-Saavedra D, Chen H, De Lisio M: **Effects of obesity and exercise on bone marrow progenitor cells after radiation**. *Medicine & Science in Sports & Exercise* 2019, **51**:1126–1136.

11. Tencerova M, Figeac F, Ditzel N, Taipaleenmäki H, Nielsen TK, Kassem M: **High-fat diet-induced obesity promotes expansion of bone marrow adipose tissue and impairs skeletal cell functions in mice**. *J Bone Miner Res* 2018, **33**:1154–1165.

12. Si Y, Tsou C-L, Croft K, Charo IF: **CCR2 mediates hematopoietic stem and progenitor cell trafficking to sites of inflammation in mice**. *J Clin Invest* 2010, **120**:1192–1203.

13. Bolus WR, Kennedy AJ, Hasty AH: **Obesity-induced reduction of adipose eosinophils is reversed with low-calorie dietary intervention**. *Physiol Rep* 2018, **6**:e13919.

14. Murray PJ: **Obesity corrupts myelopoiesis**. *Cell Metabolism* 2014, **19**:735–736.

15. Singer K, DelProposto J, Lee Morris D, Zamarron B, Mergian T, Maley N, Cho KW, Geletka L, Subbaiah P, Muir L, et al.: **Diet-induced obesity promotes myelopoiesis in hematopoietic stem cells**. *Molecular Metabolism* 2014, **3**:664–675.

16. Emmons R, Xu G, Hernández-Saavedra D, Kriska A, Pan Y-X, Chen H, De Lisio M: **Effects of obesity and exercise on colon cancer induction and hematopoiesis in mice**. *American Journal of Physiology-Endocrinology and Metabolism* 2018, **316**:E210–E220.

17. Suganami T, Tanimoto-Koyama K, Nishida J, Itoh M, Yuan X, Mizuarai S, Kotani H, Yamaoka S, Miyake K, Aoe S, et al.: **Role of the toll-like receptor 4/NF-κB pathway in saturated fatty acid-induced inflammatory changes in the interaction between adipocytes and macrophages**. *ATVB* 2007, **27**:84–91.

18. Shi H, Kokoeva MV, Inouye K, Tzameli I, Yin H, Flier JS: **TLR4 links innate immunity and fatty acid--induced insulin resistance**. *Journal of Clinical Investigation* 2006, **116**:3015–3025.

19. Liu A, Chen M, Kumar R, Stefanovic-Racic M, O'Doherty RM, Ding Y, Jahnen-Dechent W, Borghesi L: **Bone marrow lympho-myeloid malfunction in obesity requires precursor cell-autonomous TLR4**. *Nat Commun* 2018, **9**:708.

20. Liu A, Wang Y, Ding Y, Baez I, Payne KJ, Borghesi L: **Hematopoietic stem cell expansion and common lymphoid progenitor depletion requires hematopoietic-derived, cell-autonomous TLR4 in a model of chronic endotoxin**. *JI* 2015, **195**:2524–2528.

21. Xiao Y, Zhu Q, Liu X, Jiang M, Hao H, Zhu H, Cowan PJ, He X, Liu Q, Zhou S, et al.: **High-fat diet selectively decreases bone marrow lin $^{-}$ /CD117 $^{+}$ cell population in aging mice through increased ROS production**. *J Tissue Eng Regen Med* 2020, **14**:884–892.

22. Lee J-M, Govindarajah V, Goddard B, Hinge A, Muench DE, Filippi M-D, Aronow B, Cancelas JA, Salomonis N, Grimes HL, et al.: **Obesity alters the long-term fitness of the hematopoietic stem cell compartment through modulation of Gfi1 expression**. *Journal of Experimental Medicine* 2018, **215**:627–644.

23. Halade GV, Rahman MM, Williams PJ, Fernandes G: **High fat diet-induced animal model of age-associated obesity and osteoporosis**. *The Journal of Nutritional Biochemistry* 2010, **21**:1162–1169.

24. Zhou BO, Yue R, Murphy MM, Peyer JG, Morrison SJ: **Leptin-receptor-expressing mesenchymal stromal cells represent the main source of bone formed by adult bone marrow**. *Cell Stem Cell* 2014, **15**:154–168.

25. Hu L, Yin C, Zhao F, Ali A, Ma J, Qian A: **Mesenchymal stem cells: Cell fate decision to osteoblast or adipocyte and application in osteoporosis treatment**. *IJMS* 2018, **19**:360.

26. Yue R, Zhou BO, Shimada IS, Zhao Z, Morrison SJ: **Leptin receptor promotes adipogenesis and reduces osteogenesis by regulating mesenchymal stromal cells in adult bone marrow**. *Cell Stem Cell* 2016, **18**:782–796.

27. Naveiras O, Nardi V, Wenzel PL, Hauschka PV, Fahey F, Daley GQ: **Bone-marrow adipocytes as negative regulators of the haematopoietic microenvironment**. *Nature* 2009, **460**:259–263.

28. Ambrosi TH, Scialdone A, Graja A, Gohlke S, Jank A-M, Bocian C, Woelk L, Fan H, Logan DW, Schürmann A, et al.: **Adipocyte accumulation in the bone marrow during obesity and eging impairs stem cell-based hematopoietic and bone regeneration**. *Cell Stem Cell* 2017, **20**:771-784.e6.

29. Boyd AL, Reid JC, Salci KR, Aslostovar L, Benoit YD, Shapovalova Z, Nakanishi M, Porras DP, Almakadi M, Campbell CJV, et al.: **Acute myeloid leukaemia disrupts endogenous myelo-erythropoiesis by compromising the adipocyte bone marrow niche**. *Nature Cell Biology* 2017, **19**:1336–1347.

30. Frodermann V, Rohde D, Courties G, Severe N, Schloss MJ, Amatullah H, McAlpine CS, Cremer S, Hoyer FF, Ji F, et al.: **Exercise reduces inflammatory cell production and cardiovascular inflammation via instruction of hematopoietic progenitor cells**. *Nature Medicine* 2019, **25**:1761–1771.

31. Schipper HS, Nuboer R, Prop S, van den Ham HJ, de Boer FK, Kesmir Ç, Mombers IMH, van Bekkum KA, Woudstra J, Kieft JH, et al.: **Systemic inflammation in childhood obesity: circulating inflammatory mediators and activated CD14++ monocytes**. *Diabetologia* 2012, **55**:2800–2810.

32. Meng H, Liu Y, Lai L: **Diverse ways of perturbing the human arachidonic acid metabolic network to control inflammation**. *Acc Chem Res* 2015, **48**:2242–2250.

33. Varney ME, Hardman WE, Sollars VE: **Omega 3 fatty acids reduce myeloid progenitor cell frequency in the bone marrow of mice and promote progenitor cell differentiation**. *Lipids Health Dis* 2009, **8**:9.

34. Estruch R, Ros E, Salas-Salvadó J, Covas M-I, Corella D, Arós F, Gómez-Gracia E, Ruiz-Gutiérrez V, Fiol M, Lapetra J, et al.: **Primary prevention of cardiovascular disease with a mediterranean diet supplemented with extra-virgin olive oil or nuts**. *N Engl J Med* 2018, **378**:e34.

35. Shively CA, Appt SE, Vitolins MZ, Uberseder B, Michalson KT, Silverstein-Metzler MG, Register TC: **Mediterranean versus Western Diet Effects on Caloric Intake, Obesity,**

Metabolism, and Hepatosteatosis in Nonhuman Primates: Mediterranean and Western Diet in Nonhuman Primates. *Obesity* 2019, **27**:777–784.

36. Bonaccio M, Di Castelnuovo A, De Curtis A, Costanzo S, Persichillo M, Donati MB, Cerletti C, Iacoviello L, de Gaetano G: **Adherence to the Mediterranean diet is associated with lower platelet and leukocyte counts: results from the Moli-sani study**. *Blood* 2014, **123**:3037–3044.

37. Mena M-P, Sacanella E, Vazquez-Agell M, Morales M, Fitó M, Escoda R, Serrano-Martínez M, Salas-Salvadó J, Benages N, Casas R, et al.: **Inhibition of circulating immune cell activation: a molecular antiinflammatory effect of the Mediterranean diet**. *The American Journal of Clinical Nutrition* 2009, **89**:248–256.

38. Soni N, Ross A, Scheers N, Savolainen O, Nookaew I, Gabrielsson B, Sandberg A-S: **Splenic immune response is down-regulated in C57BL/6J mice fed eicosapentaenoic acid and docosahexaenoic acid enriched high fat diet**. *Nutrients* 2017, **9**:50.

39. Siddiqui NFA, Shabrani NC, Kale VP, Limaye LS: **Enhanced generation of megakaryocytes from umbilical cord blood-derived CD34+ cells expanded in the presence of two nutraceuticals, docosahexanoic acid and arachidonic acid, as supplements to the cytokine-containing medium**. *Cytotherapy* 2011, **13**:114–128.

40. Limbkar K, Dhenge A, Jadhav DD, Thulasiram HV, Kale V, Limaye L: **Oral feeding with polyunsaturated fatty acids fosters hematopoiesis and thrombopoiesis in healthy and bone marrow-transplanted mice**. *The Journal of Nutritional Biochemistry* 2017, **47**:94–105.

41. Ito K, Carracedo A, Weiss D, Arai F, Ala U, Avigan DE, Schafer ZT, Evans RM, Suda T, Lee C-H, et al.: **A PML–PPAR-δ pathway for fatty acid oxidation regulates hematopoietic stem cell maintenance**. *Nat Med* 2012, **18**:1350–1358.

42. Kinder M, Wei C, Shelat SG, Kundu M, Zhao L, Blair IA, Puré E: **Hematopoietic stem cell function requires 12/15-lipoxygenase–dependent fatty acid metabolism**. *Blood* 2010, **115**:5012–5022.

43. Shafat MS, Oellerich T, Mohr S, Robinson SD, Edwards DR, Marlein CR, Piddock RE, Fenech M, Zaitseva L, Abdul-Aziz A, et al.: **Leukemic blasts program bone marrow adipocytes to generate a protumoral microenvironment**. *Blood* 2017, **129**:1320–1332.

44. Grundy SM: **Does dietary cholesterol matter?** *Curr Atheroscler Rep* 2016, **18**:68.

45. Gomes AL, Carvalho T, Serpa J, Torre C, Dias S: **Hypercholesterolemia promotes bone marrow cell mobilization by perturbing the SDF-1:CXCR4 axis**. *Blood* 2010, **115**:3886–3894.

46. Feng Y, Schouteden S, Geenens R, Van Duppen V, Herijgers P, Holvoet P, Van Veldhoven PP, Verfaillie CM: **Hematopoietic stem/progenitor cell proliferation and differentiation is differentially regulated by high-density and low-density lipoproteins in mice**. *PLoS ONE* 2012, **7**:e47286.

47. Murphy AJ, Akhtari M, Tolani S, Pagler T, Bijl N, Kuo C-L, Wang M, Sanson M, Abramowicz S, Welch C, et al.: **ApoE regulates hematopoietic stem cell proliferation, monocytosis, and monocyte accumulation in atherosclerotic lesions in mice**. *J Clin Invest* 2011, **121**:4138–4149.

48. Seijkens T, Hoeksema MA, Beckers L, Smeets E, Meiler S, Levels J, Tjwa M, Winther MPJ, Lutgens E: **Hypercholesterolemia-induced priming of hematopoietic stem and progenitor cells aggravates atherosclerosis**. *FASEB j* 2014, **28**:2202–2213.

49. Gu Q, Yang X, Lv J, Zhang J, Xia B, Kim J, Wang R, Xiong F, Meng S, Clements TP, et al.: **AIBP-mediated cholesterol efflux instructs hematopoietic stem and progenitor cell fate**. *Science* 2019, **363**:1085–1088.

50. Ueda M, Dunbar RL, Wolska A, Sikora TU, Escobar M del R, Seliktar N, deGoma E, DerOhannessian S, Morrell L, McIntyre AD, et al.: **A novel APOC2 missense mutation causing apolipoprotein C-II deficiency with severe triglyceridemia and pancreatitis**. *The Journal of Clinical Endocrinology & Metabolism* 2017, **102**:1454–1457.

51. Komatsu T, Sakurai T, Wolska A, Amar MJ, Sakurai A, Vaisman BL, Sviridov D, Demosky S, Pryor M, Ikewaki K, et al.: **Apolipoprotein C-II mimetic peptide promotes the plasma clearance of triglyceride-rich lipid emulsion and the incorporation of fatty acids into peripheral tissues of mice**. *Journal of Nutrition and Metabolism* 2019, **2019**:1–9.

52. Merkel M, Eckel RH, Goldberg IJ: **Lipoprotein lipase: genetics, lipid uptake, and regulation**. *J Lipid Res* 2002, **43**:1997–2006.

53. Liu C, Han T, Stachura DL, Wang H, Vaisman BL, Kim J, Klemke RL, Remaley AT, Rana TM, Traver D, et al.: **Lipoprotein lipase regulates hematopoietic stem progenitor cell maintenance through DHA supply**. *Nat Commun* 2018, **9**:1310.

54. Fong LG, Young SG, Beigneux AP, Bensadoun A, Oberer M, Jiang H, Ploug M: **GPIHBP1 and plasma triglyceride metabolism**. *Trends in Endocrinology & Metabolism* 2016, **27**:455–469.

55. Dragoljevic D, Kraakman MJ, Nagareddy PR, Ngo D, Shihata W, Kammoun HL, Whillas A, Lee MKS, Al-Sharea A, Pernes G, et al.: **Defective cholesterol metabolism in haematopoietic stem cells promotes monocyte-driven atherosclerosis in rheumatoid arthritis**. *European Heart Journal* 2018, **39**:2158–2167.

56. Yvan-Charvet L, Pagler T, Gautier EL, Avagyan S, Siry RL, Han S, Welch CL, Wang N, Randolph GJ, Snoeck HW, et al.: **ATP-binding cassette transporters and HDL suppresses hematopoietic stem cell proliferation**. *Science* 2010, **328**:1689–1693.

57. Westerterp M, Gourion-Arsiquaud S, Murphy AJ, Shih A, Cremers S, Levine RL, Tall AR, Yvan-Charvet L: **Regulation of hematopoietic stem and progenitor cell mobilization by cholesterol efflux pathways**. *Cell Stem Cell* 2012, **11**:195–206.

58. Lang JK, Cimato TR: **Cholesterol and hematopoietic stem cells: Inflammatory mediators of atherosclerosis**. *STEM CELLS Translational Medicine* 2014, **3**:549–552.

59. Butko E, Pouget C, Traver D: **Complex regulation of HSC emergence by the Notch signaling pathway**. *Developmental Biology* 2016, **409**:129–138.

60. Westerterp M, Gautier EL, Ganda A, Molusky MM, Wang W, Fotakis P, Wang N, Randolph GJ, D'Agati VD, Yvan-Charvet L, et al.: **Cholesterol accumulation in dendritic cells links the inflammasome to acquired immunity**. *Cell Metabolism* 2017, **25**:1294-1304.e6.

61. Bazioti V, La Rose AM, Westerterp M: **Myeloid cells regulate plasma LDL-cholesterol levels:** *Current Opinion in Lipidology* 2018, **29**:233–239.

62. Vranić L, Mikolašević I, Milić S: **Vitamin D deficiency: Consequence or cause of obesity?** *Medicina* 2019, **55**:541.

63. Paubelle E, Zylbersztejn F, Maciel TT, Carvalho C, Mupo A, Cheok M, Lieben L, Sujobert P, Decroocq J, Yokoyama A, et al.: **Vitamin D receptor controls cell stemness in acute myeloid leukemia and in normal bone marrow**. *Cell Reports* 2020, **30**:739-754.e4.

64. Janik S, Nowak U, Łaszkiewicz A, Satyr A, Majkowski M, Marchwicka A, Śnieżewski Ł, Berkowska K, Gabryś M, Cebrat M, et al.: **Diverse regulation of Vitamin D receptor gene expression by 1,25-dihydroxyvitamin D and ATRA in murine and human blood cells at early stages of their differentiation**. *IJMS* 2017, **18**:1323.

65. Cortes M, Chen MJ, Stachura DL, Liu SY, Kwan W, Wright F, Vo LT, Theodore LN, Esain V, Frost IM, et al.: **Developmental Vitamin D availability impacts hematopoietic strem cell production**. *Cell Reports* 2016, **17**:458–468.

66. Gore AV, Pillay LM, Venero Galanternik M, Weinstein BM: **The zebrafish: A fintastic model for hematopoietic development and disease**. *WIREs Dev Biol* 2018, **7**:e312.

67. Choudhuri U, Adams JA, Byrom N, McCarthy DM, Barrett J: **1,25-Dihydroxyvitamin D3 induces normal mononuclear blood cells to differentiate in the direction of monocyte-macrophages**. *Haematologia (Budap)* 1990, **23**:9–19.

68. Katayama Y: **Vitamin D receptor: A critical regulator of inter-organ communication between skeletal and hematopoietic systems**. *The Journal of Steroid Biochemistry and Molecular Biology* 2019, **190**:281–283.

69. Kollet O, Dar A, Shivtiel S, Kalinkovich A, Lapid K, Sztainberg Y, Tesio M, Samstein RM, Goichberg P, Spiegel A, et al.: **Osteoclasts degrade endosteal components and promote mobilization of hematopoietic progenitor cells**. *Nat Med* 2006, **12**:657–664.

Chapter III: Literature Review Continued - Roles of Obesity and Exercise on Colon Cancer

Obesity and Systemic Inflammation

Obesity is associated with chronic, low-grade, systemic inflammation. Chronic caloric induces adipocyte hypertrophy and hyperplasia[16]. Lowered vascular density surrounding the enlarged adipocytes can eventually lead to hypoxia and increase inflammatory cytokine release (i.e., IL-6 and TNF-α)[17,18]. In response to the inflammatory environment, circulating monocytes enter the tissue and differentiate into macrophages via C-C chemokine ligand type 2 (CCL2) chemokine interactions with its receptor, CCR2, on the monocyte cell surface[19,20]. Of these macrophages, pro-inflammatory macrophages (M1) propagate the inflammatory condition through IL-6 and TNF-α cytokine release[21,22]. Together, adipocyte and M1 macrophage cytokine release promote a positive feedback loop[23,24]. The chronic low-grade inflammatory state seen in obesity has far-reaching effects on multiple organ systems, where TNF-α and IL-6 induce NF-κB and JAK-STAT signaling[25,26]. One organ system in particular that is impacted by obesity is the large colon, where chronic inflammation is closely linked to elevated cancer risk[27]. The following sections will review colorectal cancer, the relationship between obesity and increased colorectal cancer risk, its potential links to hematopoiesis, and how exercise may be used to mitigate these effects on colon health.

Colorectal Cancer – An Overview

Globally, colorectal cancer ranks third for cancer diagnoses and second for cancer deaths[28,29]. Diagnoses have continually risen since 1970 due to enhanced screening, Western diet consumption, cigarette smoking, excessive alcohol intake, lack of exercise, and elevated obesity

rates[11,12,30–32]. Colorectal cancer involves multiple pathologies that all include epithelial cell dysplasia at the basal layer of the colon mucosa[33,34]. Like all epithelium, these cells have a high turnover rate that leaves them susceptible to altered activity through genetic mutations. Colorectal cancer risk can be enhanced by hereditary means or through environmental factors. Hereditary colorectal cancers account for approximately 10-20% of all colorectal cancer diagnoses[35]. However, identifying a specific proportion has been challenging as many factors related to hereditary colorectal cancer initiation remain unknown[36]. Some single nucleotide polymorphisms have been identified for their role in initiating colorectal neoplasm formation, yet these recognised initiators only account for 4-10% of hereditary disease cases[36,37].

Most colorectal cancers develop initially as pre-cancerous lesions (adenomas) in colonic glands termed aberrant crypt foci (ACF). Over time, these growths become cancerous and eventually metastatic, leading to death if left untreated. There are 3 major colorectal cancer development pathways: (1) the adenoma-carcinoma, (2) serrated neoplasia, and (3) microsatellite instability pathways. The adenoma-carcinoma pathway accounts for 70-90% of colorectal cancers, with the serrated neoplasia pathway accounting for 10-20%, and 2-7% under the microsatellite instability pathway[38]. Of these, the adenoma-carcinoma is the most well-understood.

Familial (hereditary) adenomatous polyposis (FAP) and sporadic colorectal cancers are categorised within the adenoma-carcinoma colorectal cancer development pathway[39,40]. They are characterised by adenomatous polyposis coli (APC) protein gene mutations that lead to enhanced cell proliferation[41,42]. APC is a tumour suppressor gene whose protein, under normal conditions, forms part of a protein complex to promote β-catenin degradation within the Wnt

signaling pathway[43]. Under normal conditions, cytosolic and subsequent nuclear β-catenin concentrations remain low and *Myc* and *Ccnd1* proliferation gene transcription is controlled[44]. When the APC gene obtains a loss of function mutation, the protein complex responsible for marking β-catenin for degradation has a reduced capacity for β-catenin phosphorylation and ubiquitination[44]. Cytosolic β-catenin concentrations elevate, leading to tonic *Myc* and *Ccnd1* gene expression upregulation[44]. This gene upregulation is the earliest step in colorectal epithelial cell dysplasia occurrence, where gross inspection by endoscopy shows initial polyp formation. If left untreated, the polyps eventually form carcinomas enabled through late-stage tumour protein 53 (TP53) tumor suppressor gene mutations[44].

Serrated neoplasms account for 10-20% of diagnosed colorectal cancers[35], with its name derived from its histological presentation as flat lesions lining the colorectal wall[45]. The primary gene mutations strongly associated with serrated neoplasia polyp initiation include the kirsten rat sarcoma (KRAS) and v-Raf murine sarcoma viral oncogene homolog B (BRAF) genes[45,46]. These proto-oncogenes influence cell survival and proliferation through the mitogen-activated protein kinase (MAPK)/extracellular signal-regulated kinase (ERK) metabolic pathway and phosphatidylinositol-3-kinase (PI3K)/Akt/mechanistic target of rapamycin (mTOR) pathway[47–49]. Chronic hypermethylation of cytosine- and guanine-rich promoter regions induces epigenetic silencing of the DNA mismatch repair genes MutL Homolog 1 (MLH1), MutS homologs 2 and 6 (MSH2 & MSH6), and PMS1 protein homolog 2 (PMS2) mutations[50–52]. Without correct DNA mismatch repair mechanisms adenomas transition to carcinomas through microsatellite instability (increased DNA replication error rates in short, repeated sequences)[53].

A very small subset of hereditary colorectal cancers involves dysplastic growths that typically do not incorporate polyp formation that are known as hereditary non-polyposis colorectal cancer (HNPCC) or Lynch syndrome. These hereditary colorectal cancers are caused strictly by microsatellite instabilities and constitute 2-7% of all colorectal cancer diagnoses[38]. Unlike colorectal cancers formed by the adenoma-carcinoma and serrated neoplasia pathways, HNPCCs are not driven by chromosomal instability or DNA hypermethylation. Instead, germ cell inactivation mutations specific to DNA mismatch repair genes occur, thereby restricting the cell's capability to correct for gene mutations upon replication[50,51]. Human carriers will typically possess one DNA mismatch repair gene mutation and can live for many years with normal cell proliferation activity[50,51]. Once the remaining wild type allele mutates, the respective mismatch repair pathway is effectively lost[54]. As sporadic (adenoma-carcinoma) cancers are the most prevalent colorectal cancers in humans, the studies within the current thesis examined sporadic colorectal carcinogenesis within the context of exercise and obesity. This work complements previous work from our lab involving exercise and obesity with a specific focus on its links with inflammation[14].

Colorectal Cancer – The Role of Inflammation

Chronic inflammatory conditions in colorectal tissue are linked to increased colorectal cancer risk. Compared to a healthy population, patients with inflammatory bowel disease are 60% more likely to develop colorectal cancer[27]. In murine colorectal cancer models, anti-inflammatory drug provision reduces colorectal cancer development and tumor growth[55]. Furthermore, mice given dextran sodium sulfate (DSS) alongside azoxymethane (AOM) increases their susceptibility to developing colorectal cancer[56,57]. DSS is a compound used in mouse models

to replicate inflammatory bowel diseases and AOM is given to induce the genetic predisposition for colorectal cancer formation. This model provides evidence that upregulated chronic inflammatory conditions leads to elevated colorectal cancer rates. In humans, multiple studies have found a strong correlation between obesity and colorectal cancer incidence[58–60]. As described earlier, obesogenic conditions propagate a chronic systemic inflammatory condition. There is also evidence suggesting obesity invokes gene expression alterations in colonic epithelium. With obesity, intestinal barrier function can be impaired, with tight junction protein expression decreasing[61,62]. As these tight junctions are responsible for separating the external bacteria-rich environment from the sterile inner environment, loss of tight junction function provides a pathway for bacteria-derived toxin invasion to colon epithelium[63]. This phenomenon has been observed in mice accompanied by an upregulated inflammatory response and colorectal cancer development[62,64]. Finally, mice deficient in pro-inflammatory cytokine expression such as TNF-α and IL-6 display lower colon epithelial damage, attenuated inflammatory immune responses, and lower colorectal cancer development[65–67].

Colorectal Cancer – Relation to Hematopoiesis

An ongoing state of chronic inflammation is clearly partially responsible for colorectal cancer initiation and progression. As described previously, macrophages contribute substantially to systemic inflammatory responses in obesity. Macrophages can exist as tissue-resident cells that originate from the yolk sac or fetal liver during development, or they can form from differentiated monocytes from the bone marrow after birth[68]. Marrow-derived macrophages can be identified through CCR2 expression[20,69]. Colorectal cancer has been linked to elevated bone marrow-derived monocyte infiltration[70,71]. Upon CCL2-CCR2 interactions monocytes migrate

from the bone marrow to peripheral blood and to colon tissue[72]. Monocytes are short-lived cells that continually turn over[73]. Therefore, any increases in resident tissue monocyte content are directly linked to altered monocyte production in the bone marrow[73]. Our lab has previously reported exercise reduces total ACF counts in the colons of mice fed a HFD for 8 weeks compared to sedentary mice[14]. In addition, colon macrophage content is reduced in exercised mice alongside fewer common myeloid progenitor cells in the bone marrow, which differentiate to form monocytes[14]. Gene expression data from colon macrophages show sedentary mice with diet-induced obesity have elevated inflammatory marker content, including TNF-α, tumor growth factor beta (TGF-β), IL1-β, and increased STAT1 and STAT6 expression, that is reduced by exercise[14]. Bader and colleagues (2018) examined a causative role for macrophage content in colorectal cancer incidence, where vesicles loaded with clodronate were used to transiently reduce circulating macrophage populations[13]. They found a lower number of polyps in the colon and a decreased number of large polyps in particular[13]. Collectively, these data suggest exercise induces a lessened inflammatory condition through immune cell signaling to the colon. However, whether exercise attenuates HFD-induced myeloid cell accumulation in the colon and subsequent colon carcinogenesis remains unknown.

Purpose of the Thesis

HFDs and exercise have differential effects on the HSC niche and hematopoiesis. During stress hematopoiesis HFDs promote bone marrow MSC differentiation into adipocytes that in turn promote aberrant myelopoiesis[7]. Conversely, exercise promotes MSC differentiation into osteoblasts that attenuate aberrant myelopoiesis under the same conditions[7]. Systemically, myeloid cell overproduction promotes an inflammatory profile that is linked to elevated colorectal cancer risk[25]. Moreover, exercise attenuates obesity-associated inflammation and reduces colon ACF content. However, the mechanism through which bone marrow cells intercommunicate to regulate hematopoiesis under obese and exercise trained conditions remains unknown. Furthermore, whether myeloid cell accumulation in the colon is responsible for elevated ACF onset in HFD remains unknown. Therefore, identifying the cell-cell communication that promotes aberrant myelopoiesis and its importance for colon ACF onset are crucial for developing novel strategies to prevent ACF formation and progression. The current projects provide a significant foundation that will positively impact Canadians by identifying novel mechanisms by which exercise and obesity regulate hematopoiesis, and link the exercise- and obesity-induced alterations in hematopoiesis to colorectal cancer risk.

Aims and Hypotheses

The current thesis aims to further our understanding of the relationship between obesity, exercise, and hematopoiesis, and to characterize the systemic consequences of these effects on hematopoiesis in the context of colorectal carcinogenesis which is strongly linked to myeloid cell accumulation and inflammation. The thesis is split into three major aims.

Aim 1. Characterize the role of bone marrow-derived extracellular vesicles on hematopoiesis and the HSC niche. We hypothesized that extracellular vesicles from HFD mice would increase HSC and adipocyte progenitor cell concentrations in the bone marrow, and that extracellular vesicles from exercise-trained mice would attenuate these effects.

Aim 2. Understand how HFD and exercise training impacts HSC differentiation and HSC niche cell populations during steady state hematopoiesis. We hypothesized that HFD consumption would induce marrow adipose tissue accumulation and promote myeloid cell formation that would be attenuated by exercise.

Aim 3. Determine the impact of HFD and exercise training on myeloid cell accumulation in the colon and its temporal relationship with inflammation and ACF formation. We hypothesize that HFD will promote ACF formation that is preceded by myeloid cell accumulation and inflammation, and that these effects will be reversed by exercise.

Chapter IV – Thesis Aim 1

The role of exercise and high fat diet-induced bone marrow extracellular vesicles in stress hematopoiesis

James J. Vanhie[1], Wooseok Kim[1], Lisa Ek Orloff[1], Matthew Ngu[1], Nicolas Collao[1], and Michael De Lisio[1,2]

[1]School of Human Kinetics, Faculty of Health Sciences, Ottawa, ON, Canada

[2]Department of Cellular and Molecular Medicine, University of Ottawa, Ottawa, ON, Canada

Keywords: physical activity, obesity, microRNA, myelopoiesis, adipogenesis

Frontiers in Physiology

2022 Nov 23; 13: 1-14

DOI: https://doi.org/10.3389/fphys.2022.1054463

Contribution: James J. Vanhie designed the study, performed the experiments, analyzed the data, interpreted the results of experiments, prepared the figures, drafted the manuscript, and edited and revised the manuscript.

***Correspondence to:**
Michael De Lisio, PhD
Roger Guindon Hall, University of Ottawa
Phone: +1 613-562-5800 ext. 6987
Email: mdelisio@uottawa.ca

Abstract

Exercise and obesity regulate hematopoiesis, in part through alterations in cellular and soluble components of the bone marrow niche. Extracellular vesicles (EVs) are components of the bone marrow niche that regulate hematopoiesis; however, the role of exercise training or obesity induced EVs in regulating hematopoiesis remains unknown. To address this gap, donor EVs were isolated from control diet-fed, sedentary mice (CON-SED), control diet-fed exercise trained mice (CON-EX), high fat diet-fed, sedentary mice (HFD-SED), and high fat diet-fed, exercise trained mice (HFD-EX) and injected into recipient mice undergoing stress hematopoiesis. Hematopoietic and niche cell populations were quantified, and EV miRNA cargo was evaluated. EV content did not differ between the four groups. Mice receiving HFD-EX EVs had fewer hematopoietic stem cells (HSCs) ($p<0.01$), long-term HSC ($p<0.05$), multipotent progenitors ($p<0.01$), common myeloid progenitors ($p<0.01$), common lymphoid progenitors ($p<0.01$), and granulocyte-macrophage progenitors ($p<0.05$), compared to mice receiving HFD-SED EVs. Similarly, mice receiving EX EVs had fewer osteoprogenitor cells compared to SED ($p<0.05$) but enhanced mesenchymal stromal cell (MSC) osteogenic differentiation *in vitro* ($p<0.05$) compared to SED EVs. HFD EVs enhanced mesenchymal stromal cell (MSC) adipogenesis *in vitro* ($p<0.01$) compared to CON EVs. HFD-EX EVs had lower microRNA-193 and microRNA-331-5p content, microRNAs implicated in inhibiting osteogenesis and leukemic cell expansion respectively, compared to HFD-SED EVs. The results identify alterations in EV cargo as a novel mechanism by which exercise training alters stress hematopoiesis and the bone marrow niche.

Introduction

Hematopoiesis, the process of blood cell formation from hematopoietic stem cells (HSCs), occurs in the bone marrow and is regulated by complex interactions between HSCs and their niche. Cellular components of the HSC niche include mesenchymal stem/stromal cells (MSCs), endothelial cells, osteoblasts, adipocytes, neurons, as well as HSC progeny at various stages of differentiation. MSCs are particularly relevant due to their role in regulating hematopoiesis through their secretome and forming other cellular constituents of the HSC niche through their differentiation. Bone marrow cells communicate via paracrine mechanisms that have not been completely described. A greater appreciation for the role in lifestyle factors in regulating the HSC niche and hematopoiesis has recently developed. Preclinical models of diet-induced obesity results in an accelerated accumulation of bone marrow adipose tissue via promoting the adipogenic differentiation of MSCs that is related to the overproduction of inflammatory myeloid cells from HSCs (Emmons et al., 2019). This aberrant myelopoiesis is believed to contribute to systemic inflammation in obesity. Conversely, data from our lab and others have shown that participation in increased levels of physical activity and exercise training reduces marrow adipose tissue due to increased osteogenic MSC differentiation, reverses aberrant myelopoiesis, and decreases HSC turnover under obesogenic conditions (Styner et al., 2014; Emmons et al., 2019). The paracrine mechanisms responsible for the effects of obesity and physical activity/exercise training on hematopoiesis and the bone marrow niche have not been completely described.

Systemically, obesity is characterized by chronic low-grade inflammation that is accompanied by elevated levels of active immune cells in peripheral tissues that secrete pro-inflammatory cytokines (Benova and Tencerova, 2020). In bone marrow, inflammation induces

HSC proliferation that promotes pre-emptive HSC pool exhaustion and skews HSC differentiation along the myeloid lineage to form common myeloid progenitor cells (CMPs), granulocytes, and monocytes, thus further exacerbating systemic inflammation (Trottier et al., 2012; Singer et al., 2014). This myeloid cell skewing from HSCs is due, in part, to increased marrow adipose tissue content formation from MSCs (Ambrosi et al., 2017). Styner and colleagues previously linked diet-induced obesity to marrow adipose tissue content formation in mice through high-fat diet (HFD) feeding, finding that exercise was capable of mitigating adipocyte production (Styner et al., 2014). Furthermore, other reports have shown that bone marrow adipocytes are capable of promoting HSC proliferation and differentiation (Poloni et al., 2013; Zhang et al., 2019). Recent work from our lab and others has shown that exercise influences hematopoiesis through alterations to the HSC niche. For example, we have previously shown that acute exercise stimulates HSC mobilization from the bone marrow and alters MSC gene expression (Emmons et al., 2016). Other work from our lab investigating exercise training surrounding a single exposure to sublethal whole-body irradiation found lower adipose tissue accumulation and differentially expressed soluble factors in the marrow of exercise trained mice compared to sedentary groups (Emmons et al., 2019). Furthermore, Frodermann and colleagues identified leptin signaling from adipocytes and C-X-C motif chemokine ligand 12 (CXCL12) from MSCs as key mediators of HSC expansion (Frodermann et al., 2019). The current literature suggests that paracrine signaling between bone marrow cells regulate obesity- and exercise-induced alterations in hematopoiesis (Poloni et al., 2013; Emmons et al., 2016, 2019; Zhang et al., 2019).

EVs are membrane-bound particles that are secreted by all cells and act as intercellular mediators of communication (Yáñez-Mó et al., 2015; Doyle and Wang, 2019). EVs transfer miRNA

and protein to alter recipient cell activity and fate (Ratajczak et al., 2006; Valadi et al., 2007; Skog et al., 2008). Szatmári and colleagues found that injecting EVs from irradiated mice into non-irradiated mice reduced HSC content comparable to direct radiation treatment (Szatmári et al., 2017). Conversely, Wen and colleagues showed non-irradiated MSC-derived EV injections into irradiated mice improves circulating white blood cell concentration recovery, thereby suggesting a role for EVs in promoting stress hematopoiesis (Wen et al., 2016). These findings demonstrate that EVs influence HSC activity and fate. To date, there has not been a full characterization of the paracrine factors regulating hematopoiesis with exercise and HFD. However, previous reports have shown exercise impacts EV production. In skeletal muscle, miR-486 is downregulated following a bout of acute exercise (Aoi et al., 2013); miR-486 has also been linked to erythrocyte formation, thereby indicating a systemic role for EVs in affecting hematopoiesis (Shi et al., 2017). Other reports have shown exercise training increases total circulating EV and circulating endothelial cell-derived EV concentrations (Bei et al., 2017; Ma et al., 2018).

Although prior studies have examined the role of EVs in regulating stress hematopoiesis (Wen et al., 2016; Szatmári et al., 2017), no study has investigated the alterations to bone marrow-derived EV cargo by exercise or HFD, or their impact on HSC and HSC niche cell content. Therefore, the purpose of the current study was to examine the effects of EVs derived from exercise trained and sedentary mice given a HFD or control (CON) diet on stress hematopoiesis in naïve mice. We hypothesized that EVs from mice fed a HFD would increase HSC and adipocyte progenitor cell concentrations in the bone marrow, and that EVs from exercise-trained mice would attenuate these effects.

Materials and Methods

Experimental Design

All protocols were approved by the University of Ottawa Animal Care Committee in accordance with the *Animals for Research Act* and by the Canadian Council on Animal Care. Mice were maintained on a 12:12 hour light-dark schedule with food and water provided *ad libitum.* Cohort 1 was used to derive EVs. For the first cohort, male CBA (n=40; Jackson Laboratories, United States) mice aged 5 weeks were randomly selected for 8 weeks of 45% fat (HFD; D12451, Research Diets, NJ, United States) or control (CON; D10012M, Research Diets, NJ, United States) diet feeding (Figure 4.1). After 4 weeks on their respective diets, half of the mice in each condition were randomly selected for exercise training (EX) while the rest remained sedentary (SED). Cohort 2 mice were EV recipients. For Cohort 2, male and female CBA mice (n=3-4 per group) were irradiated with 3 Gy of whole-body gamma radiation using a X-Rad 320 biological irradiator (Precision X-Ray, Madison, Connecticut, USA) to induce stress hematopoiesis. At 24-hr post-irradiation, Cohort 2 mice were injected with bone marrow-derived EVs isolated from non-irradiated Cohort 1 mice. Cohort 2 mice remained sedentary and were fed standard chow (Teklad 2018 Rodent Diet, Envigo, Indianapolis, IN, USA) *ad libitum* throughout the study. Four weeks after EV injection, bone marrow was collected for cell content analysis from Cohort 2 mice.

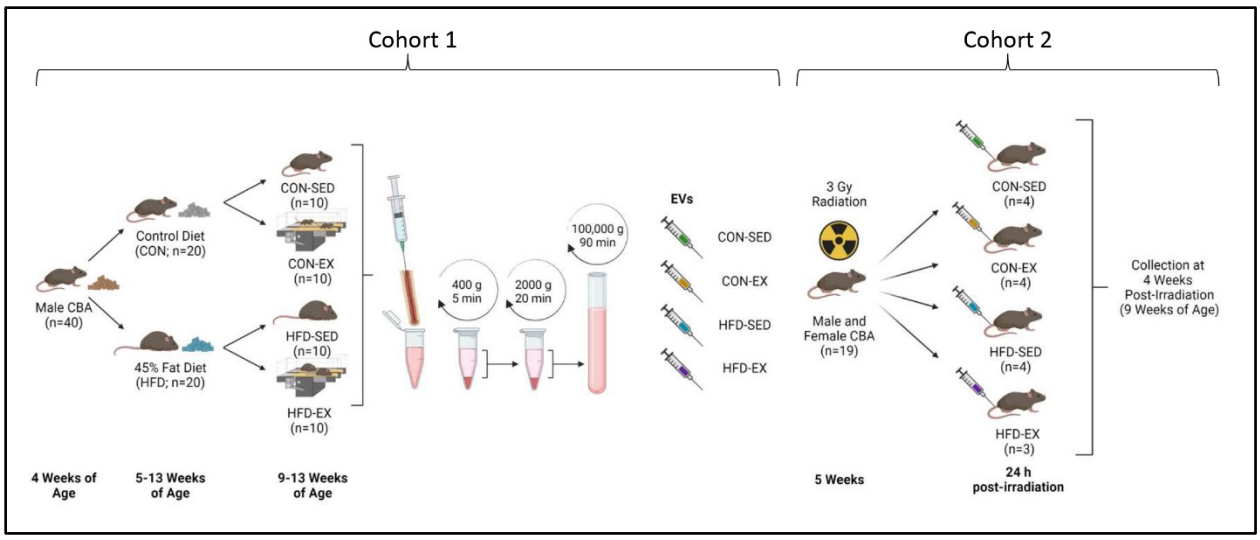

Figure 4.1. Study outline for EV isolation and injection. Male CBA mice (n=40) were placed on high-fat (HFD) or control (CON) diets for 8 weeks with the latter 4 weeks including exercise (EX) or sedentary (SED) conditions. Bone marrow was extracted, and extracellular vesicles (EVs) isolated by differential centrifugation. Collected EVs were combined by group and injected into new male and female CBA mice by tail vein 24 hours following ionising radiation injury. Bone marrow samples were collected at 4 weeks post-irradiation. Created with BioRender.com.

Endurance Test and Exercise Training

Mice in Cohort 1 underwent an endurance test using a Exer 3/6 treadmill (Columbus Instruments, Columbus, OH, USA) angled upwards at 5°, as described previously, to evaluate training status (Baker et al., 2011; De Lisio et al., 2011, 2013; De Lisio and Parise, 2012; Emmons et al., 2019; Farber et al., 2021). All mice were acclimated for 10 minutes at 8 $m \cdot min^{-1}$ the week prior to the endurance test. Cohort 1 mice ran at 10 $m \cdot min^{-1}$ and increased speed once every two minutes by 1 $m \cdot min^{-1}$ until the mice were resistant to running or were unable to keep their hind limbs on the treadmill for one full stage despite gentle encouragement. The mice were encouraged to run using a soft-bristle paint brush; electric shock was not used for any test. Following the endurance test, Cohort 1 mice underwent an exercise training program, as described previously (Baker et al., 2011; Emmons et al., 2019; Farber et al., 2021). The exercise

training program involved three exercise sessions per week for 40-60 min, depending on the training week. The exercise protocol consisted of a warm-up period at 8 $m \cdot min^{-1}$ for 10 min for the first 3 weeks (10 $m \cdot min^{-1}$ for week 4) followed by an 8-10 $m \cdot min^{-1}$ training speed for 25- (week 1), 35- (week 2), or 45- (weeks 3, 4) min and a cooldown period at 8 $m \cdot min^{-1}$ for 5 min. Sedentary mice were placed in sham treadmills on top of the running treadmill to account for any stress associated with the treadmill vibrations, noise, and handling.

Extracellular Vesicle Characterization, Injection, and miRNA Quantification

EVs were isolated from the bone marrow supernatant via differential ultracentrifugation as described previously, with minor modifications (Lobb et al., 2015). Briefly, bone marrow was extracted from Cohort 1 mice femurs and tibias using a 25-gauge needle and 1 mL of phosphate-buffered saline (PBS), followed by a 400 g centrifugation cycle at 4°C for 5 min. The supernatant was stored at -80°C for later analysis and injection. After thawing, the supernatant was centrifuged at 2000 g at 4°C for 20 minutes to remove any remaining cell fragments and apoptotic bodies. The supernatant was removed and ultracentrifuged thereafter at 100,000 g at 4°C for 90 min using an Optima MAX-Micro Ultracentrifuge (Beckman Coulter, Brea, CA, USA). EV pellets were resuspended with 110 µL sterile PBS, of which 10 µL was used for concentration and size distribution analysis at 1:100 dilution using the ZetaView PMX 110 Multiple Parameter Particle Tracking Analyzer (Particle Metrix, Meerbusch, Germany). Relative to *in vitro* isolation, bone marrow offers a small pool of EVs. Across all groups, we found that our bone marrow EV yield averaged 420 million particles per sample. Based on our quantification we were able to combine grouped samples to increase the EV injection counts to 650 million per mouse in Cohort 2, with some remaining samples available for follow-up miRNA content and *in vitro* C3H 10T1/2 MSC

adipogenic and osteogenic analysis. Following EV quantification, EVs were combined by exercise and dietary condition and injected via tail vein. Mice were weighed prior to injection with sample volumes standardised across each mouse to 8 µL/g body weight. EV isolation was confirmed by Western blot using 30 µg of protein derived from 6 combined bone marrow EV samples and MSC lysate. Antibodies included anti-TSG101 (T5701, Sigma-Aldrich), anti-Alix (SAB4200476, Sigma-Aldrich), anti-Flotillin-2 (#3436S, Cell Signaling Technology) diluted 1:1000 in 5% bovine serum albumin-diluted tris-buffered saline with 1% Tween 20 (TBST). Horseradish peroxidase-linked secondary antibody (7074S, Cell Signaling Technology) was diluted 1:10,000 in 5% milk-TBST. The membranes were incubated for 5 min using SuperSignal West Pico PLUS enhanced chemiluminescent substrate (ThermoFisher Scientific, MA, United States) and visualized using a ChemiDoc Imaging System (Bio-Rad, CA, United States)

EV miRNA cargo from individual mice in Cohort 1 (n=3 per group) was isolated using the Qiagen miRNEasy Micro kit (Hilden, Germany) according to the manufacturer's instructions. Extracted miRNA sample integrity and concentrations were measured using a Nanodrop 2000 (Thermo Fisher Scientific, Waltham, MA, USA), with concentrations ranging from 47.7-166.6 ng/µL. Using 100 ng of isolated miRNA, specific miRNA content expression was identified using the Nanostring mouse v1.5 miRNA kit as per the manufacturer's instructions (Nanostring, Seattle, WA, USA). The prepared cartridges were read using a Nanostring nCounter station. One CON-SED and two CON-EX samples did not pass quality control measures on Nanostring's proprietary nSolver 4.0 software and were excluded from statistical analysis. The HFD-SED and HFD-EX samples were analyzed using the ROSALIND analysis program (Seattle, WA, USA). Briefly, the nCounter-derived RCC files for the HFD-SED and HFD-EX conditions (n=3 per condition) were

uploaded to the ROSALIND website. The samples were normalized by positive control and codeset normalization with fold-changes and significance calculated by the Student's t-test. Absolute-fold changes of ±1.25 or greater (the default value by ROSALIND) and a p-value lower than 0.05 were considered significant. miRNAs that were differentially expressed underwent further investigation for potential gene targets using the miRWalk miRNA target mining feature (http://mirwalk.umm.uni-heidelberg.de/). All differentially expressed miRNAs were inserted to the search list and subsequent gene set enrichment analysis was selected for KEGG and GO:BP enrichment pathways. The top 5 results for the Kyoto Encyclopedia of Genes and Genomes (KEGG) and Gene Ontology: Biological Processes (GO:BP) enrichment pathways were recorded for literature investigation.

Bone Marrow Collection and Cell Quantification

Mice were euthanized at four weeks post-EV injection by CO_2 asphyxiation followed by cervical dislocation. Femurs and tibiae were isolated for bone marrow extraction. Phosphate-buffered saline (PBS) was flushed at least 6 times through the bone marrow cavity to maximize bone marrow tissue collection. The cell suspension was centrifuged at 400 g at 4 °C for 5 min and the EV-rich supernatant was frozen at -80 °C immediately. The remaining cell pellet was gently resuspended with 5% fetal bovine serum (FBS) with PBS and stored on ice until further processing. To extract any remaining cells, the bones were crushed once with a pestle and mortar, cut into tiny fragments, and chemically digested for 45 minutes with 0.2% type II collagenase diluted in high glucose DMEM. The cells were triturated every 15 minutes to promote chemical digestion. Bone marrow content from flushing and bone digestion were combined,

filtered through a 70 µm filter, and centrifuged at 400 g at 4°C for 5 min. The pellets were collected and resuspended in 5% FBS for flow cytometry staining.

Cohort 2 bone marrow bone marrow cells were quantified using an Attune NxT flow cytometer (Thermo Fisher Scientific), as described previously (De Lisio and Parise, 2012; Emmons et al., 2016, 2019). All cell identification strategies are summarized in Table 4.1, and all antibodies, fluorophores, and associated catalog numbers are summarized in Table 4.2. Live cells were used for the Zombie Yellow viability dye compensation. The flow cytometry gating was based on unstained and single-stained bone marrow cells (Figure S4.1).

Table 4.1. Flow cytometry gating strategies for HSPC and niche cell populations.

Cell Population	Gating Strategy
Hematopoietic Stem Cells (HSCs)	Lineage$^-$, Sca-1$^+$, c-Kit$^+$ (LSK)
Long-Term HSCs	LSK, CD48$^-$, CD150$^+$
Short-Term HSCs	LSK, CD48$^-$, CD150$^-$
Multipotent Progenitors	LSK, CD48$^+$, CD150$^-$
Common Myeloid Progenitors	LSK, CD16/32^{int}, CD34^{int}
Common Lymphoid Progenitors	Lineage$^-$, Sca-1^{int}, c-Kit$^-$
Granulocyte-Monocyte Progenitors	LSK, CD16/32^{hi}, CD34$^+$
Megakaryocyte-Erythroid Progenitors	LSK, CD16/32$^-$, CD34$^-$
Mesenchymal Stromal Cells	Ter119$^-$, CD45$^-$, CD31$^-$, CD51$^+$, CD140α$^+$
Endothelial Cells	Ter119$^-$, CD45$^-$, CD31$^-$, CD51$^-$
Adipocyte Progenitors	Ter119$^-$, Sca-1$^+$, CD45$^-$, CD31$^-$, CD51$^-$
Osteoblasts	Ter119$^-$, Sca-1$^-$, CD45$^-$, CD31$^-$, CD51$^+$
Osteoprogenitors	Ter119$^-$, Sca-1$^+$, CD45$^-$, CD31$^-$, CD51$^-$

C3H 10T1/2 Proliferation and Differentiation Assays

C3H 10T1/2 cells are a model of bone marrow stromal cells that are capable of induced osteogenic and adipogenic differentiation (Shea et al., 2003; Huang et al., 2009). To observe the effects of HFD- and EX-induced EVs on MSC proliferation and differentiation directly, C3H 10T1/2 cells were plated on 96-well plates (1250 cells per well) with 100 µL of growth media (10% FBS, 1% penicillin-streptomycin, in high-glucose Dulbecco's Modified Eagle Medium; DMEM) and incubated at 37°C for 72 hours to reach 90% confluence. Cells were then given either adipogenic or osteogenic differentiation media. For the initial plating and each concurrent media change, cells were supplemented with 5.1 million EVs. This value represented approximately twice the EV concentration injected into the mice and was selected to directly measure the effects of HFD- and EX-EVs on MSC differentiation and/or proliferation. Adipocyte differentiation was induced using the Mesencult adipogenic differentiation kit according to the manufacturer's instructions (Stemcell Technologies, Vancouver, BC, Canada). Two days after adding differentiation media, cells were supplemented with 1 µg/mL of insulin to induce adipocyte cell maturation for another 3 days. After 5 days of differentiation media supplementation, cells were fixed in 10% formalin on a rocker for 30 min at room temperature, washed twice with 100 µL of distilled water, and stained with 100 µL of 0.5% Oil Red O dye on a rocker for 30 min at room temperature while protected from light. Unbound dye was washed away by washing the wells 3 times with distilled water. The remaining bound dye was removed by adding 200 µL of isopropanol and was incubated on a rocker at room temperature for 10 min while protected from light. 100 µL of the isopropanol-Oil Red O dye solution was transferred to a new 96-well plate and measured by spectrophotometry at 492 nm. Osteogenesis was induced using the Mesencult osteogenic

differentiation kit according to the manufacturer's instructions (Stemcell Technologies). Osteogenic differentiation media was replaced every 3 days for 14 days. After 14 days of differentiation, cells were fixed in 10% formalin on a rocker for 30 min at room temperature, washed twice with 100 µL of distilled water, and stained with 100 µL of 0.2% Alizarin Red S dye on a rocker for 20 min at room temperature while protected from light. Alizarin Red S preparation and extraction was conducted as outlined by Gregory and colleagues using 10% of the listed volumes to account for the 96-well plate volume capacity (Gregory et al., 2004). Absorbance was read on a spectrophotometer at 405 nm.

The effects of HFD- and EX-EVs on C3H 10T1/2 cell proliferation were measured using the Alexa Fluor 488 Click-iT EdU cell proliferation kit according to the manufacturer's instructions (C10337, Thermo Fisher Scientific). Briefly, 1250 cells were added to each well in a 96-well plate with 100 µL of growth media, as described above, and were incubated for 2 hours at 37°C to allow cell adhesion to the plate. After 2 hours, 50 µL of the cell culture media was removed and replaced with 50 µL of 20 µM EdU labeling solution (for a final concentration of 10 µM) containing 5.1 million EVs per well. Cells were fixed with 100 µL 4% formaldehyde at 6-, 12-, 24-, and 48-hours post-media change, washed twice with 100 µL of 3% BSA in PBS, and permeabilized with 100 µL 0.5% Triton X-100 in PBS. To detect EdU-incorporated cells 50 µL of the Click-iT Plus reaction cocktail (85.76% 1X Click-iT reaction buffer, 4% Copper protectant, 0.24% Alexa Fluor picolyl azide, 10% 1X Click-iT EdU buffer additive) was added to each well and incubated for 30 min at room temperature while protected from light. Wells were then washed with 100 µL 3% BSA in PBS and again with 100 µL PBS. To stain all DNA, 1X Hoeschst 33342 (5 µg/mL) was added to each well and incubated for 30 minutes at room temperature while protected from light. The

wells were then washed twice with 100 µL PBS. Plates were imaged and analyzed with a ZEISS CellDiscoverer7 microscope.

Table 4.2. Antibodies used for flow cytometry.

Antibody	Conjugate	Dilution	Product Number
CD16/32	BV711	1:200	101337
CD31	BV510	1:200	563089
CD34	Pe-Cyanine5	1:200	119312
CD45	PE-Cyanine7	1:200	552848
CD48	BV510	1:200	563536
CD51	BV421	1:200	740062
Sca1 (Ly6A/E)	PE	1:200	553336
cKit (CD117)	PE-Cyanine7	1:200	558163
CD140a	PE	1:200	562776
CD150	BV421	1:200	562811
Lineage Panel (5)	Biotin	1:200 (5:200 total)	559971
Streptavidin	FITC	1:800	554060
Viability	Zombie Yellow	1:300	423104

Statistical analysis

Flow cytometry and C3H 10T1/2 *in vitro* proliferation and differentiation data were analyzed using a two-factor (diet and exercise) ANOVA followed by a Sidak post-hoc analysis for interaction effects. The two-factor ANOVAs were carried out using GraphPad Prism 9 (GraphPad Software). A Student's t-test was conducted by ROSALIND software to compare HFD-SED and HFD-EX miRNA data. All data are presented as mean ± SEM with $p<0.05$ being considered statistically significant. Investigators were blinded to all files and experimental groups for all analyses.

Results

Exercise increases EV concentration at specific sizes.

EV isolation was confirmed through Western blot analysis using the positive markers; ALIX, Flotillin-2, and TSG 101, according to recommended guidelines (Willms et al., 2016; Théry et al., 2018), with MSC lysate included as a positive control (Figure 4.2A). NTA revealed no difference in average particle concentration between any groups (n=10 per condition) (Figure 4.2B). Most EV particles were smaller than 200 nm in size, an expected observation as a large proportion of extracellular vesicles are small EVs that are typically 30-200 in size. However, EV concentration was higher in CON-EX vs. CON-SED at 225 ± 15 nm ($p<0.05$), and there was a main effect of exercise having higher EV concentrations at 315±15 and 345±15 nm ($p<0.05$) (Figure 4.2C).

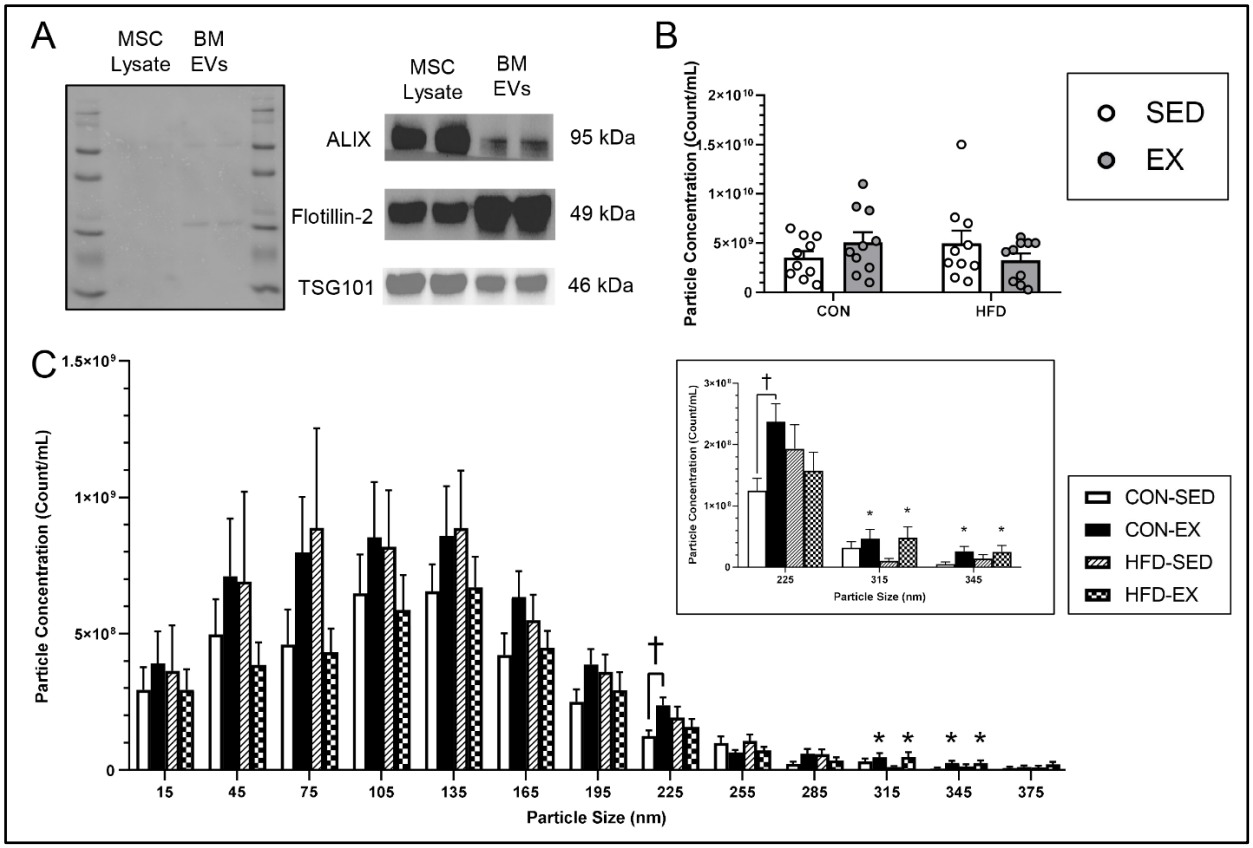

Figure 4.2. Characterization of extracellular vesicle (EVs) isolated from bone marrow supernatant of high-fat (HFD) or control (CON) diet-fed mice placed on exercise (EX) or sedentary (SED) conditions. (**A**) EV presence confirmation by mesenchymal stromal cell (MSC) lysate positive control measures of ALIX, Flotillin-2, and TSG101 proteins, (**B**) Total extracted particle concentration measured by nanoparticle tracking analysis (n=10 per group), and (**C**) EV size distribution of injected EVs. $^{\#}p<0.05$, high-fat diet difference versus control diet (n=10 per group).

Extracellular vesicles from EX mice reverse HSC expansion and myeloid progenitor cell skewing with HFD during stress hematopoiesis.

Mice injected with HFD-EX EVs had lower concentrations of HSC (Figure 4.3A), long-term HSC (LT-HSC) (Figure 4.3B), multipotent progenitor (MPP) (Figure 4.3D), CMP (Figure 4.3E), common lymphoid progenitor (CLP) (Figure 4.3F), and granulocyte-macrophage progenitor cells (Figure 4.3G) compared to mice injected with HFD-SED EVs (all $p<0.05$). There was also a trend for fewer short-term HSCs (ST-HSCs) following injection of EX EVs compared to SED (Figure 4.3C,

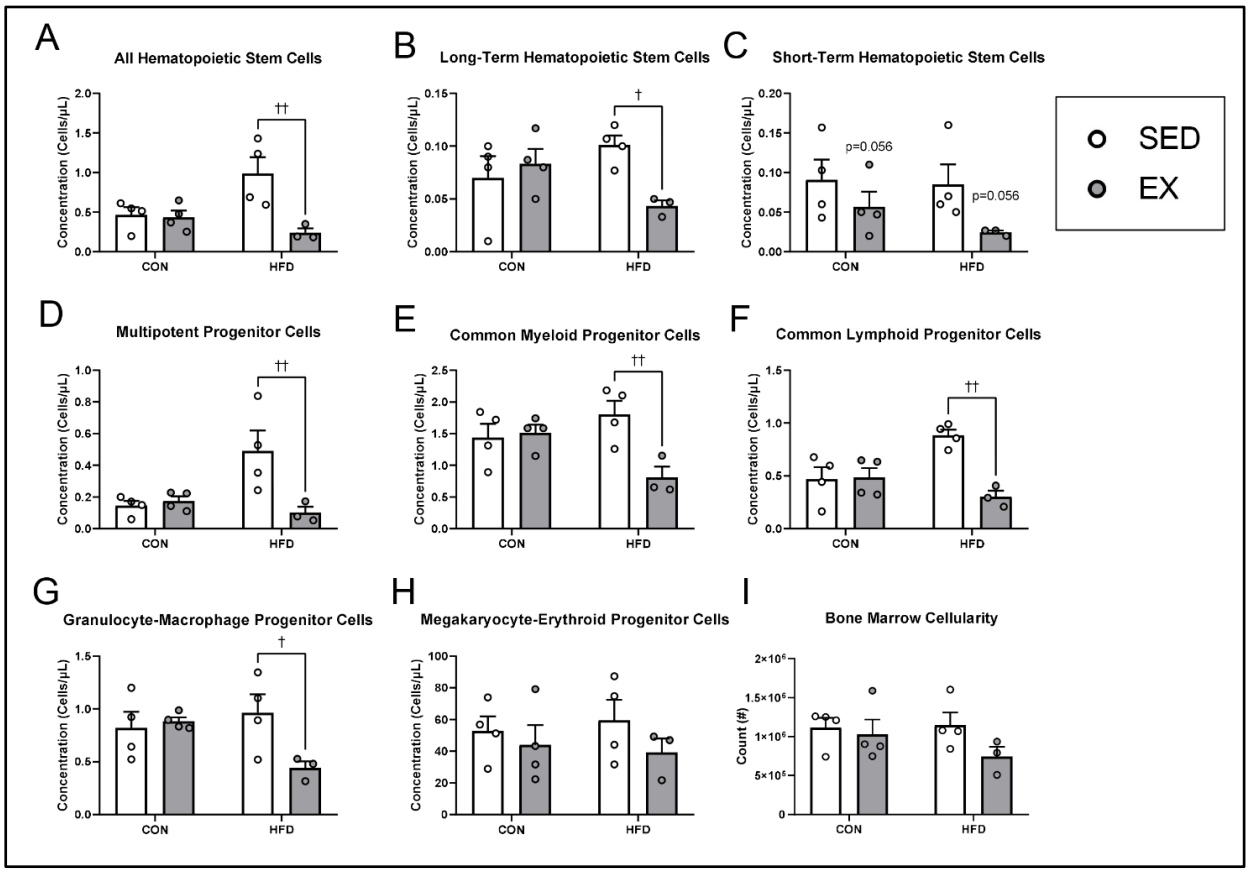

Figure 4.3. Extracellular vesicles from exercise-trained (EX) mice given a high-fat diet (HFD) return hematopoietic stem (HSC) and progenitor cell concentrations to control diet levels. (**A**) All HSCs, (**B**) long-term HSCs, (**C**) short-term HSCs, (**D**) multipotent progenitor cells, (**E**) common myeloid progenitor cells), (**F**) common lymphoid progenitor cells, (**G**) granulocyte-macrophage progenitor cells, (**H**) megakaryocyte-erythroid progenitor cells., (**I**) total bone marrow cellularity. $^{\dagger}p<0.05$ interaction effect; $^{\dagger\dagger}p<0.01$ interaction effect (n=4 per group, HFD-EX n=3).

p=0.056). There were no effects of HFD or EX EVs on megakaryocyte-erythroid progenitor (MEP) cells (Figure 4.3H) or on total bone marrow cellularity (Figure 4.3I).

EVs from EX mice reduce osteoprogenitor cell concentration during stress hematopoiesis.

Mice injected with neither EX nor HFD EVs impacted MSC (Figure 4.4A), adipocyte progenitor (HFD-EX vs. HFD-SED interaction p=0.14) (Figure 4.4B), endothelial (Figure 4.4C), or osteoblast (Figure 4.4E) concentrations during stress hematopoiesis. Mice injected with EX EVs; however, had lower osteoprogenitor cell concentrations ($p<0.05$) (Figure 4.4D).

HFD EVs increase MSC adipogenic differentiation and EX EVs increase osteogenic differentiation

Since EX EVs decreased osteoprogenitor cell concentrations, we investigated whether HFD and EX EVs directly impact MSC fate. There was no effect of HFD EVs or EX EVs on MSC proliferation, although a trend (p=0.098) was seen for higher proliferation at 6 hours post-Edu addition with CON-SED EVs compared to CON-EX EVs (Figure 4.5A). MSCs treated with HFD EVs *in vitro* had higher adipogenic differentiation ($p<0.01$) compared to MSCs treated with CON EVs (Figure 4.5B). Conversely, MSCs treated with EX EVs had higher osteogenic differentiation ($p<0.05$) compared to MSCs treated with SED EVs (Figure 4.5C).

HFD-EX EVs have lower miR-193 and miR-331-5p content compared to HFD-SED EVs.

We conducted a high-throughput miRNA screen from EVs in the current study to determine if alterations in miRNA cargo may explain our observed alterations to the various bone marrow cell

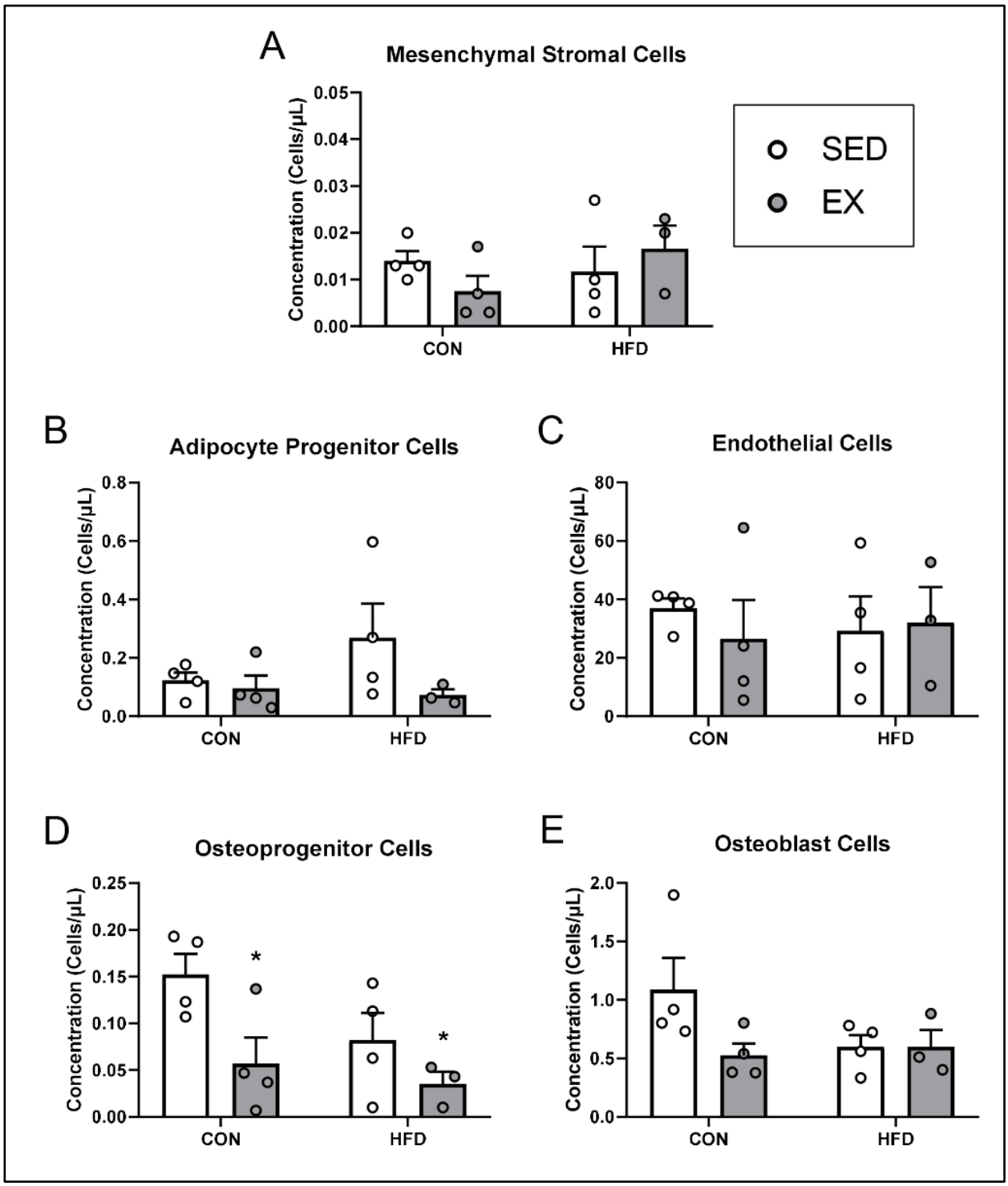

Figure 4.4. Extracellular vesicles from exercise-trained mice decrease osteoprogenitor cell concentrations. (**A**) Mesenchymal stromal cells, (**B**) adipocyte progenitor cells, (**C**) endothelial cells, (**D**) osteoprogenitor cells, and (**E**) osteoblast cells. *p<0.05 main effect of exercise (n=4 per group, HFD-EX n=3).

populations. We focused this screen on HFD-SED and HFD-EX based on changes observed in our flow cytometric results and to determine the extent to which exercise training could reverse the effects of HFD. Our analysis of 577 distinct mouse miRNAs revealed lower miR-193 (2.00 fold, p<0.01) and miR-331-5p (2.63 fold, p<0.05) content in HFD-EX (n=3) compared to HFD-SED (n=3) (Figure 4.6A).

Using miRWalk, we identified the top 5 predicted target pathways of both miR-193 and miR-331-5p combined by KEGG and GO:BP analysis (Figure 4.6B). KEGG analysis predicts miRNA control of genes and the affected general metabolic pathways while GO:BP predicts more detailed molecular functions. KEGG analysis showed predictive activity in the MAPK, ErbB, and Rap1 signaling pathways alongside pathways in cancer and axon guidance, while GO:BP analysis showed predictive interactions with the canonical Wnt signaling pathway, transcription, regulation, apoptosis, endocytosis, and intracellular signal transduction.

Discussion

Exercise and obesity induce significant alterations to bone marrow architecture and HSC activity (Styner et al., 2014; Emmons et al., 2016). Given that EVs regulate hematopoiesis (Wen et al., 2016; Szatmári et al., 2017), and exercise training increases circulating EV concentrations (Bei et al., 2017), we sought to understand the role of exercise- and high fat diet-induced EVs as molecular mediators of stress hematopoiesis and bone marrow remodeling. In diet-induced obesity, exercise-induced EVs reversed the effects of diet on HSC concentrations and induced

MSC differentiation along the osteogenic lineage during stress hematopoiesis. Interestingly, HFD-induced obesity resulted in bone marrow EVs that promoted adipogenesis *in vitro*. We further identified down-regulation of miR-193 and miR-331-5p content in exercise-induced EVs from high fat diet-fed mice as a potential molecular target responsible for these effects. Together, our findings suggest that bone-marrow derived EVs from EX mice partially reverse the effects of HFD

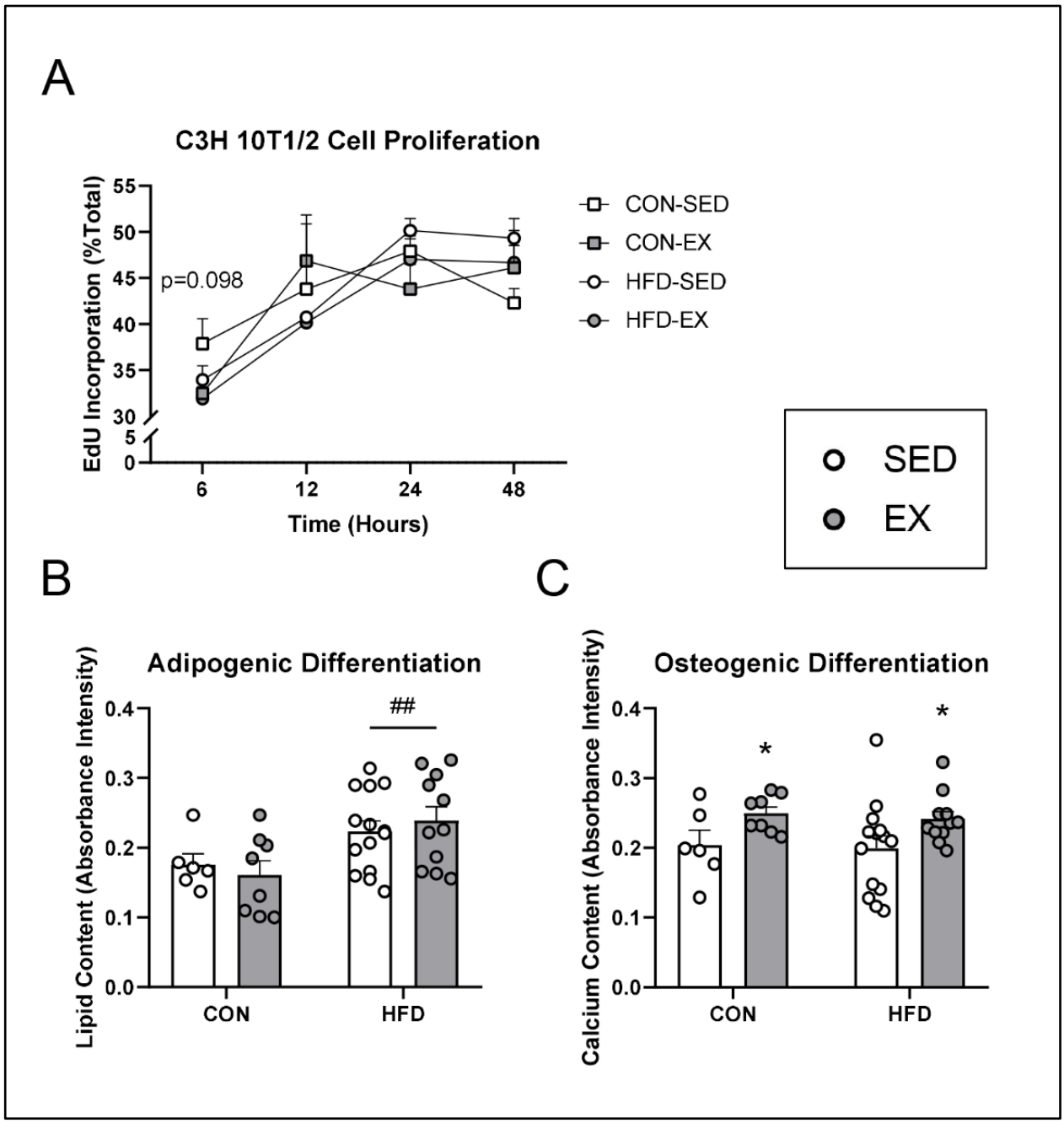

Figure 4.5. Extracellular vesicles (EVs) impact mesenchymal stromal cell (MSC) differentiation activity in vitro. C3H/10T1/2 MSCs were differentiated into either adipocytes and stained with Oil Red O or osteoblasts and stained with Alizarin Red S dye. (**A**) Proliferation by EdU stain at 6, 12, 24, and 48 hours. (**B**) EVs from high-fat diet-fed mice increased adipogenic differentiation and (**C**) EVs form exercise-trained mice increased osteogenic differentiation. *p<0.05 main effect of exercise; ##p<0.01 main effect of high-fat diet (n=6-14 per group).

EVs on hematopoiesis and the HSC niche providing a novel mechanism for the effects of exercise on hematopoiesis.

Previous studies that have examined EVs in response to exercise have focused mostly on the effects of acute exercise-induce and circulating EVs on skeletal muscle adaptations to exercise (Nederveen et al., 2021). The present study provides the first description of exercise-induced EVs specifically from the bone marrow, and also the first investigation of the effects of exercise-induced EVs on hematopoiesis. Acute exercise studies have shown elevated circulating EV concentrations immediately following a stepwise cycling test to exhaustion that subsided at 90-min post-exercise (Frühbeis et al., 2015). However, similar to our findings in bone marrow, previous work has indicated that chronic exercise training does not result in any changes to total EV concentration but found an altered miRNA expression profile (Hou et al., 2019). As such, it appears that changes in total EV concentrations may be part of the normal stress response to unaccustomed exercise, while training may have a larger impact on EV cargo. Despite no alterations to total EV concentration with HFD or EX, we found a redistribution of EV size in response to EX with EX mice having higher EV concentration at 315±15 and 345±15 nm, and specifically in CON diet condition compared to HFD at 225±15 nm. This size range corresponds to large EVs (>100 nm) which predominantly originate as microvesicles that are formed directly from plasma membrane budding (Ståhl et al., 2019). This origin disparity leads to varying cargo

profiles (Bruschi et al., 2019) that differentially impact cell function (Wen et al., 2016). These data suggest EX alters EV release in a way that partially reverses the consequences of diet-induced obesity.

Previous reports from our lab and others indicate exercise impacts hematopoiesis via paracrine actions in the HSC niche (Emmons et al., 2016; Wen et al., 2016; Szatmári et al., 2017; Frodermann et al., 2019). Therefore, to determine the role of EVs in these effects, we injected the isolated EVs from HFD and EX mice into naïve mice undergoing radiation-induced stress

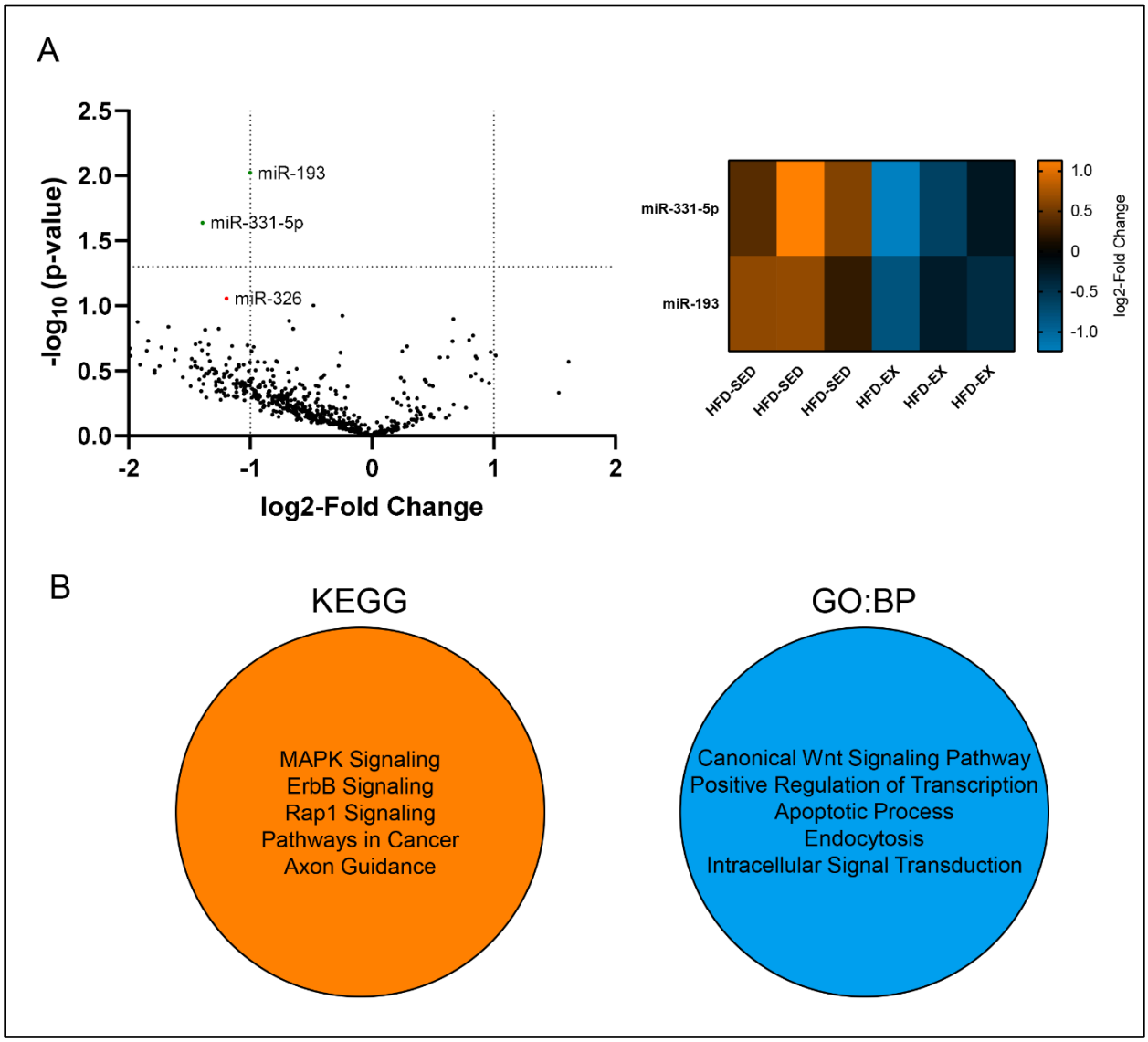

Figure 4.6. Extracellular vesicles (EVs) from high-fat diet exercise-trained (HFD-EX) mice have lower miR-331-5p ($p<0.05$) and miR-193 ($p<0.01$) expression compared to HFD-sedentary (HFD-SED) mice. **(A)** Volcano plot of all measured miRNAs and heatmap of differentially expressed miRNAs. miR-326 approached lower expression in HFD-EX EVs compared to HFD-SED ($p=0.0877$). The vertical dotted lines represent the margin for physiologically meaningful expression changes as per default ROSALIND analysis. The horizontal dotted line represents statistical significance ($p=0.05$). (n=3 per group). (**B**) Kyoto Encyclopedia of Genes and Genomes (KEGG) and Gene Ontology: Biological Processes (BP) predicted target pathways by miRWalk combined analysis of miR-193 and miR-331-5p.

hematopoiesis. We injected EVs 24 hours post-irradiation because Wen and colleagues had previously shown that injecting EVs at this timepoint following radiation altered hematopoiesis (Wen et al., 2016). Similar to previous work examining the effects of exercise in obesity on hematopoiesis (Frodermann et al., 2019), we found that exercise-induced EVs attenuated hematopoiesis in the HFD condition as evidenced by reduced concentrations of total HSC, LT-HSC, MPP, and CLP concentrations. Previous work from our lab used a similar model to the current study, where mice instead were given 3 Gy irradiation after 8 weeks of HFD or CON diet interventions and 4 weeks of EX or SED, while continuing the EX and dietary interventions for another 4 weeks after radiation (Emmons et al., 2019). Interestingly, in that study we found that EX increased LT-HSC, ST-HSC, MPP, and CLP cell counts without an effect of HFD (Emmons et al., 2019). Discrepancies in these studies could be due to different durations of exercise training, the direct effects of exercise versus indirect effects of exercise-induced EVs, or the age when the mice were irradiated. In the current study mice were irradiated at 5 weeks of age while the mice in the previous study were irradiated at 13 weeks of age. These ages represent mice pre- and post-sexual maturity (Dutta and Sengupta, 2016), which may impart differing hematopoietic and MSC differentiation responses to irradiation, exercise, and high-fat diets.

Our lab and others have previously determined that the effects of exercise on hematopoiesis are mediated by alterations in cellular communication in the bone marrow (Yamazaki et al., 2011; Kunisaki et al., 2013; Bruns et al., 2014; Hérault et al., 2017; Emmons et al., 2019). As a first step towards understanding if EVs were influencing hematopoiesis indirectly through HSC niche cells, we quantified MSCs, their progeny (i.e., osteoprogenitor, adipocyte progenitor, and osteoblast cells), and endothelial cells. These analyses revealed that EX EVs decreased osteoprogenitor cell concentrations with no effects of EX- or HFD-induced EVs on other bone marrow cell populations. HFD is known to increase bone marrow adipose tissue content which can be prevented (Styner et al., 2014; Emmons et al., 2019) or reversed (Emmons et al., 2018) by exercise training. Conversely, exercise training is known to increase osteogenesis from MSCs (Baker et al., 2011; Zhang et al., 2020), thus we hypothesized that the lower concentration of osteoprogenitors in the mice that received exercise-induced EVs may be due to enhanced differentiation. Our *in vitro* findings support this hypothesis showing that treating MSCs with exercise-induced EVs enhanced their osteogenic differentiation. Previous work has suggested that enhanced osteogenic differentiation in response to exercise training is due to mechanotransduction signaling in MSCs (Sen et al., 2011), thus our findings provide a novel paracrine mechanism whereby exercise may be enhancing osteogenesis. Interestingly, our *in vitro* analyses also revealed a role for HFD-induced EVs in enhancing adipogenesis which provides an additional mechanism explaining the enhanced adipogenic differentiation of MSCs and accumulation of marrow adipose tissue in HFD-induced obesity (Emmons et al., 2019).

As previous studies have shown alterations to cell function through variations to EV cargo (Hou et al., 2019), we reasoned that the exercise-induced effects were partially due to alterations

in EV cargo. Previous studies have examined muscle-derived EV cargo in the context of exercise, yet the EV cargo of the bone marrow environment remains unexplored. Here, we examined the miRNA cargo of the isolated EVs due to their established role in cell signaling (Avraham and Yarden, 2012; Vu et al., 2019). We found miR-331-5p ($p<0.05$) and miR-193 ($p<0.01$) downregulation in HFD-EX EVs compared to HFD-SED EVs. Correlational findings from clinical studies suggest lower miR-331-5p expression is related to leukemia relapse (Feng et al., 2011) and worsened responses to therapies for acute myeloid leukemia (Butrym et al., 2015). Previous data from our lab has shown that acute myeloid leukemia incidence is increased with HFD that is attenuated by exercise throughout the lifespan (Farber et al., 2021), thus downregulated miR-331-5p expression in HFD-EX EVs may be implicated in this observation. Relatively more information is available regarding miR-193 and hematopoiesis. Haetscher and colleagues found that miR-193b is upregulated in mouse hematopoietic stem cells while miR-193a expression is found primarily in committed myeloid cells, such as monocytes and granulocytes (Haetscher et al., 2015). Along these lines, overexpression of miR193a in HSCs impaired their regenerative capacity in transplantation assays, but had augmented granulocytic differentiation *in vitro* (Krowiorz et al., 2018), suggesting mirR-193b may be involved in maintaining HSC stemness, while mir-193a may be involved in myeloid differentiation.

miR-193a also plays a role in regulating MSC fate by suppressing osteogenic differentiation in human MSCs (Wang et al., 2018a). Further, miR-193a downregulation induced osteoblast differentiation (Wang et al., 2018b). These findings align nicely with our data as miR-193 was lower in exercise-induced EVs, and exercise-induced EVs promoted osteogenesis. miR-193a-3p has been shown to downregulate leucine-rich repeat-containing G-protein coupled

receptor 4 (LGR4) and activating transcription factor 4 (ATF4) (Wang et al., 2018b). LGR4 nonsense mutations have previously been implicated decreased bone mineral density and elevated risk of osteoporotic fractures (Styrkarsdottir et al., 2013), and ATF4 has been reported to positively regulate HSC expansion in mouse fetal liver (Zhao et al., 2015). miR-193a-3p downregulation may be promoting *lgr4* and *atf4* gene transcription to increase osteogenesis as we observed *in vitro*. Our KEGG analysis predicted the MAPK signaling pathway as a potential target for miR-331-5p and miR-193 which is corroborated by work from Lv and colleagues showing that miR-193a-3p downregulation increases MAPK signaling (Lv et al., 2020). The MAPK signaling cascade is important for cell proliferation and differentiation. The pathway is composed of multiple components, including JNK and ERK. Previous reports showed elevated JNK signaling promotes early MSC osteogenic differentiation (Brito et al., 2019; Mizerska-Kowalska et al., 2019), and others have shown that ERK inactivation in osteoprogenitors leads to decreased bone mass (Kim et al., 2019). miR-193 and 331-5p downregulation may be partially responsible for the upregulated osteogenesis seen *in vitro* in the current study.

In conclusion, our results indicate that exercise training-induced EVs restore normal hematopoiesis and enhance osteogenic differentiation in the context of HFD-induced obesity. Mechanistically, these findings may be explained by elevated large EV release alongside downregulated miR-193 and miR-331-5p content in HFD-EX EVs compared to HFD-SED EVs. These results provide a novel mechanism for the regulation of hematopoiesis and MSC fate by exercise. Future studies should identify the cellular source of these exercise-induced EVs to better-understand how intercellular crosstalk occurs between HSCs and their niche cells in the context of exercise training.

Author Contributions

JV designed and performed the experiments and drafted the manuscript and figures. WK assisted in all sample collections and assisted in drafting the methods and results sections. LEO completed the C3H 10T1/2 proliferation assay, drafted the C3H 10T1/2 proliferation assay methods section, and assisted in the Nanostring assay. MN optimized the Western Blot assay and EV isolation methods. NC assisted with flow cytometry data collection. MD supervised the project, provided funding, designed the studies, contributed to the analysis, and edited the manuscript. All authors reviewed the manuscript and approved its submission.

Funding

Support for the research program was provided by the Natural Sciences and Engineering Research Council. JV was funded by the Ontario Graduate Scholarship and the Doctoral Fellowship for Advancement of Biological Perspectives for Exercise Interventions Across the Lifespan. NC was supported by The Chilean National Agency for Research and Development (ANID) and the Doctoral Fellowship for Advancement of Biological Perspectives for Exercise Interventions Across the Lifespan.

Conflict of Interest

The authors declare that the research was conducted in the absence of any commercial or financial relationships that could be construed as a potential conflict of interest.

References

Ambrosi, T. H., Scialdone, A., Graja, A., Gohlke, S., Jank, A.-M., Bocian, C., et al. (2017). Adipocyte accumulation in the bone marrow during obesity and eging impairs stem cell-based hematopoietic and bone regeneration. *Cell Stem Cell* 20, 771-784.e6. doi: 10.1016/j.stem.2017.02.009.

Aoi, W., Ichikawa, H., Mune, K., Tanimura, Y., Mizushima, K., Naito, Y., et al. (2013). Muscle-enriched microRNA miR-486 decreases in circulation in response to exercise in young men. *Front. Physiol.* 4. doi: 10.3389/fphys.2013.00080.

Avraham, R., and Yarden, Y. (2012). Regulation of signalling by microRNAs. *Biochem. Soc. Trans.* 40, 26–30. doi: 10.1042/BST20110623.

Baker, J. M., De Lisio, M., and Parise, G. (2011). Endurance exercise training promotes medullary hematopoiesis. *FASEB J.* 25, 4348–4357. doi: 10.1096/fj.11-189043.

Bei, Y., Xu, T., Lv, D., Yu, P., Xu, J., Che, L., et al. (2017). Exercise-induced circulating extracellular vesicles protect against cardiac ischemia–reperfusion injury. *Basic Res. Cardiol.* 112, 38. doi: 10.1007/s00395-017-0628-z.

Benova, A., and Tencerova, M. (2020). Obesity-Induced Changes in Bone Marrow Homeostasis. *Front. Endocrinol.* 11, 294. doi: 10.3389/fendo.2020.00294.

Brito, V. G. B., Chaves-Neto, A. H., de Barros, T. L., and Oliveria, S. H. P. (2019). Soluble yerba mate (Ilex Paraguariensis) extract enhances in vitro osteoblastic differentiation of bone marrow-derived mesenchymal stromal cells. *J. Ethnopharmacol.* 244, 112131. doi: https://doi.org/10.1016/j.jep.2019.112131.

Bruns, I., Lucas, D., Pinho, S., Ahmed, J., Lambert, M. P., Kunisaki, Y., et al. (2014). Megakaryocytes regulate hematopoietic stem cell quiescence through CXCL4 secretion. *Nat. Med.* 20, 1315–1320. doi: 10.1038/nm.3707.

Bruschi, M., Granata, S., Santucci, L., Candiano, G., Fabris, A., Antonucci, N., et al. (2019). Proteomic Analysis of Urinary Microvesicles and Exosomes in Medullary Sponge Kidney Disease and Autosomal Dominant Polycystic Kidney Disease. *Clin. J. Am. Soc. Nephrol.* 14, 834–843. doi: 10.2215/CJN.12191018.

Butrym, A., Rybka, J., Baczyńska, D., Tukiendorf, A., Kuliczkowski, K., and Mazur, G. (2015). Expression of microRNA-331 can be used as a predictor for response to therapy and survival in acute myeloid leukemia patients. *Biomark. Med.* 9, 453–460. doi: 10.2217/bmm.14.112.

De Lisio, M., Baker, J. M., and Parise, G. (2013). Exercise promotes bone marrow cell survival and recipient reconstitution post-bone marrow transplantation, which is associated with increased survival. *Exp. Hematol.* 41, 143–154. doi: 10.1016/j.exphem.2012.10.003.

De Lisio, M., and Parise, G. (2012). Characterization of the effects of exercise training on hematopoietic stem cell quantity and function. *J. Appl. Physiol.* 113, 1576–1584. doi: 10.1152/japplphysiol.00717.2012.

De Lisio, M., Phan, N., Boreham, D. R., and Parise, G. (2011). Exercise-induced protection of bone marrow cells following exposure to radiation. *Appl. Physiol. Nutr. Metab.* 36, 80–87. doi: 10.1139/H10-087.

Doyle, L., and Wang, M. (2019). Overview of Extracellular Vesicles, Their Origin, Composition, Purpose, and Methods for Exosome Isolation and Analysis. *Cells* 8, 727. doi: 10.3390/cells8070727.

Dutta, S., and Sengupta, P. (2016). Men and mice: Relating their ages. *Life Sci.* 152, 244–248. doi: 10.1016/j.lfs.2015.10.025.

Emmons, R., Ngu, M., Xu, G., Hernández-Saavedra, D., Chen, H., and De Lisio, M. (2019). Effects of obesity and exercise on bone marrow progenitor cells after radiation. *Med. Sci. Sports Exerc.* 51, 1126–1136. doi: 10.1249/MSS.0000000000001894.

Emmons, R., Niemiro, G. M., Owolabi, O., and De Lisio, M. (2016). Acute exercise mobilizes hematopoietic stem and progenitor cells and alters the mesenchymal stromal cell secretome. *J. Appl. Physiol.* 120, 624–632. doi: 10.1152/japplphysiol.00925.2015.

Emmons, R., Xu, G., Hernández-Saavedra, D., Kriska, A., Pan, Y.-X., Chen, H., et al. (2018). Effects of obesity and exercise on colon cancer induction and hematopoiesis in mice. *Am. J. Physiol.-Endocrinol. Metab.* 316, E210–E220. doi: 10.1152/ajpendo.00237.2018.

Farber, E., Kwiecien, J. M., Bojic, D., Ngu, M., Akohene-Mensah, P., Vanhie, J. J., et al. (2021). Exercise Improves Cancer-free Survival and Health Span in a Model of Radiation-induced Cancer. *Med. Sci. Sports Exerc.* 53, 2254–2263. doi: 10.1249/MSS.0000000000002711.

Feng, D.-D., Zhang, H., Zhang, P., Zheng, Y.-S., Zhang, X.-J., Han, B.-W., et al. (2011). Down-regulated miR-331-5p and miR-27a are associated with chemotherapy resistance and relapse in leukaemia. *J. Cell. Mol. Med.* 15, 2164–2175. doi: 10.1111/j.1582-4934.2010.01213.x.

Frodermann, V., Rohde, D., Courties, G., Severe, N., Schloss, M. J., Amatullah, H., et al. (2019). Exercise reduces inflammatory cell production and cardiovascular inflammation via instruction of hematopoietic progenitor cells. *Nat. Med.* 25, 1761–1771. doi: 10.1038/s41591-019-0633-x.

Frühbeis, C., Helmig, S., Tug, S., Simon, P., and Krämer-Albers, E.-M. (2015). Physical exercise induces rapid release of small extracellular vesicles into the circulation. *J. Extracell. Vesicles* 4, 28239. doi: 10.3402/jev.v4.28239.

Gregory, C. A., Grady Gunn, W., Peister, A., and Prockop, D. J. (2004). An Alizarin red-based assay of mineralization by adherent cells in culture: comparison with cetylpyridinium chloride extraction. *Anal. Biochem.* 329, 77–84. doi: 10.1016/j.ab.2004.02.002.

Haetscher, N., Feuermann, Y., Wingert, S., Rehage, M., Thalheimer, F. B., Weiser, C., et al. (2015). STAT5-regulated microRNA-193b controls haematopoietic stem and progenitor cell expansion by modulating cytokine receptor signalling. *Nat. Commun.* 6, 8928. doi: 10.1038/ncomms9928.

Hérault, A., Binnewies, M., Leong, S., Calero-Nieto, F. J., Zhang, S. Y., Kang, Y.-A., et al. (2017). Myeloid progenitor cluster formation drives emergency and leukaemic myelopoiesis. *Nature* 544, 53–58. doi: 10.1038/nature21693.

Hou, Z., Qin, X., Hu, Y., Zhang, X., Li, G., Wu, J., et al. (2019). Longterm Exercise-Derived Exosomal miR-342-5p: A novel exerkine for cardioprotection. *Integr. Physiol.* 124, 1386–1400. doi: 10.1161/CIRCRESAHA.118.314635.

Huang, H., Song, T.-J., Li, X., Hu, L., He, Q., Liu, M., et al. (2009). BMP signaling pathway is required for commitment of C3H10T1/2 pluripotent stem cells to the adipocyte lineage. *Proc. Natl. Acad. Sci.* 106, 12670–12675. doi: 10.1073/pnas.0906266106.

Kim, J.-M., Yang, Y.-S., Park, K. H., Oh, H., Greenblatt, M. B., and Shim, J.-H. (2019). The ERK MAPK Pathway Is Essential for Skeletal Development and Homeostasis. *Int. J. Mol. Sci.* 20, 1803. doi: 10.3390/ijms20081803.

Krowiorz, K., Bhayadia, R., Jammal, R., Pabst, C., Pochert, N., Rueß, C., et al. (2018). MiR-193a Is a Negative Regulator of Hematopoietic Stem Cells and Promotes Anti-Leukemic Effects in Acute Myeloid Leukemia. *Blood* 132, 2627–2627. doi: 10.1182/blood-2018-99-116256.

Kunisaki, Y., Bruns, I., Scheiermann, C., Ahmed, J., Pinho, S., Zhang, D., et al. (2013). Arteriolar niches maintain haematopoietic stem cell quiescence. *Nature* 502, 637–643. doi: 10.1038/nature12612.

Lobb, R. J., Becker, M., Wen Wen, S., Wong, C. S. F., Wiegmans, A. P., Leimgruber, A., et al. (2015). Optimized exosome isolation protocol for cell culture supernatant and human plasma. *J. Extracell. Vesicles* 4, 27031. doi: 10.3402/jev.v4.27031.

Lv, Y., Huang, Y., Xu, M., Heng, B. C., Yang, C., Cao, C., et al. (2020). The miR-193a-3p-MAP3k3 Signaling Axis Regulates Substrate Topography-Induced Osteogenesis of Bone Marrow Stem Cells. *Adv. Sci.* 7, 1901412. doi: 10.1002/advs.201901412.

Ma, C., Wang, J., Liu, H., Chen, Y., Ma, X., Chen, S., et al. (2018). Moderate Exercise Enhances Endothelial Progenitor Cell Exosomes Release and Function. *Med. Sci. Sports Exerc.* 50, 2024–2032. doi: 10.1249/MSS.0000000000001672.

Maumus, M., Rozier, P., Boulestreau, J., Jorgensen, C., and Noël, D. (2020). Mesenchymal Stem Cell-Derived Extracellular Vesicles: Opportunities and Challenges for Clinical Translation. *Front. Bioeng. Biotechnol.* 8, 997. doi: 10.3389/fbioe.2020.00997.

Mizerska-Kowalska, M., Sławińska-Brych, A., Kaławaj, K., Żurek, A., Pawińska, B., Rzeski, W., et al. (2019). Betulin Promotes Differentiation of Human Osteoblasts In Vitro and Exerts an Osteoinductive Effect on the hFOB 1.19 Cell Line Through Activation of JNK, ERK1/2, and mTOR Kinases. *Molecules* 24, 2637. doi: 10.3390/molecules24142637.

Nederveen, J. P., Warnier, G., Di Carlo, A., Nilsson, M. I., and Tarnopolsky, M. A. (2021). Extracellular Vesicles and Exosomes: Insights From Exercise Science. *Front. Physiol.* 11, 604274. doi: 10.3389/fphys.2020.604274.

Poloni, A., Maurizi, G., Serrani, F., Mancini, S., Zingaretti, M. C., Frontini, A., et al. (2013). Molecular and functional characterization of human bone marrow adipocytes. *Exp. Hematol.* 41, 558-566.e2. doi: 10.1016/j.exphem.2013.02.005.

Ratajczak, J., Miekus, K., Kucia, M., Zhang, J., Reca, R., Dvorak, P., et al. (2006). Embryonic stem cell-derived microvesicles reprogram hematopoietic progenitors: evidence for horizontal transfer of mRNA and protein delivery. *Leukemia* 20, 847–856. doi: 10.1038/sj.leu.2404132.

Sen, B., Xie, Z., Case, N., Styner, M., Rubin, C. T., and Rubin, J. (2011). Mechanical signal influence on mesenchymal stem cell fate is enhanced by incorporation of refractory periods into the loading regimen. *J. Biomech.* 44, 593–599. doi: 10.1016/j.jbiomech.2010.11.022.

Shea, C. M., Edgar, C. M., Einhorn, T. A., and Gerstenfeld, L. C. (2003). BMP treatment of C3H10T1/2 mesenchymal stem cells induces both chondrogenesis and osteogenesis. *J. Cell. Biochem.* 90, 1112–1127. doi: 10.1002/jcb.10734.

Shi, X.-F., Wang, H., Kong, F.-X., Xu, Q.-Q., Xiao, F.-J., Yang, Y.-F., et al. (2017). Exosomal miR-486 regulates hypoxia-induced erythroid differentiation of erythroleukemia cells through targeting Sirt1. *Exp. Cell Res.* 351, 74–81. doi: 10.1016/j.yexcr.2016.12.023.

Singer, K., DelProposto, J., Lee Morris, D., Zamarron, B., Mergian, T., Maley, N., et al. (2014). Diet-induced obesity promotes myelopoiesis in hematopoietic stem cells. *Mol. Metab.* 3, 664–675. doi: 10.1016/j.molmet.2014.06.005.

Skog, J., Würdinger, T., van Rijn, S., Meijer, D. H., Gainche, L., Curry, W. T., et al. (2008). Glioblastoma microvesicles transport RNA and proteins that promote tumour growth and provide diagnostic biomarkers. *Nat. Cell Biol.* 10, 1470–1476. doi: 10.1038/ncb1800.

Ståhl, A., Johansson, K., Mossberg, M., Kahn, R., and Karpman, D. (2019). Exosomes and microvesicles in normal physiology, pathophysiology, and renal diseases. *Pediatr. Nephrol.* 34, 11–30. doi: 10.1007/s00467-017-3816-z.

Styner, M., Thompson, W. R., Galior, K., Uzer, G., Wu, X., Kadari, S., et al. (2014). Bone marrow fat accumulation accelerated by high fat diet is suppressed by exercise. *Bone* 64, 39–46. doi: 10.1016/j.bone.2014.03.044.

Styrkarsdottir, U., Thorleifsson, G., Sulem, P., Gudbjartsson, D. F., Sigurdsson, A., Jonasdottir, A., et al. (2013). Nonsense mutation in the LGR4 gene is associated with several human diseases and other traits. *Nature* 497, 517–520. doi: 10.1038/nature12124.

Szatmári, T., Kis, D., Bogdándi, E. N., Benedek, A., Bright, S., Bowler, D., et al. (2017). Extracellular Vesicles Mediate Radiation-Induced Systemic Bystander Signals in the Bone Marrow and Spleen. *Front. Immunol.* 8. doi: 10.3389/fimmu.2017.00347.

Théry, C., Witwer, K. W., Aikawa, E., Alcaraz, M. J., Anderson, J. D., Andriantsitohaina, R., et al. (2018). Minimal information for studies of extracellular vesicles 2018 (MISEV2018): a position statement of the International Society for Extracellular Vesicles and update of the MISEV2014 guidelines. *J. Extracell. Vesicles* 7, 1535750. doi: 10.1080/20013078.2018.1535750.

Trottier, M. D., Naaz, A., Li, Y., and Fraker, P. J. (2012). Enhancement of hematopoiesis and lymphopoiesis in diet-induced obese mice. *Proc. Natl. Acad. Sci.* 109, 7622–7629. doi: 10.1073/pnas.1205129109.

Valadi, H., Ekström, K., Bossios, A., Sjöstrand, M., Lee, J. J., and Lötvall, J. O. (2007). Exosome-mediated transfer of mRNAs and microRNAs is a novel mechanism of genetic exchange between cells. *Nat. Cell Biol.* 9, 654–659. doi: 10.1038/ncb1596.

Vu, L. T., Peng, B., Zhang, D. X., Ma, V., Mathey-Andrews, C. A., Lam, C. K., et al. (2019). Tumor-secreted extracellular vesicles promote the activation of cancer-associated fibroblasts via the transfer of microRNA-125b. *J. Extracell. Vesicles* 8, 1599680. doi: 10.1080/20013078.2019.1599680.

Wang, S.-N., Zhao, X.-Q., Yu, B., and Wang, B.-W. (2018a). miR-193a inhibits osteogenic differentiation of bone marrow-derived stroma cell via targeting HMGB1. *Biochem. Biophys. Res. Commun.* 503, 536–543. doi: 10.1016/j.bbrc.2018.05.132.

Wang, W., Chen, J., Hui, Y., Huang, M., and Yuan, P. (2018b). Down-regulation of miR-193a-3p promotes osteoblast differentiation through up-regulation of LGR4/ATF4 signaling. *Biochem. Biophys. Res. Commun.* 503, 2186–2193. doi: 10.1016/j.bbrc.2018.08.011.

Wen, S., Dooner, M., Cheng, Y., Papa, E., Del Tatto, M., Pereira, M., et al. (2016). Mesenchymal stromal cell-derived extracellular vesicles rescue radiation damage to murine marrow hematopoietic cells. *Leukemia* 30, 2221–2231. doi: 10.1038/leu.2016.107.

Willms, E., Johansson, H. J., Mäger, I., Lee, Y., Blomberg, K. E. M., Sadik, M., et al. (2016). Cells release subpopulations of exosomes with distinct molecular and biological properties. *Sci. Rep.* 6, 22519. doi: 10.1038/srep22519.

Yamazaki, S., Ema, H., Karlsson, G., Yamaguchi, T., Miyoshi, H., Shioda, S., et al. (2011). Nonmyelinating Schwann Cells Maintain Hematopoietic Stem Cell Hibernation in the Bone Marrow Niche. *Cell* 147, 1146–1158. doi: 10.1016/j.cell.2011.09.053.

Yáñez-Mó, M., Siljander, P. R.-M., Andreu, Z., Bedina Zavec, A., Borràs, F. E., Buzas, E. I., et al. (2015). Biological properties of extracellular vesicles and their physiological functions. *J. Extracell. Vesicles* 4, 27066. doi: 10.3402/jev.v4.27066.

Zhang, L., Yuan, Y., Wu, W., Sun, Z., Lei, L., Fan, J., et al. (2020). Medium-Intensity Treadmill Exercise Exerts Beneficial Effects on Bone Modeling Through Bone Marrow Mesenchymal Stromal Cells. *Front. Cell Dev. Biol.* 8, 600639. doi: 10.3389/fcell.2020.600639.

Zhang, Z., Huang, Z., Ong, B., Sahu, C., Zeng, H., and Ruan, H.-B. (2019). Bone marrow adipose tissue-derived stem cell factor mediates metabolic regulation of hematopoiesis. *Haematologica* 104, 1731–1743. doi: 10.3324/haematol.2018.205856.

Zhao, Y., Zhou, J., Liu, D., Dong, F., Cheng, H., Wang, W., et al. (2015). ATF4 plays a pivotal role in the development of functional hematopoietic stem cells in mouse fetal liver. *Blood* 126, 2383–2391. doi: 10.1182/blood-2015-03-633354.

Chapter V – Thesis Aim 2

High fat diets promote hematopoietic stem cell expansion and myeloid skewing during steady state hematopoiesis

James J. Vanhie[1], Wooseok Kim[1], Cole Goode[1], Nicolas Collao[1], and Michael De Lisio[1,2]

[1]School of Human Kinetics, Faculty of Health Sciences, Ottawa, ON, Canada

[2]Department of Cellular and Molecular Medicine, University of Ottawa, Ottawa, ON, Canada

Keywords: bone marrow, exercise, mesenchymal stromal cells, microRNA, myelopoiesis

Under Review in Medicine & Science in Sports & Exercise

Assigned Paper #: MSSE-D-24-00242

Contribution: James J. Vanhie designed the study, performed the experiments, analyzed the data, interpreted the results of experiments, prepared the figures, drafted the manuscript, and edited and revised the manuscript.

***Correspondence to:**
Michael De Lisio, PhD
Roger Guindon Hall, University of Ottawa
Phone: +1 613-562-5800 ext. 6987
Email: mdelisio@uottawa.ca

Abstract

Purpose: High-fat diets (HFD) and exercise (EX) exert differential impacts on inflammatory myeloid cell formation during stress hematopoiesis through altered intercellular signaling, including marrow miR-193 and miR-331-5p expression. miR-193 and miR-331-5p may derive from mesenchymal stromal cells (MSCs) whose paracrine function is altered by exercise. However, how HFDs and EX alter hematopoiesis during steady state conditions and the cells contributing to altered miR-193 and miR-331-5p marrow expression remain unknown. Therefore, the purpose of the current study was to examine hematopoietic stem and progenitor cells (HSPCs) and their surrounding niche cells during steady state hematopoiesis following a HFD and EX training intervention, and to investigate whether altered marrow miR-193 and miR-331-5p expression originates from MSCs. **Methods:** Male CBA mice (n=40) underwent 8 weeks of HFD or control (CON) diet consumption with the latter 4 weeks involving sedentary (SED) or EX training interventions. C3H10T1/2 cells, an MSC-derived cell line, were cultured in adipogenic media to mimic HFD, or were strained to model the mechanical forces experienced during EX. **Results:** HFDs promoted HSPC and myeloid progenitor cell expansion without impacting lymphoid progenitor cells while MSC concentrations were lower with EX. HSPCs derived from HFD mice displayed enhanced myeloid colony formation which was inhibited by EX. Furthermore, adipogenic conditions *in vitro* decreased miR-193 expression in MSCs with no effect of strain on miR-331-5p expression. **Conclusion:** Together, these results suggest that during steady state hematopoiesis, EX inhibits myeloid cell expansion while HFDs oppose these effects. Furthermore, adipogenic conditions may promote HSPC expansion via downregulated MSC miR-193 expression.

Introduction

Obesity rates in the United States continue to rise, with 39% of Americans having obesity (BMI ≥30 kg/m^2). This trend occurs, in part, due to a lack of physical activity combined with excessive caloric consumption via the Western diet that is high in saturated fats. High-fat diets are linked to a considerable number of detrimental health effects, including an increased risk of developing various cancers and cardiovascular disease. Compared to healthy weight individuals, those with obesity experience chronic low-grade inflammation that is driven by inflammatory myeloid cell overproduction (1,2). These myeloid cells originate from the bone marrow, where myeloid lineage-derived monocytes are recruited to external tissues via the Chemokine (C-C motif) ligand 2-receptor 2 (CCL2-CCR2) signaling axis and differentiate into inflammatory macrophages (3,4).

The bone marrow is a complex environment that is the primary site of adult hematopoiesis. Over time the marrow cavity naturally fills with adipose tissue such that up to 50% of the marrow cavity is occupied by adipose tissue by 25 years of age (5). However, a high-fat diet accelerates adipose tissue accumulation that can decrease the available space for red marrow, where active hematopoiesis occurs, leading to early hematopoietic stem cell exhaustion (1,2,6,7). Mesenchymal stromal cells (MSCs) are bone marrow resident support cells that influence hematopoietic stem and progenitor cell (HSPC) activity and can differentiate into mature HSPC niche cells such as adipocytes or osteocytes (8). Our lab has previously demonstrated that high-fat diet consumption inhibits HSPC expansion and augments marrow adipose tissue accumulation following ionizing radiation in a model of stress hematopoiesis (6). Furthermore, we have also shown that a single treadmill exercise bout in mice increases the

expression of multiple signaling factors from isolated MSCs at 15 minutes post-exercise, including granulocyte-colony stimulating factor, stem cell factor, interleukin-3, and thrombopoietin (9). Therefore, under acute stress conditions experienced following radiation exposure or intense exercise, exercise and high-fat diets regulate hematopoiesis, in part, through regulating the HSPC niche.

In addition to cytokines and growth factors, recent research has identified microRNAs (miRNAs) as novel regulators of hematopoiesis (10,11). miRNAs are non-coding RNAs that regulate translation by binding messenger RNA in a manner that is mostly repressive. Fichtel and colleagues recently demonstrated that MSC-derived extracellular vesicles (EVs) contained higher miRNA-29a (miR-29a) and miR-34a content with age, and providing aged MSC-derived EVs to HSPCs *in vitro* decreased their viability compared to MSC-derived EVs from young mice (10). We recently showed that exercise decreases miR-193 and miR-331-5p content from bone marrow-derived EVs in a mouse model involving high-fat diet consumption (7). These miRNAs have been previously implicated in osteogenesis and leukocyte expansion (12,13), yet their cell of origin remains equivocal.

MSCs are an important source for paracrine factors in the HSPC niche and exercise regulates hematopoiesis, in part, through altering paracrine signaling from MSCs (9,14,15). Mechanical forces transferred to MSCs in the bones during exercise have been shown to induce osteogenic differentiation and contribute to exercise-induced bone formation (16). However, it remains unknown whether mechanical forces experienced by bone marrow MSCs during exercise alter their paracrine function, particularly through altered MSC-derived EV miRNA cargo. Therefore, the purpose of the current study was to examine alterations to marrow cell

populations following high-fat diet consumption and exercise, and to determine whether MSCs cultured under conditions that model the mechanical strain experienced during exercise or high-fat diet *in vitro* alter their expression of miR-193 and miR-331-5p. We hypothesized that high-fat diet consumption would induce marrow adipose tissue accumulation and augment myeloid cell formation while exercise would attenuate these effects. Additionally, we hypothesized that adipogenic-induced MSCs would have greater miR-193 and miR-331-5p expression compared to control cells.

Materials and Methods

Study Design

Ethical approval was obtained from the University of Ottawa Animal Care Committee and conformed to the *Animals for Research Act* by the Canadian Council on Animal Care. Male CBA mice (n=40) (Jackson Laboratories, Maine, United States) were maintained in a 12-hour light and 12-hour dark schedule until 13 weeks of age at sacrifice. Male mice were chosen for the current study as female mice display resistance to the metabolic impacts incurred by high-fat diets (17,18). The mice arrived at the research facility at four weeks of age and were allowed to acclimate for one week. The mice were singly housed in a pathogen-free environment for the duration of the study. Mice were fed 45% fat (by calorie) chow for eight weeks to induce visceral and marrow adipose tissue accumulation with the final four weeks involving an exercise training program (Figure 5.1), as described previously (19). At five weeks of age the mice were randomized into control diet (CON; D10012M, Research Diets, NJ, United States) or high-fat diet (HFD; D12451, Research Diets, NJ, United States) conditions. The mice were fed *ad libitum* and they remained on their respective diets throughout the study (8 weeks total). After four weeks

in the diet condition, the mice were further randomized into exercise (EX) and sedentary (SED) conditions creating four experimental groups: CON-SED, CON-EX, HFD-SED, and HFD-EX. Body composition was measured once every 4 weeks using an EchoMRI-900 (EchoMRI LLC, Texas, United States) as previously described (7).

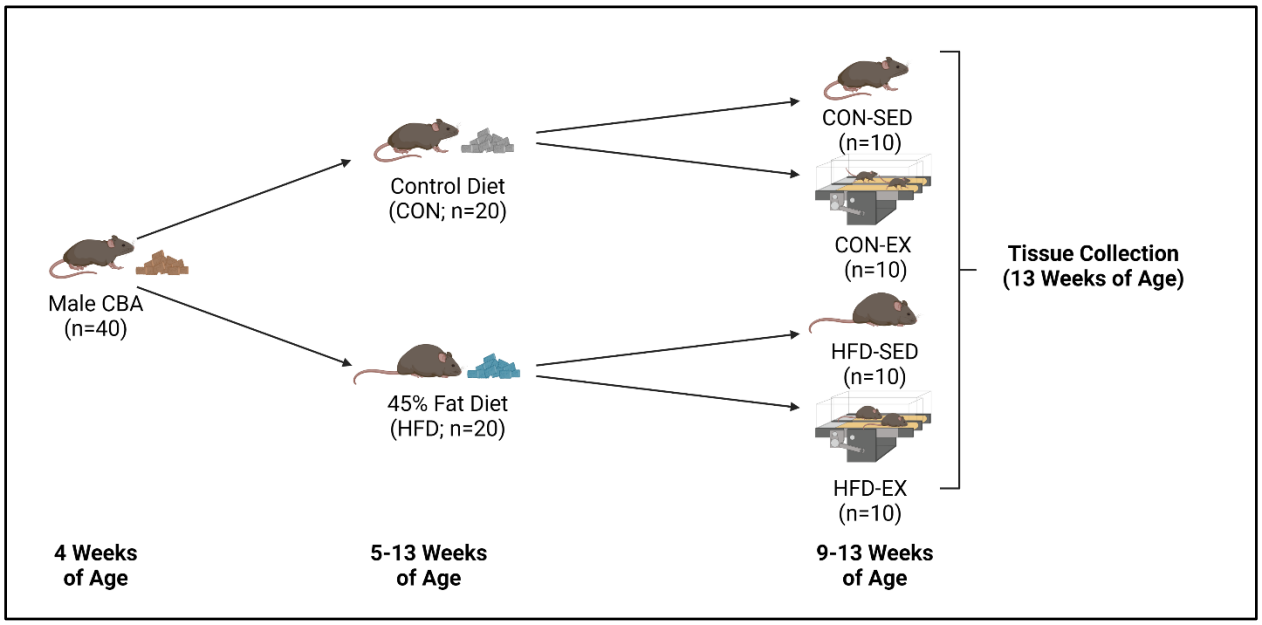

Figure 5.1. Study outline. Four-week-old male CBA mice (n=40) were acclimated for one week prior to randomized placement on either a high-fat (HFD, 45% by calorie, n=20) or control (CON, n=20) diet for 8 weeks to promote obesogenic conditions. Four weeks into the diet intervention (9 weeks of age) the mice were again randomized into either exercise (EX, n=20) or sedentary (SED, n=20) conditions until time of collection (13 weeks of age). Figure created with BioRender.com.

Progressive endurance exercise training program

All mice completed a 10-minute acclimation session on an Exer 3/6 treadmill (Columbus Instruments, Ohio, United States) at a 5° incline followed by an endurance test one week later to determine endurance capacity, as described previously (7). Briefly, mice were acclimated at 8 $m \cdot min^{-1}$ for 10 min approximately 7 days prior to the endurance test and exercise training program. The endurance test began at 10 $m \cdot min^{-1}$, and the treadmill speed increased by 1 $m \cdot min^{-}$

^{1} every 2 min until the mice were unable to run for any portion of a full stage or resisted gentle encouragement. Mice were encouraged to run by touching their lower back with a soft-bristle paint brush. Electrical stimulation was not used at any point. The mice exercised three days per week thereafter for up to one hour per session. Each exercise session included a 10-minute warmup period at 8 $m \cdot min^{-1}$, a higher speed exercise bout at 8-10 $m \cdot min^{-1}$ for 25-45 min, and a cooldown period at 8 $m \cdot min^{-1}$ for 5 min, as described previously (7). Sedentary mice were placed on sham treadmills on top of the active treadmills to mimic the treadmill vibrations, sound, and physical handling.

Bone marrow collection

Mice were euthanized at 13 weeks of age via CO_2 asphyxiation followed by cervical dislocation. All non-adherent tissues were removed from the femurs and tibias. Femur metaphyses were cut using surgical scissors and the marrow cavities were flushed with 1 mL of 5% fetal bovine serum (FBS) diluted in phosphate-buffered saline (PBS) into a 1.5 mL centrifuge tube. The cell suspension was stored on ice until later processing. The bone fragments were carefully crushed once with a mortar and pestle and chopped using scissors in 3 mL 0.2% type II collagenase (1% diluted with high-glucose Dulbecco's Modified Eagle Medium; DMEM) to isolate cells from the bone interior. This mixture was incubated at 37°C and 5% CO_2 for 45 min, and the samples were gently agitated every 15 min. These cells were combined with the marrow cell suspension through a 70 µm filter and subsequently centrifuged at 500 g at 4°C for 5 min. The supernatant was removed, and the remaining cell pellet was resuspended in 2400 µL of 5% FBS. One third of the suspension was used for flow cytometry and the other two thirds was used for HSPC magnetic cell sorting for the myeloid colony forming unit assay.

Flow Cytometry

Bone marrow-derived cells were quantified via flow cytometry as described previously (7). Cell populations of interest were identified following doublet exclusion and viability dye gating. Hematopoietic stem cells (HSCs), multipotent progenitor cells (MPPs), common myeloid progenitor cells (CMPs), common lymphoid progenitor cells (CLPs), granulocyte-macrophage progenitor cells (GMPs), and megakaryocyte-erythroid progenitor cells (MEPs) were identified using the gating strategies summarized in Table S5.1 and in our previous work (7). Representative flow cytometry gating strategies can be found in Figure S5.1. Antibody catalogue numbers, fluorophores, and dilutions are summarized in Table S5.2. Live and dead C3H10T1/2 MSCs (incubated at 95°C for 5 min to induce cell death) were used for viability dye compensation. Cell gating for all antibodies was based on unstained and single-stained bone marrow cells. Samples from four mice in the CON-EX group were excluded from flow cytometry analysis due to technical complications brought on by laboratory time and personnel restrictions during the COVID-19 pandemic.

Myeloid Colony Forming Unit Assay

To determine myeloid colony formation, HSPCs were plated for 10 days in specialized myeloid differentiation media for a myeloid colony forming unit assay (CFU). HSPCs were magnetically isolated through a negative selection kit (EasySep Mouse Hematopoietic Progenitor Isolation Kit; #19856; STEMCELL Technologies, British Columbia, Canada) that targeted unwanted non-hematopoietic stem cells and non-progenitor cells via CD5, CD11b, CD19, CD45R/B220, Gr-1, Ter119, and Ly-6B.2 (7/4) antibody binding. Isolated HSPCs were quantified using a Countess II Hemocytometer (Thermo Fisher Scientific, Massachusetts, United States) and diluted to a

concentration of 2.5 x 10^4 cells·mL^{-1} in high glucose DMEM. 0.3 mL of the diluted cell suspension and 33 µL of penicillin (1% final prepared volume) was added to 3 mL of MethoCult GF M3434 media (STEMCELL Technologies, British Columbia, Canada). The mixture was vortexed for 30 seconds to ensure uniform cell concentration within the media, as recommended by the manufacturer. Media (1.1 mL) was carefully added to two 35 mm dishes with 3 mL Syringes (#28240, STEMCELL Technologies, British Columbia, Canada) and 16-gauge blunt-end needles (#28110, STEMCELL Technologies, British Columbia, Canada), so that 2500 cells were evenly distributed in each dish. A third 35 mm dish was filled with sterile distilled water, and all three dishes were placed inside a 100 mm dish with their lids on. The cells were cultured in an incubator at 37°C and 5.0% CO_2. After 10 days the dishes were removed and imaged using a Celldiscoverer 7 microscope (ZEISS, Oberkochen, Germany). Stitched images of each dish were digitally overlaid with a translucent grid and colonies were scored according to the manufacturer's instructions using the counting tool on Adobe Photoshop CC 2018. The quantified colonies included granulocyte, erythroid, macrophage, megakaryocyte (CFU-GEMM), granulocyte, macrophage (CFU-GM), burst-forming unit-erythroid (BFU-E), and erythroid (CFU-E).

Marrow adipose tissue quantification

One femur from each mouse was resected, fixed in 10% formalin for 48 hours, then decalcified using 14% w/v EDTA at pH 7.4 (140 g Na_2-EDTA, ~14 g NaOH, topped up to 1000 mL with distilled water) for two weeks. The EDTA solution was replaced every 3-4 days. Once decalcified, the bones were stored in PBS at 4°C. The stored bones were stained using osmium tetroxide as described previously (20). Briefly, 2% osmium tetroxide solution was diluted 1:1 with 5% w/v potassium dichromate in distilled water to form a 1% osmium tetroxide/2.5% potassium

dichromate solution. The decalcified bones were transferred to new 1.5 mL tubes with 1 mL of the 1% osmium tetroxide solution and placed on a rocker for 48 hours. The bones were moved to cassettes and washed with running cold water for 2 hours. The bones were stained a second time and placed on a rocker for another 48 hours to enhance osmium tetroxide binding. After a final wash the bones were transferred to new 1.5 mL tubes with PBS and stored at 4°C until imaging. µCT imaging was conducted using a Bruker Skyscan 1272 (Bruker, Kontich, Belgium) with 70 kV, 142 µA, 0.5 mm A1 filter, 550 ms integration time, 1° rotation step, 360° angular range, and 12 µm image pixel size. Bone images were reconstructed using NRecon and analysed using CTan (Bruker, Kontich, Belgium) with a 100 global threshold value. Total marrow adipose tissue was quantified as a percentage of total bone volume.

C3H10T1/2 cell culture, miRNA extraction, and RT-qPCR

C3H10T1/2 MSCs were cultured to understand how high-fat diet and the mechanical strain component of exercise impacts miR-193 and miR-331-5p miRNA expression (21). While not fully recapitulating all of the stimuli experienced during exercise, mechanical strain is an established model for examining how physical stressors impact cell activity (22). MSCs were cultured in collagen I-coated 6-well Flexcell BioFlex culture plates (BF-3001C, Flexcell International Corporation, North Carolina, United States) so that half the wells from each plate included adipogenic media while the other half included control media. Two plates underwent tension cycling while the other two remained unstrained to make four conditions (n=6/condition): Adipogenic media ± strain and control media ± strain. We seeded 8000 cells in each well with MSC growth media (10% FBS, 1% penicillin-streptomycin, rest high-glucose DMEM) based on previous reports (23,24). After 2 days we switched the growth media with

adipogenic differentiation media in basal media and L-glutamine (2 mM) or basal media and L-glutamine (2 mM) (#05507; STEMCELL Technologies, British Columbia, Canada). At 24 hours post-adipogenic media addition the cells were subject to 100 cycles of 2% strain at 10 cycles·min^{-1} in a uniform bi-axial fashion using a Flexcell Tension System (FX5000T-FLK, Flexcell International Corporation, North Carolina, United States), as described previously (23,24) or remained unperturbed. The adipogenic media was added to the MSCs for 24 hours to promote lipid uptake while avoiding advanced MSC differentiation to adipocytes. Cell lysate was collected by scraping the wells with a cell scraper after adding lysis buffer directly to the well. miRNA was isolated directly from the cells using a Qiagen miRNEasy Micro kit (#217084, Qiagen, Hilden, Germany) according to the manufacturer's instructions. Isolated miRNA was reverse transcribed using the TaqMan MicroRNA Reverse Transcription Kit (#4366596, Thermo Fisher Scientific, Massachusetts, United States), and qPCR was conducted using the TaqMan Fast Advanced Master Mix (#4444556, Thermo Fisher Scientific, Massachusetts, United States), according to the manufacturer's instructions. TaqMan MicroRNA Assays (#4427975, Thermo Fisher Scientific, Massachusetts, United States) were used for the various miRNA-specific reactions. The miRNA primers included mmu-miR-331-5p (#002233) and mmu-miR-193 (#002577). snoRNA234 (#001234) was used as a loading control.

Statistical analysis

Body weight, body fat percentage, and lean body weight were analyzed at each time point via repeated-measures two-factor (diet and exercise) ANOVA and Sidak post-hoc correction tests. qPCR fold changes were calculated within plates using the $2^{-\Delta\Delta Ct}$ method (25). Flow cytometry, CFU, and qPCR data were analyzed on GraphPad Prism 9 by two-factor (diet and exercise or

media type and strain) ANOVA and Sidak post-hoc correction tests. All data are presented as mean ± SEM with $p<0.05$ considered significant. All investigators conducting analyses were blinded.

Results

Chronic high-fat diet consumption induces adipose tissue accumulation that is not reversed by exercise.

Body weight was higher in HFD mice compared to CON mice ($p<0.001$ at 6 weeks, $p<0.0001$ at 7-13 weeks, Figure 5.2A) at 6-13 weeks of age and higher in EX mice compared to SED at 13 weeks ($p<0.05$). Body fat percentage ($p<0.0001$, Figure 5.2B) and lean body weight (Figure 5.2C) were also elevated at 9 ($p<0.01$) and 13 ($p<0.0001$) weeks of age in HFD compared to CON. There was a trend for more marrow adipose tissue in HFD without any effect of exercise ($p=0.08$, Figure 5.2D). CON-EX mice had a greater post-exercise training endurance test duration ($p<0.001$, Figure 5.2E) while the HFD group did not ($p=0.15$).

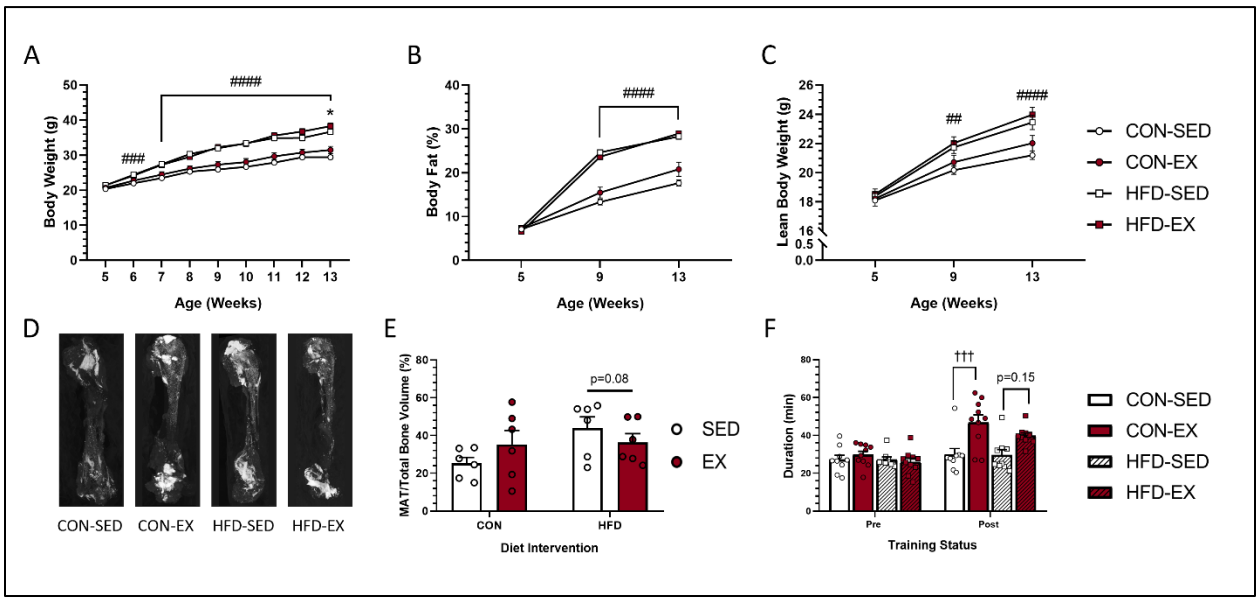

Figure 5.2. High-fat diet consumption increases total body weight and body fat percentage. (A) Total body weight. (B) body fat percentage and (C) lean body weight measured by echo MRI. (D) representative bone marrow adipose tissue (MAT) µCT images, (E) MAT-to-total bone volume fraction (n=6 per group), and (E) endurance test exercise duration. ##p<0.01 main effect of diet. ###p<0.001 main effect of diet. ####p<0.0001 main effect of diet. †††p<0.001 interaction effect.

Chronic high-fat diet consumption, but not exercise, increases bone marrow stem and progenitor cell concentrations.

We used flow cytometry to quantify changes to bone marrow cell populations in HFD and EX conditions during steady state hematopoiesis using the gating strategies listed in Table S5.1. HFD mice had higher hematopoietic stem cell (HSC; p<0.05), long-term HSC (p<0.01), and multipotent progenitor (p<0.05) cell concentrations (Figure 5.3A-D). Common

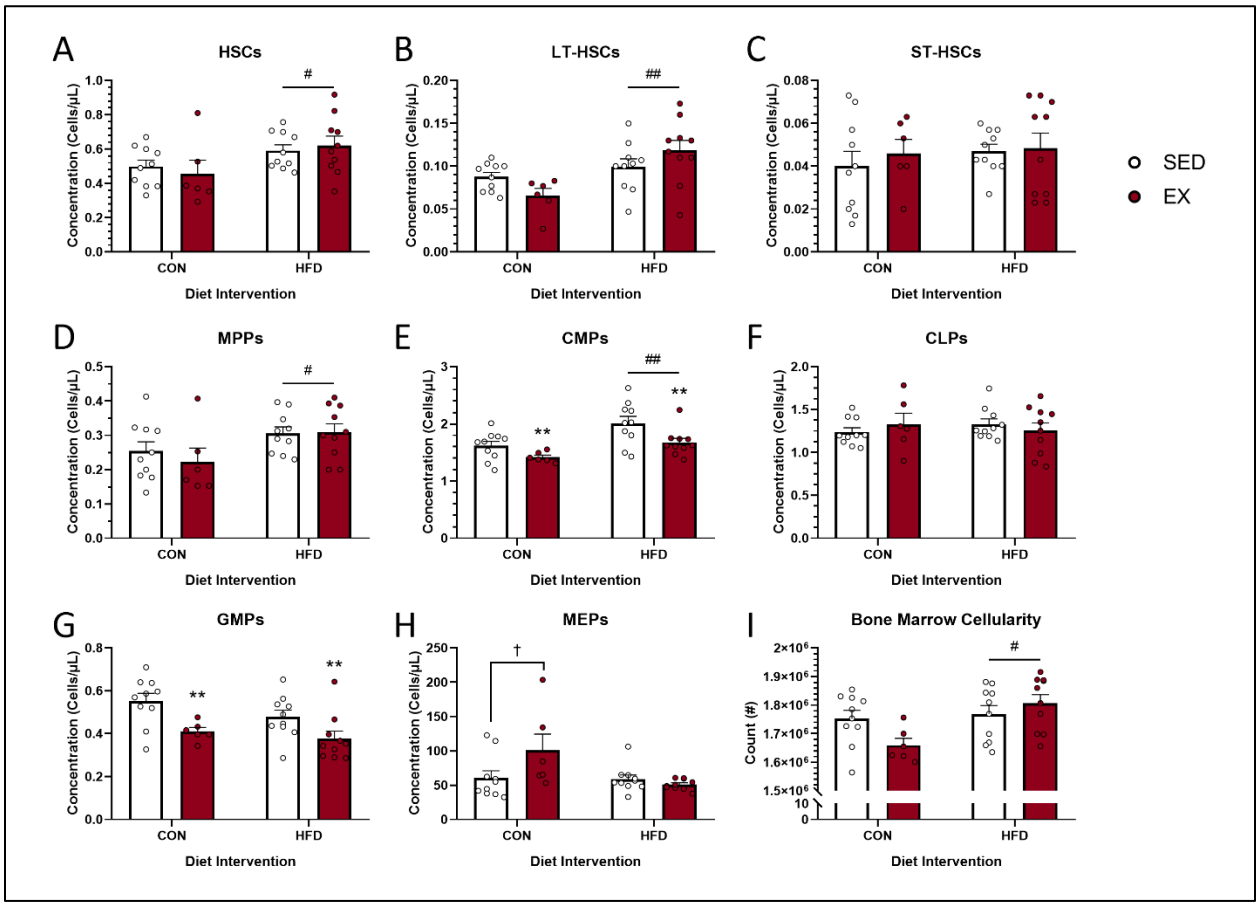

Figure 5.3. High-fat diet consumption increases hematopoietic stem cell and progenitor cell concentrations. Flow cytometry data showing HSPC cell concentrations. (A) Hematopoietic stem cells (HSCs), (B) long-term HSCs (LT-HSCs), (C) short-term HSCs (ST-HSCs), (D) multipotent progenitor cells (MPPs), (E) common myeloid progenitor cells (CMPs) (F) common lymphoid progenitor cells (CLPs), (G) granulocyte-macrophage progenitor cells (GMPs), (H) megakaryocyte-erythroid progenitor cells (MEP) and (I) total bone marrow cellularity. **p<0.01 main effect of exercise. #p<0.05 main effect of diet. ##p<0.01 main effect of diet. †p<0.05 interaction effect. (n=6 for CON-EX for HSCs, LT-HSCs, ST-HSCs, MPPs, CMPs, GMPs, and MEPs. n=10 per group for all other conditions, CLPs, and bone marrow cellularity).

myeloid progenitor cell concentrations were also higher in HFD (p<0.01; Figure 5.3E); however, there was no impact on common lymphoid progenitor cell concentrations with either intervention (Figure 5.3F). Granulocyte-macrophage progenitor cell concentrations were lower with exercise (Figure 5.3G; p<0.01). Megakaryocyte-erythroid progenitor cell concentrations were higher in CON-EX compared to CON-SED (p<0.05, Figure 5.3H). HFD had higher bone marrow cellularity (p<0.05, Figure 5.3I) compared to CON.

Exercise decreases myeloid colony formation.

To functionally quantify HSPCs with myeloid lineage potential we magnetically sorted HSPCs and conducted a standardised CFU assay (Stem Cell Technologies Methocult GF M3434). Exercise mice had fewer CFUs for each colony subpopulation (p<0.05, Figures 5.4A-D) and the total CFU counts (p<0.0001, Figure 4E). HFD promoted CFU-GM, CFU-E, and total CFU formation (p<0.05, Figure 5.4B, C, and E).

Adipogenic conditions reduce miR-193 expression in C3H 10T1/2 cells *in vitro.*

We previously reported that marrow-derived EVs from HFD-EX mice had lower miR-193 and miR-331-5p compared to HFD-SED mice (7). These miRNAs may play a role in leukemia relapse (13) and osteogenesis through upregulated MAPK signaling (12,26). MSCs regulate leukemia genesis

through paracrine factors impacting tumor cell p38 MAPK activity (27) and are the source of osteoblasts (28); therefore, we speculated that these miRNAs may originate from MSCs. To understand whether MSCs could be responsible for the reduced marrow-derived EV miR-193 and miR-331-5p content, we quantified these miRNAs using RT-qPCR from MSCs exposed to *in vitro* models of HFD and mechanical aspects of EX. To mimic the HFD conditions we provided the MSCs with adipogenic differentiation media for 24 hours prior to miRNA extraction alongside 10 min of 2% strain to mimic exercise, as described previously (23) (Figure 5.5A). We found that the adipogenic media led to decreased miR-193 expression compared to control media ($p<0.05$, (Figure 5.5B) and a trend for more miR-193 expression ($p=0.06$, (Figure 5.5B) following strain. We also found a trend for less miR-331-5p expression with adipogenic media ($p=0.09$, (Figure 5.5C) without any impact of strain.

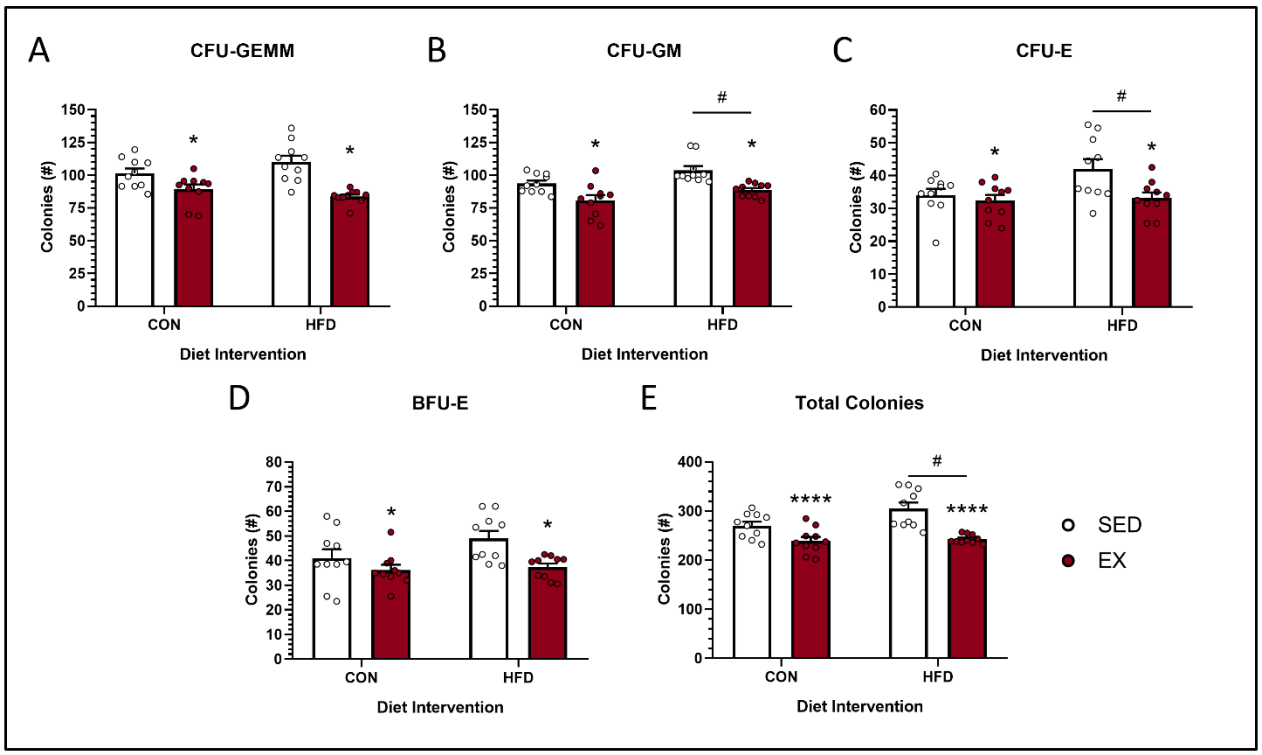

Figure 5.4. Exercise reduces myeloid colony formation. Colony forming unit data following 10 days of HSC culture in specialized differentiation media promoting myeloid colony formation. (A) colony forming unit-granulocyte, erythroid, monocyte, megakaryocyte (CFU-GEMM), (B) colony forming unit-granulocyte, monocyte (CFU-GM), (C) colony forming unit erythroid (CFU-E), (D) blast-forming unit-erythroid (BFU-E), and (E) total colony count. *p<0.05 main effect of exercise. ****p<0.0001 main effect of exercise. #p<0.05 main effect of diet (n=10 per group).

Discussion

The objective of the current study was to determine how exercise and HFD consumption impacts bone marrow cell populations during steady state hematopoiesis and to determine whether MSCs express greater miR-193 and miR-331-5p under *in vitro* adipogenic conditions. Our main findings were that HFD consumption promoted HSPC expansion and myeloid skewing, that exercise prevented HSPC priming towards the myeloid lineage, and that MSCs cultured under adipogenic conditions expressed lower miR-193 compared to control culture conditions. Overall, these results suggest that HFDs promote HSPC and myeloid cell expansion that may be related to MSC-derived miR-193 expression at steady state. Previous investigations of bone marrow cellularity in the context of HFDs and exercise have involved acute exercise interventions (9), disease states (15), and imposed stress hematopoiesis (6,29). Stress hematopoiesis involves transient blood cell reductions followed by rapid hematopoietic regeneration. Using radiation-induced hematopoietic stem cell depletion, our lab showed that exercise can mitigate negative HSPC and HPSC niche cell impacts induced by HFDs (6). In that study, several HSPC populations were lower in sedentary HFD mice compared to their exercise-trained counterparts 4 weeks following radiation exposure, indicating that exercise was stimulatory during stress hematopoiesis. Frodermann and colleagues (2019) showed that exercise promotes bone marrow mononuclear cell quiescence during steady state conditions, yet exercise also promotes their

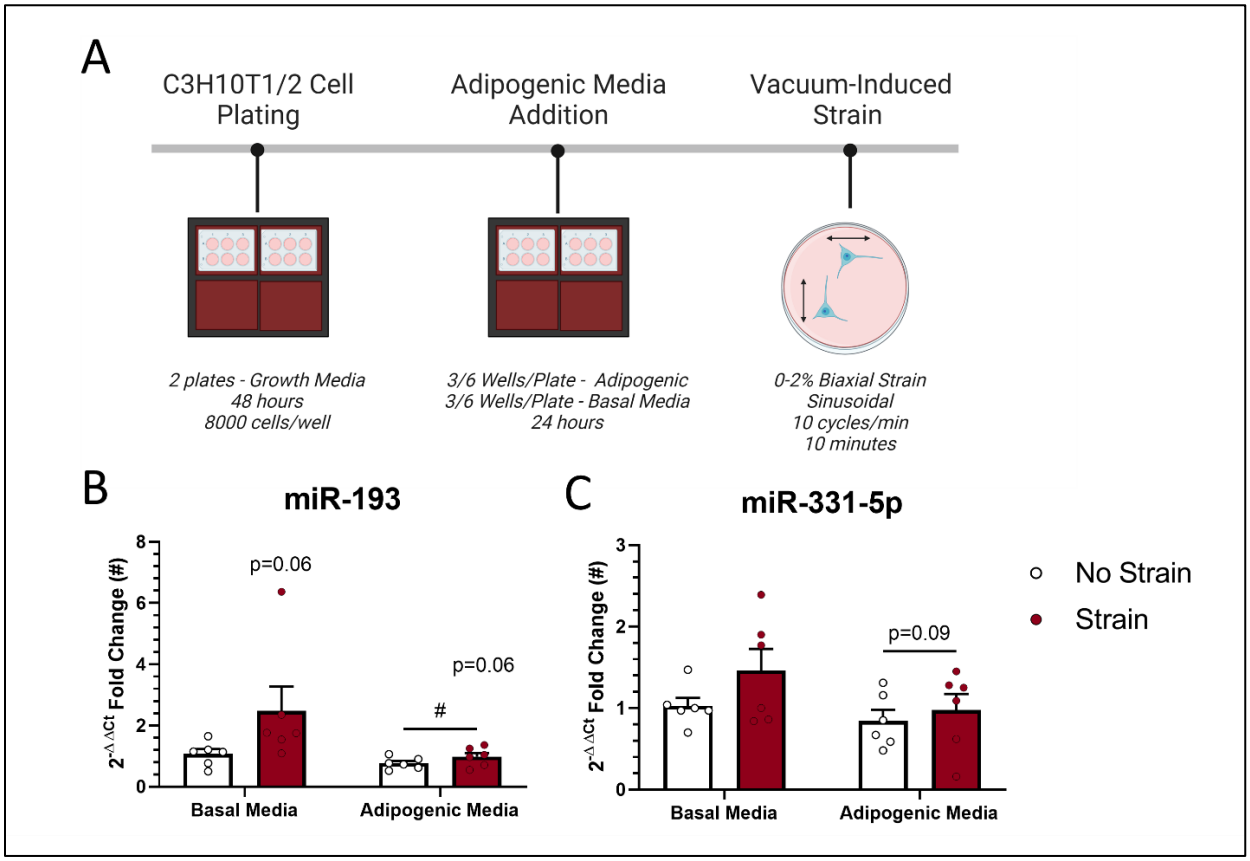

Figure 5.5. Adipogenic conditions reduce miR-193 expression in C3H 10T1/2 cells *in vitro*. (A) Outline of the Flexcell BioFlex plate seeding, Flexcell strain, miRNA extraction, and qPCR protocol. qPCR data showing miRNA $2^{-\Delta\Delta Ct}$ fold changes for (B) miR-193 and (C) miR-331-5p. There was a trend for strain in increasing miR-193 expression (p=0.0639) and for adipogenic media in decreasing miR-331-5p expression. #p<0.05 main effect of media (n=6 per group). Figure A created with BioRender.com.

expansion during lipopolysaccharide-induced stress hematopoiesis (15). These findings agree with the present study results, suggesting that EX inhibits HSPC expansion and myelopoiesis during steady state hematopoiesis.

Marrow adipose tissue accumulation is a natural occurrence with age. By adulthood over 50% of the marrow cavity is occupied by adipose tissue in humans (5). Interestingly, Styner and colleagues (2014) previously showed exercise prevents marrow adipose tissue formation during

HFD consumption (16). These results differ from ours potentially because their investigation involved 6 weeks of HFD and exercise interventions that initiated simultaneously, while our investigation initiated the exercise intervention after body weight gain and whole-body adiposity were already significantly elevated. Furthermore, their exercise model used a running wheel where the volume of exercise is much higher than the treadmill protocol used in the present study which included exercise for 1 hour three times per week for the latter 4 weeks. As such, the discrepancy between our findings and those from Styner and colleagues may be consequent to exercise volume as mice in their study ran over 9 km per day (30). By the final exercise training week our mice ran 570 meters per 1-hour session for three sessions. Exercise volume variation has been shown to impact hematopoiesis (31), and these effects may extend to bone marrow adipogenesis. Our approach is translational as most individuals with obesity will engage in a structured exercise intervention to improve health. Interestingly, a subsequent study from the same group found similar results as ours when the HFD intervention was initiated 3 months prior to exercise initiation (30).

We used flow cytometry to gain insight into how HSPCs and their differentiated progeny are impacted by HFDs and exercise under steady state conditions. Here, we found HFD increased bone marrow cellularity and promoted HSPC and HSPC-subpopulation expansion alongside common myeloid progenitor cells without impacting common lymphoid progenitor cell concentrations. Furthermore, EX reduced common myeloid progenitor and granulocyte-macrophage progenitor cell concentrations. These findings are similar to previous reports (1,2,6,7). While concentration data provides meaningful insight into the cellular makeup of the marrow environment, it does not provide a functional window into HSPC activity. To functionally

quantify the role of HFDs and exercise on HSPC myeloid populations, we plated HSPCs into specialized myeloid differentiation media to observe their myeloid differentiation potential. This assay provides critical information into the extent to which HSPCs are primed for myeloid lineage potency. Here, we found HFD consumption promoted CFU-GM, CFU-E, and total colony formation. However, exercise had lower colony formation for all colony forming units. Together, these discrepant *in vitro* and *in vivo* findings suggest that cell populations present *in vivo* may interfere via intercellular signaling to diminish the myeloid cell expansion pattern that was observed *in vitro*.

Intercellular communication is critical to HSPC activity. Our lab previously reported the impact of acute exercise on MSC paracrine factor expression (9). In that study we found a significant increase in multiple paracrine factors with acute exercise, including granulocyte colony-stimulating factor and stem cell factor (9). These factors have been shown to promote HSPC egress from the marrow (32–34). Aside from protein paracrine factors, EVs play important endocrine and paracrine roles in regulating cell function. For example, Wen and colleagues (2016) found that MSC-derived EVs accelerated leukocyte recovery in irradiated mice (35). Szatmári and colleagues (2017) isolated EVs from irradiated mice and injected them into non-irradiated bystander mice. They found DNA damage and HSPC reductions in the mice receiving EVs from irradiated mice that was similar to direct radiation (36). Together, these results imply that EVs contain cargo that regulates HSPC fate. Our lab recently conducted a study to identify potential miRNAs in marrow-derived EVs that could be altered with HFDs and exercise (7). In that study we found that marrow-derived EVs from exercised HFD mice contained lower miR-193 and miR-331-5p cargo compared to their sedentary counterparts (7). In the current study we found that

adipogenic conditions decreased miR-193 expression in MSCs while strain induced a trend for an upregulation in miR-193, which is contrary to our findings from marrow-derived EVs. Interestingly, Ying and colleagues (2020) reported that human marrow-derived MSC EVs carrying miR-193a impede colon cancer cell proliferation, migration, and invasion (37). In particular, the authors determined the mechanism for these trends was through downregulated focal adhesion kinase (FAK) signaling. Using a FAK knockout model, Lu and colleagues (2012) observed elevated HSC cell cycling while progenitor and mature blood cells remained unaffected (38). Together, these results suggest a potential role for the observed miR-193 downregulation in adipogenic MSCs in promoting HSPC expansion if they are the source of the marrow-derived EVs.

The current study did not detect alterations in miR-331-5p expression in MSCs *in vitro*, suggesting its lower presence observed in exercised HFD mice in our previous report (7) may originate from another cell source. We were unable to measure EV-derived miRNA in cell culture media due to low yield using 6-well plates in the Flexcell system; however, we can conclude that adipogenic and strained conditions differentially impact MSC miRNA expression under acute timelines (<20 min), and that these alterations could play a significant role in HSPC proliferation and differentiation.

A limitation of our *in vitro* model is that only the mechanical strain component of exercise was examined. Exercise may also induce metabolic effects or alter intercellular signaling that affects miRNA expression. It was not possible to isolate MSCs directly from HFD or EX mice in the present study due to tissue limitations which would have required expansion *in vitro*. Future work will examine miRNA-expression in bone marrow MSCs *in vivo*.

In conclusion, our results demonstrate the roles of exercise and HFDs on HSPC and HSPC niche cell content and HSPC potential for myeloid colony formation during steady state hematopoiesis. These effects may occur, in part, due to altered miRNA signaling from MSCs, specifically through downregulation of miR-193. The current findings remain correlative and the MSC lysate data are only suggestive of potential for intercellular signaling; however, they provide the basis for future studies to better understand how HFD and exercise alter MSC-derived EVs to regulate HSPC fate. Our findings contribute to the literature examining the mechanisms responsible for the systemic effects of exercise on hematopoiesis showing that exercise inhibits myelopoiesis at steady state.

Acknowledgements

We thank the University of Ottawa Faculty of Medicine Animal Behaviour and Physiology Core for their assistance with organizing treadmill availability and EchoMRI data collection. We also thank the Burger lab for their assistance with extracellular vesicle concentration quantification, and to the Micro CT Core Facility at the Ottawa Hospital Research Institute for their assistance with the marrow adipose tissue analysis.

Grants

Funding for the current project was provided by the National Sciences and Engineering Research Council (NSERC) of Canada (RGPIN-2017-04320).

Conflict of Interest

The authors declare no conflict of interest. The results of the current study do not constitute endorsement by ACSM. The results of the study are presented clearly, honestly, and without fabrication, falsification, or inappropriate data manipulation.

Author Contributions

JV designed the study, performed the experiments, analyzed the data, interpreted the results of experiments, prepared the figures, drafted the manuscript, and edited and revised the manuscript. WK assisted in bone marrow sample collection, completed the flow cytometry data analysis, and assisted in drafting the methods section of the manuscript. CG analyzed the flow cytometry data analysis and assisted in drafting the methods section of the manuscript. NC assisted in HSPC magnetic sorting and flow cytometry data collection. MD designed the study, supervised the project, contributed to data interpretation, and edited the manuscript. All authors reviewed the manuscript and approved its submission.

References

1. Singer K, DelProposto J, Lee Morris D, et al. Diet-induced obesity promotes myelopoiesis in hematopoietic stem cells. *Molecular Metabolism*. 2014;3(6):664–75.

2. Trottier MD, Naaz A, Li Y, Fraker PJ. Enhancement of hematopoiesis and lymphopoiesis in diet-induced obese mice. *Proceedings of the National Academy of Sciences*. 2012;109(20):7622–9.

3. Chen C, He W, Huang J, et al. LNMAT1 promotes lymphatic metastasis of bladder cancer via CCL2 dependent macrophage recruitment. *Nat Commun*. 2018;9(3826):1–18.

4. Li C, Xu X, Wei S, Jiang P, Xue L, Wang J. Tumor-associated macrophages: potential therapeutic strategies and future prospects in cancer. *J Immunother Cancer*. 2021;9(1):e001341.

5. Moore SG, Dawson KL. Red and yellow marrow in the femur: age-related changes in appearance at MR imaging. *Radiology*. 1990;175(1):219–23.

6. Emmons R, Ngu M, Xu G, Hernández-Saavedra D, Chen H, De Lisio M. Effects of obesity and exercise on bone marrow progenitor cells after radiation. *Medicine & Science in Sports & Exercise*. 2019;51(6):1126–36.

7. Vanhie JJ, Kim W, Ek Orloff L, Ngu M, Collao N, De Lisio M. The role of exercise-and high fat diet-induced bone marrow extracellular vesicles in stress hematopoiesis. *Front Physiol*. 2022;13:1054463.

8. Chen Q, Shou P, Zheng C, et al. Fate decision of mesenchymal stem cells: adipocytes or osteoblasts? *Cell Death Differ*. 2016;23(7):1128–39.

9. Emmons R, Niemiro GM, Owolabi O, De Lisio M. Acute exercise mobilizes hematopoietic stem and progenitor cells and alters the mesenchymal stromal cell secretome. *Journal of Applied Physiology*. 2016;120(6):624–32.

10. Fichtel P, Von Bonin M, Kuhnert R, Möbus K, Bornhäuser M, Wobus M. Mesenchymal Stromal Cell-Derived Extracellular Vesicles Modulate Hematopoietic Stem and Progenitor Cell Viability and the Expression of Cell Cycle Regulators in an Age-dependent Manner. *Front Bioeng Biotechnol*. 2022;10:892661.

11. Vu LT, Peng B, Zhang DX, et al. Tumor-secreted extracellular vesicles promote the activation of cancer-associated fibroblasts via the transfer of microRNA-125b. *Journal of Extracellular Vesicles*. 2019;8(1):1599680.

12. Lv Y, Huang Y, Xu M, et al. The miR-193a-3p-MAP3k3 Signaling Axis Regulates Substrate Topography-Induced Osteogenesis of Bone Marrow Stem Cells. *Adv Sci*. 2020;7(1):1901412.

13. Feng D-D, Zhang H, Zhang P, et al. Down-regulated miR-331-5p and miR-27a are associated with chemotherapy resistance and relapse in leukaemia. *Journal of Cellular and Molecular Medicine*. 2011;15(10):2164–75.

14. Pendse S, Kale V, Vaidya A. The Intercellular Communication Between Mesenchymal Stromal Cells and Hematopoietic Stem Cells Critically Depends on NF-κB Signalling in the Mesenchymal Stromal Cells. *Stem Cell Rev and Rep*. 2022;18(7):2458–73.

15. Frodermann V, Rohde D, Courties G, et al. Exercise reduces inflammatory cell production and cardiovascular inflammation via instruction of hematopoietic progenitor cells. *Nature Medicine*. 2019;25:1761–71.

16. Styner M, Thompson WR, Galior K, et al. Bone marrow fat accumulation accelerated by high fat diet is suppressed by exercise. *Bone*. 2014;64:39–46.

17. Kim SJ, Gajbhiye A, Lyu A-R, et al. Sex differences in hearing impairment due to diet-induced obesity in CBA/Ca mice. *Biol Sex Differ*. 2023;14(1):10.

18. Pettersson US, Waldén TB, Carlsson P-O, Jansson L, Phillipson M. Female Mice are Protected against High-Fat Diet Induced Metabolic Syndrome and Increase the Regulatory T Cell Population in Adipose Tissue. *PLoS ONE*. 2012;7(9):e46057.

19. Farber E, Kwiecien JM, Bojic D, et al. Exercise Improves Cancer-free Survival and Health Span in a Model of Radiation-induced Cancer. *Medicine & Science in Sports & Exercise*. 2021;53(11):2254–63.

20. Scheller EL, Troiano N, VanHoutan JN, et al. Use of Osmium Tetroxide Staining with Microcomputerized Tomography to Visualize and Quantify Bone Marrow Adipose Tissue In Vivo. *Methods in Enzymology*. Elsevier; 2014. p. 123–39. [cited 2020 May 13] Available from: https://linkinghub.elsevier.com/retrieve/pii/B9780124116191000070.

21. Huang H, Song T-J, Li X, et al. BMP signaling pathway is required for commitment of C3H10T1/2 pluripotent stem cells to the adipocyte lineage. *Proc Natl Acad Sci USA*. 2009;106(31):12670–5.

22. Ouyang N, Zhang P, Fu R, Shen G, Jiang L, Fang B. Mechanical strain promotes osteogenic differentiation of bone mesenchymal stem cells from ovariectomized rats via the phosphoinositide 3-kinase/Akt signaling pathway. *Mol Med Report* [Internet]. 2017 [cited 2024 Feb 19]; Available from: http://www.spandidos-publications.com/10.3892/mmr.2017.8030. doi:10.3892/mmr.2017.8030.

23. Sen B, Xie Z, Case N, Ma M, Rubin C, Rubin J. Mechanical Strain Inhibits Adipogenesis in Mesenchymal Stem Cells by Stimulating a Durable β-Catenin Signal. *Endocrinology*. 2008;149(12):6065–75.

24. Sen B, Xie Z, Case N, et al. mTORC2 Regulates Mechanically Induced Cytoskeletal Reorganization and Lineage Selection in Marrow-Derived Mesenchymal Stem Cells: mTORC2 REGULATES CYTOSKELETAL REORGANIZATION AND LINEAGE SELECTION. *J Bone Miner Res*. 2014;29(1):78–89.

25. Livak KJ, Schmittgen TD. Analysis of Relative Gene Expression Data Using Real-Time Quantitative PCR and the 2−ΔΔCT Method. *Methods*. 2001;25(4):402–8.

26. Mizerska-Kowalska M, Sławińska-Brych A, Kaławaj K, et al. Betulin Promotes Differentiation of Human Osteoblasts In Vitro and Exerts an Osteoinductive Effect on the hFOB 1.19 Cell Line Through Activation of JNK, ERK1/2, and mTOR Kinases. *Molecules*. 2019;24(14):2637.

27. Tian K, Yang S, Ren Q, et al. p38 MAPK Contributes to the Growth Inhibition of Leukemic Tumor Cells Mediated by Human Umbilical Cord Mesenchymal Stem Cells. *Cell Physiol Biochem*. 2010;26(6):799–808.

28. Liao L, Yang X, Su X, et al. Redundant miR-3077-5p and miR-705 mediate the shift of mesenchymal stem cell lineage commitment to adipocyte in osteoporosis bone marrow. *Cell Death Dis*. 2013;4(4):e600–e600.

29. De Lisio M, Phan N, Boreham DR, Parise G. Exercise-induced protection of bone marrow cells following exposure to radiation. *Appl Physiol Nutr Metab*. 2011;36(1):80–7.

30. Styner M, Pagnotti GM, McGrath C, et al. Exercise Decreases Marrow Adipose Tissue Through ß-Oxidation in Obese Running Mice. *J of Bone & Mineral Res*. 2017;32(8):1692–702.

31. Magalhães F de C, Fernandes T, Bassaneze V, et al. High-volume endurance exercise training stimulates hematopoiesis by increasing ACE NH2-terminal activity. *Clinical Science*. 2021;135(20):2377–91.

32. Reddy RL. Mobilization and collection of peripheral blood progenitor cells for transplantation. *Transfusion and Apheresis Science*. 2005;32(1):63–72.

33. Janowska-Wieczorek A, Marquez LA, Dobrowsky A, Ratajczak MZ, Cabuhat ML. Differential MMP and TIMP production by human marrow and peripheral blood CD34(+) cells in response to chemokines. *Experimental Hematology*. 2000;28(11):1274–85.

34. Liu F, Poursine-Laurent J, Link DC. Expression of the G-CSF receptor on hematopoietic progenitor cells is not required for their mobilization by G-CSF. 2000;95(10).

35. Wen S, Dooner M, Cheng Y, et al. Mesenchymal stromal cell-derived extracellular vesicles rescue radiation damage to murine marrow hematopoietic cells. *Leukemia*. 2016;30(11):2221–31.

36. Szatmári T, Kis D, Bogdándi EN, et al. Extracellular Vesicles Mediate Radiation-Induced Systemic Bystander Signals in the Bone Marrow and Spleen. *Front Immunol* [Internet]. 2017 [cited 2020 Nov 3];8 Available from: http://journal.frontiersin.org/article/10.3389/fimmu.2017.00347/full. doi:10.3389/fimmu.2017.00347.

37. Ying H, Lin F, Ding R, Wang W, Hong W. Extracellular vesicles carrying miR-193a derived from mesenchymal stem cells impede cell proliferation, migration and invasion of colon cancer by downregulating FAK. *Experimental Cell Research*. 2020;394(2):112144.

38. Lu J, Sun Y, Nombela-Arrieta C, et al. Fak depletion in both hematopoietic and nonhematopoietic niche cells leads to hematopoietic stem cell expansion. *Experimental Hematology*. 2012;40(4):307-317.e3.

Chapter VI – Thesis Aim 3

Obesity promotes marrow-derived myeloid cell accumulation while exercise reduces proliferative signaling in colon cancer

James J. Vanhie[1], Lisa Ek Orloff[1], Alice Tate[1], Cole Goode[1], Nicolas Collao[1,2], Anastasia Pisanko[2], Krista A. Power[3,4], and Michael De Lisio[1,2]

[1]School of Human Kinetics; [2]Department of Cellular and Molecular Medicine; [3]School of Nutrition Sciences, [4]Department of Biochemistry, Microbiology and Immunology, University of Ottawa, Ottawa, ON, Canada

Keywords: azoxymethane; bone marrow; hematopoiesis; inflammation; myelopoiesis

Under Review in Medicine & Science in Sports & Exercise

Assigned Paper #: Pending

Contribution: James J. Vanhie designed the study, performed the experiments, analyzed the data, interpreted the results of experiments, prepared the figures, drafted the manuscript, and edited and revised the manuscript.

***Correspondence to:**
Michael De Lisio, PhD
Roger Guindon Hall, University of Ottawa
Phone: +1 613-562-5800 ext. 6987
Email: mdelisio@uottawa.ca

Abstract

Purpose: Obesity increases colon cancer risk that has been previously linked to marrow-derived myeloid cells. We previously demonstrated that exercise training (EX) prevents colon cancer initiation, potentially through reduced myelopoiesis. However, it remains unknown whether early myeloid cell accumulation and inflammation in the colon precedes carcinogenesis with high-fat diet (HFD)-induced obesity, and if EX can attenuate these effects. We hypothesized that obesity would promote colon carcinogenesis that was preceded by myeloid cell accumulation and inflammation that would be attenuated by EX. **Methods:** C57BL/6 mice were randomized to a HFD or control (CON) diet for 8 weeks. The HFD mice switched to CON diet and all mice were given intraperitoneal injections of azoxymethane (AOM) to induce colon cancer and randomized into EX or sedentary (SED) conditions. **Results:** HFD mice developed more aberrant crypt foci (ACF), a marker for early carcinogenesis, compared to CON ($p<0.01$), and EX developed fewer ACF compared to SED ($p<0.0001$). Marrow-derived ($p<0.001$) $CD206^+$ macrophages were elevated in HFD compared to CON at study week 16 ($p<0.01$). Marrow-derived $CD206^-$ macrophages ($p<0.05$) and marrow-derived ($p<0.05$) $CD206^+$ macrophages were more abundant in HFD compared to CON at study week 42. EX did not alter colon immune cell populations. β-Catenin protein was higher in HFD compared to CON at study week 42 ($p<0.05$), and STAT3 protein content was lower at study week 28 with EX compared to SED ($p<0.05$). **Conclusion:** The results suggest that obesity promotes colon ACF formation, potentially through early inflammatory myeloid cell accumulation. Despite attenuating ACF, EX did not alter myeloid cell accumulation in the colon, suggesting that EX inhibits ACF formation through alternative mechanisms which may include reduced β-Catenin and STAT3 signaling.

Introduction

Colorectal cancer is the third most commonly diagnosed cancer and accounts for the second highest number of cancer deaths (1). While the overall incidence of colorectal cancer has decreased, young adults (<50 years) who are below the standard population screening age are being diagnosed at an increasing rate (2). The elevated rate in young adults is related to higher obesity rates and sedentary behavior (3). As of 2018, approximately 31% of American adults were classified as overweight (BMI 25≤29.9 $kg \cdot m^2$) while another 42% were categorized as having obesity (BMI ≥30 $kg \cdot m^2$) or severe obesity (BMI ≥40 $kg \cdot m^2$) (4). By 2030 it is projected that the percentage of overweight American adults will remain the same but 49% will be classified as having obesity or severe obesity (5). Therefore, understanding the link between early-onset colorectal cancer and increasing obesity rates is a significant clinical concern.

Western diets consisting of a high concentration of saturated fats, promote adipocyte hypertrophy and contribute to a considerable proportion of the obesity epidemic (6). Obesogenic conditions propagated by high-fat diet (HFD) consumption leads to chronic systemic low-grade inflammation caused, in part, by myeloid cell overproduction (7). Our lab and others have shown that HFDs promote inflammatory myeloid cell overproduction in the bone marrow that can be attenuated by exercise, and our lab has shown that exercise, not weight loss alone, decreases colorectal carcinogenesis in mice (8, 9). Our lab has also shown that myeloid cell overproduction could be consequent to altered hematopoietic stem cell (HSC) niche population concentrations, differentiation patterns, and mesenchymal stromal cell paracrine signaling (10, 11).

Monocytes and macrophages promote adipose tissue inflammation via interleukin-6 (IL-6) and tumor necrosis factor α (TNFα) release that imposes a positive inflammatory feedback

loop (12). Bone marrow-derived monocytes bind the C-C chemokine (C-C Motif) receptor 2 (CCR2) chemoattractant ligand (CCL2) to migrate from the bone marrow to the blood and peripheral tissues (13, 14). Using a macrophage-specific CCR2 knockout mouse model, Kawano and colleagues (2016) showed that macrophage-deficient mice had lower colonic pro-inflammatory macrophage infiltration, reduced intestinal permeability, downregulation of the inflammasome, and lower adipose tissue inflammation (15). These findings are pertinent to the current study as colon monocyte and macrophage accumulation is positively correlated with elevated colon cancer development (16). Bader and colleagues (2018) transiently induced macrophage knockdown in colon tumors via clodronate injection and found that the number of large and total colon neoplasms was lower in the clodronate group compared to vehicle (16). Together, these data suggest a role for myeloid cell-induced inflammation in promoting colorectal cancer onset.

Colon cancer risk is elevated in obesity alongside inflammatory cell accumulation and colon inflammation. Conversely, exercise training reduces colorectal carcinogenesis, colon inflammation, and aberrant myelopoiesis. However, a direct link between alterations in myelopoiesis, subsequent myeloid cell accumulation in the colon, and colorectal carcinogenesis remains unknown. Therefore, as a first step to address this gap, the present study aimed to determine the time course for inflammatory myeloid cell infiltration into the colon during colorectal carcinogenesis in obesity and EX conditions using a heterozygous CCR2^{gfp} mouse model to track bone marrow-derived cells. We hypothesized that obesity would promote marrow-derived myeloid cell accumulation in the colon which will enhance ACF formation, and that ACF formation would be inhibited by exercise.

Materials and Methods

Experimental Design

All animal experiments were approved by the University of Ottawa Animal Care Committee and in accordance with the Canadian Council on Animal Care and the *Animals for Research Act*. All mice were housed at room temperature on a 12:12 hour day-night cycle with water and food provided *ad libitum*. B6(C)-Ccr2$^{tm1.1Cln}$/J mice (Strain #027619, Jackson Laboratories) were bred with C57BL/6J mice (Strain #000664, Jackson Laboratories) to produce mice that were heterozygous for C-C motif chemokine receptor 2 (CCR2) possessing an enhanced green fluorescent protein. We used this model to track bone marrow-derived cell migration from the bone marrow to the blood and colon. At 5 weeks of age (study week 0) the mice were randomly assigned to either a control (CON; D100012M, Research Diets) or 45% kcal high fat (HFD; D12451, Research Diets) diet for 8 weeks, as described previously (9, 10) (Figure 6.1). At the end of the 8-week period the HFD was replaced with CON. Mice were given intraperitoneal injections of azoxymethane (AOM; 10 mg·kg-1 body mass) once weekly for 4 weeks (study weeks 9-12) to promote colorectal cancer development, similar to previous work from our lab (9). Compared to our previous study (9), dosages were reduced from 15 to 10 mg·kg^{-1} body mass to minimize lethal acute liver toxicity. At study week 16 the mice were randomized into one of three time points for sample collection; study weeks 16, 28, or 42. These time points were selected to observe the temporal relationship between myeloid cell migration to the blood and colon, inflammatory and proliferative protein marker elevation, and colorectal aberrant crypt foci formation and they are equal to 4-, 16, and 30 weeks following the final AOM injection. Mice that were placed in the 28- or 42-week time points were randomly selected to remain sedentary (SED)

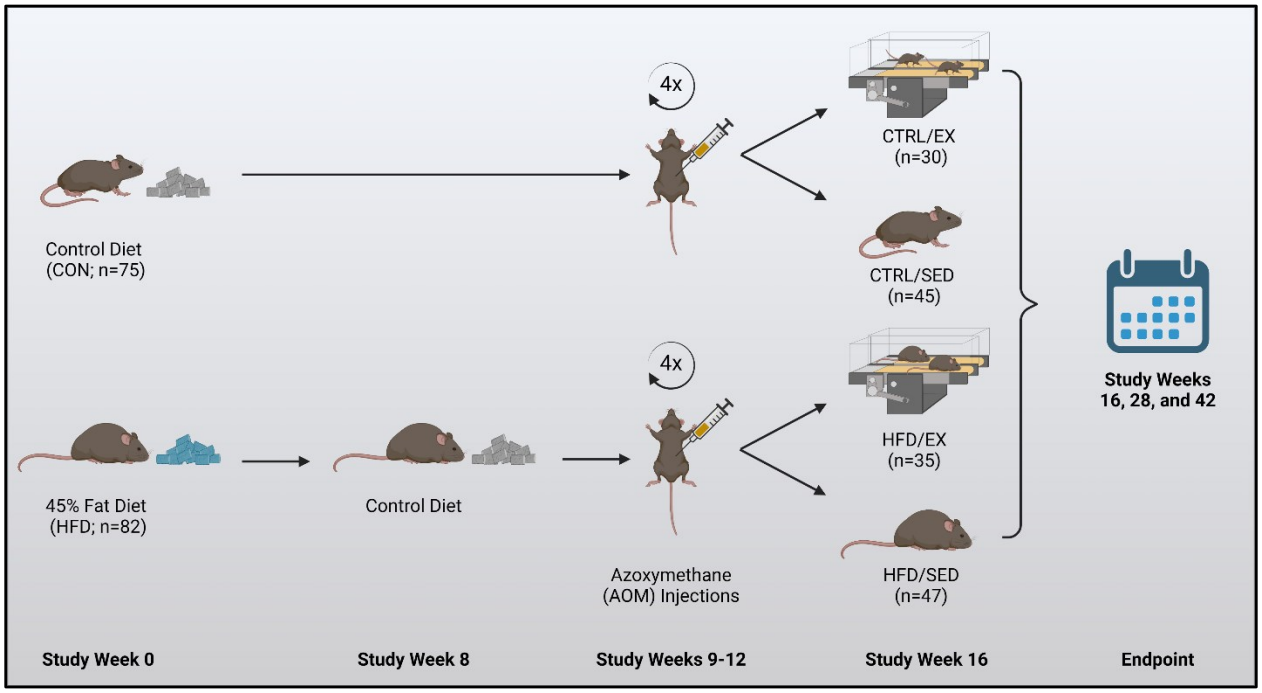

Figure 6.1. Study outline. Five-week-old male and female CCR2$^{gfp/+}$ mice (n=157, 73 male, 84 female) were randomly placed on a high-fat (HFD; 45% by calorie; n=82, 39 male, 43 female) or control (CON, n=75, 34 male, 41 female) diet for 8 weeks to promote body fat accumulation. HFD mice switched to CON diet after 8 weeks to induce weight loss, 1 week prior to the first azoxymethane (AOM) injection. AOM injections occurred in all mice once weekly during the 9th-12th weeks. Mice were randomly placed into exercise trained (EX; n=65) or sedentary (SED; n=92) conditions until the time of collection. Collections occurred at 16, 28, and 42 weeks into the study. The 16-week mice did not undergo exercise training and were categorized as SED.

or undergo an exercise (EX) training intervention. All mice underwent EchoMRI for body composition measures once every 4 weeks beginning at 5 weeks of age using an EchoMRI-900 (EchoMRI LLC), as previously described (17).

Exercise Training Intervention

EX mice completed the exercise training program as described previously, with some minor modifications (10, 11, 17) (Table S6.1). EX mice exercised three days per week for 40-60 min using an Exer 3/6 treadmill (Columbus Instruments). Weeks 1 and 2 were conducted at 8 m·min^{-1} for 25 and 35 min, respectively, and week 3 was completed at 9 m·min^{-1} for 45 min. From

weeks 4 to 18, the duration of each exercise session remained constant at 45 min, while speeds increased by 2 $m \cdot min^{-1}$ every two weeks. This progression continued until week 18, where a maximum speed of 24 $m \cdot min^{-1}$ was reached. All exercise sessions included a 10 min warmup at 10 $m \cdot min^{-1}$ (8 $m \cdot min^{-1}$ for the first 3 weeks), and a 5 min cooldown at 8 $m \cdot min^{-1}$. SED and EX mice were housed together so that stress from handling and treadmill noise was equal between groups.

Endurance Performance Test

Endurance performance tests were completed in all mice at weeks 28 (pre-training) and 42 (post-training) using an Exer 3/6 treadmill (Columbus Instruments) angled at +5°, as described previously (10, 17). The mice were acclimated to the treadmill for 10 minutes at 8 $m \cdot min^{-1}$ two days prior to completing the initial endurance test. The endurance tests began at 10 m·min-1 and increased by 1 $m \cdot min^{-1}$ in a stepwise fashion once every two minutes. The test ended when mice were unable to keep their hindlimbs on the treadmill for a full stage despite gentle encouragement using a soft-bristled paintbrush.

Blood Collection

Mice were euthanized at 16-, 28-, or 42-weeks by CO2 asphyxiation and cervical dislocation. The chest cavity was quickly exposed by separating the ribcage away from the heart and lungs. Any adipose tissue on the heart surface was removed and the heart apex was placed inside a 6.0 mL dipotassium-ethylenediaminetetraacetic acid (K_2-EDTA) BD Vacutainer (BD, Cat #367863). The right ventricle was cut using fine scissors and the blood was allowed to flow into the tube. The tubes were carefully inverted multiple times to prevent coagulation. To isolate white blood cells, 5 mL of ammonium-chloride-potassium (ACK) lysis buffer (Thermo Fisher

Scientific, Cat #A1049201) was added to the 6.0 mL K_2-EDTA tube and gently inverted for one minute. The samples were incubated at room temperature for 2 minutes. The lysed blood was carefully transferred to 15 mL conical tubes. The fluid was centrifuged at 500 g at 4 °C for 5 min and the supernatant was removed. The blood cell pellet was resuspended with 5 mL of phosphate-buffered saline (PBS) and was centrifuged again at 500 g at 4 °C for 5 min. The supernatant was once again removed and the pellet was resuspended with 5 mL of 5% fetal bovine serum (FBS) diluted in PBS, then stored on ice for later processing.

Bone Marrow Isolation

Bone marrow was collected as described previously (10, 11, 18). Briefly, the femurs were isolated, and the ends were removed. The marrow cavities were flushed with 1 mL of PBS using a 25-gauge needle. The cell suspension was centrifuged at 500 g at 4°C for 5 min. The supernatant was removed, flash frozen, and stored at -80°C. The remaining cell pellet was resuspended in 1 mL 5% FBS and stored on ice for later processing. The femurs were then carefully crushed once using a pestle and mortar, rinsed with 0.2% type II collagenase diluted in Dulbecco's Modified Eagle Medium (DMEM, high glucose), and cut into tiny fragments. Once the fragments resembled a paste, they were placed inside an incubator at 37°C and 5% CO_2 for 45 min. The cells were mixed every 15 min to assist the chemical digestion. Once the incubation was complete the cells were filtered through a 70 µm filter along with the previously isolated bone marrow cells and centrifuged at 500 g at 4°C for 5 min. The cell pellets were resuspended in 5% FBS, and one third of the cells were aliquoted for antibody staining for flow cytometry. The remaining cells were centrifuged again at 500 g at 4°C for 5 min. The supernatant was discarded, and the remaining cell pellet was flash frozen and stored at -80°C.

Flow Cytometry

Flow cytometry samples were prepared as described previously (10). Briefly, cell suspensions were centrifuged at 500 g at 4°C for 5 min and were resuspended with 100 µL Zombie Yellow viability dye in the dark for 15 min at room temperature. Following incubation, the cells were quenched with 500 µL of PBS, centrifuged at 500 g at 4°C for 5 min, and resuspended with the 200 µL of the appropriate primary antibody cocktails in the dark for 60 min on ice. Following incubation, the cells were once again quenched with 500 µL PBS, centrifuged at 500 g at 4°C for 5 min, and resuspended with 200 µL of streptavidin secondary antibody in the dark for 30 min on ice for antibody cocktails involving lineage marker primary antibodies. The gating strategies for the bone marrow, blood, and colon cells are summarized in Table S6.2, and the antibodies, conjugates, dilutions, and product numbers are summarized in Table S6.3. Representative gating figures can be found in Figures S6.1-3. Once fully stained the cells underwent a final centrifuge cycle at 500 g at 4°C for 5 min, were resuspended with 500 µL of 5% FBS, and analyzed using an Attune NxT (Thermo Fisher Scientific).

Colon Collection and Cell Isolation

The entire length of the colon was harvested and cleaned of adipose tissue. The feces were removed by rolling with a small wooden rod dipped in PBS. The colon was divided transversally into thirds. Each third was cut longitudinally and carefully placed onto a glass slide exposing the lumen. $1/8^{th}$ of the colon was cut again longitudinally from each segment and flash-frozen in liquid nitrogen for protein analysis. $1/4^{th}$ of the colon was cut longitudinally from each third and digested in 1mL of 0.2% type II collagenase (1% FBS, diluted in high-glucose DMEM) for flow cytometry analysis. The colon tissue was chopped with scissors until it resembled a paste.

The tissue was placed in a 50 mL conical tube with an additional 9 mL of 0.2% type II collagenase and incubated on a shaker at 225 rpm at 37°C for 45 min. The remaining colon tissue on the glass slide was placed in 10% formalin on a rocker for 24 hours at room temperature. The slides were carefully rinsed with deionized water, transferred to 70% ethanol, and stored at 4°C for ACF analysis.

Colon Aberrant Crypt Foci Analysis

Fixed colons were rinsed in deionized water to remove any remaining 70% ethanol. The colons were immersed in freshly prepared 0.05% w/v methylene blue/deionized water solution at room temperature by dipping the slides twenty times for one second per cycle before fully immersing the slides in the solution for 3 minutes. The colons were rinsed again in deionized water at room temperature until the excess dye was removed. Stained slides were stored in 70% ethanol until they were ready for imaging. Prior to imaging the slides were dipped in deionized water to avoid sample dehydration. Areas suspected for ACF were color-imaged with a SteREO Discovery V.20 stereo microscope (ZEISS) with Zen software v3.8 (ZEISS). Aberrant crypts were identified as being 2-3 times the size of surrounding crypts, stained darker than the surrounding crypts, and had thickened epithelial lining. Groups of aberrant crypts were collectively categorized as one ACF.

Western Blot

Western blot from colon samples were prepared as described previously with some modifications (19). We measured (p)STAT3, NF-κB, and β-catenin in the colon via western blot to understand the timeline of inflammation and proliferation relative to ACF onset. Flash-frozen colon samples were transferred from a -80°C freezer to liquid nitrogen. Samples were

homogenized in RIPA buffer (10 µL·mg^{-1}) with protease and phosphatase inhibitors using a bead homogenizer (Fisher Scientific Bead Mill 24, Thermo Fisher Scientific) for two 1-min cycles at 6 m·s^{-1}, separated by 5 seconds. The homogenized samples were centrifuged at 21,000 g for 30 seconds. The samples were transferred to a new 1.5 mL microcentrifuge tube and centrifuged at 21,000 g for 8 minutes at 4°C to isolate the protein supernatant from the tissue pellet. The samples were stored at -80°C, and an aliquot was used for protein quantification by Bradford. Samples were diluted with 4x Laemmli buffer, and 20 µg of protein for NF-κB and (p)STAT3 or 10 ug for β-catenin was resolved using SDS-PAGE. A standard sample was prepared using 2 µL of each sample and added to each gel to account for inter-gel variability. Resolved proteins were transferred to polyvinylidene fluoride membranes then stained with Ponceau. The membranes were blocked with 5% milk-TBST, washed, then stained for primary antibodies overnight at 4°C. After primary incubation the membranes were washed 3 times with TBST and incubated with secondary antibody (1:10,000 anti-rabbit HRP-linked antibody in 5% milk-TBST; Cell Signaling, Cat #7074S). After imaging on a ChemiDoc imaging system (Bio-Rad), the secondary antibody was stripped for 45 min at room temperature using Restore Western Blot stripping buffer (Thermo Fisher Scientific, Cat #21059). The membranes were then washed, re-blocked with 5% milk-TBST, and stained for the next primary antibody overnight at 4°C.

Statistical Analysis

All flow cytometry data was extracted using Attune NxT Software v4.0.0. Body weight, body fat percentage and lean body weight were analyzed at each time point using a two-factor (diet and exercise) ANOVA and Sidak post-hoc analysis to resolve significant interactions. Endurance tests, flow cytometry, ACF, and western blot data at 28 and 42 weeks were analyzed

using a two-factor (diet and exercise) ANOVA and Sidak post-hoc analysis to resolve significant interactions. Flow cytometry, ACF analysis, and western blot data at 16 weeks were analyzed by Student's t-test (diet). All statistical analysis was completed using GraphPad Prism v9 (GraphPad). All data are represented as mean ± SEM, and statistical significance was accepted at $p<0.05$. The investigators were blind to all files and experimental groups for all analyses.

Results

High-fat diet induces reversible increases in body weight and adiposity and impairs endurance performance.

Total body weight was higher in HFD compared to CON at weeks 4-12 (4 and 8 weeks, $p<0.0001$, 12 weeks, $p<0.05$, Figure 6.2A). Body fat percentage was higher in HFD compared to CON at 4 ($p<0.0001$), 8 ($p<0.0001$), 21 ($p<0.05$), 33 ($p<0.05$), and 41 ($p<0.05$) weeks, but was lower in EX compared to SED at 29 ($p<0.01$), 37 ($p<0.05$), and 41 ($p<0.05$) weeks (Figure 6.2B). Lean body weight was higher in HFD compared to CON at 4 ($p<0.0001$), 8 ($p<0.001$), and 12 ($p<0.05$) weeks (Figure 6.2C). EX mice had higher post-exercise training endurance compared to SED mice at 28 ($p<0.0001$) and 42 ($p<0.05$) weeks, and HFD mice had lower post-exercise training endurance compared to CON mice at 28 and 42 weeks ($p<0.01$, Figures 6.2D and E).

High-fat diet-induced ACF accumulation is prevented by EX.

We quantified colon ACF formation using light microscopy (Figure 6.3A). ACF formed at 16 weeks, but HFD did not differ from CON (Figure 6.3B). ACF counts were similar between diet and exercise conditions at 28 weeks (Figure 6.3C). However, HFD had greater ACF counts compared to CON at 42 weeks ($p<0.01$) and EX had lower counts compared to SED at 42 weeks ($p<0.0001$, Figure 6.3D).

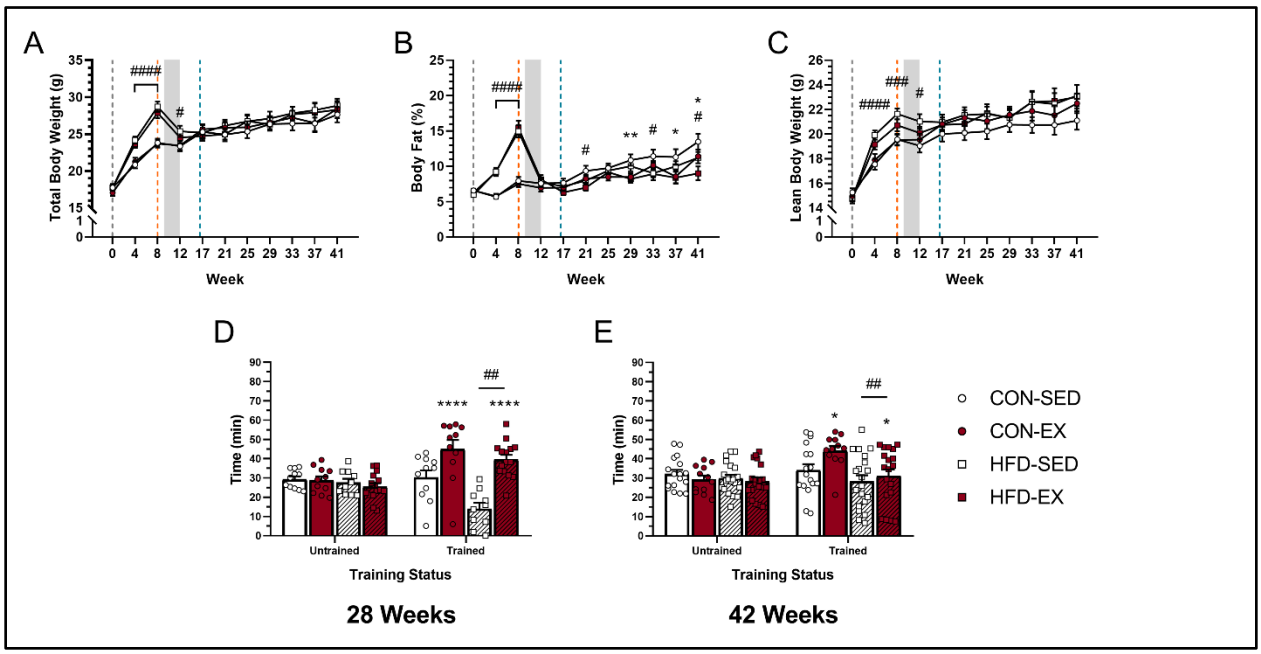

Figure 6.2. High-fat diet consumption induces temporary body weight accumulation that is reversed by control diet consumption. (A) Total body weight, (B) body fat percentage and (C) lean body weight (n=14-82 per group). Pre- and post-exercise training endurance duration tests for study weeks (D) 28 and (E) 42 (n=10-20 per group). Grey dotted line represents diet intervention initiation. Orange dotted line indicates HFD switch to CON diet. Blue dotted line represents exercise training initiation. The solid grey bar indicates the time of AOM injection. *p<0.05 main effect of exercise. **p<0.01 main effect of exercise. ****p<0.0001 main effect of exercise. #p<0.05 main effect of diet. ##p<0.01 main effect of exercise. ###p<0.001 main effect of diet. ####p<0.0001 main effect of diet. n=14-82 per group.

High-fat diet promotes early hematopoietic stem cell accumulation in the colon.

HFD led to colon HSC accumulation at 16 weeks (p<0.01, Figure 6.4A). Neither HFD nor EX impacted HSC concentration in the colon at 28 (Figures 6.4B) or 42 weeks (Figures 6.4C).

High-fat diet promotes monocyte accumulation in the colon.

HFD led to colon classical monocyte accumulation at 16 weeks (p<0.05, Figure 6.5A) that persisted at 28 weeks (p<0.05, Figure 6.5B), and there was a trend for the concentration of these cells to remain elevated at 42 weeks (p=0.10, Figures 6.5C) compared to CON. Non-classical monocytes were also higher with HFD compared to CON at 16 weeks (p<0.05, Figure 6.5D), but

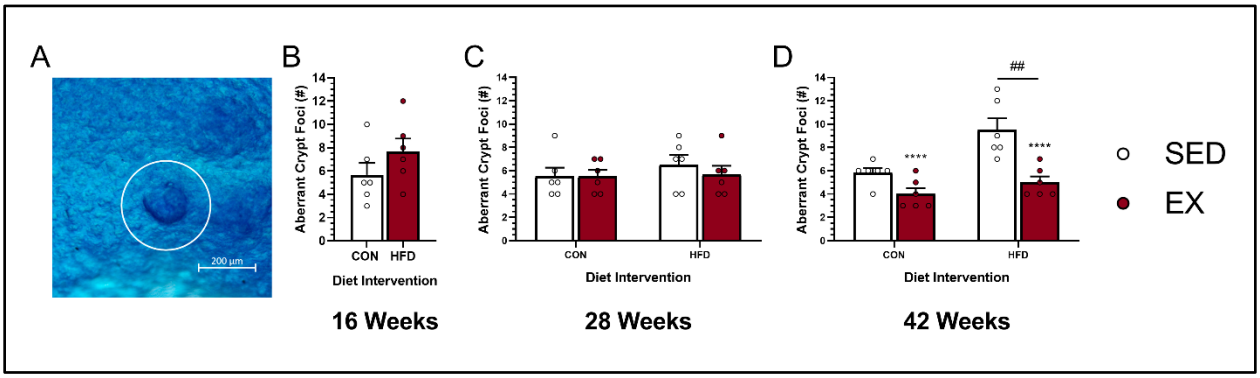

Figure 6.3. High-fat diets promote- and exercise inhibits azoxymethane-induced colon aberrant crypt formation. (A) Representative colon aberrant crypt (ACF), ACF counts at (B) 16, (C) 28, and (D) 42 weeks post-azoxymethane injection. ****p<0.0001 main effect of exercise. ##p<0.01 main effect of diet (n=6 per group).

not at 28 weeks (Figure 6.5E), but similarly exhibited a trend to remain elevated at 42 weeks (p=0.09, Figure 6.5F).

High-fat diet promotes bone marrow-derived macrophage accumulation in the colon that persists.

Total $CD206^-$ macrophages were higher with HFD compared to SED at 16 ($p<0.05$, Figure 6.6A), 28 ($p<0.05$, Figure 6.6B), and 42 ($p<0.01$, Figure 6.6C) weeks which seemed to be driven by a trend for marrow-derived $CD206^-$ macrophages to be more abundant with HFD compared to CON at 16 weeks (p=0.06, Figure 6.6D). Marrow-derived $CD206^-$ macrophages were not impacted by HFD nor EX at 28 weeks (Figure 6.6E) but were more abundant in HFD at 42 weeks compared to CON ($p<0.05$, Figure 6.6F). Total $CD206^+$ macrophages were elevated with HFD compared to CON at 16 weeks ($p<0.01$, Figure 6.6G), EX trended lower compared to SED at 28 weeks (p=0.09, Figure 6.6H), and HFD was higher compared to CON at 42 weeks ($p<0.01$, Figure 6.6I). Marrow-derived $CD206^+$ macrophages were similarly elevated at 16 weeks ($p<0.001$, Figure 6.6J) without any impact at 28 weeks (Figure 6.6K) before being higher at 42 weeks ($p<0.05$, Figure 6.6L).

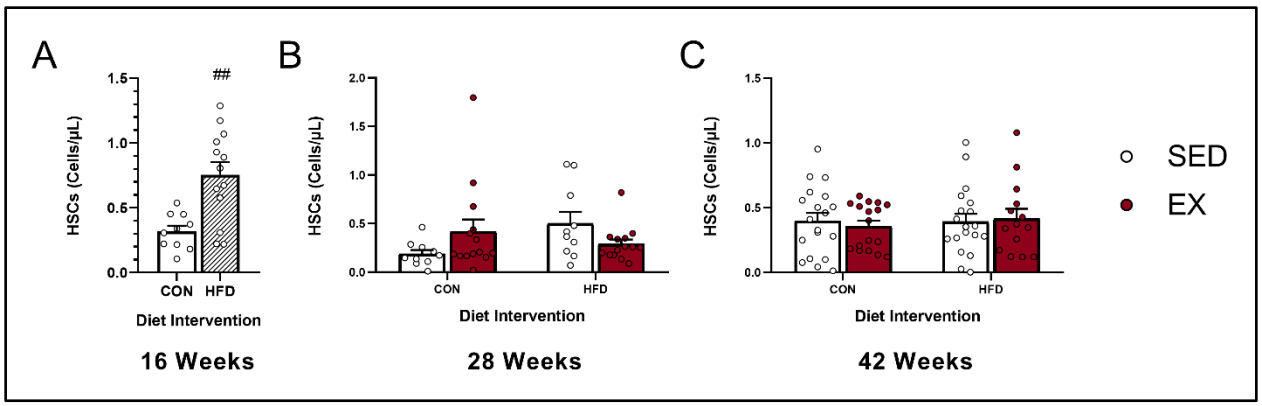

Figure 6.4. High-fat diets promote hematopoietic stem cell accumulation in the colon. Hematopoietic stem cell concentrations at (A) 16, (B) 28, and (C) 42 weeks post-azoxymethane injection. ##p<0.01 main effect of diet (n=10-19 per group).

High-fat diet promotes early myeloid-derived suppressor cell accumulation in the colon.

Total MDSC concentrations were elevated at 16 weeks with HFD compared to CON (p<0.01, Figure 6.7A) but there was no effect of HFD or EX at 28 weeks (Figures 6.7B). There was a trend for more MDSCs in HFD at 42 weeks (p=0.09, Figure 6.7C). This effect was driven by more marrow-derived MDSCs in HFD compared to CON at 16 weeks (p<0.01, Figure 6.7D), but there was no impact of HFD nor EX at 28 (Figure 6.7E) or 42 weeks (Figure 6.7F).

Exercise inhibits proliferative markers in the colon.

β-catenin was not impacted by HFD nor EX at 16 weeks (Figure 6.8A), but there was a trend for lower β-catenin with EX at 28 weeks (p=0.07, Figure 6.8B) and was higher with HFD at 42 weeks (p<0.05, Figure 6.8C). NF-κB was unaltered at all time points (Figures 6.8D-F). No difference in the pSTAT3/STAT3 ratio was detected at all time points (Figures 6.8G-I). Total STAT3 was unaltered at 16 weeks (Figure 6.8J); however, EX decreased STAT3 at 28 weeks (p<0.05, Figure 6.8K) before returning to control levels at 42 weeks (Figure 6.8L).

Discussion

Previous reports show an important role for mature myeloid cells in promoting colon ACF formation (9, 16). Our lab has also previously shown that exercise, not weight loss alone, attenuates colon ACF formation which was associated with an EX-induced reduction of inflammatory cells in the colon (9). Therefore, the current study investigated the timing of myeloid cell accumulation in the colon and its relationship to ACF onset in the context of obesity and EX. Our main findings were that mature myeloid cells accumulate in the colon with obesity at 16 weeks after study initiation that is primarily due to marrow-derived cell infiltration. The marrow-derived myeloid cell accumulation occurred at the same time point as ACF development. ACF further accumulated in HFD at 42 weeks. However, the enhanced ACF accumulation was prevented in EX and was not related to further myeloid cell accumulation. Rather, EX diminished proliferative signaling in the colon at 28 weeks, suggesting a local anti-proliferative effect as the mechanism responsible for the beneficial effects of EX on colorectal carcinogenesis.

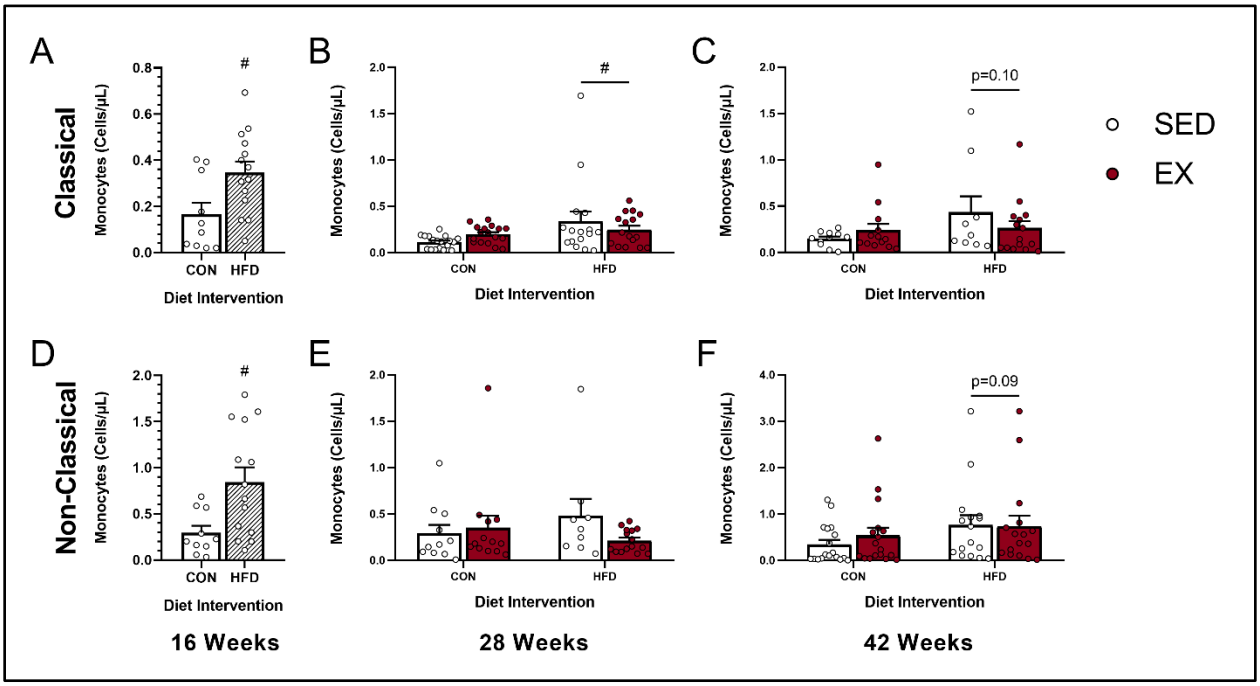

Figure 6.5. High-fat diets promote monocyte accumulation in the colon. Classical monocyte concentrations at (A) 16, (B) 28, and (C) 42 weeks post-azoxymethane (AOM) injection. Non-classical monocyte concentrations at (D) 4, (E) 16, and (F) 30 weeks post-AOM injection. #$p<0.05$ main effect of diet (n=10-18 per group).

The current study is the first to show that HSCs accumulate in colon tissue in response to obesity and colorectal carcinogenesis, that their accumulation is concomitant with marrow-derived myeloid cell accumulation, and that the myeloid cell accumulation is not deterred by EX. Accumulation of HSCs and their progenitor cells (collectively termed *HSPCs*) has been previously linked to enhanced tumor growth. Using a Lewis Lung carcinoma model, Kane and colleagues (2013) reported a direct positive correlation between marrow-derived HSPC accumulation and tumor regrowth rates (20). The elevated tumor regrowth rate was suggested to be related to HSPCs in the tumor microenvironment upregulating colony stimulating factor (CSF) release that promotes HSPC differentiation into tumor-supportive macrophages (21). These findings may extend to colorectal cancer as colon tumors have a marked increase in CSF1(22). Using a glioblastoma model, Lu and colleagues (2021) showed that HSPC accumulation in tumor tissue is positively linked to glioblastoma progression in humans (23). In that study, HSPCs co-cultured with the glioblastoma cell lines T98G, LN229, and U87 had higher cell proliferation compared to cultures without HSPCs (23). Furthermore, HSPC co-culture upregulated programmed death-ligand 1 (PD-L1) expression in the tumor cells (23). PD-L1 is a critical immune checkpoint inhibitor that moderates T cell attacks on cells, thereby allowing for unimpeded cancer cell growth (23, 24). In the context of human colon cancer, PD-L1 expression is upregulated in colon cancer tissue, and greater expression is positively correlated with enhanced tumor invasion, metastasis, and poorer survival outcomes (25). Together, these data suggest HSPC accumulation in the colon may

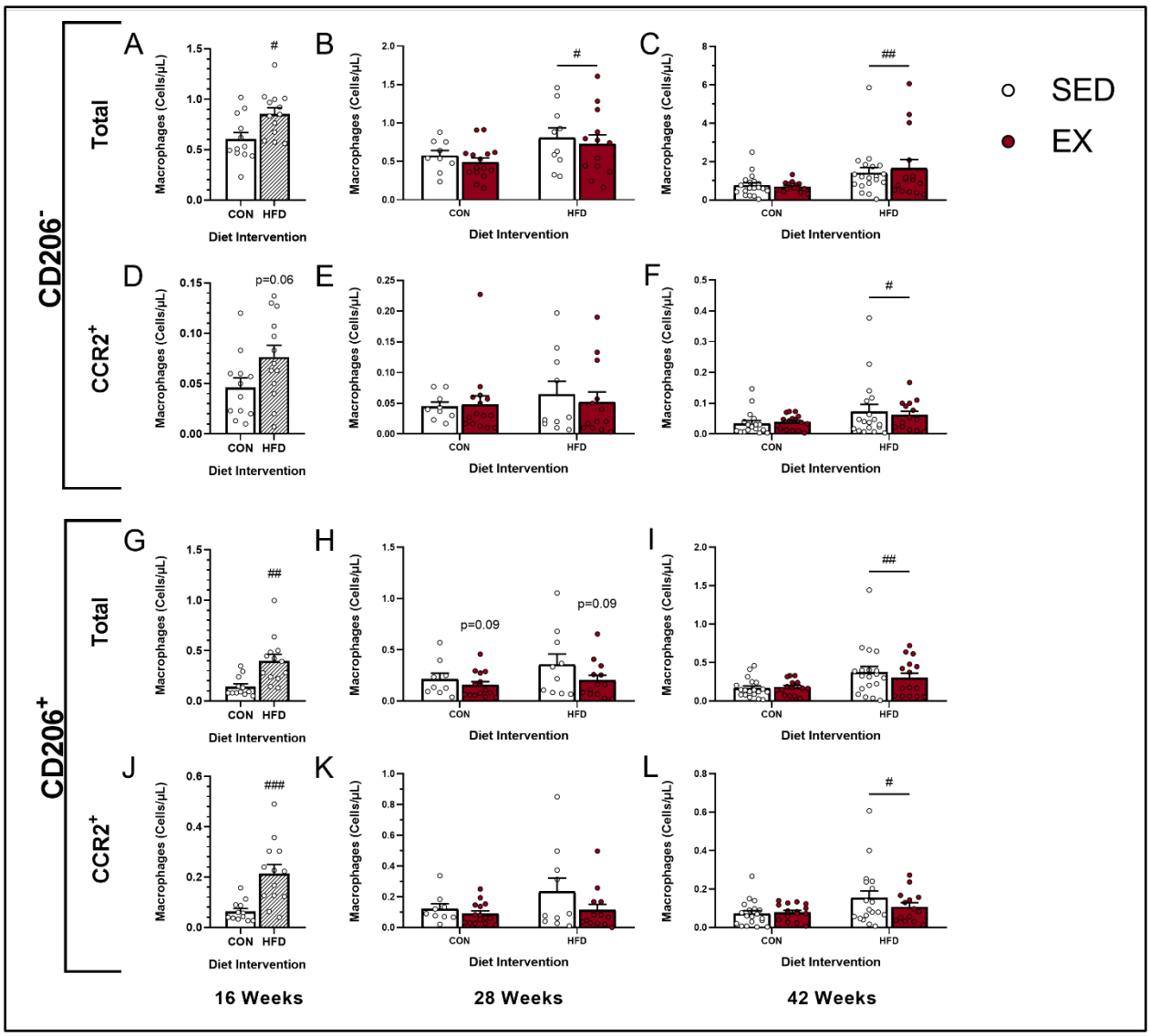

Figure 6.6. High-fat diets promote total- and marrow-derived colon macrophage accumulation in the colon. Total classically activated macrophage concentrations (A) 16, (B) 28, and (C) 42 weeks post-azoxymethane (AOM) injection. Marrow-derived classically activated macrophage concentrations at (D) 16, (E) 28, and (F) 42 weeks post-AOM injection. Total alternatively activated macrophage concentrations at (G) 16, (H) 28, and (I) 42 weeks post-azoxymethane (AOM) injection. Marrow-derived alternatively activated macrophage concentrations at (J) 16, (K) 28, and (L) 42 weeks post-AOM injection. #p<0.05 main effect of diet. ##p<0.01 main effect of diet (n=9-19 per group).

promote cancer cell resistance to T cells through intercellular signaling. Lu and colleagues (2021) also found that HSPC accumulation was positively linked to cancer severity, with glioblastoma

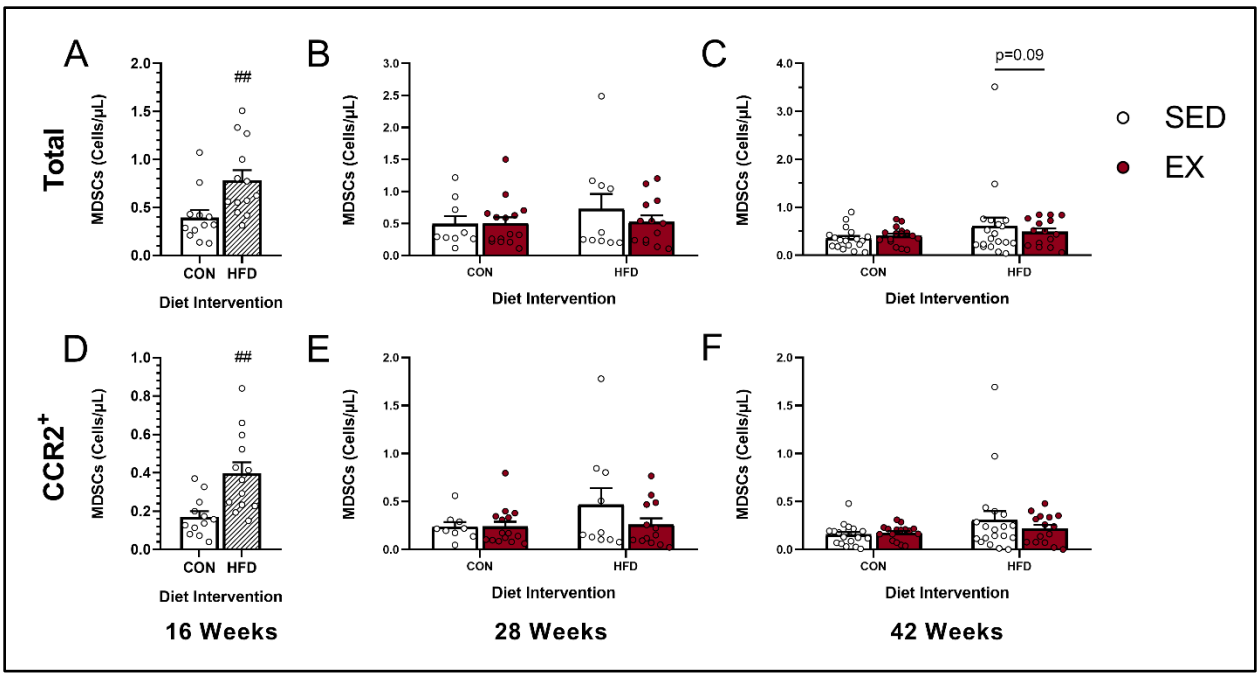

Figure 6.7. High-fat diets promote total- and marrow-derived colon myeloid-derived suppressor cell accumulation in the colon. Total myeloid-derived suppressor cell (MDSC) concentrations at (A) 16, (B) 28, and (C) 42 weeks post-azoxymethane (AOM) injection. Marrow-derived MDSC concentrations at (D) 16, (E) 28, and (F) 42 weeks post-AOM injection. ##p<0.01 main effect of diet (n=9-19 per group).

patients having higher HSC and myeloid progenitor cell populations compared to grade II and III gliomas (23). When cultured *ex vivo*, glioblastoma-derived HSCs were skewed towards myeloid differentiation compared to lower grade gliomas, suggesting tumor-associated HSCs are primed for myelopoiesis *in situ* (23). These findings align with our study, where HFD promoted mature myeloid cell accumulation, including monocytes, macrophages, and MDSCs throughout the study. Colorectal cancer cells are also capable of releasing the HSC maintenance chemokines osteopontin (26) and CXCL12 (27), providing further evidence that the colon tumor microenvironment is favourable to HSPC maintenance. Together, our results when considered in the context of previous work suggests that obesity may promote CRC initiation by recruiting HSPCs to the colon that subsequently differentiate into myeloid cells that encourage a tumor-

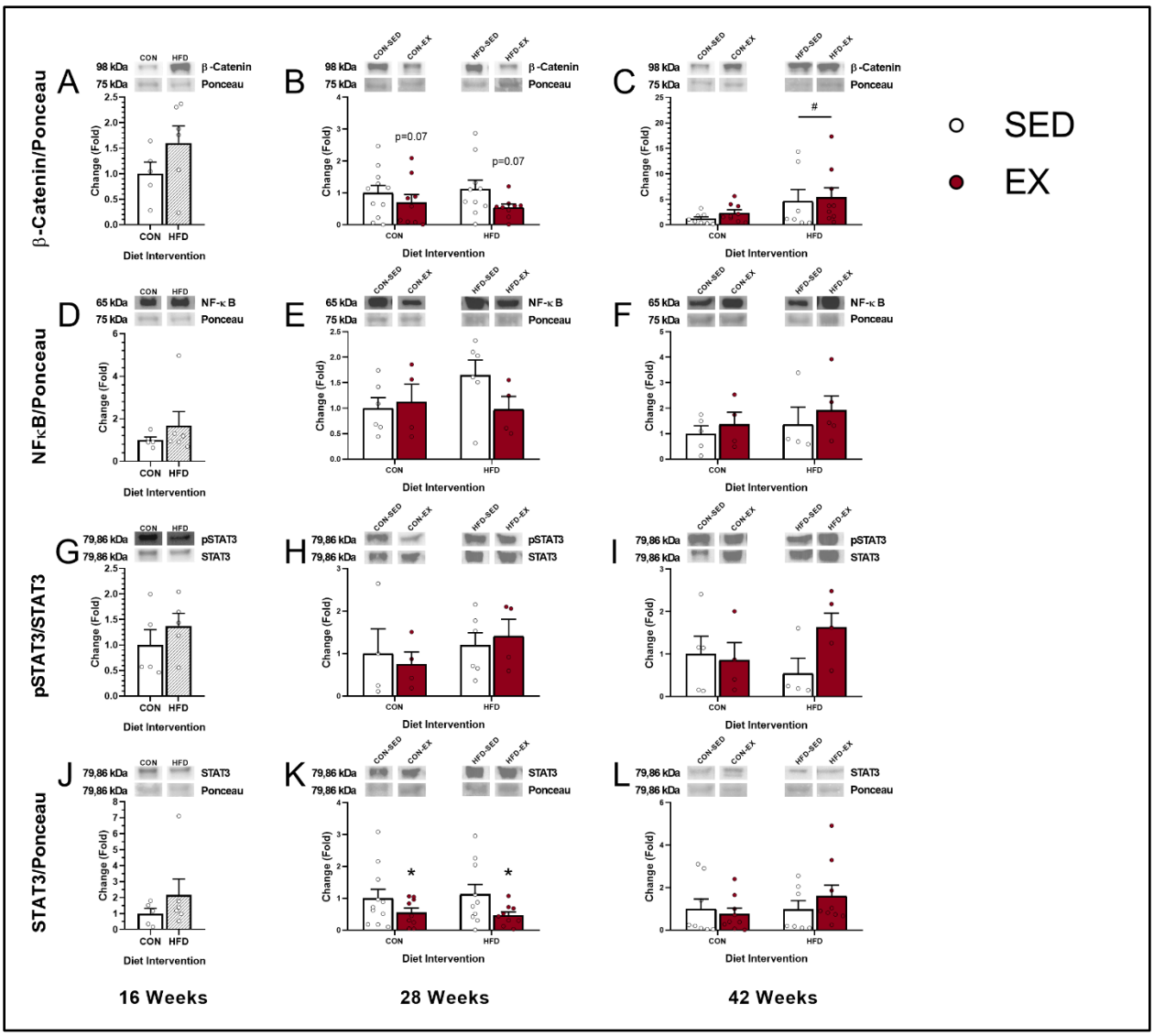

Figure 6.8. Exercise inhibits colon STAT3 presence and high-fat diet promotes β-Catenin presence. β-Catenin protein content at (A) 16, (B) 28, and (C) 42 weeks. NF-κB protein content at (D) 16, (E) 28, and (F) 42 weeks. pSTAT3/STAT3 protein content at (G) 16, (H) 28, and (I) 42 weeks. pSTAT3 protein content at (M) 16, (N) 28, and (O) 42 weeks. *p<0.05 main effect of exercise. #p<0.05 main effect of diet (n=4-11 per group).

promoting immune cell microenvironment. Since cell mobilization is energy-intensive (28, 29), HSPC differentiation at the tumor site may offer a more energy-efficient method for promoting tumor growth compared to myeloid differentiation in the marrow.

Our lab has previously shown that EX reduces colon cancer onset through downregulated inflammation (9, 30), yet our current findings suggest EX may reduce colon carcinogenesis by targeting cell proliferation pathways at early stages of colorectal carcinogenesis. We found that neither obesity nor EX altered NF-κB signaling at any time point, but instead STAT3 was lower with EX at 28 weeks, there was a trend for lower β-Catenin with EX at 28 weeks, and β-Catenin was elevated in HFD at 42 weeks. Similar to the current study, Velázquez and colleagues observed no alterations to pSTAT3/STAT3 or NF-κB via western blot following low- and high-fat diet consumption despite following a similar diet and AOM administration protocol (31). Combined, these results suggest AOM and obesity promote ACF formation through mechanisms not directly related to local inflammatory signaling in the colon. However, these conclusions are at odds with the literature, which may be due to our study design using AOM exclusively. Most studies examining the inflammatory influence on colon carcinogenesis do so using AOM and dextran sodium sulfate (DSS) to replicate inflammatory bowel syndrome and/or Crohn's disease. DSS is a polysaccharide that induces colitis by damaging the gut epithelial lining (32), thereby replicating the inflammasome observed in colitis-induced colon cancer. Colitis-induced CRC is relatively rare compared to the prevalence of non-colitis-induced CRC, and the AOM-exclusive model is the most applicable preclinical model for determining the efficacy of spontaneous tumor prevention strategies in humans (33). Further, the objective of the current study was to examine the impact of obesity and EX on innate gut inflammation and sporadic colon cancer development. We therefore opted for an AOM model of disease while excluding DSS to understand how inflammation in response to obesity and EX alters colon carcinogenesis. Our data suggest EX and obesity target cell proliferation pathways in an AOM-exclusive CRC model, and there is evidence

in the literature that demonstrates that EX mediates cell proliferation and apoptosis in humans (34). Schwappacher and colleagues (2020) found attenuated CRC cell viability *in vitro* following whole-body electrical stimulation (34). These findings were consistent when HT29 colorectal adenocarcinoma cells were supplemented with conditioned media from electrically stimulated myotubes, and gene expression analysis showed upregulated activity for apoptosis and downregulation for proliferation (34). These data align with a previous report showing that EX-induced secreted protein acidic and rich in cysteine (SPARC) secretion suppresses colon tumorigenesis (35). Combined, these data suggest EX may be inhibiting ACF formation in an AOM-exclusive model through systemic crosstalk originating from contracting skeletal muscle, ultimately leading to downregulated colon cell proliferation via altered STAT3 and β-Catenin signaling. However, the role of myokines in colon carcinogenesis remains largely understudied.

Our results show that early life obesity, followed by weight loss promotes HSC and marrow-derived myeloid cell accumulation in the colon and promotes ACF formation. However, adding EX to the weight loss stimulus inhibits further ACF formation via early alterations to proliferative signaling in the colon as evidenced by alterations in β-catenin and STAT3. Despite these findings, EX does not appear to reduce the inflammatory state in whole colon tissue. Together these findings suggest different mechanisms responsible for the differential effects of obesity and EX on colorectal cancer risk. Our findings provide an important first step in understanding the role of EX and HFDs on the time course of myeloid cell accumulation to colon carcinogenesis and show that EX is an effective strategy for attenuating colon carcinogenesis.

Acknowledgements

We would like to acknowledge the University of Ottawa Animal Care and Veterinary Service for their support with animal care. We would also like to recognise the Faculty of Medicine Animal Behaviour and Physiology Core for their support with Echo MRI and treadmill exercise.

Grants

This work was supported by the Natural Sciences and Engineering Research Council of Canada (NSERC) (RGPIN-2017-04320) and the American Institute for Cancer Research. J.V. was supported by the uOttawa/CHEO Research Institute's Doctoral Fellowship for Advancement of Biological Perspectives for Exercise Interventions Across the Lifespan and the Ontario Graduate Scholarship (OGS). N.C was supported by The Chilean National Agency for Research and Development (Agencia Nacional de Investigacion y Desarrollo [ANID]), the uOttawa/CHEO Research Institute's Doctoral Fellowship for Advancement of Biological Perspectives for Exercise Interventions Across the Lifespan, and the uOttawa Eric Poulin Centre for Neuromuscular Disease (CNMD) Scholarship in Translational Research (STaR).

Conflict of Interest

The authors declare no conflict of interest. The results of the current study are presented honestly, clearly, and without falsification, fabrication, or inappropriate data manipulation. The results of the present study do not constitute endorsement by ACSM.

Author Contributions

JV designed the study, managed the study, performed the experiments, analyzed the data, interpreted the results of the experiments, prepared the figures, drafted the manuscript,

and edited and revised the manuscript. LEO assisted in managing the study, isolated the colons, prepared the samples, and assisted in drafting the methods section of the manuscript. AT assisted in bone marrow sample collection, extracted and analyzed the flow cytometry data, and assisted in drafting the methods section of the manuscript. CG completed the colon methylene blue staining and imaging and assisted in drafting the methods section of the manuscript. NC performed and analyzed the western blots. AP assisted with bone marrow sample collection and extracted the flow cytometry data. KP assisted with the study design. KP designed the study, assisted with colon extraction techniques, and contributed to funding. MD designed the study, supervised the project, funded the project, contributed to data interpretation, and edited the manuscript. All authors reviewed the manuscript and approved its submission.

References

1. Bray F, Ferlay J, Soerjomataram I, Siegel RL, Torre LA, Jemal A. Global cancer statistics 2018: GLOBOCAN estimates of incidence and mortality worldwide for 36 cancers in 185 countries. *CA: A Cancer Journal for Clinicians*. 2018;68(6):394–424.

2. Murphy CC, Sandler RS, Sanoff HK, Yang YC, Lund JL, Baron JA. Decrease in Incidence of Colorectal Cancer Among Individuals 50 Years or Older After Recommendations for Population-based Screening. *Clinical Gastroenterology and Hepatology*. 2017;15(6):903-909.e6.

3. Nunez C, Nair-Shalliker V, Egger S, Sitas F, Bauman A. Physical activity, obesity and sedentary behaviour and the risks of colon and rectal cancers in the 45 and up study. *BMC Public Health*. 2018;18(1):325.

4. Hales CM, Carroll MD, Fryar CD, Ogden CL. Prevalence of Obesity and Severe Obesity Among Adults: United States, 2017–2018. 2020; Available from: https://www.cdc.gov/nchs/products/databriefs/db360.htm.

5. Ward ZJ, Bleich SN, Cradock AL, et al. Projected U.S. State-Level Prevalence of Adult Obesity and Severe Obesity. *N Engl J Med*. 2019;381(25):2440–50.

6. Folie S, Radlinger B, Goebel G, et al. Changing the dietary composition improves inflammation but not adipocyte thermogenesis in diet-induced obese mice. *The Journal of Nutritional Biochemistry*. 2022;99:108837.

7. Benova A, Tencerova M. Obesity-Induced Changes in Bone Marrow Homeostasis. *Front Endocrinol*. 2020;11:294.

8. Frodermann V, Rohde D, Courties G, et al. Exercise reduces inflammatory cell production and cardiovascular inflammation via instruction of hematopoietic progenitor cells. *Nature Medicine*. 2019;25:1761–71.

9. Emmons R, Xu G, Hernández-Saavedra D, et al. Effects of obesity and exercise on colon cancer induction and hematopoiesis in mice. *American Journal of Physiology-Endocrinology and Metabolism*. 2018;316(2):E210–20.

10. Vanhie JJ, Kim W, Ek Orloff L, Ngu M, Collao N, De Lisio M. The role of exercise-and high fat diet-induced bone marrow extracellular vesicles in stress hematopoiesis. *Front Physiol*. 2022;13:1054463.

11. Emmons R, Ngu M, Xu G, Hernández-Saavedra D, Chen H, De Lisio M. Effects of obesity and exercise on bone marrow progenitor cells after radiation. *Medicine & Science in Sports & Exercise*. 2019;51(6):1126–36.

12. Weisberg SP, McCann D, Desai M, Rosenbaum M, Leibel RL, Ferrante AW. Obesity is associated with macrophage accumulation in adipose tissue. *J Clin Invest*. 2003;112(12):1796–808.

13. Lu B, Rutledge BJ, Gu L, et al. Abnormalities in Monocyte Recruitment and Cytokine Expression in Monocyte Chemoattractant Protein 1–deficient Mice. *The Journal of Experimental Medicine*. 1998;187(4):601–8.

14. Huang D, Wang J, Kivisakk P, Rollins BJ, Ransohoff RM. Absence of Monocyte Chemoattractant Protein 1 in Mice Leads to Decreased Local Macrophage Recruitment and Antigen-Specific T Helper Cell Type 1 Immune Response in Experimental Autoimmune Encephalomyelitis. *The Journal of Experimental Medicine*. 2001;193(6):713–26.

15. Kawano Y, Nakae J, Watanabe N, et al. Colonic Pro-inflammatory Macrophages Cause Insulin Resistance in an Intestinal Ccl2/Ccr2-Dependent Manner. *Cell Metabolism*. 2016;24(2):295–310.

16. Bader JE, Enos RT, Velázquez KT, et al. Macrophage depletion using clodronate liposomes decreases tumorigenesis and alters gut microbiota in the AOM/DSS mouse model of colon cancer. *American Journal of Physiology-Gastrointestinal and Liver Physiology*. 2018;314(1):G22–31.

17. Farber E, Kwiecien JM, Bojic D, et al. Exercise Improves Cancer-free Survival and Health Span in a Model of Radiation-induced Cancer. *Medicine & Science in Sports & Exercise*. 2021;53(11):2254–63.

18. Emmons R, Niemiro GM, Owolabi O, De Lisio M. Acute exercise mobilizes hematopoietic stem and progenitor cells and alters the mesenchymal stromal cell secretome. *Journal of Applied Physiology*. 2016;120(6):624–32.

19. Collao N, D'Souza D, Messeiller L, et al. Radiation induces long-term muscle fibrosis and promotes a fibrotic phenotype in fibro-adipogenic progenitors. *J cachexia sarcopenia muscle*. 2023;14(5):2335–49.

20. Kane J, Krueger SA, Dilworth JT, et al. Hematopoietic Stem and Progenitor Cell Migration After Hypofractionated Radiation Therapy in a Murine Model. *International Journal of Radiation Oncology*Biology*Physics*. 2013;87(5):1162–70.

21. Parsons TM, Buelow KL, Hanna A, et al. Intratumoural haematopoietic stem and progenitor cell differentiation into M2 macrophages facilitates the regrowth of solid tumours after radiation therapy. *Br J Cancer*. 2022;126(6):927–36.

22. Wang H, Shao Q, Sun J, et al. Interactions between colon cancer cells and tumor-infiltrated macrophages depending on cancer cell-derived colony stimulating factor 1. *OncoImmunology*. 2016;5(4):e1122157.

23. Lu I-N, Dobersalske C, Rauschenbach L, et al. Tumor-associated hematopoietic stem and progenitor cells positively linked to glioblastoma progression. *Nat Commun*. 2021;12(1):3895.

24. Ghosh C, Luong G, Sun Y. A snapshot of the PD-1/PD-L1 pathway. *J Cancer*. 2021;12(9):2735–46.

25. Shan T, Chen S, Wu T, Yang Y, Li S, Chen X. PD-L1 expression in colon cancer and its relationship with clinical prognosis. *International Journal of Clinical and Experimental Pathology*. 2019;12(5):1764–9.

26. Klement JD, Poschel DB, Lu C, et al. Osteopontin Blockade Immunotherapy Increases Cytotoxic T Lymphocyte Lytic Activity and Suppresses Colon Tumor Progression. *Cancers*. 2021;13(5):1006.

27. Goïta AA, Guenot D. Colorectal Cancer: The Contribution of CXCL12 and Its Receptors CXCR4 and CXCR7. *Cancers*. 2022;14(7):1810.

28. Alghamdi A, Tamra A, Rakhmatulina A, et al. Nanoscopic Characterization of Cell Migration under Flow Using Optical and Electron Microscopy. *Anal Chem*. 2023;95(3):1958–66.

29. Li Y, Yao L, Mori Y, Sun SX. On the energy efficiency of cell migration in diverse physical environments. *Proc Natl Acad Sci USA*. 2019;116(48):23894–900.

30. Roubos S, D'Souza D, Hernández-Saavedra D, et al. Weight loss with exercise improves muscle architecture and progenitor cell populations compared with weight loss alone in mice with preneoplastic colorectal lesions. *Appl Physiol Nutr Metab*. 2021;46(7):837–45.

31. Velázquez KT, Enos RT, Carson MS, et al. Weight loss following diet-induced obesity does not alter colon tumorigenesis in the AOM mouse model. *American Journal of Physiology-Gastrointestinal and Liver Physiology*. 2016;311(4):G699–712.

32. Okayasu I, Hatakeyama S, Yamada M, Ohkusa T, Inagaki Y, Nakaya R. A novel method in the induction of reliable experimental acute and chronic ulcerative colitis in mice. *Gastroenterology*. 1990;98(3):694–702.

33. McIntyre RE, Buczacki SJA, Arends MJ, Adams DJ. Mouse models of colorectal cancer as preclinical models. *BioEssays*. 2015;37(8):909–20.

34. Schwappacher R, Schink K, Sologub S, et al. Physical activity and advanced cancer: evidence of exercise-sensitive genes regulating prostate cancer cell proliferation and apoptosis. *The Journal of Physiology*. 2020;598(18):3871–89.

35. Aoi W, Naito Y, Takagi T, et al. A novel myokine, secreted protein acidic and rich in cysteine (SPARC), suppresses colon tumorigenesis via regular exercise. *Gut*. 2013;62(6):882–9.

Chapter VII – Global Discussion

The aim of the current thesis was to address a critical gap in the literature on how obesity and EX alter hematopoiesis and the systemic consequences of those effects, particularly in colorectal carcinogenesis. Frodermann and colleagues (2019) previously reported that HFDs promote atherosclerotic development through aberrant myelopoiesis[74]. Further, they showed that EX mitigates the risk of aberrant myelopoiesis, and in turn, atherosclerotic severity[74]. Our lab has also previously shown that HFDs promote aberrant myelopoiesis in mice that is attenuated by EX during radiation-induced stress hematopoiesis[7,14]. Aberrant myelopoiesis has been linked to enhanced colorectal carcinogenesis onset which may occur by promoting an inflammatory response in the colon[13]. However, a direct inquiry into the role of HFDs and EX on myelopoiesis during steady state hematopoiesis and its implications for colorectal carcinogenesis has not been completed. To address this gap in the literature we first established the impact of EVs from HFD and EX-trained mice on HSC differentiation in naïve mice. We also explored the impacts of HFD and EX training on HSC differentiation and the niche cell populations during steady state hematopoiesis. Finally, we examined the systemic role of HFD and EX on myeloid cell accumulation and inflammation in the colon and their effects on colorectal carcinogenesis. The major findings of this thesis are as follows: First, marrow-derived EVs from HFD-SED mice promote HSC differentiation that is attenuated in HFD-EX mice, which may be due, in part, to altered miR-193 and miR-311-5p packaging (EV study, Chapter IV). Second, aberrant myelopoiesis with HFD that has been observed previously during radiation-induced stress hematopoiesis also occurs during steady state hematopoiesis (steady state hematopoiesis study, Chapter V). Third, HFDs promote myeloid cell accumulation in the colon without an effect of EX, yet EX inhibits ACF

formation, potentially through β-Catenin and STAT3 signaling cascade maintenance (CRC study, Chapter VI). Collectively, these studies identify HFDs as a major contributor to aberrant myelopoiesis, partially through EV communication. A systemic consequence of this effect is that HFD-induced HSC myelopoietic skewing promotes marrow-derived myeloid cell accumulation in the colon that contributes to colon ACF formation. Despite no effect of EX on colon marrow-derived myeloid cell accumulation, EX training emerged as a significant mitigator of ACF formation (Figure 7.1). The purpose of this chapter is to globally discuss the implications of the current studies presented herein, identify limitations, and offer future directions for subsequent investigations.

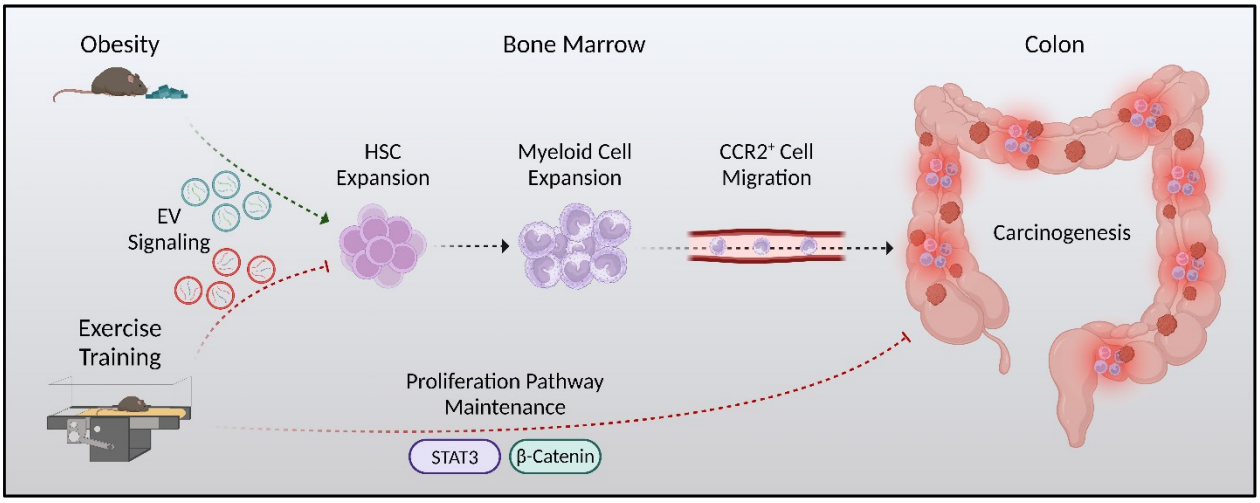

Figure 7.1. Thesis summary. Obesity and exercise training release extracellular vesicles (EVs) with altered miRNA packaging that is partially responsible for hematopoietic stem cell (HSC) expansion. Obesity also promotes myeloid cell expansion and C-C chemokine receptor 2-positive ($CCR2^+$) myeloid cell migration. $CCR2^+$ cells accumulate in the colon and promote carcinogenesis. Exercise training attenuates carcinogenesis, in part, by maintaining colon cell STAT3 and β-Catenin proliferation pathway signaling. Created with BioRender.com.

The hematopoietic stem cell niche contains a large number of cell populations that communicate with one another to maintain the immune system, forming approximately 500

billion new cells per day[75]. The hematopoietic system is capable of quickly responding to stress through multiple signaling mechanisms. Infection from external sources such as bacteria or unknown pathogens promote local inflammatory signaling at the site of the bacteria or pathogen that stimulates innate immune system interactions. Further, infection from a previously known invader can be quickly resolved by adaptive immune cells. However, internal stressors can also elicit an immune response. In our first study (Chapter IV) we examined HFD- and EX-induced effects on hematopoiesis through EV communication. Wen and colleagues (2016) previously reported that MSC-derived EVs promote leukocyte recovery following radiation damage[8]. Szatmári and colleagues (2017) showed that EVs from irradiated mice reduced HSC populations in bystander mice that were similar to irradiated mice[9]. Moreover, dendritic cell populations were expanded in the bystander mice compared to non-irradiated control EVs[9]. Together, these data suggest a significant role for EVs in bone marrow intercellular signaling and HSC differentiation. The findings from Szatmári and colleagues (2017) resemble previous work that shows that aberrant myelopoiesis occurs in response to a multitude of stress-induction mechanisms, including radiation[14] and HFDs[74].

Radiation-induced stress hematopoiesis forms genetic mutations that induce cell apoptosis[76]. In the context of the blood system, ionizing radiation promotes a transient decrease in immune cell populations, leading to HSC expansion and differentiation[76,77]. Therefore, radiation can be used to stimulate blood cell regeneration when applied at sub-lethal doses. Using a model of sub-lethal irradiation in our EV study (Chapter IV), we showed that EVs from HFD-EX mice return HSC, CMP, and CLP cell concentrations to CON levels without impacting bone marrow cellularity. Further, our EV study was the first to show in the context of EX that marrow-

derived EVs have a direct impact on HSPC expansion and differentiation. Previous studies examining EVs and EX have focused on muscle-derived or circulating EVs[78]. The interaction effects observed in HFD-EX compared to HFD-SED in our EV study (Chapter IV) were not found in the original mice from the steady state hematopoiesis study (Chapter V). Instead, the mice in Chapter V had higher HSC, MPP, and CMP concentrations with HFD without any impact on the CLPs while EX had lower CMPs and GMPs compared to SED. Further, HSPCs from EX mice had lower myeloid colony forming unit development compared to HFD in Chapter V. The observation that HFDs promote myelopoiesis that is inhibited by EX in those studies are in alignment with previous data from our lab[7,14,79] and others[74]. However, variation in the HSC expansion and differentiation responses could be due to signaling aside from EVs. The HSC niche consists of highly complex cell signaling interactions that are not exclusive to intercellular EV signaling[80]. Instead, a complex array of cytokines interact across many cell types that influence HSC differentiation. Our lab previously reported altered bone marrow cytokine signaling 4 weeks after a single session of radiation when mice underwent EX training until collection[7]. Marrow-derived macrophage colony-stimulation factor (M-CSF) and macrophage inflammatory protein-2 (MIP-2) in particular were greater in EX-trained mice compared to HFD-SED mice[7]. M-CSF and MIP-2 activate hematopoiesis without exhausting the HSPC pool, which is critical for HSPC maintenance[81]. A previous study from our lab also showed an important role for MSC intercellular signaling in hematopoiesis[82]. In that study, Lin^- $CD45^-$ MSCs from mice undergoing a single bout of exercise were isolated and cultured for 24 hours[82]. Granulocyte colony-stimulating factor (G-CSF), stem cell factor (SCF), interleukin-2 (IL-2), interleukin-17 (IL-17), and Interleukin-3 (IL-3) were all upregulated with EX[82]. In addition, interferon-γ (IFN-γ) and IL-5 were lower in EX

compared to CON MSCs[82]. These data suggest an important role for MSC signaling in hematopoiesis. These findings could not be corroborated in Chapters IV and V as we did not consider cytokine signaling in our research questions. Instead, we focused on a novel mechanism of intercellular communication via EVs and their miRNA cargo.

In Chapter IV, we found that marrow-derived EVs had lower miR-331-5p and miR-193 content in HFD-EX-derived EVs compared to HFD-SED. Bone marrow miR-331-5p content has been previously linked to worsened acute myeloid leukemia outcomes[83] and leukemia relapse[84]. Similarly, miR-193 overexpression is linked to HSC regenerative impairment and enhanced granulocytic differentiation[85]. In our steady state hematopoiesis study (Chapter V) we found a trend for lower miR-331-5p expression in MSCs *in vitro* undergoing early adipogenic differentiation and was lower for miR-193. Together, these data suggest bone marrow MSCs are the source of altered miRNA expression in marrow-derived EVs. MSC-derived EVs from the bone marrow directly regulate HSC function[86]. Fichtel and colleagues (2022) showed that marrow-derived MSC EVs from aged (median 70 years) human donors had higher miR-29a and miR-34a cargo compared to young (median 22 years) donors[86]. Further, HSPCs incubated with EVs from young donors exhibited significantly greater cell viability and expansion compared to HSPCs incubated with EVs from aged donors[86]. In the context of diet, adipose tissue-derived EVs from patients with obesity promote kidney inflammation that is attenuated by EVs from lean patients[87]. Together, our studies suggest MSCs are a significant source of marrow-derived EVs that alter HSC differentiation, and that HFDs promote EV miRNA packaging that leads to inflammatory cell formation.

While in Chapters IV and V we observed aberrant myelopoiesis in the bone marrow with HFD, Chapter VI showed that marrow-derived myeloid cell accumulation in the colon is higher with HFD alongside higher colon ACF formation. The HFD-induced marrow-derived myeloid accumulation in the colon in Chapter VI occurred despite the switch from HFD to CON diet, suggesting there is a long-term local effect that drives marrow-derived myeloid cell accumulation and differentiation that remains following HFD cessation and subsequent weight loss. Long-term impacts by HFD on the colon environment may occur through several mechanisms. Long-term myeloid accumulative effects may be secondary to HFD-induced metabolic syndrome. Metabolic syndrome involves the dysregulation of several critical cell functions, including glucose handling, dyslipidemia, and hypertension that is characterized in obesity in humans with chronic low-grade systemic inflammation[88]. While not measured in the current collection of studies, insulin resistance has been observed alongside excessive and persistent adipokine release[89]. Continual adipokine release may promote localized insulin resistance in colon cells through autocrine and paracrine signaling while also enhancing local chronic inflammation through a positive myeloid cell cytokine release loop that may persist following HFD cessation[90]. Cottam and colleagues (2022) observed T cell exhaustion and upregulated lipid handling (*Trem2, Cd36, and Cd9*) and co-stimulation (*Cd86 and Cd40*) genes in adipose tissue monocytes that was not reversed with weight loss[91]. These findings may extend to the colon tissue where we found persistent HFD-induced myeloid cell accumulation (Chapter VI).

A second mechanism through which HFDs may impose long-term alterations to the colon environment is through epigenetic modifications. HFDs are capable of inducing epigenetic modifications to the leptin promotor gene, where enhanced methylation has been observed in

rats following 11 weeks of 60% HFD compared to CON[92]. As we observed consistent long-term myeloid cell accumulation in the absence of a HFD (Chapter VI), one may speculate that there could be an epigenetic memory supporting myeloid cell accumulation in the colon. Many epigenetic modifications are at the forefront of altered hematopoiesis that invoke blood diseases, including acute myeloid leukemia and lymphomas[93]. Edillor and colleagues (2019) fed mice a HFD for 8 weeks followed by a low-fat chow diet for 4 weeks to examine DNA methylation alterations in the liver[94]. In their study, 83 candidate sites underwent epigenetic changes that were linked to body fat accumulation and elevated plasma glucose concentrations[94]. Of the 83 candidate sites, 36 had persistent epigenetic changes despite returning to a low-fat chow diet and lean body composition[94], suggesting that HFDs promote long-term alterations to gene availability that could impact distant tissues. These findings may be especially important given the positive relationship between hyperlipidemia and aberrant myelopoiesis[95–97]. Understanding how HFDs and EX alter the epigenetic makeup of HSCs could have direct implications for CRC development by restricting aberrant myelopoiesis, which may in turn mitigate CRC onset and development. Therefore, future studies should investigate gene sites altered by HFDs and EX, and importantly, how these sites retain an epigenetic memory that predisposes them to aberrant myelopoiesis. To accomplish this goal, single cell analysis for assay for transposase-accessible chromatin using sequencing (scATAC-seq) and single nucleus analysis pipeline for ATAC-seq (SnapATAC) software can be used[98]. scATAC-seq can be used to examine accessible chromatin across the colon tissue without requiring cell sorting, thereby offering comprehensive insight into the diversity of gene accessibility with HFD and EX.

Limitations

The studies completed in the current thesis were carefully planned to provide insight into hematopoiesis, the HSC niche, and systemic effects of HFDs and EX, yet the conclusions of the data should be made carefully as some limitations were present.

In Chapter IV we injected non-irradiated EVs into mice given whole-body sublethal irradiation. Radiation damages all blood cells and leads to reductions in blood cell counts. To compensate, HSCs undergo a state of stress hematopoiesis where they proliferate and differentiate at an accelerated rate to restore the immune system. While stress hematopoiesis allowed us to observe the impact of exogenous marrow-derived EVs on blood cell regeneration, we were unable to directly interpret how EVs impact hematopoiesis at steady state. Furthermore, we were unable to isolate the cell source of the EVs. Previous studies indicate that MSCs impose altered HSC differentiation through EV communication[8,86], but we could not confirm that in Chapter IV. EVs from specific tissues have been found to include specific markers based on cell origin[99]. Therefore, future studies should isolate and identify EV surface markers from marrow-derived cells via fluorescence-activated cell sorting (FACS) or magnetic-activated cell sorting (MACS) to promote our understanding of EV-based intercellular communication.

In Chapter V we investigated whether MSCs were the source of altered miR-193 and miR-331-5p packaging in EVs that we saw in Chapter IV. There were several limitations with this method. First, the EV yield from the media was too low to obtain miRNA samples pure enough for RT-qPCR. We therefore had to obtain the miRNA from MSC lysate. There are limitations in understanding how cells choose which components are packaged into EVs and released[100]. Since we used a cell line (C3H/10T1/2) instead of marrow-derived cells, we could not entirely

recapitulate the bone marrow milieu. Therefore, our observation that miR-193 was lower with lipid accumulation in C3H/10T1/2 MSCs *in vitro* may not directly translate to miR-193 packaging and release in EVs *in vivo*. While we did observe a trend for lower miR-193 and miR-331-5p expression in MSCs under adipogenic conditions, the cells were undergoing early differentiation. The model used for that test included adipogenic differentiation media to promote lipid uptake alongside mechanical strain to induce a physical stress response in the cells. This model allowed us to study the contribution of lipid uptake and physical strain on MSC EV miRNA cargo incorporation. While mechanical strain has been used to model the mechanical signals induced by exercise in vivo[101,102], it does not fully capitulate the complex *in vivo* conditions.

Chapter VI included an extensive study examining the role of inflammation on colon cancer initiation. Inflammation was inferred using the inflammatory protein NF-κB as NF-κB signaling induces inflammatory cytokine production[103]. However, there are several caveats. This method of inferring inflammation was used to understand how the accumulative inflammation signal could be impacted by HFD and EX but does not measure specific cytokines. Since immunohistochemistry was not used, we were unable to identify the spatial relationships between ACF formation, inflammatory marker presence, and marrow-derived myeloid cell accumulation. Similarly, we did not visualize the colon epithelial lining and therefore could not measure alterations in bacteria-induced inflammation via lipopolysaccharide release[104].

Final Remarks

The studies presented in the current thesis demonstrate a critical role for obesity and EX in HSC differentiation. Furthermore, obesity and EX impose significant differential effects on colorectal carcinogenesis. Specifically, obesity promotes myelopoiesis and myeloid cell egress from the marrow that promote colorectal carcinogenesis, while EX attenuates colorectal carcinogenesis despite not impacting myeloid cell accumulation. Collectively, the thesis proposes regular endurance training and avoidance of obesity to attenuate the risk of myelopoiesis and the associated colorectal carcinogenesis. Future studies are required to further our understanding of the mechanisms underlying HFDs, EX, and colorectal carcinogenesis at the cellular level. Overall, the current collection of studies demonstrate that EVs are important intercellular messengers for miRNA across the bone marrow that directly impact hematopoiesis. Further, we show that MSCs could play a direct role in varied miRNA signaling that promotes or inhibits aberrant myelopoiesis under adipogenic or physically strained conditions. Finally, we show that a transient HFD intervention has a long-term detrimental effect myeloid cell accumulation in the colon and colorectal carcinogenesis which can be attenuated by EX training. Furthering our understanding of impacted metabolic pathways and cell communication from the marrow to the colon could lead to novel EX and diet-inspired avoidance strategies for colorectal cancer onset. Overall, the findings presented herein provide a significant foundation that will positively impact Canadians by improving our understanding of the mechanisms by which obesity and exercise regulate hematopoiesis and colorectal cancer formation.

References for Thesis Abstract, Chapter III, and Chapter VII

1. Hales, C. M., Carroll, M. D., Fryar, C. D. & Ogden, C. L. Prevalence of Obesity and Severe Obesity Among Adults: United States, 2017–2018. https://www.cdc.gov/nchs/products/databriefs/db360.htm (2020).

2. Folie, S. *et al.* Changing the dietary composition improves inflammation but not adipocyte thermogenesis in diet-induced obese mice. *The Journal of Nutritional Biochemistry* **99**, 108837 (2022).

3. Singer, K. *et al.* Diet-induced obesity promotes myelopoiesis in hematopoietic stem cells. *Molecular Metabolism* **3**, 664–675 (2014).

4. Trottier, M. D., Naaz, A., Li, Y. & Fraker, P. J. Enhancement of hematopoiesis and lymphopoiesis in diet-induced obese mice. *Proceedings of the National Academy of Sciences* **109**, 7622–7629 (2012).

5. Chen, C. *et al.* LNMAT1 promotes lymphatic metastasis of bladder cancer via CCL2 dependent macrophage recruitment. *Nat Commun* **9**, 1–18 (2018).

6. Li, C. *et al.* Tumor-associated macrophages: potential therapeutic strategies and future prospects in cancer. *J Immunother Cancer* **9**, e001341 (2021).

7. Emmons, R. *et al.* Effects of obesity and exercise on bone marrow progenitor cells after radiation. *Medicine & Science in Sports & Exercise* **51**, 1126–1136 (2019).

8. Wen, S. *et al.* Mesenchymal stromal cell-derived extracellular vesicles rescue radiation damage to murine marrow hematopoietic cells. *Leukemia* **30**, 2221–2231 (2016).

9. Szatmári, T. *et al.* Extracellular Vesicles Mediate Radiation-Induced Systemic Bystander Signals in the Bone Marrow and Spleen. *Front. Immunol.* **8**, (2017).

10. Nunez, C., Nair-Shalliker, V., Egger, S., Sitas, F. & Bauman, A. Physical activity, obesity and sedentary behaviour and the risks of colon and rectal cancers in the 45 and up study. *BMC Public Health* **18**, 325 (2018).

11. Cai, S., Li, Y., Ding, Y., Chen, K. & Jin, M. Alcohol drinking and the risk of colorectal cancer death: a meta-analysis. *European Journal of Cancer Prevention* **23**, 532–539 (2014).

12. Chan, D. S. M. *et al.* Red and Processed Meat and Colorectal Cancer Incidence: Meta-Analysis of Prospective Studies. *PLoS ONE* **6**, e20456 (2011).

13. Bader, J. E. *et al.* Macrophage depletion using clodronate liposomes decreases tumorigenesis and alters gut microbiota in the AOM/DSS mouse model of colon cancer. *American Journal of Physiology-Gastrointestinal and Liver Physiology* **314**, G22–G31 (2018).

14. Emmons, R. *et al.* Effects of obesity and exercise on colon cancer induction and hematopoiesis in mice. *American Journal of Physiology-Endocrinology and Metabolism* **316**, E210–E220 (2018).

15. Velázquez, K. T. *et al.* Weight loss following diet-induced obesity does not alter colon tumorigenesis in the AOM mouse model. *American Journal of Physiology-Gastrointestinal and Liver Physiology* **311**, G699–G712 (2016).

16. Halberg, N., Wernstedt-Asterholm, I. & Scherer, P. E. The Adipocyte as an Endocrine Cell. *Endocrinology and Metabolism Clinics of North America* **37**, 753–768 (2008).

17. Cinti, S. *et al.* Adipocyte death defines macrophage localization and function in adipose tissue of obese mice and humans. *Journal of Lipid Research* **46**, 2347–2355 (2005).

18. Trayhurn, P. & Wood, I. S. Adipokines: inflammation and the pleiotropic role of white adipose tissue. *Br J Nutr* **92**, 347–355 (2004).

19. Italiani, P. & Boraschi, D. From Monocytes to M1/M2 Macrophages: Phenotypical vs. Functional Differentiation. *Front. Immunol.* **5**, (2014).

20. Fujimura, N. *et al.* CCR2 inhibition sequesters multiple subsets of leukocytes in the bone marrow. *Sci Rep* **5**, 11664 (2015).

21. Murano, I. *et al.* Dead adipocytes, detected as crown-like structures, are prevalent in visceral fat depots of genetically obese mice. *Journal of Lipid Research* **49**, 1562–1568 (2008).

22. Revelo, X. S., Luck, H., Winer, S. & Winer, D. A. Morphological and Inflammatory Changes in Visceral Adipose Tissue During Obesity. *Endocr Pathol* **25**, 93–101 (2014).

23. Weisberg, S. P. *et al.* Obesity is associated with macrophage accumulation in adipose tissue. *J. Clin. Invest.* **112**, 1796–1808 (2003).

24. Hotamisligil, G. S., Shargill, N. S. & Spiegelman, B. M. Adipose Expression of Tumor Necrosis Factor-α: Direct Role in Obesity-Linked Insulin Resistance. *Science* **259**, 87–91 (1993).

25. Kern, L. *et al.* Obesity-Induced TNFα and IL-6 Signaling: The Missing Link between Obesity and Inflammation—Driven Liver and Colorectal Cancers. *Cancers* **11**, 24 (2018).

26. Jais, A. & Brüning, J. C. Hypothalamic inflammation in obesity and metabolic disease. *Journal of Clinical Investigation* **127**, 24–32 (2017).

27. Marshall, J. R. Prevention of Colorectal Cancer: Diet, Chemoprevention, and Lifestyle. *Gastroenterology Clinics of North America* **37**, 73–82 (2008).

28. Bray, F. *et al.* Global cancer statistics 2018: GLOBOCAN estimates of incidence and mortality worldwide for 36 cancers in 185 countries. *CA: A Cancer Journal for Clinicians* **68**, 394–424 (2018).

29. Haggar, F. & Boushey, R. Colorectal Cancer Epidemiology: Incidence, Mortality, Survival, and Risk Factors. *Clinics in Colon and Rectal Surgery* **22**, 191–197 (2009).

30. Ait Ouakrim, D. *et al.* Trends in colorectal cancer mortality in Europe: retrospective analysis of the WHO mortality database. *BMJ* h4970 (2015) doi:10.1136/bmj.h4970.

31. Botteri, E. *et al.* Smoking and Colorectal Cancer: A Meta-analysis. *JAMA* **300**, 2765 (2008).

32. Kyrgiou, M. *et al.* Adiposity and cancer at major anatomical sites: umbrella review of the literature. *BMJ* j477 (2017) doi:10.1136/bmj.j477.

33. Nassar, D. & Blanpain, C. Cancer Stem Cells: Basic Concepts and Therapeutic Implications. *Annu. Rev. Pathol. Mech. Dis.* **11**, 47–76 (2016).

34. Medema, J. P. Cancer stem cells: The challenges ahead. *Nat Cell Biol* **15**, 338–344 (2013).

35. Henrikson, N. B. *et al.* Family history and the natural history of colorectal cancer: systematic review. *Genet Med* **17**, 702–712 (2015).

36. Jiao, S. *et al.* Estimating the heritability of colorectal cancer. *Human Molecular Genetics* **23**, 3898–3905 (2014).

37. Syngal, S. *et al.* ACG Clinical Guideline: Genetic Testing and Management of Hereditary Gastrointestinal Cancer Syndromes. *American Journal of Gastroenterology* **110**, 223–262 (2015).

38. The Cancer Genome Atlas Network. Comprehensive molecular characterization of human colon and rectal cancer. *Nature* **487**, 330–337 (2012).

39. Groden, J. *et al.* Identification and characterization of the familial adenomatous polyposis coli gene. *Cell* **66**, 589–600 (1991).

40. Kinzler, K. *et al.* Identification of a gene located at chromosome 5q21 that is mutated in colorectal cancers. *Science* **251**, 1366–1370 (1991).

41. Forrester, K., Almoguera, C., Han, K., Grizzle, W. E. & Perucho, M. Detection of high incidence of K-ras oncogenes during human colon tumorigenesis. *Nature* **327**, 298–303 (1987).

42. Nagase, H. & Nakamura, Y. Mutations of the APC (Adenomatsus Polyposis Coli) Gene. 10 (1992).

43. Komiya, Y. & Habas, R. Wnt signal transduction pathways. *Organogenesis* **4**, 68–75 (2008).

44. Fearon, E. R. Molecular Genetics of Colorectal Cancer. *Annual Review of Pathology: Mechanisms of Disease* **6**, 479–507 (2011).

45. Kim, D. H., Lubner, M. G., Cahoon, A. R., Pooler, B. D. & Pickhardt, P. J. Flat Serrated Polyps at CT Colonography: Relevance, Appearance, and Optimizing Interpretation. *RadioGraphics* **38**, 60–74 (2018).

46. Li, Z.-N., Zhao, L., Yu, L.-F. & Wei, M.-J. BRAF and KRAS mutations in metastatic colorectal cancer: future perspectives for personalized therapy. *Gastroenterology Report* **8**, 192–205 (2020).

47. Montagut, C. & Settleman, J. Targeting the RAF–MEK–ERK pathway in cancer therapy. *Cancer Letters* **283**, 125–134 (2009).

48. Benvenuti, S. *et al.* Oncogenic Activation of the RAS/RAF Signaling Pathway Impairs the Response of Metastatic Colorectal Cancers to Anti–Epidermal Growth Factor Receptor Antibody Therapies. *Cancer Res* **67**, 2643–2648 (2007).

49. Downward, J. Targeting RAS signalling pathways in cancer therapy. *Nat Rev Cancer* **3**, 11–22 (2003).

50. Vasen, H. F. A. *et al.* Guidelines for surveillance of individuals with constitutional mismatch repair-deficiency proposed by the European Consortium “Care for CMMR-D” (C4CMMR-D). *J Med Genet* **51**, 283–293 (2014).

51. Thompson, B. A. *et al.* Application of a 5-tiered scheme for standardized classification of 2,360 unique mismatch repair gene variants in the InSiGHT locus-specific database. *Nat Genet* **46**, 107–115 (2014).

52. Sanchez, J. A. *et al.* Genetic and epigenetic classifications define clinical phenotypes and determine patient outcomes in colorectal cancer. *Br J Surg* **96**, 1196–1204 (2009).

53. Umar, A. Lynch Syndrome (HNPCC) and Microsatellite Instability. *Disease Markers* **20**, 179–180 (2004).

54. Poulogiannis, G., Frayling, I. M. & Arends, M. J. DNA mismatch repair deficiency in sporadic colorectal cancer and Lynch syndrome. *Histopathology* **56**, 167–179 (2010).

55. Gupta, R. A. & DuBois, R. N. Colorectal cancer prevention and treatment by inhibition of cyclooxygenase-2. *Nat Rev Cancer* **1**, 11–21 (2001).

56. Tanaka, T. *et al.* Dextran sodium sulfate strongly promotes colorectal carcinogenesis inApcMin/+ mice: Inflammatory stimuli by dextran sodium sulfate results in development of multiple colonic neoplasms. *Int. J. Cancer* **118**, 25–34 (2006).

57. Neufert, C., Becker, C. & Neurath, M. F. An inducible mouse model of colon carcinogenesis for the analysis of sporadic and inflammation-driven tumor progression. *Nat Protoc* **2**, 1998–2004 (2007).

58. Bhaskaran, K. *et al.* Body-mass index and risk of 22 specific cancers: a population-based cohort study of 5·24 million UK adults. *The Lancet* **384**, 755–765 (2014).

59. Calle, E. E., Rodriguez, C., Walker-Thurmond, K. & Thun, M. J. Overweight, Obesity, and Mortality from Cancer in a Prospectively Studied Cohort of U.S. Adults. *The New England Journal of Medicine* **348**, 1625–1638 (2003).

60. Dignam, J. J. *et al.* Body Mass Index and Outcomes in Patients Who Receive Adjuvant Chemotherapy for Colon Cancer. *JNCI: Journal of the National Cancer Institute* **98**, 1647–1654 (2006).

61. Gulhane, M. *et al.* High Fat Diets Induce Colonic Epithelial Cell Stress and Inflammation that is Reversed by IL-22. *Sci Rep* **6**, 28990 (2016).

62. Ahmad, R., Rah, B., Bastola, D., Dhawan, P. & Singh, A. B. Obesity-induces Organ and Tissue Specific Tight Junction Restructuring and Barrier Deregulation by Claudin Switching. *Sci Rep* **7**, 5125 (2017).

63. Panneerselvam, J. *et al.* Inflammatory Mediators and Gut Microbial Toxins Drive Colon Tumorigenesis by IL-23 Dependent Mechanism. *Cancers* **13**, 5159 (2021).

64. Suzuki, T., Yoshinaga, N. & Tanabe, S. Interleukin-6 (IL-6) Regulates Claudin-2 Expression and Tight Junction Permeability in Intestinal Epithelium. *Journal of Biological Chemistry* **286**, 31263–31271 (2011).

65. Grivennikov, S. *et al.* IL-6 and Stat3 Are Required for Survival of Intestinal Epithelial Cells and Development of Colitis-Associated Cancer. *Cancer Cell* **15**, 103–113 (2009).

66. Popivanova, B. K. *et al.* Blocking TNF-α in mice reduces colorectal carcinogenesis associated with chronic colitis. *J. Clin. Invest.* JCI32453 (2008) doi:10.1172/JCI32453.

67. Wunderlich, C. M. *et al.* Obesity exacerbates colitis-associated cancer via IL-6-regulated macrophage polarisation and CCL-20/CCR-6-mediated lymphocyte recruitment. *Nat Commun* **9**, 1646 (2018).

68. Davies, L. C., Jenkins, S. J., Allen, J. E. & Taylor, P. R. Tissue-resident macrophages. *Nature Immunology* **14**, 986–995 (2013).

69. Si, Y., Tsou, C.-L., Croft, K. & Charo, I. F. CCR2 mediates hematopoietic stem and progenitor cell trafficking to sites of inflammation in mice. *J. Clin. Invest.* **120**, 1192–1203 (2010).

70. Chun, E. *et al.* CCL2 Promotes Colorectal Carcinogenesis by Enhancing Polymorphonuclear Myeloid-Derived Suppressor Cell Population and Function. *Cell Reports* **12**, 244–257 (2015).

71. Wang, H. *et al.* Interactions between colon cancer cells and tumor-infiltrated macrophages depending on cancer cell-derived colony stimulating factor 1. *OncoImmunology* **5**, e1122157 (2016).

72. Barrett, T. J., Murphy, A. J., Goldberg, I. J. & Fisher, E. A. Diabetes-mediated myelopoiesis and the relationship to cardiovascular risk. *Annals of the New York Academy of Sciences* **1402**, 31–42 (2017).

73. Patel, A. A. *et al.* The fate and lifespan of human monocyte subsets in steady state and systemic inflammation. *The Journal of Experimental Medicine* **214**, 1913–1923 (2017).

74. Frodermann, V. *et al.* Exercise reduces inflammatory cell production and cardiovascular inflammation via instruction of hematopoietic progenitor cells. *Nature Medicine* **25**, 1761–1771 (2019).

75. Kaushansky, K. Lineage-Specific Hematopoietic Growth Factors. *The New England Journal of Medicine* **354**, 2034–2045 (2006).

76. Jiao, Y., Cao, F. & Liu, H. Radiation-induced Cell Death and Its Mechanisms. *Health Physics* **123**, 376–386 (2022).

77. Shao, L., Luo, Y. & Zhou, D. Hematopoietic Stem Cell Injury Induced by Ionizing Radiation. *Antioxidants & Redox Signaling* **20**, 1447–1462 (2014).

78. Nederveen, J. P., Warnier, G., Di Carlo, A., Nilsson, M. I. & Tarnopolsky, M. A. Extracellular Vesicles and Exosomes: Insights From Exercise Science. *Front. Physiol.* **11**, 604274 (2021).

79. Vanhie, J. J. *et al.* The role of exercise-and high fat diet-induced bone marrow extracellular vesicles in stress hematopoiesis. *Front. Physiol.* **13**, 1054463 (2022).

80. Birbrair, A. & Frenette, P. S. Niche heterogeneity in the bone marrow. *Annals of the New York Academy of Sciences* **1370**, 82–96 (2016).

81. Kandalla, P. K. *et al.* M-CSF improves protection against bacterial and fungal infections after hematopoietic stem/progenitor cell transplantation. *Journal of Experimental Medicine* **213**, 2269–2279 (2016).

82. Emmons, R., Niemiro, G. M., Owolabi, O. & De Lisio, M. Acute exercise mobilizes hematopoietic stem and progenitor cells and alters the mesenchymal stromal cell secretome. *Journal of Applied Physiology* **120**, 624–632 (2016).

83. Butrym, A. *et al.* Expression of microRNA-331 can be used as a predictor for response to therapy and survival in acute myeloid leukemia patients. *Biomarkers in Medicine* **9**, 453–460 (2015).

84. Feng, D.-D. *et al.* Down-regulated miR-331-5p and miR-27a are associated with chemotherapy resistance and relapse in leukaemia. *Journal of Cellular and Molecular Medicine* **15**, 2164–2175 (2011).

85. Krowiorz, K. *et al.* MiR-193a Is a Negative Regulator of Hematopoietic Stem Cells and Promotes Anti-Leukemic Effects in Acute Myeloid Leukemia. *Blood* **132**, 2627–2627 (2018).

86. Fichtel, P. *et al.* Mesenchymal Stromal Cell-Derived Extracellular Vesicles Modulate Hematopoietic Stem and Progenitor Cell Viability and the Expression of Cell Cycle Regulators in an Age-dependent Manner. *Front. Bioeng. Biotechnol.* **10**, 892661 (2022).

87. Huang, W. *et al.* Obesity Blunts the Effect of Mesenchymal Stem Cell-Derived Extracellular Vesicles. *Kidney International Reports* **8**, 1841–1851 (2023).

88. De Ferranti, S. & Mozaffarian, D. The Perfect Storm: Obesity, Adipocyte Dysfunction, and Metabolic Consequences. *Clinical Chemistry* **54**, 945–955 (2008).

89. Versini, M., Jeandel, P.-Y., Rosenthal, E. & Shoenfeld, Y. Obesity in autoimmune diseases: Not a passive bystander. *Autoimmunity Reviews* **13**, 981–1000 (2014).

90. de Luca, C. & Olefsky, J. M. Inflammation and Insulin Resistance. *FEBS Letters* **582**, 97–105 (2009).

91. Cottam, M. A., Caslin, H. L., Winn, N. C. & Hasty, A. H. Multiomics reveals persistence of obesity-associated immune cell phenotypes in adipose tissue during weight loss and weight regain in mice. *Nat Commun* **13**, 2950 (2022).

92. Milagro, F. I. *et al.* High fat diet-induced obesity modifies the methylation pattern of leptin promoter in rats. *J. Physiol. Biochem.* **65**, 1–9 (2009).

93. Goyama, S. & Kitamura, T. Epigenetics in normal and malignant hematopoiesis: An overview and update 2017. *Cancer Science* **108**, 553–562 (2017).

94. Edillor, C. R., Parks, B. W., Mehrabian, M., Lusis, A. J. & Pellegrini, M. DNA Methylation Changes More Slowly Than Physiological States in Response to Weight Loss in Genetically Diverse Mouse Strains. *Front. Endocrinol.* **10**, 882 (2019).

95. Yvan-Charvet, L. *et al.* ATP-binding cassette transporters and HDL suppresses hematopoietic stem cell proliferation. *Science* **328**, 1689–1693 (2010).

96. Gao, M. *et al.* Regulation of HDL on hematopoietic stem/progenitor cells in atherosclerosis requires SR-BI expression. *Atherosclerosis, Thrombosis, and Vascular Biology* **34**, 1900–1909 (2015).

97. Ma, X. & Feng, Y. Hypercholesterolemia Tunes Hematopoietic Stem/Progenitor Cells for Inflammation and Atherosclerosis. *IJMS* **17**, 1162 (2016).

98. Fang, R. *et al.* Comprehensive analysis of single cell ATAC-seq data with SnapATAC. *Nat Commun* **12**, 1337 (2021).

99. Ekström, K. *et al.* Characterization of surface markers on extracellular vesicles isolated from lymphatic exudate from patients with breast cancer. *BMC Cancer* **22**, 50 (2022).

100. Welsh, J. A. *et al.* Minimal information for studies of extracellular vesicles (MISEV2023): From basic to advanced approaches. *J of Extracellular Vesicle* **13**, e12404 (2024).

101. De Lisio, M., Jensen, T., Sukiennik, R. A., Huntsman, H. D. & Boppart, M. D. Substrate and strain alter the muscle-derived mesenchymal stem cell secretome to promote myogenesis. *Stem Cell Res Ther* **5**, 74 (2014).

102. Styner, M. *et al.* Mechanical Strain Downregulates C/EBPβ in MSC and Decreases Endoplasmic Reticulum Stress. *PLoS ONE* **7**, e51613 (2012).

103. Ghosh, A. *et al.* Telomerase directly regulates NF-κB-dependent transcription. *Nat Cell Biol* **14**, 1270–1281 (2012).

104. Li, Q. *et al.* Gut Barrier Dysfunction and Bacterial Lipopolysaccharides in Colorectal Cancer. *Journal of Gastrointestinal Surgery* **27**, 1466–1472 (2023).

Chapter VIII – Supplemental Information

Chapter IV

Supplemental Figures

The role of exercise and high fat diet-induced bone marrow extracellular vesicles in stress hematopoiesis

James J. Vanhie[1], Wooseok Kim[1], Lisa Ek Orloff[1], Matthew Ngu[1], Nicolas Collao[1], and Michael De Lisio[1]

[1]School of Human Kinetics, Faculty of Health Sciences, Ottawa, ON, Canada

[2]Department of Cellular and Molecular Medicine, University of Ottawa, Ottawa, ON, Canada

Keywords: physical activity, obesity, microRNA, myelopoiesis, adipogenesis

Frontiers in Physiology

2022 Nov 23; 13: 1-14

DOI: https://doi.org/10.3389/fphys.2022.1054463

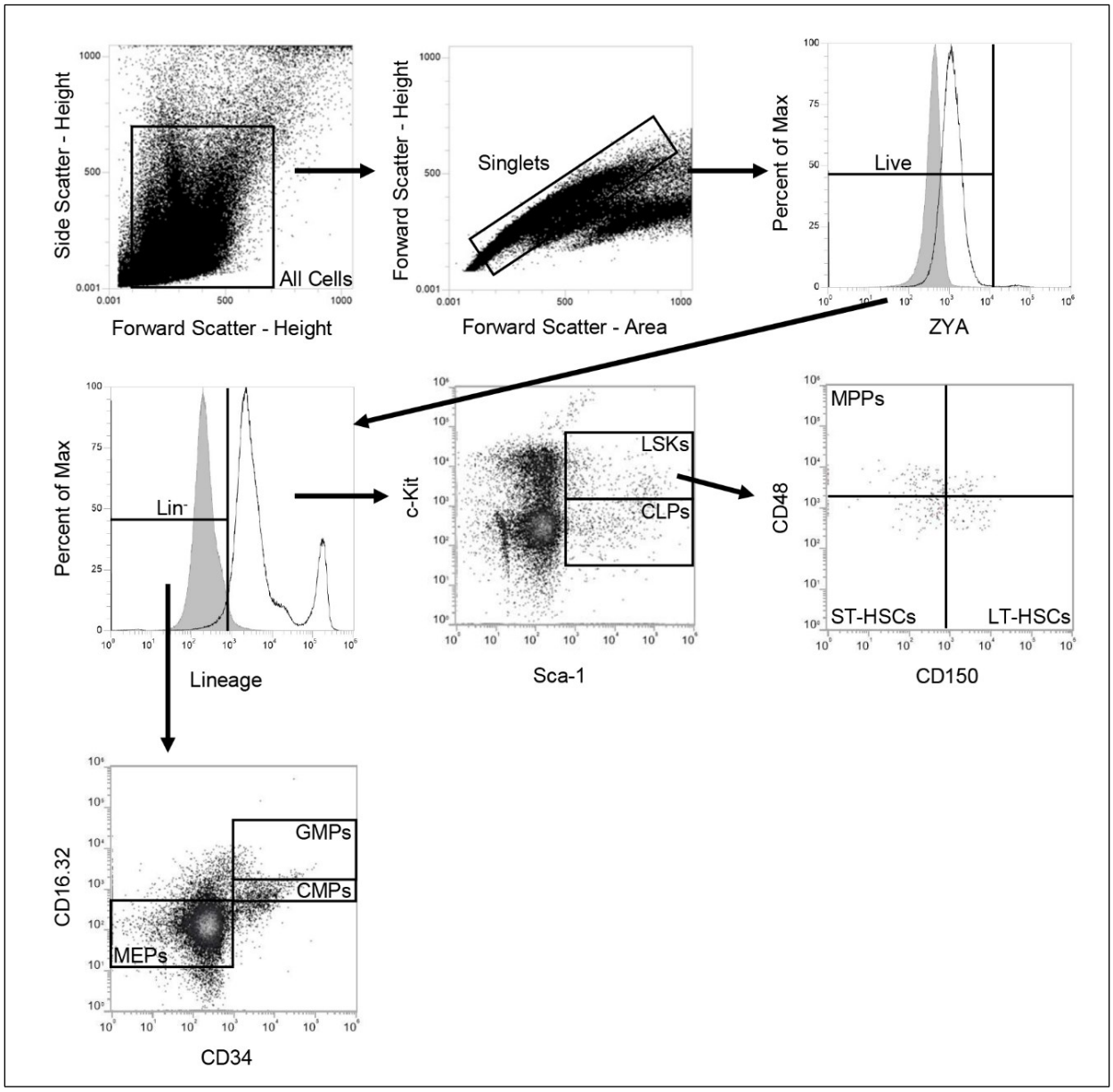

Figure S4.1. Flow cytometry gating strategy for hematopoietic stem cells (LSKs), common lymphoid progenitor cells (CLPs), multipotent progenitor cells (MPPs), short-term (ST-HSCs) and long-term HSCs (LT-HSCs), megakaryocyte-erythroid progenitor (MEPs), granulocyte-macrophage progenitor, and common myeloid progenitor cells. The shaded curves in the histograms represent unstained controls and the black lines represent fully stained positive samples.

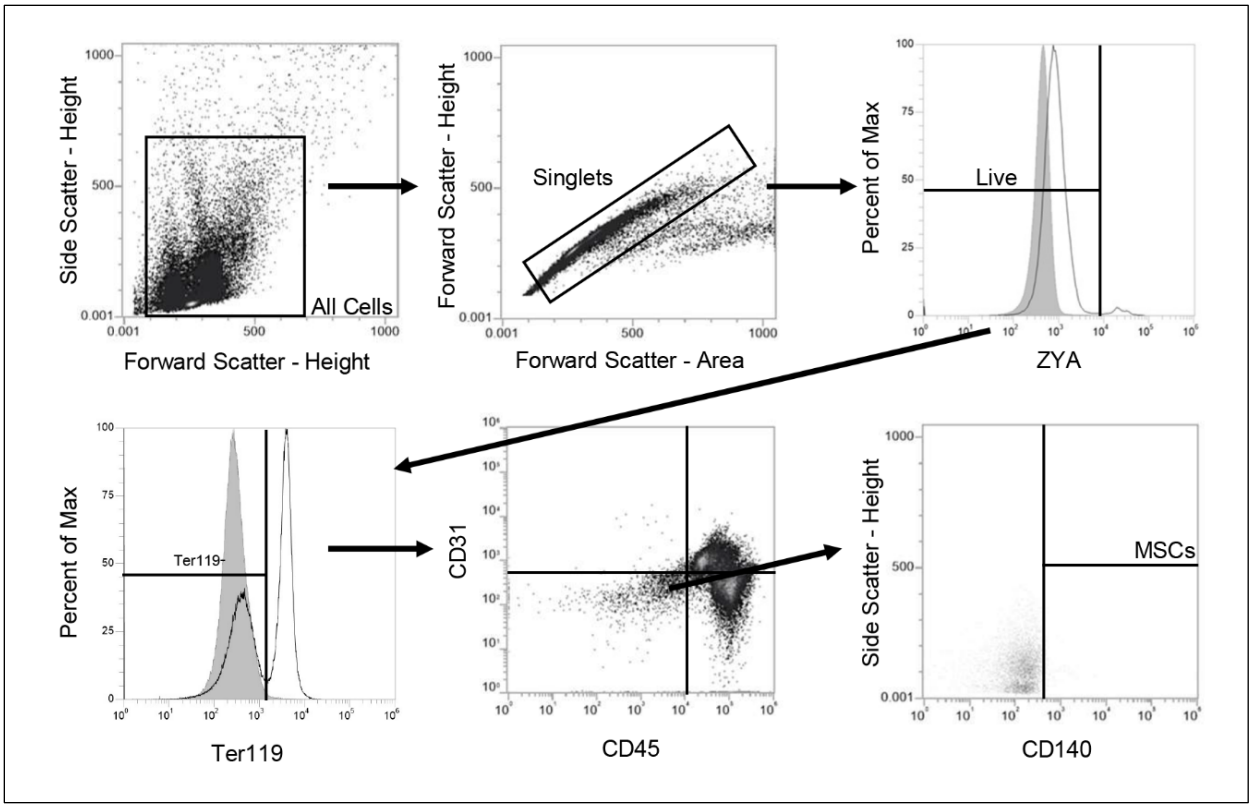

Figure S4.2. Flow cytometry gating strategy for mesenchymal stromal cells (MSCs). The shaded curves in the histograms represent unstained controls and the black lines represent fully stained positive samples.

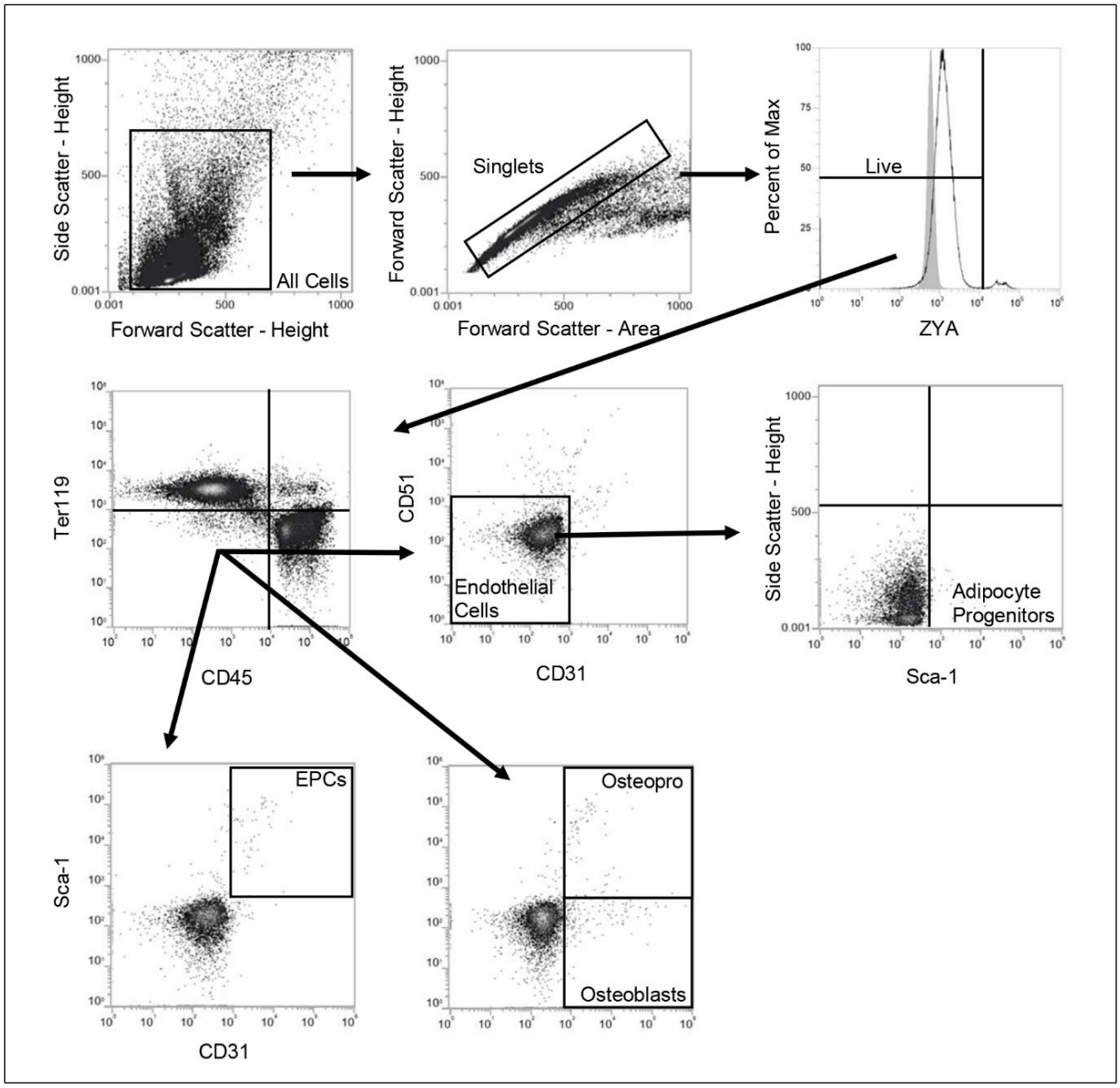

Figure S4.3. Flow cytometry gating strategy for endothelial cells, adipocyte progenitor cells, endothelial progenitor cells, osteoprogenitor cells, and osteoblasts. The shaded curves in the histograms represent unstained controls and the black lines represent fully stained positive samples.

Chapter V

Supplemental Figures and Tables

High-fat diets promote hematopoietic stem cell expansion and myeloid skewing during steady state hematopoiesis

James J. Vanhie[1], Wooseok Kim[1], Cole Goode[1], Nicolas Collao[1], and Michael De Lisio[1,2]

[1]School of Human Kinetics, Faculty of Health Sciences, Ottawa, ON, Canada

[2]Department of Cellular and Molecular Medicine, University of Ottawa, Ottawa, ON, Canada

Keywords: bone marrow, exercise, mesenchymal stromal cells, microRNA, myelopoiesis

Under Review in Medicine & Science in Sports & Exercise

Assigned Paper #: MSSE-D-24-00242

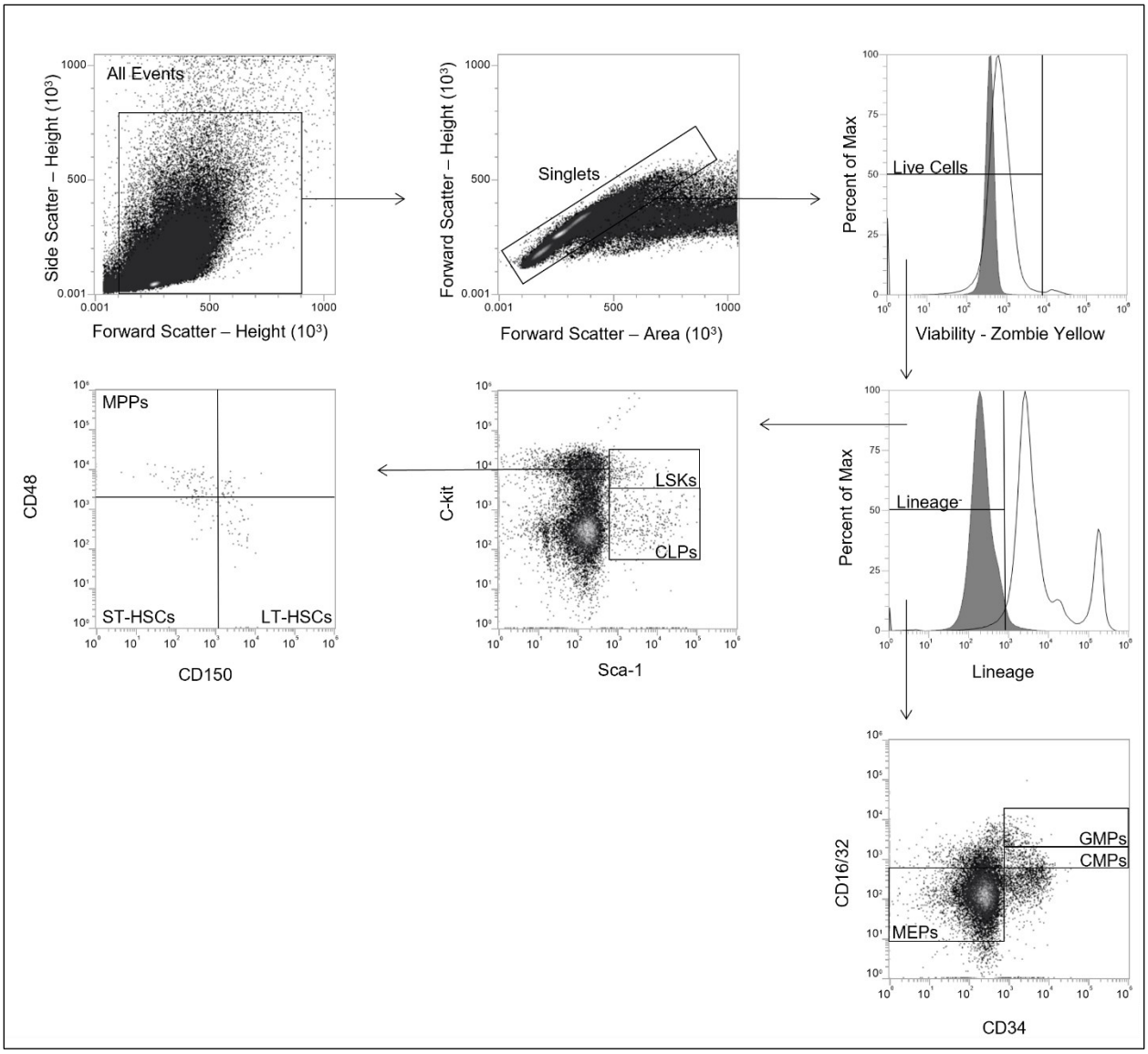

Figure S5.1. Flow cytometry gating strategy for total hematopoietic stem cells (LSKs), multipotent progenitor cells (MPPs), short-term (ST-HSCs), long-term HSCs (LT-HSCs), common lymphoid progenitor (CLP), megakaryocyte-erythroid progenitor (MEP), granulocyte-macrophage progenitor (GMP), and common myeloid progenitor (CMP) cells. In the viability and lineage histograms the unshaded curves represent fully stained positive samples and the shaded grey curves represent unstained control samples.

Table S5.1. Flow cytometry gating strategies for bone marrow hematopoietic stem and progenitor cells.

Population of Interest	Flow Cytometry Gating Strategy
Total Hematopoietic Stem Cells (HSCs)	Lineage$^-$, Sca-1$^+$, c-Kit$^+$ (LSK)
Common Lymphoid Progenitors (CLPs)	Lineage$^-$, Sca-1$^+$, c-Kit$^-$
Long-Term HSCs (LT-HSCs)	LSK, CD48$^-$, CD150$^+$
Short-Term HSCs (ST-HSCs)	LSK, CD48$^-$, CD150$^-$
Multipotent Progenitors (MPPs)	LSK, CD48$^+$, CD150$^-$
Common Myeloid Progenitors (CMPs)	Lineage$^-$, CD16/32^{int}, CD34$^+$
Granulocyte-Monocyte Progenitors (GMPs)	Lineage$^-$, CD16/32^{hi}, CD34$^+$
Megakaryocyte-Erythroid Progenitors (MEPs)	Lineage$^-$, CD16/32$^-$, CD34$^-$

Table S5.2. Flow cytometry antibodies.

Antibody	Fluorophore	Dilution (Solvent)	Product ID
Viability	Zombie Yellow	1:300 (PBS)	423104
Lineage (5 Antibodies)	Biotinylated	1:200 (5% FBS)	559971
Streptavidin	FITC	1:800 (5% FBS)	554060
Sca-1 (Ly6A/E)	PE	1:200 (5% FBS)	553336
c-Kit (CD117)	PE-Cyanine7	1:200 (5% FBS)	561681
CD16/32	BV711	1:200 (5% FBS)	101337
CD31	BV510	1:200 (5% FBS)	563089
CD34	PE-Cyanine5	1:200 (5% FBS)	119312
CD45	PE-Cyanine7	1:200 (5% FBS)	552848
CD48	BV510	1:200 (5% FBS)	563536
CD51	BV421	1:200 (5% FBS)	BDB740062
CD140α	PE	1:200 (5% FBS)	562776
CD150	BV421	1:200 (5% FBS)	562811

Chapter VI

Supplemental Figures and Tables

Obesity promotes marrow-derived myeloid cell accumulation while exercise reduces proliferative signaling in colon cancer

James J. Vanhie[1], Lisa Ek Orloff[1], Alice Tate[1], Cole Goode[1], Nicolas Collao[1,2], Anastasia Pisanko[2], Krista A. Power[3,4], and Michael De Lisio[1,2].

[1]School of Human Kinetics; [2]Department of Cellular and Molecular Medicine; [3]School of Nutrition Sciences, [4]Department of Biochemistry, Microbiology and Immunology, University of Ottawa, Ottawa, ON, Canada

Keywords: bone marrow, exercise, mesenchymal stromal cells, microRNA, myelopoiesis

Under Review in Medicine & Science in Sports & Exercise

Assigned Paper #: Pending

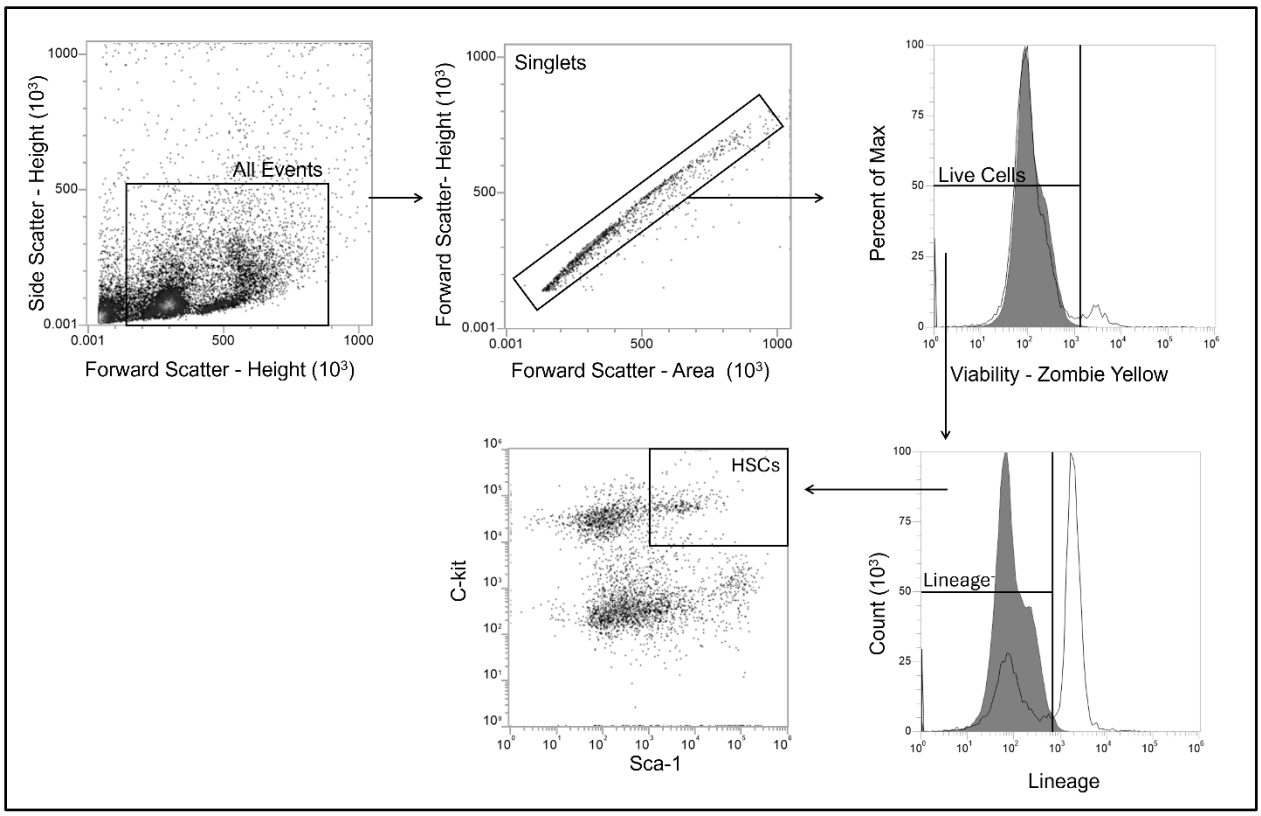

Figure S6.1. Flow cytometry gating strategies for hematopoietic stem cells (HSCs).

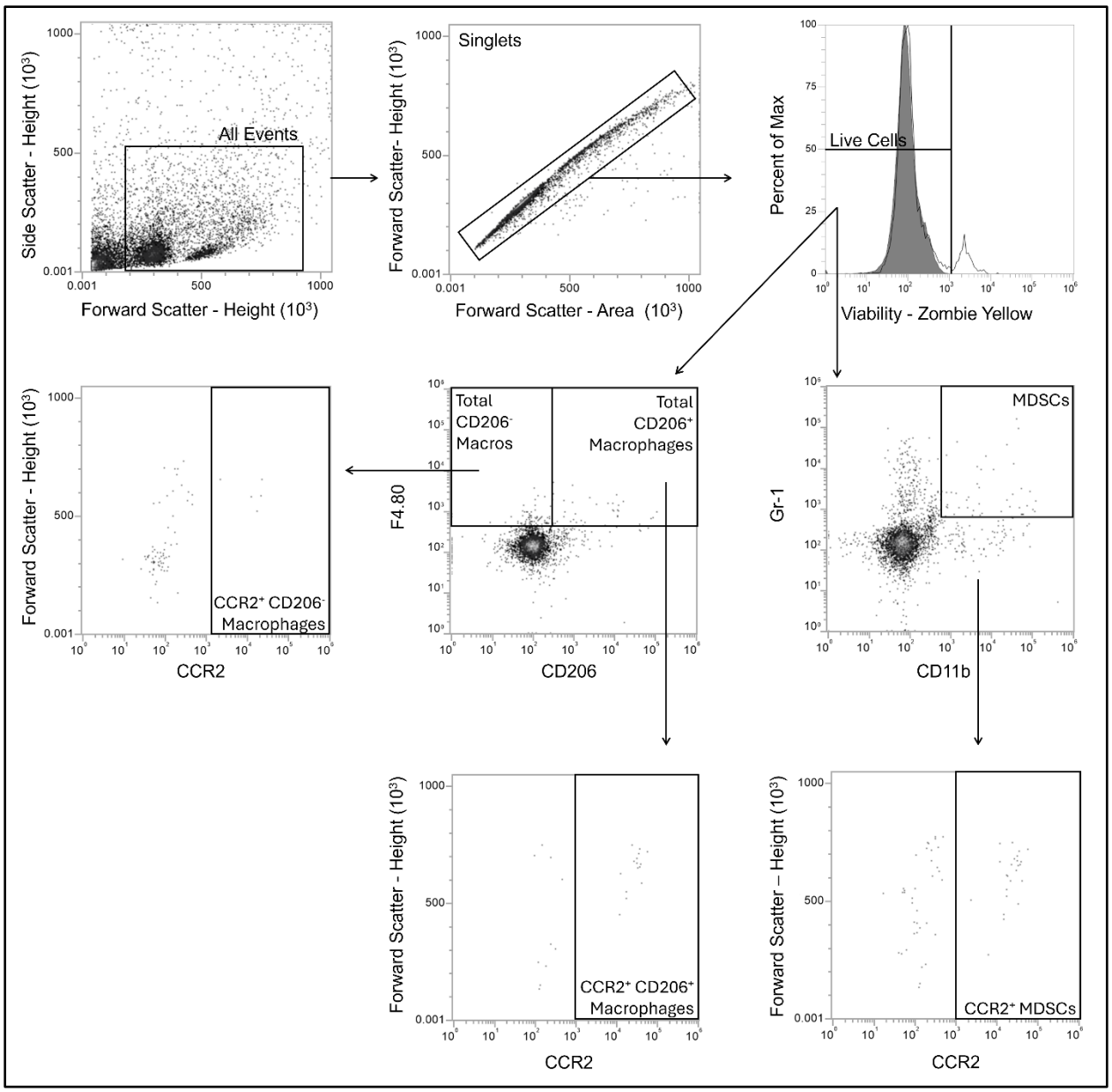

Figure S6.2. Flow cytometry gating strategies for macrophages and myeloid-derived suppressor cells (MDSCs).

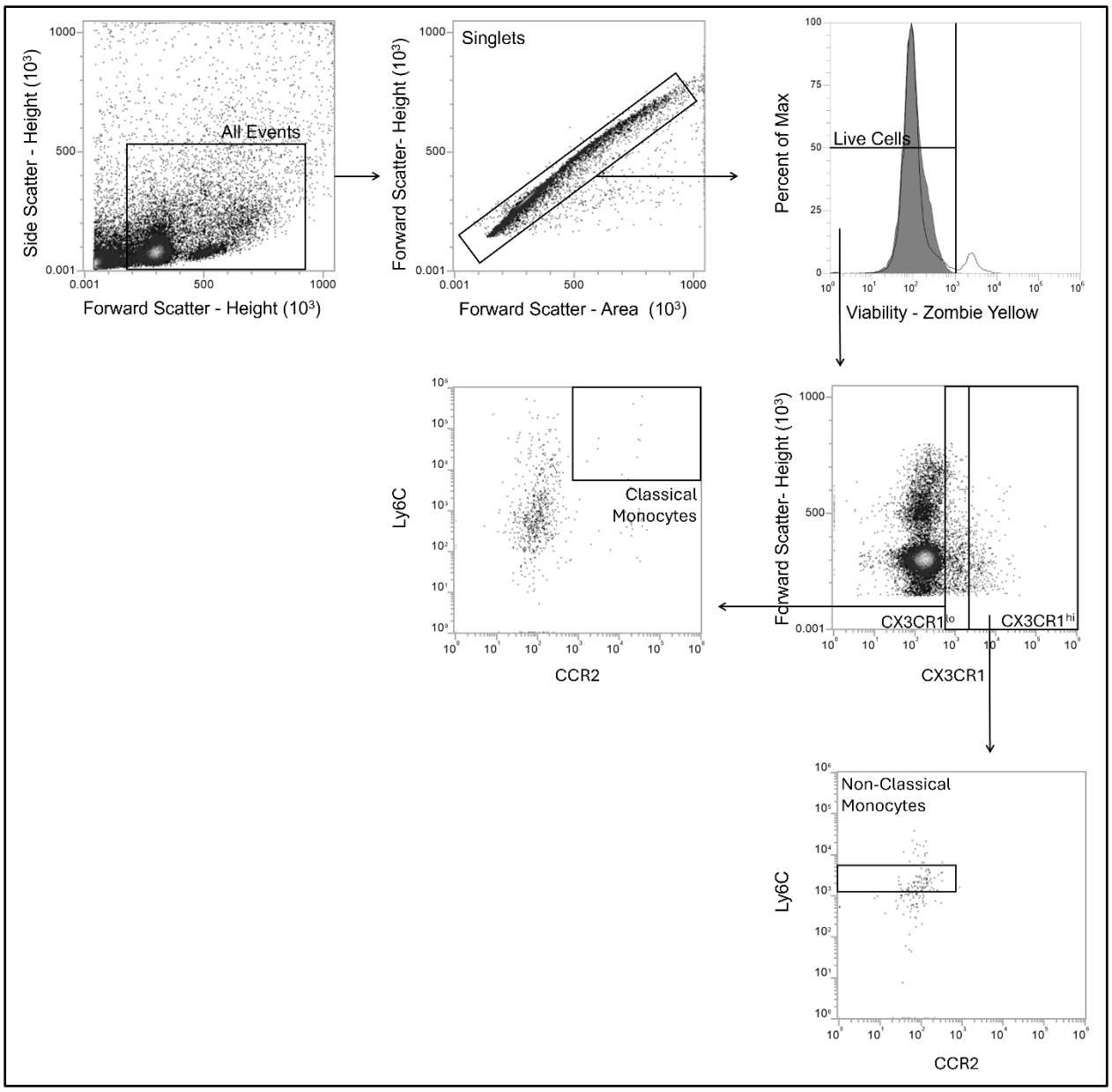

Figure S6.3. Flow cytometry gating strategies for classical and non-classical monocytes.

Table S6.1. Treadmill exercise training protocol.

EXERCISE TRAINING PROTOCOL						
Exercise Week	**Warmup**	**Duration**	**Training**	**Duration**	**Cooldown**	**Duration**
1	8 m/min	10 min	8 m/min	25 min	8m/min	5 min
2	8 m/min	10 min	8 m/min	35 min	8m/min	5 min
3	8 m/min	10 min	9 m/min	45 min	8m/min	5 min
4,5	10 m/min	10 min	10 m/min	45 min	8m/min	5 min
6,7	10 m/min	10 min	12 m/min	45 min	8m/min	5 min
8,9	10 m/min	10 min	14 m/min	45 min	8m/min	5 min
10,11	10 m/min	10 min	16 m/min	45 min	8m/min	5 min
12,13	10 m/min	10 min	18 m/min	45 min	8m/min	5 min
14,15	10 m/min	10 min	20 m/min	45 min	8m/min	5 min
16,17	10 m/min	10 min	22 m/min	45 min	8m/min	5 min
18+	10 m/min	10 min	24 m/min	45 min	8m/min	5 min

Table S6.2. Flow cytometry gating strategies.

Cell Population	Gating Strategy
Hematopoietic Stem Cells	Lineage^{-}, Sca-1^{+}, c-Kit^{+}
Classically Activated Monocytes	CX3CR1^{lo}, Ly6C^{+}, CCR2^{+}
Non-Classically Activated Monocytes	CX3CR1^{hi}, Ly6C^{lo}, CCR2^{-}
Myeloid-Derived Suppressor Cells	c-Kit^{+}, CD11b^{+}
Classically Activated Macrophages	F4.80^{+}, CD206^{-}
Marrow-Derived Classically Activated Macrophages	F4.80^{+}, CD206^{-}, CCR2^{+}
Alternatively Activated Macrophages	F4.80^{+}, CD206^{+}
Marrow-Derived Alternatively Activated Macrophages	F4.80^{+}, CD206^{+}, CCR2^{+}

Table S6.3. Antibodies used for flow cytometry.

Antibody	Conjugate	Laser	Product Number
CCR2	eGFP	BL1	N/A (Genetic)
CD11b	Biotin	VL1	559971
CD16/32	BV711	VL4	101337
CD31	BV510	VL2	563089
CD34	Pe-Cyanine5	BL3	119312
CD45	PE-Cyanine7	BL4	552848
CD48	BV510	VL2	563536
CD51	BV711	VL4	740755
CD93	PerCP/Cy5.5	BL3	136512
CD206	PE	BL2	12-2061-82
CX_3CR_1	PerCP/Cy5.5	BL3	567531
F4/80	SB702	VL4	67-4801-82
Gr-1 (Ly6G/Ly6C)	PE-Cyanine7	BL4	25-5931-82
Sca1 (Ly6A/E)	PE	BL2	553336
cKit (CD117)	PE-Cyanine7	BL4	558163
CD127 (IL-7Rα)	BV510	VL2	135033
CD140a	PE	BL2	562776
CD150 - WT Panel	BV421	VL1	562811
Lineage	Biotin	VL1	559971
Viability - Zombie Yellow	Zombie Yellow	VL3	423104
Streptavidin (Binds Biotin)	BV421	VL1	563259

Appendix A - Detailed Methods

Control and High-Fat Diets
Data Obtained from: https://researchdiets.com/formulas/d12451
D10012M - AIN-93M Mature Rodent Diet (Control Diet)
Caloric Information (Physiological Fuel Values):
Protein: 15% kcal - Fat: 9.4% kcal - Carbohydrate: 76% kcal - Energy Density: 3.81 kcal/g

Table A1. D10012M – AIN-93M Control Diet Composition.

Class Description	Ingredients	Weight (Grams)
Protein	Casein, Lactic, 30 Mesh	140.00
Protein	Cystine, L	1.80
Carbohydrate	Sucrose, Fine Granulated	100.00
Carbohydrate	Lodex 10	125.00
Carbohydrate	Starch, Corn	495.69
Fiber	Solka Floc, FCC200	50.00
Fat	Soybean Oil, USP	40.00
Mineral	S10022M (AIN-93 Mineral Mix for Mature Rodents)	35.00
Vitamin	Choline Bitartrate	10.00
Vitamin	V10037 (Vitamin Mix for AIN-93 Rodent Diets)	1.00
Anti-oxidant	tert-Butylhydroquinone (tBHQ)	0.01
Total	N/A	1000.00

D12451 - Rodent Diet with 45% kcal Fat (High-Fat Diet)
Caloric Information (Physiological Fuel Values):
Protein: 20% kcal - Fat: 45% kcal - Carbohydrate: 35% kcal - Energy Density: 4.7 kcal/g

Table A2. D12451 – High-Fat Diet Composition.

Class Description	Ingredients	Weight (Grams)
Protein	Casein, Lactic, 30 Mesh	200.00
Protein	Cystine, L	3.00
Carbohydrate	Sucrose, Fine Granulated	176.80
Carbohydrate	Lodex 10	100.00
Carbohydrate	Starch, Corn	72.80
Fiber	Solka Floc, FCC200	50.00
Fat	Lard	177.50
Fat	Soybean Oil, USP	25.00
Mineral	S10026B (RD-96 Mineral Mix)	50.00
Vitamin	Choline Bitartrate	2.00
Vitamin	V10001C (AIN-76A Vitamin Mix, 10X Concentration)	1.00
Dye	Dye, Red FD&C #40, Alum. Lake 35-42%	0.05
Total	N/A	858.15

Flow Cytometry Panels

Table A3. Bone marrow antibody cocktail preparation for flow cytometry – Wild-type CBA.

Antibody Cocktail Description	Antibodies in Cocktail	Dilution of Respective Antibody (5% FBS)	Laser (Conjugate)
A. HSC; CMP/GMP/MEP	Lineage Panel (5 total), FITC	1:200 (5:200 total)	BL1 (FITC)
	Sca1 (Ly-6A/E)	1:200	BL2 (PE)
	c-Kit (CD117)	1:200	BL4 (PE-Cy7)
	CD48	1:200	VL2 (BV510)
	CD150	1:200	VL1 (BV421)
	CD34	1:200	BL3 (Pe-Cy5)
	CD16/32	1:200	VL4 (BV711)
B. CLP	Lineage Panel, FITC	1:200 (5:200 total)	BL1 (FITC)
	Sca1 (Ly-6A/E)	1:200	BL2 (PE)
	c-Kit (CD117)	1:200	BL4 (PE-Cy7)
C. MSC	Ter119, FITC	1:200	BL1 (FITC)
	CD31	1:200	VL2 (BV510)
	CD45	1:200	BL4 (PE-Cy7)
	CD140a	1:200	BL2 (PE)
D. EPCs Adipo/Osteo Prog	Ter119, FITC	1:200	BL1 (FITC)
	Sca1 (Ly-6A/E)	1:200	BL2 (PE)
	CD31	1:200	VL2 (BV510)
	CD45	1:200	BL4 (PE-Cy7)
	CD51	1:200	VL1 (BV421)

**All samples will include Zombie Yellow Dye on the VL3 channel.

Flow Cytometer: Life Technologies Attune NxT (Blue and Violet Lasers)

Blue Laser – 488nm
Blue Laser Filters – BL1 (530/30), BL2 (574/26), BL3 (695/40), BL4 (750/60)

Violet Laser – 405nm
Violet Laser Filters – VL1 (440/50), VL2 (512/25), VL3 (603/48), VL4 (710/50)

Table A4. Bone marrow antibody cocktail preparation for flow cytometry - CCR2$^{gfp/+}$ C57BL/6J.

Antibody Cocktail Description	Antibodies in Cocktail	Dilution of Respective Antibody (5% FBS)	Laser (Conjugate)
A. HSC	Lineage Panel (5 total) Sca1 (Ly-6A/E) c-Kit (CD117) CD48 CD150	1:200 (5:200 total) 1:200 1:200 1:200 1:200	VL1 (BV421) BL2 (PE) BL4 (PE-Cy7) VL2 (BV510) BL3 (PerCP-eF710)
B. CMP/GMP/MEP	Lineage Panel (5 total), Sca1 (Ly-6A/E) c-Kit (CD117) CD34 CD16/32	1:200 (5:200 total) 1:200 1:200 1:200 1:200	VL1 (BV421) BL2 (PE) BL4 (PE-Cy7) BL3 (PE-Cy5) VL4 (BV711)
C. CLP	CD135 Sca1 (Ly-6A/E) CD127 Lineage Panel c-Kit (CD117)	1:200 1:200 1:200 1:200 (5:200 total) 1:200	BL3 (PerCP-eF710) BL2 (PE) VL2 (BV510) VL1 (BV421) BL4 (PE-Cy7)
D. MSC	CD45 Ter119 CD31 CD140a	1:200 1:200 1:200 1:200	BL4 (PE-Cy7) VL1 (BV421) VL2 (BV510) BL2 (PE)
E. EPCs Adipo/Osteo Prog	CD45 Ter119 Sca1 (Ly-6A/E) CD31 CD51	1:200 1:200 1:200 1:200 1:200	BL4 (PE-Cy7) VL1 (BV421) BL2 (PE) VL2 (BV510) VL4 (BV711)

**All samples will include Zombie Yellow Dye on the VL3 channel.

**All samples will include CCR2^{gfp} on the BL1 channel. All lineage samples use BV421 Streptavidin, not FITC.

Table A5. Blood and colon antibody cocktail preparation for flow cytometry - CCR2$^{gfp/+}$ C57BL/6J.

Antibody Cocktail Description	Antibodies in Cocktail	Dilution of Respective Antibody (5% FBS)	Laser (Conjugate)
F. HSCs, T-Lymphocytes	Lineage Panel (5 total), Sca1 (Ly-6A/E) c-Kit (CD117) CD4 CD8	1:200 (5:200 total) 1:200 1:200 1:200 1:200	VL1 (BV421) BL2 (PE) BL4 (PE-Cy7) VL4 (SB702) BL3 (PerCP-eF710)
G. MDSCs and Macrophages	CD11b (from Lin panel) F4/80 CD206 CX3CR1 Gr-1 (Ly6C/Ly6G)	1:200 1:200 1:200 1:200 1:200	VL1 (BV421) VL4 (SB702) BL2 (PE) BL3 (PerCP-Cy5.5) BL4 (PE-Cy7)
H. Monocytes	CCR2 CX3CR1 Ly6C	1:200 1:200 1:200	BL1 (eGFP) BL3 (PerCP/Cy5.5) BL4 (PE-Cy7)

**All samples will include Zombie Yellow Dye on the VL3 channel.
**All samples will include CCR2^{gfp} on the BL1 channel.
**Monocyte gating strategy is based on Rahman et al. (2017).

Table A6. Full antibody list for wild-type CBA and CCR2$^{gfp/+}$ C57BL/6J Panels Combined.

Antibody	Conjugate	Laser	Product Number
CCR2	eGFP	BL1	N/A (Genetic)
CD4	SB702	VL4	67-0042-82
CD8	PerCP-eFluor 710	BL3	46-0081-82
CD11b	Biotin (Lin Panel, BV421)	VL1	559971
CD16/32	BV711	VL4	101337
CD31	BV510	VL2	563089
CD34	Pe-Cyanine5	BL3	119312
CD45	PE-Cyanine7	BL4	552848
CD48	BV510	VL2	563536
CD51 - WT Panel	BV421	VL1	740062
CD51 - CCR2 eGFP Panel	BV711	VL4	740755
CD51 - CCR2 eGFP Panel	PE	BL2	12-0512-83
CD93	PerCP/Cy5.5	BL3	136512
CD206	PE	BL2	12-2061-82
CX_3CR_1	PerCP/Cy5.5	BL3	567531
F4/80	SB702	VL4	67-4801-82
Ly6C	PE-Cyanine7	BL4	25-5932-82
Gr-1 (Ly6G/Ly6C)	PE-Cyanine7	BL4	25-5931-82
Sca1 (Ly6A/E)	PE	BL2	553336
Sca-1 (Ly6A/E)	BV711	VL4	407-5981-82
cKit (CD117)	PE-Cyanine7	BL4	558163
CD127 (IL-7Rα)	BV510	VL2	135033
CD135	BL3 (PerCP-eF710)	BL3	46-1351-82
CD140a	PE	BL2	562776
CD150 - WT Panel	BV421	VL1	562811
CD150 - CCR2 eGFP Panel	PerCP-eFluor710	BL3	46-1502-82
Lineage	Biotin (Binds Streptavidin)	BL1 or VL1	559971
Viability - Zombie Yellow	Zombie Yellow	VL3	423104
Streptavidin - WT Panel	FITC	BL1	554060
Streptavidin - CCR2 eGFP Panel	BV421	VL1	563259

Note: CD51 BV711 (Cat #740755) was discontinued in January 2023 and no other CD51 with the BV711 conjugate was available. A new version of CD51 (Cat #12-0512-83) with PE conjugate was used. The original Sca-1 PE (Cat #553336) was therefore switched to a another Sca-1 antibody using BV711 (Cat #407-5981-82).

Flow Cytometry Compensation Protocol

1. Resuspend ABC beads (in fridge door - top shelf) by inverting tube 10x and vortexing gently (level 7) for 2 seconds.
2. Label sample tubes with appropriate fluorochrome and add 1 drop of ABC beads to each tube.
3. Add 1 µL of Antibody to compensate to each tube (1 Ab per tube). Mix well.
4. Incubate for 15 min at room temperature in the dark.
5. Add 1 mL of 1X PBS or other buffer and centrifuge for 5 min at 250 g at room temperature.
6. Remove supernatant (leave 50 µL because you cannot visualise the beads).
7. Resuspend the pellet with 500 µL of 1X PBS.
8. Vortex the negative beads and add 1 drop to each tube.
9. Vortex well and analyze using the flow cytometer. Start with a 100 µL sample at 100 µL/min. FSC voltage at 260, SSC voltage at 375.

Mouse Exercise Training (Aims 1 and 2)

Acclimation:

1. On the week prior to the first Monday of exercise training, allow the mice to habituate to the testing room for 30 minutes.
2. Gently place each mouse on a treadmill lane. Record the mouse cage and lane numbers in the lab book.
3. Once mice are on the treadmill, turn the treadmill on (10 $m \cdot min^{-1}$) and allow the mice to run for no longer than 10 minutes.
4. Repeat steps 2 and 3 until all mice have been trained. Clean the treadmill and lane barriers with antiseptic solution between each exercise session.

Mouse Endurance Test

1. Begin test at 11 $m \cdot min^{-1}$.
2. Increase speed by 1 $m \cdot min^{-1}$ every 2 minutes.
3. Stop test if:
    - Mouse remains on platform for >1 min.
    - Mouse attempts to return to treadmill with forelimbs but cannot maintain pace.

Table A7. Exercise protocol for mice in the high-fat diet and exercise study (Aim 2).

EX Week	Warmup	Duration	Training	Duration	Cooldown	Duration
1	8 m·min^{-1}	10 min	7 m·min^{-1}	25 min	8 m·min^{-1}	5 min
2	8 m·min^{-1}	10 min	8 m·min^{-1}	35 min	8 m·min^{-1}	5 min
3	8 m·min^{-1}	10 min	9 m·min^{-1}	45 min	8 m·min^{-1}	5 min
4	10 m·min^{-1}	10 min	10 m·min^{-1}	45 min	8 m·min^{-1}	5 min
5	10 m·min^{-1}	10 min	11 m·min^{-1}	45 min	8 m·min^{-1}	5 min
6	10 m·min^{-1}	10 min	12 m·min^{-1}	45 min	8 m·min^{-1}	5 min
7	10 m·min^{-1}	10 min	13 m·min^{-1}	45 min	8 m·min^{-1}	5 min
8	10 m·min^{-1}	10 min	14 m·min^{-1}	45 min	8 m·min^{-1}	5 min
9	10 m·min^{-1}	10 min	15 m·min^{-1}	45 min	8 m·min^{-1}	5 min
10	10 m·min^{-1}	10 min	16 m·min^{-1}	45 min	8 m·min^{-1}	5 min
11	10 m·min^{-1}	10 min	17 m·min^{-1}	45 min	8 m·min^{-1}	5 min
12	10 m·min^{-1}	10 min	18 m·min^{-1}	45 min	8 m·min^{-1}	5 min
13	10 m·min^{-1}	10 min	19 m·min^{-1}	45 min	8 m·min^{-1}	5 min
14	10 m·min^{-1}	10 min	20 m·min^{-1}	45 min	8 m·min^{-1}	5 min
15	10 m·min^{-1}	10 min	21 m·min^{-1}	45 min	8 m·min^{-1}	5 min
16	10 m·min^{-1}	10 min	22 m·min^{-1}	45 min	8 m·min^{-1}	5 min
17	10 m·min^{-1}	10 min	23 m·min^{-1}	45 min	8 m·min^{-1}	5 min
18-26	10 m·min^{-1}	10 min	24 m·min^{-1}	45 min	8 m·min^{-1}	5 min

Table A8. Exercise protocol for mice in the colorectal cancer study (Aim 3).

EX Week	Warmup	Duration	Training	Duration	Cooldown	Duration
1	8 m/min	10 min	8 m/min	25 min	8m/min	5 min
2	8 m/min	10 min	8 m/min	35 min	8m/min	5 min
3	8 m/min	10 min	9 m/min	45 min	8m/min	5 min
4,5	10 m/min	10 min	10 m/min	45 min	8m/min	5 min
6,7	10 m/min	10 min	12 m/min	45 min	8m/min	5 min
8,9	10 m/min	10 min	14 m/min	45 min	8m/min	5 min
10,11	10 m/min	10 min	16 m/min	45 min	8m/min	5 min
12,13	10 m/min	10 min	18 m/min	45 min	8m/min	5 min
14,15	10 m/min	10 min	20 m/min	45 min	8m/min	5 min
16,17	10 m/min	10 min	22 m/min	45 min	8m/min	5 min
18+	10 m/min	10 min	24 m/min	45 min	8m/min	5 min
Week	Warmup	Duration	Training	Duration	Cooldown	Duration

Mouse Sample Collection Protocols

Blood, Liver, and Colon Extraction Protocol

Blood:

1. Carefully observe the respiration rate of the mouse. Once respiration ceases, quickly cervically dislocate the mouse and transfer to the flow hood with the mouse in anatomical position (facing upwards with the head towards the back of the flow hood). **The heart will continue to beat for approximately 4 minutes.**
2. Using small, sharp scissors and standard forceps, cut the abdomen and carefully through the subcutaneous adipose until the liver is exposed.
3. Keeping the scissors closed, push the liver downward so that the diaphragm is visualized. It appears as a thin sheath connecting to the ribcage.
4. Starting from the right edge (if cutting with scissors in right hand), cut away a small piece of the diaphragm close to the ribs.
5. Carefully cut across the diaphragm, lightly pulling the muscle inferiorly (towards the legs). This will help minimise the risk of cutting either the heart or the lungs.
6. Once the diaphragm is cut away the chest cavity should be available to visualise from an inferior angle.
7. Using larger scissors, cut through the ribs along the mid-axial plane. **Make sure not to cut the lungs or too superiorly – there is a risk of cutting the subclavian arteries and veins.**
8. Using your right thumb, fold the ribcage upwards while lightly pulling down just below the heart to make the apex approximately 90°.
9. Use your left thumb to hold the ribcage (as the right thumb had prior) and your 4^{th} and 5^{th} fingers to hold the bottom half of the mouse.
10. While inverted, place the heart inside a capless 6 mL K_2-EDTA-sprayed blood collection tube. Use small scissors to cut the left ventricle, allowing blood to enter the tube.
11. Using your 4^{th} and 5^{th} fingers, gently squeeze to promote further blood transfer into the blood collection tube.
12. Once all blood is collected, place the mouse down, return the cap to the collection tube, and gently invert the tube to minimise blood clotting. **Be conscious of any hairs that surround the collection tube – try to remove as many as possible before placing the cap on top of the collection tube.**

Liver:

1. Once the blood has been collected, use the small scissors and forceps to carefully remove the liver. **Never adjust the liver by pulling with the forceps or pushing with open scissors. The liver will tear and/or cut**.

2. Start from the superior side of the liver, first by cutting the aorta, connected diaphragm, and the stomach.
3. Using closed scissors and/or forceps, gently push the liver superiorly to observe any attachment points. Carefully cut away until the liver becomes loose.
4. Continue to manipulate the liver to observe any remaining attachment points and cut them.
5. Once the liver is fully released, carefully lift it with the forceps and place directly into a labelled 50 mL conical tube with at least 35 mL of 10% formalin.

Colon:

Items Required

Permanent Marker
Ice
Truncated 1000uL pipette tips
70% Ethanol Spray
Beaker with 70% Ethanol
Surgical Scissors and Forceps
Centrifuge Tubes (1.5 mL)
15 mL Tubes
50 mL Tubes
35 mm Culture Dishes
70 µM Cell Strainers
Kim Wipes
1 x PBS
5% **EV-Rich** FBS (FBS in -20°C freezer; PBS-diluted) - **FOR FLOW SAMPLES ONLY!**
5% EV-Depleted FBS
10 mL 0.2% Collagenase (DMEM-diluted) - 7 mL DMEM; 2 mL 1% Collagenase; 1ml FBS (10 mL/mouse)
Styrofoam ice box lid
Pins
Absorbent paper
Ruler
Scale
Razor
Weigh boats
Wooden sticks
Microscope slide
Liquid nitrogen

Parafilm

Protocol

1. Once legs removed (See Bone Marrow Protocol), place absorbent orange paper on Styrofoam ice box lid.
2. Use pins to secure mouse hands and base of tail to Styrofoam.
3. Using **small** scissors and forceps, carefully cut through tissue in the abdomen until colon is visible.
4. Locate the base of the colon and make a cut to remove the most distal part of the colon.
5. Use forceps to hold onto the distal end of the colon and carefully pull the colon out of the abdominal cavity, using small scissors to cut connective tissue under the colon.
6. Once the full colon is pulled out, make a cut right above the cecum (cecum will indicate the proximal end of the colon).
7. Align the colon against the ruler and measure the length of the colon from the most distal end to the right below the cecum (proximal end of the colon).
8. Make note of the proximal and distal ends of the colon and use a razor to remove the cecum.
9. Dip a wooden stick in a weigh boat of PBS to wet the stick, and carefully roll out all fecal matter from the colon.
10. Use a razor to remove any fat on the outside of the colon.
11. Tare the scare with the weigh boat of PBS and add colon to weigh boat to measure weight.
12. Cut colon into thirds using the razor so there is a proximal third, middle third, distal third.
13. Place the proximal colon third on a weigh paper, and using the small scissors carefully make a cut down the middle of the colon so the lumen is facing up on the weight paper.
14. Using forceps, transfer the colon to the top right side of the microscope slide and flatten out against the slide with the forceps.
15. Use the razor to cut ¼ longitudinally of the colon on the slide and transfer to a 35mm plate with 1 mL of prepared collagenase.
16. Use the razor to cut 1/8 of the colon on the slide longitudinally and transfer to a 1.5 mL tube labelled colon freeze for later protein analysis.
17. Repeat steps 13-16 with the middle and distal portions of the colon, adding the ¼ and 1/8 pieces to the same plate and 1.5mL tube, respectively.
18. Flash freeze the colon sample in the 1.5 mL tube in liquid nitrogen.
19. Store at -80°C.
20. Use small scissors to finely chop the ¼ colon sample in the 35mm plate with collagenase.
21. Place the remaining colon sample and slide into at 50 mL conical tube with 10% formalin and transfer to a rocker for 48 hours to fix the tissue for later aberrant crypt foci analysis.

22. Transfer chopped sample to a 50mL and add the remaining 9mL of collagenase to the tube.
23. Close tube tight and parafilm around the lid to secure the tube.
24. Place in orbital shaker for 45 min at 225rpm at 37°C.
25. Run 2 mL of PBS through a 70 µm filter into a 50 mL tube then filter colon cells through the filter using a truncated colon pipette tip.
26. Spin cells at 400g x, 4°C for 5 mins.
27. Remove supernatant and resuspend cells in 300uL prepared zombie yellow antibody (1:300 in PBS).
    - Incubate at room temperature for 15 mins.
28. Divide cells into each Flow Cytometry sample tube (F, G, H) and continue with Flow Cytometry Sample Instructions for Colon and Blood).

Colon Methylene Blue Staining and Aberrant Crypt Foci (ACF) Analysis

1. Once the colon tissue has been fixed in 10% formalin for 48 hours, remove the sample, lightly rinse with ddH_2O, and submerse them in new 50 mL conical tubes in 70% EtoH. Store the samples at 4 °C.
2. When ready for analysis, rinse the 70% EtoH away lightly with ddH_2O.
3. Prepare a 0.05% (yes, that low!) w/v methylene blue dye in ddH_2O at room temperature.
4. Dip the slides for one second at a time in the methylene blue dye for 20 cycles, then immerse fully for 3 minutes.
5. Rinse the slides again in ddH_2O to remove any excess dye.
6. Store the slides in 70% EtOH until ready for imaging.
7. Image the slides with the SteREO Discovery V.20 microscope at the microscopy core.
    - Make sure to keep the samples hydrated with water throughout the imaging session.
    - If the tissue is not hydrated properly the 70% EtOH will evaporate, leading to colon tissue curling off of the slide.
8. Look for any suspicious lesions and image them. Keep experiment files for each image for full analysis capability after the fact.

Whole Blood Collection – Serum

Items Required:

Permanent Marker
1.5 mL Eppendorf tubes (5 or 6 - 1 per mouse plus an extra 1-2)
Punch

Protocol

1. Collect blood from facial bleed into tube.

2. Let blood clot for approx. 15 min.
3. Spin down at 1500g for 10 min at 4°C.
4. Remove supernatant (serum) and place into new tubes.
5. Store at -20°C.
6. Transfer to -80°C ASAP.

Bone Marrow, Extracellular Vesicles Extraction

Items Required:

Permanent Marker
Ice
70% Ethanol Spray
Beaker with 70% Ethanol
Surgical Scissors and Forceps
Pestle and Mortar
Cell Strainer (70 µm)
Centrifuge Tubes (1.5 mL)
15 mL Tubes
50 mL Tubes
35 mm Culture Dishes
60 mm Culture Dishes
70 µM Cell Strainers
25G Needles (**Cat #309581 - CanMedDirect**)
Kim Wipes
Permanent Marker PBS
5% **EV-Rich** FBS (FBS in -20°C freezer; PBS-diluted) - **FOR FLOW SAMPLES ONLY!**
5% EV-Depleted FBS
20 mL 0.2% Collagenase (DMEM-diluted) - 16 mL DMEM; 4 mL 1% Collagenase (5 mL per mouse)

Protocol

1. Sacrifice mice 1-4.
2. Spray Mouse liberally with 70% Etoh
3. Dissect mouse and remove bottom half of fur and skin.
4. Remove all non-adherent tissues from the femurs and tibias, cut off feet, and place bones in ice-cold PBS (4 mL in a 15 mL tube) while working on other leg.
5. Remove any remaining muscle with KimWipes and cut free any tendons or ligaments with fine scissors.
6. Cut the ends of the bones with **large** scissors.

7. Flush the bone marrow with 500 µL PBS into a 1.5 mL tube until the bone is white (no remaining marrow).
8. Spin the samples at 500 g at 4 °C for 5 min. Remove the supernatant and transfer to a new 1.5 mL tube (EVs). Flash freeze or place in -80 °C freezer.
9. Soak a gauze pad in PBS and wrap the remaining femur. Place in a new 1.5 mL tube and store on ice. Set in the -80 °C freezer for later strength and microarchitecture analysis.
10. Another femur can be placed in a cassette in 10% formalin for marrow adipose tissue analysis.
11. Resuspend the pellet with 500 µL 5% FBS-PBS and set on ice.
12. Place bones in sterile mortar + pestle and rush bones gently.
    - Aim for approximately one bone fracture per bone, excessive crushing will damage the MSCs and reduce yield.
13. Add 2mL of 0.2% collagenase to the mortar. Transfer collagenase and bones to 60mm dish.
14. Cut the bone fragments into tiny pieces with **large** scissors.
    - Should take at least 5 minutes to ensure adequate chopping. Bones should be extremely fine (resemble paste).
15. After chopping, add 3mL of 0.2% collagenase to culture dish to bring final volume to 5mL.
16. Incubate at 37C for 45 min. Triturate samples in 25 mL pipets 15 minutes.
17. Run 2 mL of PBS through a 70 µm filter into a 50 mL tube. Filter resuspended bone marrow cells from ice through the filter, then the incubated cell suspension. **Ensure each sample is of equal volume with PBS**.
18. Spin cells at 400g x, 4°C for 5 mins
19. Remove supernatant and resuspend cells in 3 mL 5% EV-Depleted FBS, and store on ice.
20. **Once all samples from all mice are stored on ice, spin down at 400g, 4°C for 5 min.**
21. Aspirate the supernatant and resuspend the pellet in **2400 µL 5% FBS (marrow flushing FBS)**.
    - **Set 200 µL** into each **Flow Cytometry** sample tube (A,B,C,D; approx. 9.5 x 10^6 cells) and continue with Flow Cytometry Sample Instructions.
    - **Remaining cells** are for **HSC and MSC Isolation** Samples (approx. 15.5 x 10^6 cells). Spin down the **HSC and MSC Isolation** sample and resuspend in **100 µL Isolation Media**, then continue with MACS Instructions.

Bone MAT Staining

1. After isolating the femur and removing all muscle tissue, place in labelled cassette (pencil or permanent marker) and fix with 10% formalin for 48 hours.
    - Keep the cassettes in a beaker on the rocker.
2. Remove the cassettes and place under running water for 1 hour.
3. Decalcify the femur with 14% w/v EDTA (any type should be fine) at pH 7.4 for two weeks.

- Replace the EDTA solution once every 3-4 days.

4. Store the bones in PBS at 4 °C.
5. Mix 2% osmium tetroxide 1:1 with 5% w/v potassium dichromate to produce a 1% osmium tetroxide/2.5% potassium dichromate solution. The osmium tetroxide can be removed using a 25-gauge needle.
    - **IMPORTANT! ALL OSMIUM TETROXIDE HANDLING SHOULD BE DONE UNDER THE CHEMICAL FUMEHOOD. BE EXTREMELY CAREFUL NOT TO HAVE ANY OSMIUM TETROXIDE TOUCH YOUR SKIN OR FACE. IT IS HIGHLY TOXIC. USE 2 LAYERS OF NITRILE GLOVES AND A FACE SHIELD WITH THE SASH BETWEEN YOURSELF AND THE CHEMICAL. USE A SLIGHTLY OVERSIZED LABCOAT WITH ELASTIC CUFFS TO ENSURE FULL SKIN COVERAGE.**
    - All waste needs to go into a chemical waste bin specific for the osmium tetroxide.
    - Neutralize everything with any type of oil (corn oil is fine).
6. Transfer the decalcified bones to a 1.5 mL tube and add 1 mL of the staining solution. Set on rocker for 48 hours.
7. Move the bones to cassettes and run under cool water for 2 hours, then re-stain for 48 hours.
8. Wash bones once again then store in 1.5 mL tubes in PBS at 4 °C until imaging.
9. Settings for MAT imaging on Bruker Skyscan 1272 at OHRI: 70 kV, 142 µA, 0.5 mm A1 filter, 550 ms integration time, 1° rotation step, 360° angular range, and 12 µm image pixel.
10. Reconstruct the images using NRecon and CTan with a 100 global threshold value.

Flow Cytometry

Samples for Each Mouse – Aims 1 and 2 (For Wild-Type CBA Mice - Adjust as Necessary for CCR2 eGFP Mice):

A. HSCs, CMPs/GMPs/MEPs
B. CLPs
C. MSCs
D. EPCs and Adipo/Osteo Progenitors
ZYO. Zombie Yellow Only (Only for first mouse of study)
Ø. Unstained (Only for first mouse of study)

Dilution of Flow Cytometry Sample

Viability Staining-Zombie Yellow -Standard Cell Staining Protocol:

- Prior to reconstitution, spin down the vial of lyophilized reagent in a microcentrifuge to ensure the reagent is at the bottom of the vial.

- For reconstitution, pre-warm the kit to room temperature; add 100 µl of DMSO (the dessicant) to one vial of Zombie Yellow™ dye and mix until fully dissolved. Zombie Yellow Dye with DMSO is termed "reconstituted Zombie Yellow Dye".
- Store kit at -20°C upon receipt. Do not open vials until needed. Once the DMSO is added to the Zombie Yellow™ dye, use immediately, or store at -20°C in a dry place and protected from light. Use within one month.

1. Dilute cells with 1 mL 5% FBS.
2. Dilute Zombie Yellow™ dye at 1:300 in PBS (i.e., for 16 samples, need 16x 100 uL). Make one 15 mL tube with **1744 µL PBS, 5.8 µL** reconstituted Zombie Yellow.
3. Spin cells at 400g, 4°C for 5 minutes. Remove supernatant.
4. Resuspend the unstained (Ø) sample in 500 uL 5% FBS and store on ice in dark. This sample is ready to be analysed on the flow cytometer. **This sample is only required for the first test day.**
5. Resuspend cells of **#A-D and Zombie Yellow Only (ZYO) samples, not Ø,** in 100 µL of the prepared diluted Zombie Yellow solution. **Leave Ø on ice.**
6. Incubate the cells at **room temperature**, in the dark, for 15 minutes.
7. After incubation, quench with 500 µL PBS and spin cells (**not Ø**) at 400g, 4°C for 5 minutes.
8. Resuspend **Zombie Yellow** sample with 500 uL 5% FBS, store on ice in dark. This sample is ready to be analysed on the flow cytometer. **This sample is only required for the first test day.**
9. Remove supernatant. **Re-suspend cells in appropriate 200 uL anti-body cocktail**.
10. Incubate on ice for 1 hour in dark. **Work on Part IV during this time (have a partner).**
11. After incubation quench with 500 µL of PBS **(A-D Samples ONLY! Not ZYO or Ø samples).**
12. Spin at 400g x 4°C x 5mins
13. Remove supernatant. Re-suspend in 200uL of 5% FBS-diluted streptavidin-FITC (1:800) (Required for Lineage markers, including Ter119-only).
    - Required for **#A,B,C,D (16 total)**, therefore **make 3350 µL total (4.2 µL FITC, 3345.8 µL 5% FBS) in one 15 mL conical tube.** 3200 is for the samples, 150 is extra.
14. Incubate on ice for 30 minutes.
15. Quench with 1mL of PBS
16. Spin at 400g x 4°C x 5mins
17. Remove supernatant from **#A-D**. Re-suspend cells in 500uL 5% FBS
18. Samples are ready to be analysed on the flow. Keep samples on ice and covered.

*****Cocktails made up in 5% FBS*****

Single stain cocktails are required when initially optimizing an antibody.

If your antibody can only bind to cells and can't bind to compensation beads, you must prepare a single stain for that antibody (e.g., Zombie Yellow, as it binds to DNA). This single stain will be needed to set the compensation for the viability anti-body. Once you have this for the first group, they do not need to be re-made. The same goes for the initial unstained samples.

StemCell Tech HSC & MSC Negative Selection Magnetic Sorting (MACS)

Items Required:

Permanent Marker
EasySep Magnet
Rat Serum (Stored in -20°C Freezer in small box) (**Cat #13551**) *The entire kit is **Cat #19856.**
Isolation Antibody Cocktail (Stored in 4°C Fridge) (**Cat #19856C**)
RapidSpheres (Stored in 4°C Fridge) (**Cat #50001**)
Falcon Tubes (same ones used for flow cytometry)
15 mL Polypropylene Tubes
"Isolation Media" - 2% **EV-Depleted** FBS + 1mM EDTA (Recommended Medium)

Protocol

1. (Step 21 from previous protocol) - Samples containing 2 x 10^7 cells or fewer should be suspended in 100 µL of buffer (In FAQ "Can EasySep be used to isolate rare cells?".
2. Add 5 µL of Rat Serum to sample.
3. Transfer sample from 15 mL tube to 5 mL Falcon tube.
4. Add 5 µL of Isolation Antibody Cocktail to the sample.
5. Mix and Incubate: **2-8°C** for 15 minutes.
6. Vortex **RapidSpheres, NOT the samples** for 30 s.
7. Add 7.5 µL of RapidSpheres to the sample.
8. Mix and Incubate: **2-8°C** for 10 minutes.
9. Top up the sample to 2.5 mL with **Isolation Media**. Mix by gently pipetting up and down 5-6 times.
10. Place the tube **without the lid** into the magnet and incubate at **Room Temperature** for 3 min.
11. Pick up the magnet, and in one continuous motion, invert the magnet, pouring the enriched cell suspension (HSCs and MSCs) into a new 15 mL polypropylene tube.
12. Remove the tube from the magnet and top up to 2.5 mL with **Isolation Media**. Mix by gently pipetting up and down 5-6 times.
13. Place the tube **without the lid** into the magnet and incubate at **Room Temperature** for 3 min.
14. Pick up the magnet, and in one continuous motion, invert the magnet **and tube**, pouring the enriched cell suspension into the same 15 mL polypropylene tube.

15. Wash the MSCs in the new centrifuge tubes with **2 mL PBS.**
16. Throw away the remaining cell suspension (5 mL Falcon tubes - keep the 15 mL tubes).
17. Spin down the HSCs/MSCs (15 mL tubes) at 400g x 4°C x 5 min.
18. Resuspend HSC Isolated cells in **250 µL of HSC media with 20-200 µL pipette - 2x 125 mL transfers for volume accuracy!**
19. Pipette 10 µL of each HSC and MSC sample into a 1.5 mL tube to count cells.

Post-MACS - MSC Plating

Items Required:

Permanent Marker
Trypan Blue Stain
4 Hemocytometer Slides
Micropipette Tips
65 mm Culture Dishes
Complete DMEM Medium:

- 83 mL **High Glucose** DMEM (**GIBCO, Cat #11995065**)
- 2 mL Penicillin/Streptomycin
- 15 mL **EV-Depleted FBS**

Protocol:

1. Find cell count using hemocytometer slides - place 10 µL of diluted sample into a new 1.5 mL Eppendorf tube.
2. Add 10 µL of Trypan Blue dye into the Eppendorf tube with the sample.
3. Take the slide to the hemocytometer and obtain cell count.
4. **Manually adjust focus to ensure cell count is accurate.**
5. Further dilute cells to 2-3 x 10^5 cells/mL, so that the final concentration plated is 2-3 x 10^4 cells/mL.
6. Add **0.15 mL** of the diluted cells to **1.5 mL** media (**1.65 mL total**).
7. Transfer the cells to a 35 mm dish.
8. Plate the rest of the cells in another 35 mm dish with 1.5 mL media.
9. Change cell media every 24 hours for the 35 mm dish for 72 h, then every 3 days thereafter.
10. Cells should be ready to collect protein in approximately two weeks. These cells are difficult to release with trypsin. Extract protein and store in -80 °C freezer.

Post-MACS - HSC Plating

Items Required:

Trypan Blue Stain

4 Hemocytometer Slides
HSC Media - IMDM + 2% **EV-Depleted FBS**.
1x 13 mL Complete MethoCult M3434 Medium Aliquot (3 mL per mouse (in duplicate) (**Cat #03434 - StemCell Tech**)
2x 3 cc Syringes (**Cat #28240 - StemCell Tech**)
2x Blunt-End Needles; 16 Gauge (1 for use; 1 extra; **Cat #28110 - StemCell Tech**)
Micropipette Tips
12x 35 mm Culture Dishes (3 per mouse)
4x 100 mm Culture Dishes (1 per mouse)
Permanent Marker
150 µL Pen/Strep

HSC Plating Protocol:

1. Dilute cell with 250 µL **HSC Media**.
2. Find cell count using hemocytometer slides - place 10 µL of diluted sample into a new 1.5 mL Eppendorf tube.
3. Add 10 µL of Trypan Blue dye into the Eppendorf tube with the sample.
4. Take the slide to the hemocytometer and obtain cell count.
5. **Manually adjust focus to ensure cell count is accurate.**
6. Thaw the pre-aliquoted tube of complete MethoCult medium at room temperature or overnight at 2-8°C.
7. Prepare culture dishes by placing 2 x 35 mm culture dishes with lids inside a 100 mm Petri dish with a lid.
8. Add a third 35 mm culture dish without a lid as a water dish. This set of dishes is sufficient for one duplicate assay.
9. Dilute the cells with IMDM + 2% EV-Depleted FBS to 2-3 x 10^5 cells/mL so that the final concentration plated is 2-3 x 10^4 cells/mL.
10. For a duplicate assay, add 0.3 mL of diluted cells to a pre-aliquoted 3 mL MethoCult tube.
11. Add 33 µL of Penicillin/Streptomycin (to make 1% media) to the MethoCult tube.
12. Vortex the tube vigorously to mix the contents thoroughly.
13. Let the tube stand for at least 5 minutes to allow the bubbles to rise to the top.
14. To dispense the MethoCult™ mixture containing cells into culture dishes, attach a sterile 16 gauge blunt-end needle to a sterile 3 mL luer lock syringe.
    - For each tube plated, use a new sterile disposable 3 mL syringe fitted with a new 16 gauge blunt-end needle to prevent contamination between samples.
15. To expel the air from the syringe, place the needle below the surface of the solution to draw up approx. 1 mL of MethoCult. Depress the plunger to expel the medium and the air.

- Repeat until there is no air space visible.

16. Draw up the MethoCult mixture (containing the cells) into the syringe and dispense a volume of 1.1 mL into each 35 mm dish.
17. Position the syringe over the center of the dish and dispense 1.1 mL
    - **Do not expel the medium to the "0" mark on the syringe. Do 1.5 mL down to 0.4 mL rather than 1.1 mL to 0 mL for an accurate measure.**
18. Gently tilt and rotate the dish to evenly distribute the medium across the dish surface.
    - If any medium contacts the lid, replace the lid of the dish.
19. Place the dishes into the 100 mm dish.
20. Add approx. 3 mL of ddH_2O to the uncovered 35 mm dish to maintain humidity.
21. Count colonies at 10 days.

HSC CFU Imaging and Scoring Protocol

Celldiscoverer 7 HSC CFU Imaging:

At 10 days post-plating, the CFUs are imaged on the Celldiscoverer 7.

1. Place the 35 mm dish into the holder.
2. Using the Zen software, uncheck the "automatically detect plate" option.
3. Choose the entering plate option as a 60 mm dish. This will allow you to image the entire 35 mm dish. If 35 mm is selected the microscope will not capture the edges of the dish.
4. Image each plate using the stitching option.
5. Export the images as BigTIFF files to provide maximum resolution for later scoring.

HSC CFU Scoring:

1. Using Photoshop, resize the image to 48"x48" at 300ppi.
2. Make a 4"x4" grid as a pattern at 300ppi.
3. Lay the grid pattern over the image at 300% scale and 25% opacity.
4. To make the grid overlay, follow these instructions.
5. If the grid has been made previously, on the right side of the window go to "Layers" (left of *Channels*), select the "Fill" option (half-black, half-white option), then select "pattern" (third from the top).
6. To score colonies, use the "Count" tool.
7. Marker Size = 5, Label Size = 50.
8. Colour codes used for each colony type:
    - CFU-GEMM: #1922d4
    - CFU-GM: #039536
    - CFU-E: #d7290d
    - BFU-E: #d70dd0

9. Move upwards and downwards, not side to side, to score. Score one type of colony at a time to analyse more quickly.
10. To view previous scores, you must open the file in Photoshop. Use the count tool to score the colonies.

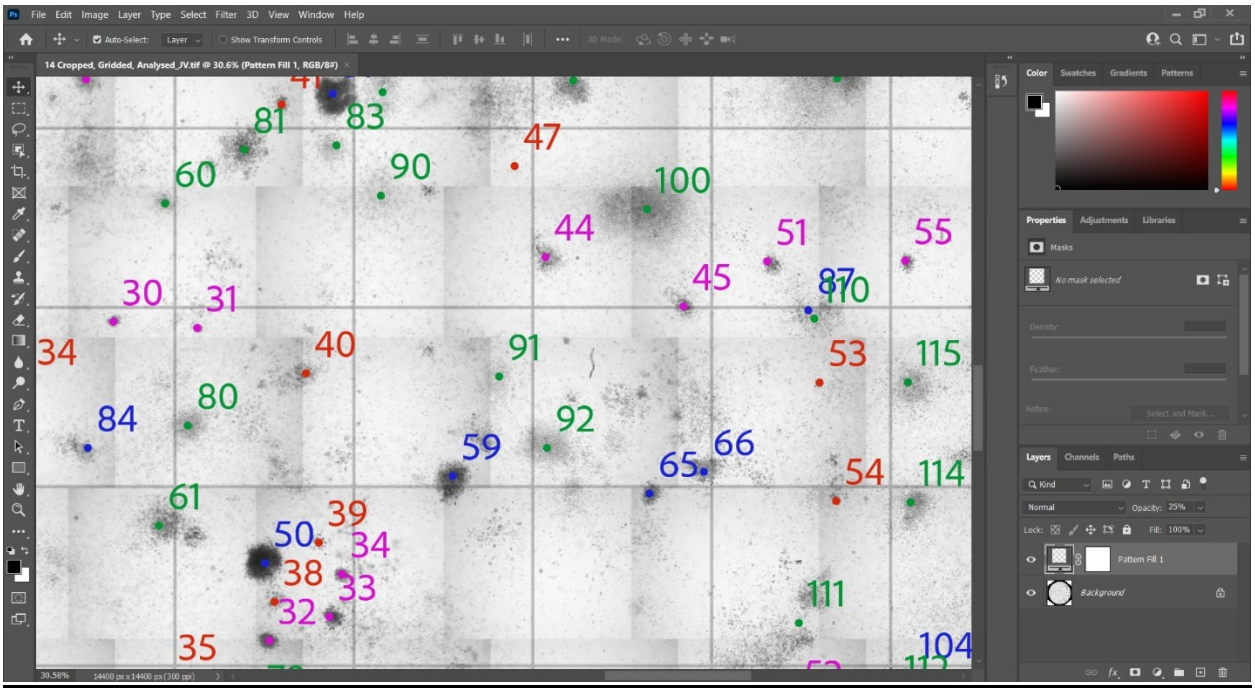

Figure A1. Example of a grid overlay and scoring technique.

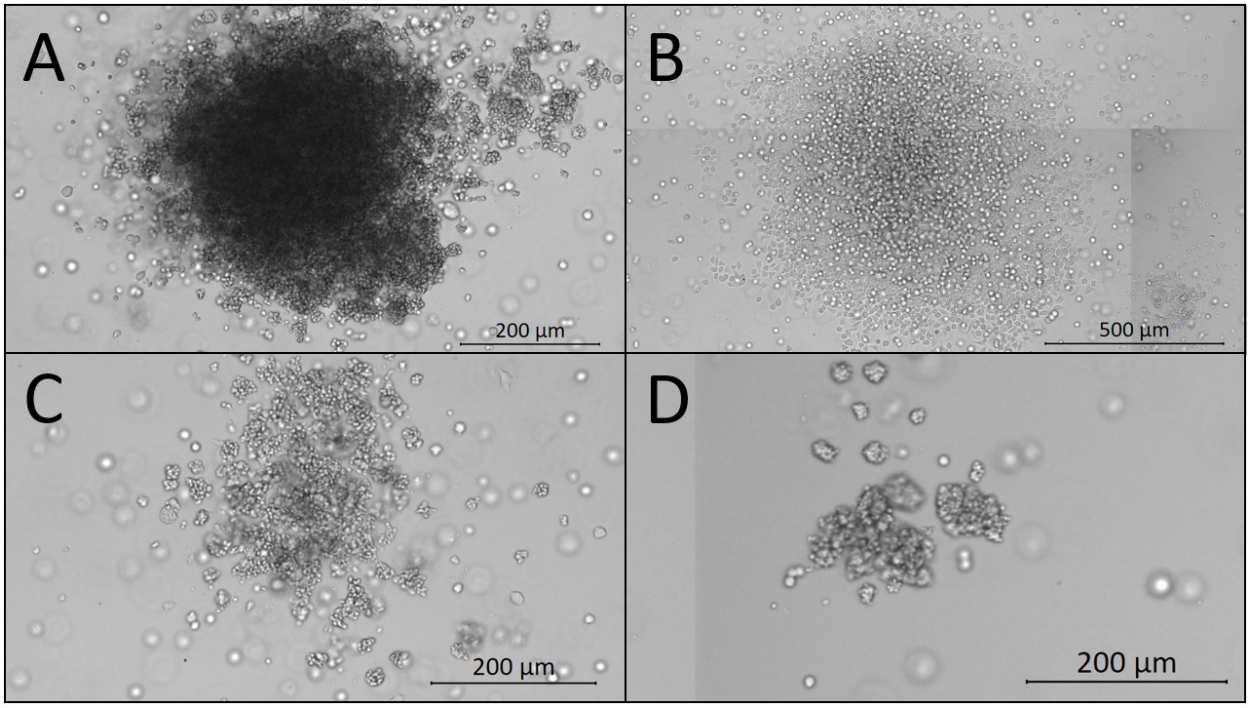

Figure A2. Examples of various hematopoietic stem cell colon forming units (HSC CFUs). (A) CFU-granulocyte, erythroid, macrophage, megakaryocyte (CFU-GEMM); (B) CFU-granulocyte, macrophage (CFU-GM); (C) Blast-forming unit-erythroid (BFU-E); and (D) CFU-erythroid (CFU-E).

Isolation of Extracellular Vesicles by Ultracentrifugation

1. TLA 100.3 - rotor to be used in 100,000 g (49,000 RPM) spin; UCF is the Optima MAX micro (room 3156). (Tubes - 3 mL polycarbonate 349622)
2. Supernatant from flushed bone marrow is centrifuged at 2,000 × *g* for 20 min at 4°C.
3. After 2,000 × *g* spin transfer supernatant to new tube.
    - An optional spin for 40 min at 15,000 x *g* at 4°C can be done following the 2,000 x *g* spin to separate large from small EVs.
4. Spin for 90 min at 100,000 × *g* (49,000 RPM) at 4°C.
5. Resuspend pellet with 110 µL of sterile PBS.
6. Add 10 µL of resuspended solution to 990 µL of 1X PBS (1:100 dilution).
7. To clean used tube:
    - Place in beaker with 70% EtoH.
    - Incubate for 5 minutes.
    - Pour out EtoH and clean the inside using forceps and a KimWipe. Repeat with ddh_2O.
    - Place in clean beaker, take up to autoclave.

Extracellular Vesicle Sample Nanoparticle-Tracking Analysis

1. Turn on Zetaview machine first. Allow to warm up for 5 minutes.
2. Open Zetaview softwarePress cancel on first pop up
3. Wash system using ddH_2O
    - Use 10mL syringe to push water through.
    - Aim for less than 10 particles.
    - Click cell quality check.
4. Focus machine by injecting bead sample (provided)
    - Inject 700 µL.
5. Set exposure value. Samples from animal is 80-92.
6. Clear system with ddH_2O.
7. Draw up 1000 µL of sample and inject first 700µL.
    - For bone marrow EV samples, dilute to no more than 1:100.
    - **Remember to incorporate this dilution factor when calculating the final concentration**.
    - Add the dilution factor to the software upon initial sample injection.
8. Analyze sample.
9. Select file location to be saved.

10. Select the default SOP.
11. Frame rate “15” for microvesicles and “30” for exosomes. If both, select 15.
12. Ensure the exposure value is correct.
13. Analyze.
14. Wash machine with ddH_2O between each sample.

EV and C3H10T1/2 miRNA Extraction - miRNeasy Micro Kit Protocol

Storage:

- The kit is shipped at RT. Store the RNeasy MinElute spin columns at 4 °C. The QIAzol Lysis Reagent can be stored at RT or at 4 °C. All other components are stored at RT. All products will be stable for at least 9 months.
- If buffer RWT forms precipitate upon storage, redissolve by warming then place at RT.

Equipment/reagents supplied by the user:

- Chloroform (without added isoamyl alcohol - important!).
- Ethanol (70%, 80%, and 100%)
- RNase-free ddH_2O (for ethanol dilution)
- 1.5 mL centrifuge tubes (autoclaved)

Protocol - EVs

1. Isolate EVs via ultracentrifugation at 100,000 g/49k RPM at 4 °C for 90 min.
2. Remove all supernatant and add 700 µL of QIAzol lysis reagent. Make sure it is mixed well and the pellet is released. Vortex the sample for 1 minute.

Protocol – C3H10T1/2 Cells

1. Wash cells twice with warm PBS and add 0.25% Trypsin in DMEM.
2. Incubate cells for 5 minutes at 37 °C.
3. Tap dish to agitate cells. Add 5% FBS and transfer cells to a new tube. Spin at 500 g at 5 °C for 5 minutes.
4. Remove super and resuspend cells in 250 µL 5% FBS. Move 10 µL to PCR tube for Cell Countess quantification.
    - Add 10 µL of Trypan blue dye to cells and mix.
    - Add 10 µL to each half of Countess slide.
    - Insert the slide upside down and focus so that the cells resemble donuts. Live cells are intact, dead cells will show stain inside the cell.
    - Use the average of the live cell counts to obtain value for dilution calculation.
    - If concentrations vary wildly, repeat the process.

- $C_1V_1 = C_2V_2$. C_1 is what is measured, V_1 is the volume you will require. C_2 is the desired concentration. V_2 is the desired final volume. Rearrange to solve for V_1.
- For the miRNA extraction the final concentration does not matter much. Make sure that you include no more than $1x10^6$ cells.

5. Add 700 µL of QIAzol Lysis Reagent make sure it is mixed well by vortexing for 1 minute.

Protocol – EVs and C3H10T1/2 Cells

1. Transfer the EV/lysis fluid mixture to a new 1.5 mL tube.
2. Let the mixture incubate at RT for 5 min.
3. Add 140 µL of chloroform to the tube containing the homogenate and cap it securely. **Perform this step inside the flow hood!**
4. Secure the cap and shake vigorously for 15 s.
5. Incubate the tube at RT for 2-3 min.
6. Centrifuge the tube at 12,000 g at 4 °C for 15 min. **Heat the centrifuge up to RT for the remaining centrifuge steps**.
7. Transfer the upper aqueous phase to a new 1.5 mL tube. Add 1.5 volumes (usually 525 µL) of 100% ethanol and mix thoroughly. **Do not centrifuge. Continue without delay to the next step.** Any precipitate formed here will not affect the procedure.
8. Pipet up to 700 µL of the sample into an RNeasy MinElute spin column in a 2 mL collection tube (supplied). Discard the flow-through.
9. Centrifuge at 8000 g for 15 s at RT. Discard the flow-through. Reuse the collection tube and repeat.
10. Add 700 µL **Buffer RWT** to the spin column. Centrifuge at 8000 g for 15 s at RT. Discard the flow-through.
11. Add 500 µL of **Buffer RPE** onto the spin column. Centrifuge at 8000 g for 15 s at RT.
12. Add 500 µL of **80% ethanol** into the spin column and centrifuge at 8000 g for **2 min into a new 2 mL collection tube (supplied)**. Discard the collection tube containing the flow-through. **Make sure not to touch the flow-through against the spin column.**
13. Open the lid of the spin column **(important)** and centrifuge at max speed for 5 min to dry the membrane. Discard the follow-through. Keep at least one empty position and point the lids in the direction opposite to the rotation of the rotor (i.e., if the rotor rotates clockwise, orient the lids counter-clockwise).
14. Place the spin column in a new 1.5 mL collection tube (supplied).
15. Add 14 µL RNase-free ddH_2O directly into the center of the spin column membrane. Close the lid gently and centrifuge for 1 min at full speed to elute the RNA. ***The dead volume of the spin column is 2 µL. Elution with 14 µL results in a 12 µL eluate.**

16. Check RNA sample concentration on nanodrop (2 µL of ddH_2O as the blank, 2 µL of sample for the measure). Lightly dry with a KimWipe between samples. Record the concentration, the A_{260}/A_{280} and A_{260}/A_{230} ratios.
17. Store RNA samples at -80 °C.

Nanostring nCounter miRNA Expression Assay

1. The RNA A_{260}/A_{280} ratio should be >1.9 and the RNA A_{260}/A_{230} ratio should be >1.8 for optimal results. Samples with concentrations below 10 ng/µL can be quite inaccurate.
2. Prepare RNA samples so that there is a 5 µL sample prepared at 33 ng/µL. 3 µL will eventually be used to provide a ~100 ng sample.
3. Prepare 500 µL of the miRNA assay control at a 1:500 ratio (1 µL assay control to 499 µL sterile H_2O) and keep on ice.
4. Prepare the **annealing master mix** – 13 µL annealing buffer, 26 µL tag reagent, and 6.5 µL of the prepared 1:500 assay control.
5. Aliquot 3.5 µL of the annealing master mix to each tube in the strip tube.
6. Add 3 µL of the diluted 33 ng/µL RNA sample to a designated tube. Flick the tubes gently and spin down.
7. Initiate the annealing protocol.

Table A9. Thermocycler settings for Nanostring nCounter miRNA annealing step.

Temp	Time
94 °C	1 min
65 °C	2 min
45 °C	10 min
48 °C	Hold

8. Prepare a **ligation master mix** with 19.5 µL of PEG (slowly! It's viscous) and 13 µL of the ligation buffer.
9. Add 2.5 µL the ligation master mix to each tube, flick the tubes, and spin down.
10. Set the tubes in the cycler and incubate at 48 °C for 5 min. **Keep them there at 48 °C.**
11. Keeping the tubes in the cycler, carefully add 1 µL of the ligase master mix to the bottom of each tube. **Do not mix the solution at this step.**
12. Recap the tubes and continue with the ligation protocol.

Table A10. Thermocycler settings for Nanostring nCounter miRNA ligation step.

Temp	Time
48 °C	3 min
47 °C	3 min
46 °C	3 min
45 °C	5 min
65 °C	10 min
4 °C	Hold

13. Remove the tubes and add 1 µL of the ligation clean-up enzyme to each tube. Flick the tubes and spin down.
14. Place the tubes in the cycler and continue with the final purification protocol.

Table A11. Thermocycler settings for Nanostring nCounter miRNA final purification step.

Temp	Time
37 °C	1 hour
70 °C	10 min
4 °C	Hold

15. Add 40 µL of sterile H_2O to each sample, mix, and spin down. The samples are ready for hybridization. **The hybridization was completed by the Rayner Lab tech.**
16. Upload data to nSolver 4.0 for quality control and normalization, then ROSALIND for analysis.

Protein Extraction

Protein Extraction – All Methods

1. Thaw RIPA buffer and keep on ice.
2. Add ½ a protease inhibitor tablet and ½ a phosphatase inhibitor tablet to each 5 mL RIPA buffer aliquot.

Protein Extraction – Nanoparticles

1. Remove samples from -80 °C freezer and keep on dry ice.
2. Spin samples at 2000 g at 4 °C for 20 minutes to form a cell debris pellet.
3. Move the supernatant into ultracentrifuge tubes (Beckman Coulter Cat #349622).
    - Set tubes into TLA100.3 rotor and balance tubes within 0.01 g with PBS.
4. Spin at 100,000 g (49,000 RPM) in Optima MAX Micro centrifuge 4 °C for 90 minutes.
    - Check 45 minutes into the spin to ensure the samples are still being centrifuged.
5. Carefully remove the supernatant and discard.

6. Resuspend the pellet using 60 µL of RIPA buffer. The pellet is often not visible. Mix thoroughly, transfer the RIPA and EVs to new 1.5 mL tubes, and place on inverter at 4 °C for 30 minutes.
7. Spin the samples down in the microcentrifuge at max RPM at 4 °C for 5 minutes.
8. Continue protein quantification via Bradford Assay.

Protein Extraction – *In Vitro* Cells (Adherent)

1. Remove media from dishes and place on ice immediately. Always keep the cells cold.
2. Add 100 µL of prepared RIPA buffer to a 35 mm dish or 250 µL to a 60 mm dish.
3. Use a cell scraper to remove/force the cells off the plate. Scraping the cells will promote cell lysis.
4. Transfer all of the RIPA-cell mixture to new 1.5 mL tubes and invert at 4 °C for 30 minutes.
5. Spin the samples down in the microcentrifuge at max RPM at 4 °C for 5 minutes.
6. Transfer protein supernatant to new 1.5 mL tube and proceed with protein quantification via Bradford Assay.

Protein Extraction – Colon Tissue

1. Remove samples from -80 °C freezer and keep in liquid nitrogen dewar.
2. Using an ultrasensitive scale, add an empty bead homogenizer tube and cap dry at room temperature, and tare the scale. **Make sure the tube is already labelled for your sample.**
3. Quickly remove the colon sample tube from the dewar and face the opening of the sample tube to the homogenizer tube.
4. Transfer the colon sample by tapping both tubes against the desk. The colon sample should fully transfer.
5. Quickly place the homogenizer tube to the scale and record the new weight.
6. Apply the homogenizer tube cap **tightly** and throw into the liquid nitrogen immediately. **This step is critical to keep the sample cold.** Make sure the cap is very tight on the tube. The cold will compress the tube and there is a risk of the cap becoming loose.
7. Move the tubes from the liquid nitrogen to ice.
8. Add 4 clean homogenization spheres (decontaminated by 70% EtoH and dry) to each tube and add 10 µL of prepared RIPA for every 1 mg. Add at least 60 µL to the tube (even if weight is below 6 mg).
9. Run the bead homogenizer at the following settings:
    - (S)peed: 6.00
    - (T)ime per cycle: 1:00
    - (C)ycles in total: 2
    - (D)ivision of time between cycles: 0:05

10. After homogenization, transfer all of the sample to a new 1.5 mL tube and spin at max RPM for 30 seconds at 4 °C.
11. Remove the clear supernatant and place into new 1.5 mL tube. Set aside 5 µL in a PCR tube for later protein quantification. Place both tubes in the -80 °C for storage.

Bradford Assay

1. Acquire the previously stored 5 µL protein sample (or 12 µL sample for nanoparticles) from the -80 °C freezer and keep on ice.
2. Prepare protein standards at 0, 0.125, 0.25, 0.5, 1.0, and 2.0 µg/µL via serial dilution in 1.5 mL tubes.
3. Prepare 10x dilution PCR tubes for colon homogenate or *in vitro* extractions; nanoparticles should not be diluted (keep at 1X).
4. Add 1.5 µL sample into 13.5 µL of ddH_2O to prepare a 15 µL 10x diluted sample. This will allow for two 5 µL samples to be transferred without risk of running out of sample. Keep the samples on ice at all times.
5. Prepare 250 µL of 1 part Bio-Rad Bradford Reagent (Cat #5000006) and 4 parts PBS for each well with an extra margin to ensure enough is prepared for all of the wells. Keep at room temperature in the dark – use aluminum foil to cover a 5, 15, or 50 mL tube.
6. Add 5 µL of each protein standard into a 96-well plate in duplicate.
7. Add 5 µL of each 10x-diluted sample into a 96-well plate in duplicate.
8. Quickly add 250 µL of the prepared dye to each well.
9. Scan the plate using the spectrophotometer at 595 nm.

Extracellular Vesicle Western Blot Protocol

Western Blot - Reagents Needed:

- 10x Running Buffer - to make 1x Running Buffer (with ddH_2O)
  - 30.3g Tris Base (NOT Tris-HCl)
  - 144.0g Glycine
  - 10.0g Sodium Dodecyl Sulfate (SDS)
  - Top up to 1L with ddH_2O
  - Adjust pH to 8.3 (Approximately 9.5 mL of 37% HCl)
- 10x Transfer Buffer - to make 1x Transfer Buffer (10% Transfer Buffer, 70% ddH_2O, 20% Methanol)
  - 30.3g Tris Base (NOT Tris-HCl)
  - 144.0g Glycine
  - Top up to 1L with ddH_2O
- 10x Tris-Buffered Saline (TBS) - to make 1x TBS (with ddH_2O)

- 24.2g Tris Base (NOT Tris-HCl)
- 80g Sodium Chloride (NaCl)
- Top up to 1L with ddH_2O
- Adjust pH to 7.6 (Approximately 12 mL of 37% HCl)

- 1.5 M Tris-HCl (for Running Gel) – 600 mL Preparation
  - 108.9g Tris Base (NOT Tris-HCl)
  - Top up to 600 mL ddH_2O
  - Adjust pH to 8.8 (Approximately 18.5 mL of 37% HCl)
- 1.0 M Tris-HCl (for Stacking Gel) – 200 mL Preparation
  - 24.2g Tris Base (NOT Tris-HCl)
  - Top up to 200 mL ddH_2O
  - Adjust pH to 6.8 (Approximately 15 mL of 37% HCl)
- 0.1% TBST (1 mL Tween 20 in 999 mL TBS) - Cut off end of 1 mL pipette tip with scissors. Tween is viscous and some will stay inside. Eject the empty pipette tip into the 1000 mL tube, cover with parafilm paper, and mix. Pour the fluid into a new capped glass jar.
- 10% Ammonium Persulfate (APS) (In -20°C freezer)
  - 1g Ammonium Persulfate
  - 10mL ddH_2O
  - Aliquot in 1mL, store in -20°C freezer
- 4x Laemmli Buffer (In -20°C freezer)
  - 2.4mL 1M Tris-HCl (NOT Tris Base)
  - 0.8g SDS
  - 4mL Glycerol
  - 1mg Bromophenol Blue
  - 1mL β-mercaptoethanol
  - 2.8mL ddH_2O
  - Aliquot in 1mL, store in -20°C freezer
- 30% Acrylamide (In 4°C Fridge - Brown Bio-Rad bottle)
- TEMED (in flammables cabinet)
- APS (In -20°C freezer)
- 5% Milk-TBST (for 50 mL: 250 mg powder milk and top up to 50 mL with TBST).

Prepare Resolving Gel (10%) – 1.5 gels with 1.5 mm spacing.

- 5.9 mL ddH_2O
- 5 mL 30% Acrylamide
- 3.8 mL Tris 1.5 M (pH 8.8)
- 150 µL 10% SDS

- 150 µL 10% APS - **Only add this component when ready to form gel – it's an active component.**
- 6 µL TEMED - **Only add this component when ready to form gel – it's an active component.**

Prepare Stacking Gel (5%) – 1.5 gels with 1.5mm spacing.

- 5.1 mL ddH_2O
- 1.25 mL 30% Acrylamide
- 960 µL Tris 1.5 M (pH 6.8)
- 75 µL 10% SDS
- 75 µL 10% APS - **Only add this component when ready to form gel – it's an active component.**
- 8 µL TEMED - **Only add this component when ready to form gel – it's an active component.**

Prepare Running Buffer

- 100 mL 10x running buffer (pre-made on shelf), 900 mL ddH_2O

Day 1 - Protein Separation via SDS-PAGE:

1. Thaw protein sample (95°C x 5 min on thermocycler).
2. While samples are boiling/denaturing, remove combs from gel and remove all bubbles with ddH_2O.
3. Load plates onto cassette. Use plastic dam when only running 1 gel.
4. Fill cassette 50-75% capacity with running buffer to check for leaks on bottom of cassette.
5. Load ladders and samples to wells.
6. Fill cassette with running buffer to the top, then the container with remaining buffer. Make sure the buffer runs over the top of the cassette (fully submerged).
7. Run at 90V x 30 min, then at 120V for approximately 60 minutes.

Day 1 - Protein Transfer to PVDF Membrane:

8. Stop the run when the ladder reaches the bottom green line.
9. Prepare the membrane.
    - Use the glass plate as a template and mark blue cover with pencil.
    - Use scissors to cut around.
10. Activate the PDVF membrane in methanol for approx. 10 seconds, then wash in ddH_2O and place in transfer buffer.
11. Wet the sponges and filters in transfer buffer.
12. Make the sandwich (order). The proteins will run to red (i.e., make sure the membrane is towards the red electrode, which is also the white/clear portion of the cassette).

- White/Clear Side
- Sponge
- Filter
- Membrane
- Gel
- Filter
- Sponge
- Black Side

13. Place the sandwich in the container (red and black) and fill with transfer buffer. **Make sure there is enough transfer buffer to cover the entire membrane, not just the bottom half.** The temperature gradient can impact the transfer.
14. Add an ice pack from the freezer and run in the cold storage room at 120V for 60 minutes **sharp. Do not turn off before or after this time point. The proteins may not transfer enough if stopped earlier and may pass through the membrane and lost if left running too long.**
15. After run, add 25 mL of Ponceau stain to the dish.
    - Place the membrane inside and set on a shaker until bands appear (2-5 min).
16. Remove the membrane from the stain and rinse with ddH_2O. Hold the membrane by the corner with forceps and dab on paper towel.
17. Place the membrane in between plastic sheets (new sheets in drawers underneath Cell Countess).
18. Image membrane on the Biorad Chemidoc. **This will tell you that your proteins have transferred successfully.**

<u>Day 1 - Primary Antibody Staining and Incubation:</u>

19. Cut the portions of the membrane you want to isolate for proteins. Use the protein ladder for reference.
    - Rinse in ddH_2O.
    - Add TBST and tilt for 5 min at 45 RPM.
    - Dump TBST and re-rinse 3x total.
20. Submerge membranes with 5% powdered milk on shaker at room temperature at 16 RPM for 1 hour. This step will reduce nonspecific binding of the antibodies later.
21. Prepare the primary antibodies (dilution).
22. Prepare 5 mL of each antibody (in 15 mL conical tube).
    - 250 mg of BSA (4°C fridge)
    - Top up to 5 mL of TBST
    - Add 5 µL of antibody (-20°C freezer in small blue shelving unit)
23. After block with 5% milk, wash membrane 3 x 5 min with TBST.

- Set on shaker at 45 RPM each time.

24. Pour off TBST and add primary antibodies listed below (diluted Flotillin-2 and Alix).
25. Place on shaker in cold room for overnight incubation.

Table A12. Antibodies used for the extracellular vesicle study.

Aim 2: Primary Antibody	Category Number	MW (kDa)	Dilution (5% BSA-TBST)
Flotillin-2	3436S	49, 58	1:1000
Alix	SAB4200476-200UL	95	1:1000
TSG 101	T5701-200UL	46	1:1000

Table A13. Antibodies used for the colorectal cancer study.

Aim 3: Primary Antibody	Category Number	MW (kDa)	Dilution (5% Milk-TBST)
β-Actin	4970T	45	1:1000
p-STAT3	9145T	79, 86	1:1000
STAT3	4904T	79, 86	1:1000
NF-κB	8242T	65	1:500
β-Catenin	9562S	92	1:1000

***pNF-κB was not for this study as we were unable to detect it in any colon sample. It was faint but present in skeletal muscle homogenate.**

Day 2 - Adding HRP Secondary Antibody and Imaging:

1. Remove primary antibodies and place in -20°C for later use. Make note on the tube how many uses the antibody has had.
2. Wash the membrane 3 x 5 min on shaker at room temperature at 45 RPM with TBST.
3. Prepare secondary antibody (Horseradish Peroxidase - HRP) in 5% milk with TBST.
    - Dilute HRP at 1:10,000 to make 10 mL total (1 µL HRP, 10 mL 5% milk with TBST).
4. Add secondary HRP antibody to membranes and incubate for 1 hour at room temperature at 16 RPM.
5. Wash membranes 3 x 5 min with TBST on shaker at 45 RPM.
6. Prepare chemiluminescence stain (1:1 ratio) when ready to image - on shelf with other Western Blot reagents (ECL mixture).
    - 500 µL per membrane section.
    - Only 2 sections for this stain. Therefore prepare 1.0 mL (500 µL from each bottle into 1.5 mL tube)

7. Place membranes flat on glass panel (from Day 1 gel) and add ECL mixture. It will react with HRP.
    - Cover with Styrofoam box for 5 minutes - light-sensitive!
8. Blot-dry membranes on Kimwipe or paper towel **quickly** and place membranes inside plastic sleeve.
9. Image on the Biorad Chemidoc
    - Colorimetric - Auto
    - Chemiluminescence - Auto

Day 2 - Removing Flotillin-2 and Alix Antibodies and Staining TSG-101 Antibody:

10. Wash flotillin membrane 3 x 5 min with TBST (can keep Alix strip in fridge if desired).
11. Add 7 mL stripping buffer to membrane.
    - Place on shaker for 20 min at room temperature at 45 RPM.
12. Wash membrane 3 x 5 min with TBST on shaker at 45 RPM.
13. Add secondary HRP antibody at 1:10,000 in 5% milk-TBST and incubate for 1 hour on shaker at 16 RPM to ensure there is no residual primary antibody.
14. Wash 3 x 5 min with TBST on shaker at 45 RPM.
15. Prepare chemiluminescent mixture.
    - Need 500 µL total - only 1 membrane strip this time.
16. Place on glass plate, add 500 µL and set Styrofoam box overtop for 5 minutes.
17. Blot-dry membrane on Kimwipe or paper towel **quickly** and place in plastic sleeve.
18. Image membrane on Biorad Chemidoc to ensure no antibody is remaining.
    - Colorimetric - Auto
    - Chemiluminescence - Auto
    - You shouldn't be able to visualise any chemiluminescent signal. The Chemidoc will take a series of test images and should return an error stating the sample is too faint to use the autoexposure setting. **This is what you want to see at this step.** The antibody was stripped and therefore not visualised.
19. If a signal is seen, repeat steps 12-18. If no signal is seen, continue to step 20.
20. Wash membrane 3 x 5 min with TBST.
21. Block for 60 min with 5% powder milk at room temperature on shaker at 16 RPM.
22. Wash membrane 3 x 5 min with TBST.
23. Add TSG-101 primary antibody (1:1000, prepared on Day 1) to membrane.
    - Incubate overnight in cold room on shaker.

Day 3 - Adding HRP Secondary Antibody and Imaging:

1. Remove primary antibodies and place in -20°C for later use. Make note on the tube how many uses the antibody has had.

2. Wash the membrane 3 x 5 min on shaker at room temperature at 45 RPM with TBST.
3. Prepare secondary antibody (Horseradish Peroxidase - HRP) in 5% milk with TBST.
    - Dilute HRP at 1:10,000 to make 10 mL total (1 µL HRP, 10 mL 5% milk with TBST).
4. Add secondary HRP antibody to membranes and incubate for 1 hour at room temperature at 16 RPM.
5. Wash membranes 3 x 5 min with TBST on shaker at 45 RPM.
6. Prepare chemiluminescence stain (1:1 ratio) when ready to image - on shelf with other Western Blot reagents (ECL mixture).
    - 500 µL per membrane section.
    - Only 1 section for this stain. Therefore prepare 250 µL from each bottle into 1.5 mL tube.
7. Place membranes flat on glass panel (from Day 1 gel) and add ECL mixture. It will react with HRP.
    - Cover with Styrofoam box for 5 minutes - light-sensitive!
8. Blot-dry membranes on Kimwipe or paper towel **quickly** and place membranes inside plastic sleeve.
9. Image on the Biorad Chemidoc
    - Colorimetric - Auto
    - Chemiluminescence - Auto

CCR2 eGFP Mouse Genotyping

<u>Ordering Primers</u>

Primers are ordered through the ThermoFisher Custom DNA Oligo Primer form online. An account must be made with the information linked to the Medpurch Shipping Bay at RGN. Once an account is made the shipping and billing information must be entered. The shipping and billing addresses are the same:

Company or Institution: UNIV OF OTTAWA
Address: 451 Smyth Rd, Ottawa ON, K1H 8M5, Canada
Attention to: University of Ottawa
Building and Room Number: Roger Guindon Hall (Shipping), Roger Guindon Bldg (Billing)
Lab or Department: Health Sciences

Once this information is entered there should be an option to select the shipping center, and the billing and shipping account numbers should be automatically entered. Check “My Profile” to confirm.

1. Oligo Primer Resuspension

- GFP Mutant Reverse 15020
- GFP Common/WT 24128
- GFP Common/WT Reverse 24129
- Take sample mass (nanomoles), multiply by 10, and add DNAse-free ddH_2O in that volume in µL to the primer tubes.

e.g., 26.5 nmol of primer. Add 265 µL of DNAse-free ddH_2O to make 100 µM stock.

2. Crude DNA Extraction: Adapted from Lopez (2012).

Reagents

- 50 mM NaOH (Anhydrous - M.W. 39.99 g/mole)
- 99.975 mg of NaOH in 50 mL
- 300 mM Sodium Acetate (NaOAc; Anhydrous - M.W. 82.03 g/mole)
- 1.23045 g of Anhydrous NaOAc in 50 mL

e.g., Add 250 µL of 1 M NaOH to 4.75 mL of ddH_2O, and 123 mg of sodium acetate to 5 mL ddH_2O.

Methods

1. Add 50 µL of 50 mM sodium hydroxide (NaOH) to PCR tube containing mouse ear clip sample.
2. Incubate at 98 °C for 30-60 min. Flick occasionally to keep liquid at bottom.
3. Once done, flick/vortex tubes vigorously while still hot.
4. Add 50 µL of 300 mM NaOAc to neutralize NaOH.
5. Add 150 µL of DNAse-free ddH_2O to get ~100 ng/µL (can check concentration on Nanodrop).
6. Spin sample at 1500 g for 3 min.
7. Use 1-2 µL for the reaction.

Table A14. PCR reaction preparation.

Item	Volume
WT Reverse 24129 Primer	0.5 µL (1 µM)
WT Common/Forward 24128 Primer	0.5 µL (1 µM)
Mutant Reverse 15020 Primer	0.5 µL (1 µM)
Template DNA (from extraction step)	1 µL
DreamTaq Green PCR Master Mix (2x)	25 µL
DNAse-free ddH_2O	22.5 µL (to make 50 µL total)

Table A15. PCR thermocycler settings for CCR2^{+} mouse genotyping.

Step	Temperature (°C)	Time	Number of Cycles
Initial Denature	95	2 min	1
Denature	95	30 s	32
Annealing	*Tm-5 (61 °C)	30 s	32
Extension	72	1 min	32
Final Extension	72	10 min	1
Hold	4	N/A	N/A

*Tm is the melting point of the primers. Tm = 4(G+C) + 2(A+T). The Tm for the current set of primers is approx. 66 °C. The annealing temp requested for the DreamTaq PCR master mix is Tm-5 °C. Therefore, the annealing temp for this protocol is set to 61 °C.

Run PCR with the "ccr2 gfp" file in James' folder on the thermocycler.
Prepare the agarose gel while PCR is running.

Agarose Gel Electrophoresis

1. For the small blue container, approx. 90 mL is required. Therefore make 100 mL.
2. 100 mL 2% agarose gel = 100 mL TBE (or TAE) and 2 g agarose powder into an Erlenmeyer flask.
3. Gently mix by swirling the flask.
4. Place in the microwave and heat for 30 s. Remove and swirl the flask and place back in for more 30 s cycles until the agarose has been fully dissolved. **IMPORTANT: Do not let the agarose solution boil over. Use a glove to handle the flask as it will be very hot.**
5. Allow the solution to cool down enough to be able to be touched. Add 10 µL of 10,000x SYBR safe gel stain to the solution and swirl until fully mixed.
6. Pour the solution into the plastic mold and allow to dry. The mold needs to be perpendicular to the rest of the plate to stop any leak from occurring.
7. Place the comb in the solution.
8. Once the gel is formed, remove the comb straight up to keep the wells intact.
9. Turn the plastic holding the gel 90 degrees so that the walls are closer to the black electrode (**Run to Red**).
10. Add ladder, PCR samples, and +ve/-ve controls (if wanted).
11. Run the gel at 100 V until the marker is approx. 75% down the gel (approx. 90 mins).

C3H10T1/2 MSC Adipogenic Assay

1. Plate 1250 cells per well in a 96-well flat bottom dish in 100 µL of growth media (10% FBS, 1% penicillin-streptomycin, rest high glucose DMEM) and 5.1 million EVs.
2. Incubate the cells for 72 hours until the wells are 90% confluent.
3. Begin adipogenic differentiation using the Mesencult adipogenic differentiation kit along with 5.1 million EVs and incubate for 48 hours.
4. Add 1 µg/mL of insulin and incubate for 72 hours with 5.1 million EVs.
5. Fix the cells in 10% formalin for 30 minutes at room temperature.
6. Wash the cells twice with ddH_2O.
7. Stain the cells with 0.5% Oil Red O dye (100 µL) for 30 minutes at room temperature in the dark.
8. Carefully wash excess dye away with ddH_2O 3 times.
9. Add 200 µL of isopropanol and set the plate on a rocker for 10 minutes at room temperature in the dark.
10. Transfer 100 µL of the isopropanol to a new plate.
11. Measure the absorption on the spectrophotometer at 492 nm.

C3H10T1/2 MSC Osteogenic Assay

This protocol was adapted from Gregory and colleagues (2004) using 10% of their listed volumes to account for the 96-well plates.

1. Plate 1250 cells per well in a 96-well flat bottom dish in 100 µL of growth media (10% FBS, 1% penicillin-streptomycin, rest high glucose DMEM) with 5.1 million EVs.
2. Incubate the cells for 72 hours until the wells are 90% confluent.
3. Begin osteogenic differentiation using the Mesencult osteogenic differentiation kit along with 5.1 million EVs.
4. Replace the media every 72 hours with 5.1 million EVs per media change for a total of 14 days.
5. Fix the cells in 10% formalin for 30 minutes at room temperature.
6. Was the cells twice with ddH_2O.
7. Stain the cells with 0.2% Alizarin Red S dye (100 µL) for 20 minutes at room temperature in the dark.
8. Read the absorbance on the spectrophotometer at 405 nm.

C3H10T1/2 MSC Proliferation Assay

Prepare the solutions according to the manufacturer's instructions.

1. Warm up the vials to room temperature.

2. Add 2 mL of dimethyl sulfoxide to the EdU to prepare a **10 mM EdU solution**.
    - Keep unused solution at -20 °C or colder.
3. Transfer 4 mL of the **1X reaction buffer** to 36 mL of ddH_2O.
4. Add 2 mL of ddH_2O to the buffer additive to prepare a 10X solution.
    - Keep unused solution at -20 °C or colder.
5. Prepare a 1X Hoechst 33342 by a 1:2000 dilution with PBS.

Label the cells with EdU.

1. Grow 1250 C3H10T1/2 cells in a 96-well dish with 100 µL of growth media for 2 hours.
2. Prepare a 20 µM solution from the 10 mM EdU solution with new cell media.
3. Replace 50 µL of the original growth media with 50 µL of the 20 µM EdU-rich media (for a final concentration of 10 µM) alongside 5.1 million EVs.

Fix and permeabilize the cells.

1. Fix the cells with 4% formaldehyde at 6-, 12-, 24-, and 48-h after the EdU-rich media addition.
2. Wash the cells twice with 3% BSA-PBS and permeabilize with 100 µL of 0.5% Triton X-100-PBS for 20 minutes at room temperature.

Detect the EdU.

1. Add 50 µL of the reaction cocktail to each well and incubate for 30 minutes in the dark at room temperature.
2. Wash the cells with 100 µL of 3% BSA-PBS and a second time with PBS.
3. Stain the DNA with 1X Hoechst 33342 and incubate for 30 minutes in the dark at room temperature.
4. Wash the cells twice with 100 µL of PBS.
5. Image on the Celldiscoverer7.
    - Excitation λ: 350 nm
    - Emission λ: 461 nm

C3H10T1/2 MSC Flexcell Tension Assay – Lipid Accumulation Assay

The following is a general protocol for using the Flexcell.

1. Seed desired number of cells in a 6-well collagen I-coated plate (BF-3001C) in the appropriate growth media. Some time must be allowed for cell adhesion. This time window will be dependent upon the type of cell.
2. Open the Flexcell software and switch the vacuum to “Auto”. The vacuum should turn on.
    - The vacuum pump oil should be replaced annually or every 100 hours of use (whichever is first). The oil to be replaced is LVO 100 (Thermo Fisher, Cat

#NC0313679). Make sure the oil is filled between the appropriate lines on the front.

3. Clean the large black plate holder with 70% EtoH and paper towel. **Make sure there are no liquid particles entering the tubes. They must remain dry.**
4. Apply silicone-based grease to the large plate holder where the orange rubber gaskets attach. This layer must be thick enough to ensure that no air can escape. Air leakage violates the integrity of the vacuum forcing.
5. Attach the rubber gaskets and apply another thick layer of grease to the inside of the orange rubber gaskets to ensure air cannot pass through.
6. Set a small amount of grease on each white post. The membranes will slide along the posts due to the vacuum forcing.
7. Attach the 6-well plates into the gaskets. The fit should be tight. Add another layer of grease around each plate to ensure air cannot pass through. Four plates must be used for the vacuum forcing to function properly. If using fewer than 4, add a 4th empty plate.

Figure A3. Flexcell vacuum pump. The bottom right plug is used to drain the LVO 100 oil. The plug directly above the oil line is used to refill the oil. The oil should be between the lines on the plate surrounding the oil level visualizer and should resemble the level shown above.

8. Set the large black plate inside the incubator.
9. Set the heavy glass plate overtop of the 6-well plates and set the black weights overtop. Prior to their addition, make sure each component is sprayed with 70% EtoH to sterilize them.
10. Carefully attach the quick-connect tubes without touching any component of the plates or incubator.
11. Turn on the FX5000T-FLK Tension system by setting the white switch at the back to “On”.
12. Open the Flexcell software and set the vacuum pump to “On”
13. Load the regiment for the C3H assay. Regimen/Assign/BFIx Loading Station (25mm)/James – C3H EV Study/C3H Adipo – Aim 1 – SIN – 0.167 Hz – 100.
14. Check for any air leaks in the loading stations. Add more grease if necessary.
15. Once the run is complete, collect the cell media for EV isolation and RT-qPCR preparation.

16. Clean the loading station with soap and water before leaving the lab. An initial cleaning with 70% EtoH and KimWipes will remove most of the grease. If the grease is not removed the gaskets will harden and stick to the loading station.

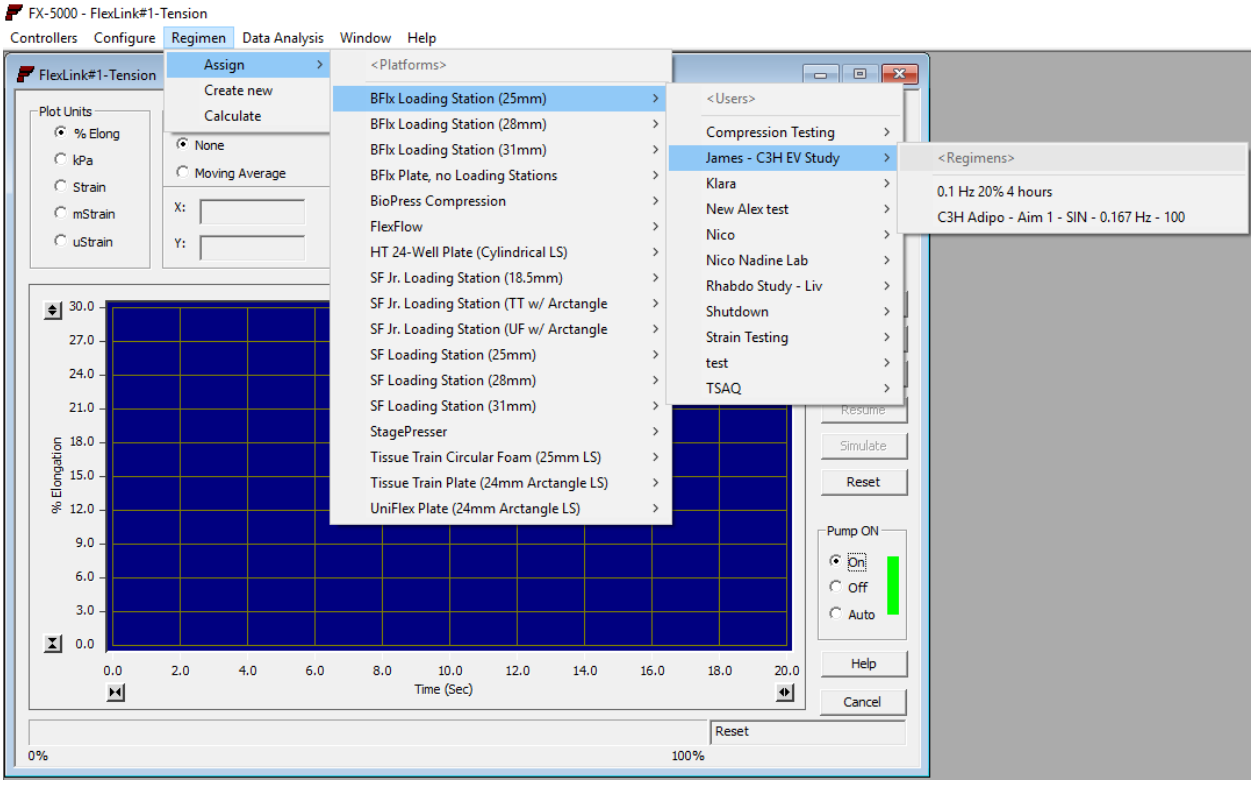

Figure A4. Outline of the Flexcell software and regimen loading step.

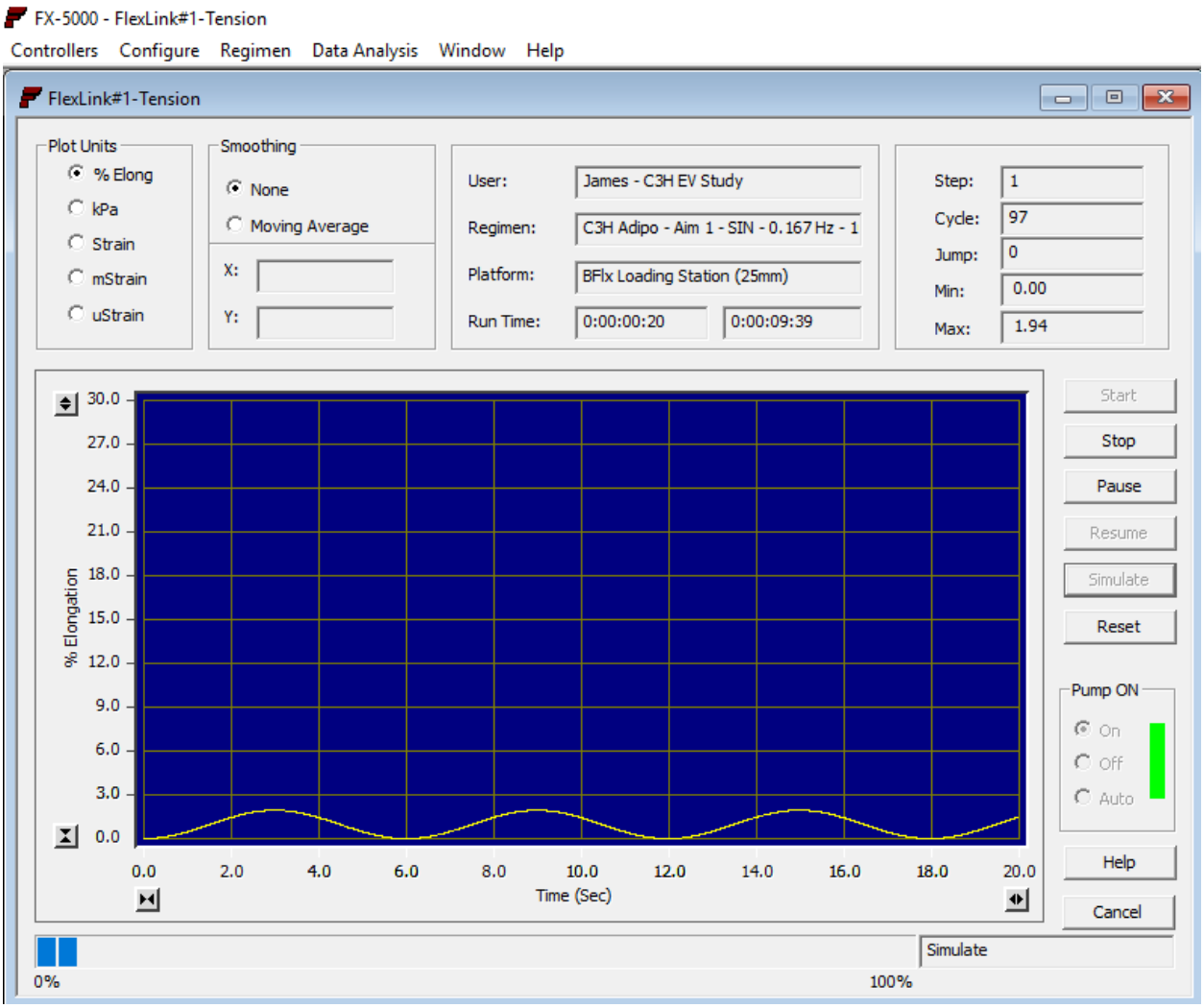

Figure A5. Simulation of the SIN wave regimen run at 0.167 Hz.

C3H10T1/2 RT-qPCR Assay

miRNA RT-qPCR requires (1) miRNA extraction, (2) complementary DNA formation via reverse transcription, and (3) a polymerase chain reaction that is quantified via fluorescence. A quick reference guide can be found here. A full guide can be found here. The PDFs are available in my OneDrive folder in Studies/Aim 1/C3H Flexcell Assay/RT-qPCR/User Guides.

Required Components:

- Taqman MicroRNA Reverse Transcription Kit (Thermo Fisher, Cat #4366596)
- TaqMan Fast Advanced Master Mix for qPCR (Thermo Fisher, Cat #4444556)
- TaqMan MicroRNA Assay and 5X Primer – hsa-miR-331-5p – Assay ID #002233 (Thermo Fisher, Cat #4427975)
- TaqMan MicroRNA Assay and 5X Primer – mmu-miR-193 – Assay ID #002577 (Thermo Fisher, Cat #4427975)

- TaqMan MicroRNA Assay and 5X Primer– sno234 – Assay ID #001234 (Thermo Fisher, Cat #4427975)

1. Isolate and C3H10T1/2 miRNA using the Qiagen miRNEasy Micro kit and quantify via Nanodrop.
2. Dilute samples to 1 ng/µL. Make an aliquot of the original sample and dilute, then reassess with Nanodrop until the samples are in the 5 ng/µL region. Finalize the dilution to 1 ng/µL.
3. Thaw, vortex briefly, and spin the 5X primer briefly.
4. Prepare the reverse transcription reaction mix for 42 reactions:

Table A16. miRNA reverse transcription reaction cocktail preparation.

Component	Vol (1 rxn)	Vol (42 rxn)
100 mM dNTPs (with dTTP)	0.15 µL	6.3 µL
MultiScribe RTase, 50 U/µL	1.00 µL	42 µL
10X RT Buffer	1.50 µL	63 µL
RNase Inhibitor, 20U/µL	0.19 µL	7.98 µL
Nuclease-free H_2O	4.16 µL	174.72 µL
Total RT Rxn Vol	7.00 µL	294 µL

5. Invert to mix and spin briefly. Keep the components on ice.
6. Add 7 µL of the RT reaction mix and 5 µL of template RNA to a qPCR reaction plate. The plate wells must resemble PCR tubes, **not** flat-bottom!
7. Add 3 µL of 5X RT primer to each well. Seal the plate and spin briefly.
8. Place the plate in the thermocycler and complete RT with the following settings:

Table A17. Thermocycler settings for miRNA reverse transcription.

Step	Temperature	Time
RT	16 °C	30 min
	42 °C	30 min
Stop Rxn	85 °C	5 min
Hold	4 °C	Hold

9. The cDNA can be stored at -20 °C.
10. Prepare a separate qPCR master mix for each assay (test samples in duplicate).

Table A18. cDNA qPCR master mix cocktail preparation.

Component	96-well plate (0.2 mL)	For 1 Plate (x29)
miRNA Assay (20X)	1 µL	29 µL
PCR Master Mix (2X)	10 µL	290 µL
Nuclease-Free ddH_2O	7.67 µL	222.43 µL
Total PCR Rxn Mix Vol	18.67 µL	541.43 µL
Template cDNA	1.33 µL	N/A

11. Add 18.67 µL of the prepared qPCR master mix to each well of a PCR reaction plate. Add 1.33 µL of the cDNA and mix thoroughly.
    - Make sure to include a no template control to assess DNA carryover for each primer.
12. Seal the plate and spin briefly.
13. Place the plate in the Bio-Rad CFX96 RT-qPCR System.
    - The user guide for the TaqMan Fast Advanced Master Mix on the CFX96 system can be found here. The PDF is available on my OneDrive folder in Studies/Aim 1/C3H Flexcell Assay/RT-qPCR/User Guides.
14. Initiate the thermocycler and qPCR.

Table A19. Thermocycler settings for cDNA qPCR.

Step	Temperature	Time
UNG Activation (1 Cycle)	50 °C	2 minutes
Polymerase Activation (1Cycle)	95 °C	20 seconds
PCR (40 Cycles)	95 °C	3 seconds
	60 °C	30 seconds

Appendix B – Resource List

Table A20. Resource table for flow cytometry and western blot antibodies, miscellaneous reagents, specialized sample collection consumables, experimental mice and cell lines, software, and hardware used throughout the thesis.

Item/Reagent	Supplier	Cat #
Flow Cytometry Antibodies		
CCR2	N/A – Genetic	N/A - Genetic
CD4	Thermo Fisher Scientific	67-0042-82
CD8	Thermo Fisher Scientific	46-0081-82
CD11b (from Lineage Panel)	BD Biosciences	559971
CD16/32	BioLegend	101337
CD31	BD Biosciences	563089
CD34	BioLegend	119312
CD45	BD Biosciences	552848
CD48	BD Biosciences	563536
CD51 - WT Panel	Fisher Scientific	740062
CD51 - CCR2 eGFP Panel	BD Biosciences	740755
CD51 – CCR2 eGFP Panel	Thermo Fisher Scientific	12-0512-83
CD93	BioLegend	136512
CD206	Thermo Fisher Scientific	12-2061-82
CX_3CR_1	BioLegend	567531
F4/80	Thermo Fisher Scientific	67-4801-82
Ly6C	Thermo Fisher Scientific	25-5932-82
Gr-1 (Ly6G/Ly6C)	Thermo Fisher Scientific	25-5931-82
Sca-1 (Ly6A/E)	BD Biosciences	553336
Sca-1 (Ly6A/E)	Thermo Fisher Scientific	407-5981-82
cKit (CD117)	BD Biosciences	558163
CD127 (IL-7Rα)	BioLegend	135033
CD135	Thermo Fisher Scientific	46-1351-82
CD140a	BD Biosciences	562776
CD150 - WT Panel	BD Biosciences	562811
CD150 - CCR2 eGFP Panel	Thermo Fisher Scientific	46-1502-82
Lineage	BD Biosciences	559971
Viability - Zombie Yellow	BioLegend	423104
Streptavidin - WT Panel	BD Biosciences	554060
Streptavidin – CCR2 eGFP Panel	BD Biosciences	563259

Western Blot Antibodies		
TSG-101	Millipore Sigma	T5701
Alix	Millipore Sigma	SAB4200476
Flotillin-2	Cell Signaling Technology	3436S
pSTAT3 (Tyr705)	Cell Signaling Technology	9145T
STAT3	Cell Signaling Technology	4904T
pNF-κB p65 (Ser468)	Cell Signaling Technology	3039S
NF-κB	Cell Signaling Technology	8242T
β-Catenin	Cell Signaling Technology	9562S
β-Actin	Cell Signaling Technology	4970S
HRP-Linked Secondary – Anti Rabbit	Cell Signaling Technology	7074S
Ladder Precision Plus Dual Standard	Bio-Rad	161-0374
Other Reagents		
Collagenase II (Powder)	Thermo Fisher Scientific	17101015
ACK Lysis Buffer	Gibco	A1049201
Premium Frosted Microscope Slides	Fisher Scientific	12-544-2
Na_2-EDTA	Fisher Scientific	0219482283
Sodium Hydroxide	Millipore Sigma	221465-1KG
Hydrochloric Acid (37% Concentrate)	Millipore Sigma	320331-500ML
Azoxymethane	Millipore Sigma	A5486-25MG
High Glucose DMEM	Wisent Bioproducts	319-005-CL
Fetal Bovine Serum (FBS)	Thermo Fisher Scientific	12483020
Phosphate-Buffered Saline (PBS)	Wisent Bioproducts	311-010-CL
100X Penicillin/Streptomycin (P/S)	Thermo Fisher Scientific	15140-122
EasySep Mouse HSPC Isolation Kit	STEMCELL Technologies	19856
MethoCult HSPC CFU Assay Kit	STEMCELL Technologies	GF M3434
Mesencult Adipogenic Differentiation Kit	STEMCELL Technologies	05507
Mesencult Osteogenic Differentiation Kit	STEMCELL Technologies	05504
L-glutamine 200 mM	STEMCELL Technologies	07100
Oil Red O	Millipore Sigma	O1391
Alizarin Red S	Millipore Sigma	A5533
Isopropanol	Fisher Scientific	A416-500
Click-iT EdU Assay Kits	Thermo Fisher Scientific	C10337
Insulin (1 µg/mL)	Millipore Sigma	I9278
Triton X-100	Millipore Sigma	9036-19-5
70 µm Cell Strainer	Fisher Scientific	22-363-548
Mortar and Pestle	Fisher Scientific	S337631
Large Scissors (9 cm)	Fine Science Tools	14060-09

Small Scissors (9 cm)	Fine Science Tools	14184-09
Large Forceps (16 cm)	Concord Surgical	OEL-J-27-271
Small Forceps (4.5”)	Life Supply	MDL MDS10724
Protease Inhibitor Cocktail	Millipore Sigma	04693116001
Phosphatase Inhibitor	Millipore Sigma	4906837001
Bradford Reagent	Bio-Rad	5000006
PVDF Membranes	Bio-Rad	1620177
4x Laemmli Buffer	Bio-Rad	1610747
Tris Base	Thermo Fisher Scientific	15504020
Glycine	Bio-Rad	1610718
Sodium Dodecyl Sulfate	Thermo Fisher Scientific	15525017
Ammonium Persulfate	Thermo Fisher Scientific	327081000
Glycerol	Fisher Scientific	BP2291
Bromophenol Blue	Millipore Sigma	B0126
β-Mercaptoethanol	Bio-Rad	1610710
TEMED	Bio-Rad	1610801
Acrylamide (30%)	Bio-Rad	1610158
Sodium Acetate	Millipore Sigma	S7899
Agarose	Millipore Sigma	A6013
EZ Load 100 bp Molecular Ruler	Bio-Rad	1708352
4% Formaldehyde	Millipore Sigma	1004960700
Restore Western Blot Stripping Buffer	Thermo Fisher Scientific	21059
miRNEasy Micro RNA Extraction Kit	Qiagen	217084
Chloroform	Fisher Scientific	ICN19400290
TaqMan MicroRNA Reverse Transcription	Thermo Fisher Scientific	4366596
TaqMan Fast Advanced Master Mix	Thermo Fisher Scientific	4444556
TaqMan miRNA Assays	Thermo Fisher Scientific	4427975
45% kcal High-Fat Diet	Research Diets	D12451
Control Diet	Research Diets	D10012M
Teklad 2018 Standard Diet	Inotiv	2018
Bovine Serum Albumin (BSA)	Fisher Scientific	BP1600-100
Tween 20 (Polysorbate 20)	Fisher Scientific	BP337500
SuperSignal West Pico PLUS Enhanced	Thermo Fisher Scientific	34580
Mini Trans-Blot Filter Paper 7.5x10cm	Bio-Rad	1703932
Epredia 10% Neutral Buffered Formalin	Fisher Scientific	22-050-104
Ethyl Alcohol Anhydrous	Greenfield	P016EAAN
Osmium Tetroxide	Polysciences	23311-10
Potassium Dichromate	Millipore Sigma	207802

Dimethyl Sulfoxide	Millipore Sigma	D2438
Specialized Sample Collection Consumables		
3 mL Syringes	STEMCELL Technologies	28240
16-Gauge Blunt-End Needles	STEMCELL Technologies	28110
25-Gauge Needles (3cc)	CanMedDirect	309581
BioFlex Collagen I-Coated 6-Well Plates	Flexcell	BF-3001C
Cell Scrapers	Fisher Scientific	08-100-241
K_2-EDTA 6.0 mL Vacutainers	BD Biosciences	367863
Wooden Dowel Rods – 0.2”x11.8”	Amazon	044484545
Bel-Art SP Plastic-Backed Roll	Fisher Scientific	11-999-19
70 mL Polycarbonate Bottle Assembly	Beckman Coulter	355622
3.5 mL Open-Top Polycarbonate Tube	Beckman Coulter	349622
Experimental Mice and Cell Lines		
CBA/J	The Jackson Laboratory	000656
C57Bl/6J	The Jackson Laboratory	000664
B6(C)-Ccr2$^{tm1.1Cln}$/J	The Jackson Laboratory	027619
C3H10T1/2 Clone 8	ATCC	CCL-226
Software		
GraphPad Prism v9	GraphPad Software	Website
Zen Blue v2.6	ZEISS	Website
Zen Software v3.8	ZEISS	Website
Nanostring Mouse v1.5 miRNA Library	Nanostring Technologies	Website
Nanostring nSolver 4.0	Nanostring Technologies	Website
ROSALIND nCounter Data Analysis	ROSALIND	Website
Photoshop CC 2018	Adobe	Website
BioRender	BioRender	Website
NRecon	Micro Photonics Inc	Website
CTan	Blue Scientific	Website
Attune NxT v4.0.0	Thermo Fisher Scientific	Website
Hardware		
X-RAD 320	Precision X-Ray	Website
Attune NxT Flow Cytometer	Thermo Fisher Scientific	Website
Celldiscoverer 7 Microscope	ZEISS	Website
Bio-Rad ChemiDoc	Bio-Rad	Website
NanoDrop 2000	Thermo Fisher Scientific	Website
EchoMRI-900	EchoMRI LLC	Website
Exer 3/6 Treadmill	Columbus Instruments	Website
Sorvall ST 16R Centrifuge	Thermo Fisher Scientific	Website

5430 R Centrifuge	Eppendorf	Website
Optima MAX-Micro Ultracentrifuge	Beckman Coulter	Website
Optima XPN Ultracentrifuge	Beckman Coulter	Website
Optima MAX-XP Ultracentrifuge	Beckman Coulter	Website
TLA 100.3 Ultracentrifuge Rotor (3 mL)	Beckman Coulter	Website
Type 45 Ti Ultracentrifuge Rotor (70 mL)	Beckman Coulter	Website
ZetaView PMX 110 NTA	Particle Metrix	Website
EasyEights EasySep Magnet	STEMCELL Technologies	Website
Cell Countess II Hemocytometer	Thermo Fisher Scientific	Website
SkyScan 1272	Bruker	Website
Flexcell FX5000T-FLK Tension System	Flexcell	Website
SteREO Discovery.V20 Stereo Microscope	ZEISS	Website
Fisher Scientific Bead Mill 24	Thermo Fisher Scientific	Website
PowerPac Basic Power Supply (1645050)	Bio-Rad	Website
Mini-PROTEAN Tetra Cell	Bio-Rad	Website